1990

Origin, sedimentary geochemistry, and correlation of Middle and Late Ordovician K-bentonites: constraints from melt inclusions and zircon morphology

Carsten Schirnick
University at Albany, State University of New York

Origin, sedimentary geochemistry, and correlation

of Middle and Late Ordovician K-bentonites:

Constraints from melt inclusions and zircon morphology.

A Thesis presented to the Faculty

of the State University of New York

at Albany

in partial fulfillment of the requirements

for the degree of

Master of Science

College of Science and Mathematics

Department of Geological Sciences

Carsten Schirnick

1990

Origin, sedimentary geochemistry, and correlation

of Middle and Late Ordovician K-bentonites:

Constraints from melt inclusions and zircon morphology.

Abstract of a thesis presented to the Faculty

of the State University of New York

at Albany

in partial fulfillment of the requirements

for the degree of

Master of Science

College of Science and Mathematics

Department of Geological Sciences

Carsten Schirnick

1990

Abstract

The present study of Paleozoic K-bentonites demonstrates that the geochemistry of melt inclusions and the morphology of zircons can be studied by inexpensive and simple-to-use methods, which rely on phenocrysts. Constraints are obtained that lead to (a) the origin of these altered volcanic ashes, (b) the geochemistry of ash-to-K-bentonite-alteration, and (c) the reliable correlation of extensively altered volcanic ashes (i.e. K-bentonites).

Silicic melt inclusions (i.e. non-devitrified) have been found in quartz and zircon phenocrysts contained within Ordovician and Devonian K-bentonites from New York State, the Upper Mississippi Valley, and Pennsylvania. Origin, source, and tectonic setting of the volcanism that produced these Paleozoic volcanic ashes (i.e. K-bentonites) are constrained by the geochemistry of these inclusions. The major element compositions of the inclusions, which are small samples of the non-degassed pre-eruptive melt trapped during growth of the phenocrysts, indicate that the K-bentonites were generated by explosive eruptions of rhyolitic, high-K type magmas in a continental volcanic arc. The geochemistry of melt inclusions may furthermore be used for correlation of these volcanic ashes since stratigraphically distinct K-bentonites contain inclusions with different major element composition.

Diagenetic alteration of the rhyolitic ashes to K-bentonites has strongly affected their mineralogy and bulk geochemistry. The major element composition of altered K-bentonites, which apparently depends on the composition of the dominating clay minerals and other authigenic phases (e.g., pyrite, calcite), has been compared with unaltered melt inclusions and shows the direction and magnitude of the geochemical changes that occur during diagenesis. Relative to aluminum, substantial amounts of Si, Na, K and Mn have been lost, whereas Ti, Fe and Mg have been gained in the K-bentonites. The surrounding sediments, which are enriched in

SiO_2 compared with sediments further away, apparently acted as a sink for the silica released from the volcanic ash. The observed enrichment of TiO_2 in the K-bentonites relative to aluminum seems best explained as a result of contamination by pelagic, TiO_2-rich clay particles that have settled into the voids within the unaltered volcanic ashes.

The morphology of zircon populations from several K-bentonites has been studied using the classification scheme of Pupin and Turco (1972b). Applied as a petrogenetic indicator, the morphologies suggest crystallization of the zircons in I-type magmas at temperatures common for silicic volcanic rocks (i.e. >750°C). It can be demonstrated that stratigraphically different K-bentonites contain zircon populations that are morphologically distinct and can be used for correlation. At least two different K-bentonites seem to be correlated between New York State and the upper Mississippi Valley based on the morphology of zircons.

The trace element abundances of Hf, Ti, P, Y, Yb, Ce, U and Th in individual zircons from several K-bentonites have been analyzed by electron microprobe. Single grains have been selected from layers which can be correlated by stratigraphy and by zircon morphology. It was found, however, that the geochemistry of zircons from stratigraphically different layers is indistinguishable and can not be used for correlation of the Paleozoic K-bentonites.

Acknowledgements

Before all, I thank everyone here in the Department of Geological Sciences and abroad in Germany, especially my parents, who made it possible for me to stay and study in Albany and gather the experience, which I would never want to miss.

Special thanks go to the members of my committee J.W. Delano, W.S.F. Kidd, S.D. Samson, and K. Hollocher for reading my thesis and making helpful comments and suggestions which greatly improved this thesis.

Many thanks to W.S.F. Kidd for his experience and help during the fieldwork in New York State.

My particular gratitude goes to J.W. Delano, who has had the most important and valuable influence as advisor and friend, while he "made" me grow from a student to a scientist over the past three years. Without his outstanding support and continous encouragement, this thesis as the documentation of my research, and the research itself, wouldn't have been possible. The financial support that he provided and which allowed me to conduct all this research, is gratefully acknowledged.

I thank Brian Taylor in the machine shop for the great craftmanship and patience in making all these last-minute custom built orders; David Wark at RPI, who taught me how to use the electron microprobe and how to get along with all its fancy features, particularly late at night or on the weekend; and Jeff Travis in the SUNY Biology department, who introduced me to the use of the SEM and who took Noah's flood so easy.

Among the friends in the department I thank Barbara B. for all the fun (and pain) we shared during the field and laboratory work as well as for putting up with my moods, particularly during the final stage of writing the thesis. It has to be pointed out that this work on K-bentonites could only be so extensive since Barbara and I shared the work involved in collecting and processing all sample material (i.e. K-bentonites), allowing each of us to conduct the research on almost the same sample set but different subjects.

Table of contents

List of tables

List of figures

Chapter 1 "General introduction"

1.1. Study of Paleozoic K-bentonites

K-bentonites are clay-rich alteration products of silicic vitric ashes that have undergone extensive chemical and mineralogical changes during diagenesis. Occurrences of K-bentonites of Ordovician age are numerous in eastern North America (e.g., Allen, 1929, 1932; Brun and Chagnon, 1979; Cullen-Lollis and Huff, 1986; Delano et al., 1990; Huff, 1983; Kay, 1931, 1935; Kolata et al., 1986; Mossler and Hayes, 1966; Nelson, 1922; Weaver and Bates, 1951) and distributed over large areas (about 1,000,000 km^2; Bergström, 1983; Kolata et al., 1986; Nelson, 1922). Because of their widespread distribution and representation of short depositional events (i.e. duration of volcanic eruption), these altered ashes ideally serve as time markers (event horizons) for correlation within sedimentary strata (e.g. Bergström, 1983; Cisne et al., 1978, 1982; Cullen-Lollis and Huff, 1986; Huff, 1983; Kay, 1931; Kolata et al., 1986, 1987; Rosenkrans, 1934; Samson et al., 1988; Smith et al., 1988; Way et al., 1986). Various methods (e.g. chemical fingerprinting, apatite chemistry, biostratigraphy, lithostratigraphy, bed tracing) have been used for correlation of Ordovician K-bentonites, although their successful application has been commonly restricted to local outcrop areas (e.g. New York State, Mississippi Valley, Pennsylvania).

Furthermore, recent studies of Paleozoic K-bentonites have demonstrated that correlation is only a single aspect of their geologic record because isotopic, geochemical and petrologic constraints can be placed on the origin of the volcanism that produced those K-bentonites, despite the extensive alteration they have undergone (e.g., Delano et al., 1990; Samson, 1986; Samson et al., 1989).

1.2. Purpose of this study

The goal of the present study was to (a) constrain the origin of the Paleozoic K-bentonites and (b) develop criteria leading to the reliable correlation of K-bentonites despite the altered character of these ashes. For this latter purpose, two approaches were selected: (a) the geochemistry of melt inclusions; and (b) the morphology and geochemistry of zircons.

Melt inclusions contained within quartz and zircon phenocrysts from various K-bentonites were analyzed for their major element composition. Since the inclusions represent small fractions of pre-eruptive melt from which the phenocrysts grew, they yield evidence for the composition of the unaltered volcanic ashes amd provide important insights into the magmatic processes and tectonic setting of the volcanic arc that generated the K-bentonites.

In a comparison of altered (i.e. K-bentonite) with unaltered (i.e. melt inclusion) compositions, it is possible to determine the magnitude and direction of geochemical changes that occurred during diagenesis.

The morphology of zircon populations contained within the K-bentonites was investigated and compared with previous studies (e.g., Pupin, 1980; Pupin and Turco, 1972, 1975), which allow an estimate of the magma type (i.e. I-type, S-type, A-type) from which the zircon populations crystallized. Furthermore, since zircon morphology has been successfully used for correlation of altered volcanic ashes (Kowallis and Christiansen, 1990; Winter 1981, 1984), the applicability of this method was tested on several K-bentonites in the present study. Individual zircons were geochemically analyzed to detect (1) a possible correlation between geochemistry and morphology and (2) whether the geochemistry of zircons can also be used for correlation.

1.3. Geologic setting at the time of ash deposition

The volcanism recorded by Middle- and Late-Ordovician K-bentonites in the eastern United States is generally linked to eastward dipping subduction underneath an approaching volcanic arc, which ended in an arc-continent collision (i.e. Taconic orogeny). Although remnants of the volcanic arc are found along the Appalachians and Caledonides (e.g., Ammonoosuc, Tetagouche, Borrowdale Volcanics), none of these volcanic centers has yet been confidently identified as the source area for the North American K-bentonites (Delano et al., 1990; Kay, 1935; Kolata et al., 1986; Samson et al., 1989; Sloan, 1987).

At the time of ash deposition, the eastern margin of the North American continent evolved from a passive margin to a foreland basin (Rowley and Kidd, 1981; Cisne et al., 1982). This transformation resulted from the approach of the volcanic arc and its associated accretionary prism, which caused the gradual subsidence of the eastern continental margin of North America. The record of subsidence is evident from a sediment sequence in the central Mohawk Valley (New York State) consisting of thin (i.e. 5-100 meters) shallow water carbonates (Trenton Group) overlain by 200-500 meters of black, in part calcareous, shales (Utica Formation) (Fisher, 1977; Rickard, 1973), which represent the deep water facies (Cisne et al., 1982). These black shales are overlain by a thick pile (up to several thousand meters) of alternating argillaceous and turbiditic flysch sediments (Frankfort/Schenectady Formations).

The relative ages of the formation boundaries (e.g., carbonate to shale, shale to flysch deposition) become progressively younger to the west (Fisher, 1977; Rowley and Kidd, 1981; Ruedemann and Chadwick, 1935) (Figure 1).

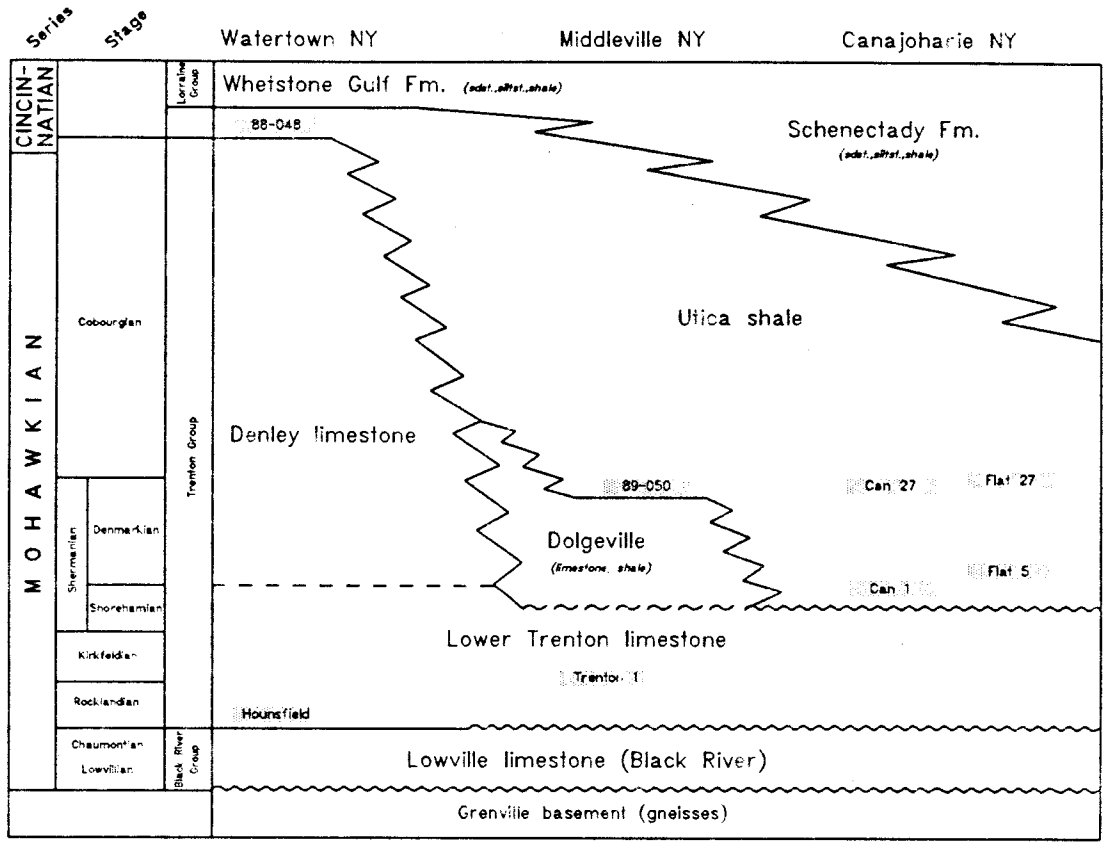

Figure 1: Schematic illustration of the Middle and Late Ordovician K-bentonites in New York State and their stratigraphic relation to the hosting sediments, which were deposited on the subsiding eastern margin of the North American continent. Deposition of this carbonate-shale-flysch sequence was diachronous such that the facies changes are progressively younger to the west. Terminology and stratigraphic relations after Fisher (1977) and Cisne et al. (1982).

1.4. Stratigraphy of K-bentonites

At least 30 different K-bentonites have been recognized in Middle- and Late-Ordovician sediments in New York State. These altered volcanic ashes occur in carbonates (Trenton Group) and in black, calcareous shales (Utica Formation) as thin (<10 cm), nonlithified, clay-rich layers. They are easily recognized in outcrop because they (a) form prominent reentrants resulting from preferred erosion relative to the lithified over- and underlying strata (Figure 2) and (b) generate orange surface-staining on underlying shales, which is caused by weathering of authigenic, Fe-rich sulfides contained within the K-bentonites.

More than 15 different K-bentonites are reported to occur in three different clusters of Middle- and Late-Ordovician strata in the upper Mississippi Valley (Kolata et al., 1986; Sloan, 1987). They are hosted by sediments, dominantly carbonates and minor shales, that were deposited onto the North American craton in an epicontinental sea to the west of the subsiding continental margin (Cisne et al., 1984).

All of the K-bentonites from New York State and the upper Mississippi Valley that were investigated in the present study occur stratigraphically above the Black River-Trenton boundary (Cisne et al., 1982; Fisher, 1977; Kay, 1935; Sloan, 1987; Templeton and Willman, 1963). This boundary appears to be represented by the Deicke K-bentonite (Sloan, 1987) in the Mississippi Valley, which has been dated independently at 454.2±6.0 Ma (^{40}Ar-^{39}Ar method on biotites; Kunk and Sutter, 1984) and 457.1±1.0 Ma (U-Pb method on zircons; Samson et al., 1989). A brief summary of the stratigraphy and terminology used for K-bentonites in the present study, as well as in other studies (i.e., Cisne et al., 1982; Delano et al., 1990; Hay and Cisne, 1988), follows (see also Table I).

Figure 2: Photograph of Utica shale outcrop in Canajoharie Creek. Dark, horizontal lines mark reentrants that were formed by preferred erosion of nonlithified K-bentonites. Lowermost reentrant is formed by K-bentonite Can 10; uppermost K-bentonite exposed in this cliff is Can 23 (Figure 3). A 2 meter scale bar stands upright on debris pile at level of K-bentonite Can 10.


Can23
22
20+21
19
18
17
16
15
14
13
12
11
Can 10

Table I.

Summary of terminology used in different studies (present study; Cisne et al., 1982; Hay and Cisne, 1988) for identical K-bentonites in New York State. Labels are printed in brackets where uncertainties remained due to different number and/or position of K-bentonites recognized in the field.
See appendices D,E,F for localities and geographic positions.

Present study	Cisne et al. (1982)	Hay and Cisne (1988)
Canajoharie Creek:		
Can 27	not recognized	# 21
Can 26	not recognized	# 20
Can 25	not recognized	# 19
Can 24	not recognized	# 18
Can 21;22;23	M 39	(# 16;17)
Can 18;19;20	not recognized	not recognized
Can 17	M 37	# 15
Can 16	M 37	# 14
Can 15	M 37	# 13
Can 14	M 37	# 12
Can 13	M 35	# 11
Can 12	M 32	# 10
Can 11	M 32	# 9
Can 10	M 32	# 8
Can 9	M 31	(# 7)
Can 7;8	M ?	(# 6)
Can 3;4;5;6	not recognized	(# 5)
Can 2	M 15	# 4
Can 1	M 14	# 3
Can 1-1	M 11	# 2
Can 1-2	M 8	# 1
Middleville NY.:		
89-050	M 37	# 2
Trenton-1	M-25	not recognized

The Hounsfield K-bentonite is stratigraphically the oldest altered ash that was sampled for the present study in New York State at its type locality near Dexter, Jefferson County, NY (Kay, 1930, 1931). It occurs in limestone of the Rocklandian stage (Kay, 1935) and was correlated with the Millbrig K-bentonite in the upper Mississippi Valley (Kay, 1931). Cisne et al. (1982) assign the Hounsfield to their two M-25 beds in the upper Mohawk Valley further east, although these two K-bentonites occur in the Kings Falls limestone of Kirkfeldian stage, which is the stage following the Rocklandian (Figure 1). The lower of the two M-25 K-bentonites has been sampled in an outcrop east of Middleville, NY (Cameron and Kamal, 1977) and was named Trenton-1 (Delano et al., 1990; present study). The 89-050 K-bentonite (M37 bed of Cisne et al., 1982) was sampled south of Middleville, NY., where it occurs in black Utica shale immediately above the contact with Dolgeville facies (upper Shermanian stage) (Kay, 1953). This altered ash is therefore younger than the Trenton-1 K-bentonite (Figure 1). A succession of about thirty (30) K-bentonites is exposed in Canajoharie Creek and Flat Creek in the central Mohawk Valley, NY, where they occur throughout in black shales of the Utica Formation (upper Shorehamian to Cobourgian stage; Cisne et al., 1982; Fisher, 1977) (Figure 1). Both sections have been measured and are correlated based on the stratigraphy of the K-bentonites, which have been labeled in ascending order starting with the oldest layers near the bottom of the sections (Figure 3). They are younger than the Trenton-1 but either time-equivalent, or older than, the 89-050 K-bentonite (Figure 1; see also Chapters 2 and 4).

The Millbrig and Dickeyville K-bentonites were sampled in the upper Mississippi Valley northwest of Dickeyville, WI. They occur in carbonates and carbonaceous shales of the Spechts Ferry (Millbrig), and Guttenberg Formations (Dickeyville), which belong to the Rocklandian stage (Kolata et al., 1986; Sloan, 1987). Another sample, which is believed to be the Nasset K-bentonite, was sampled

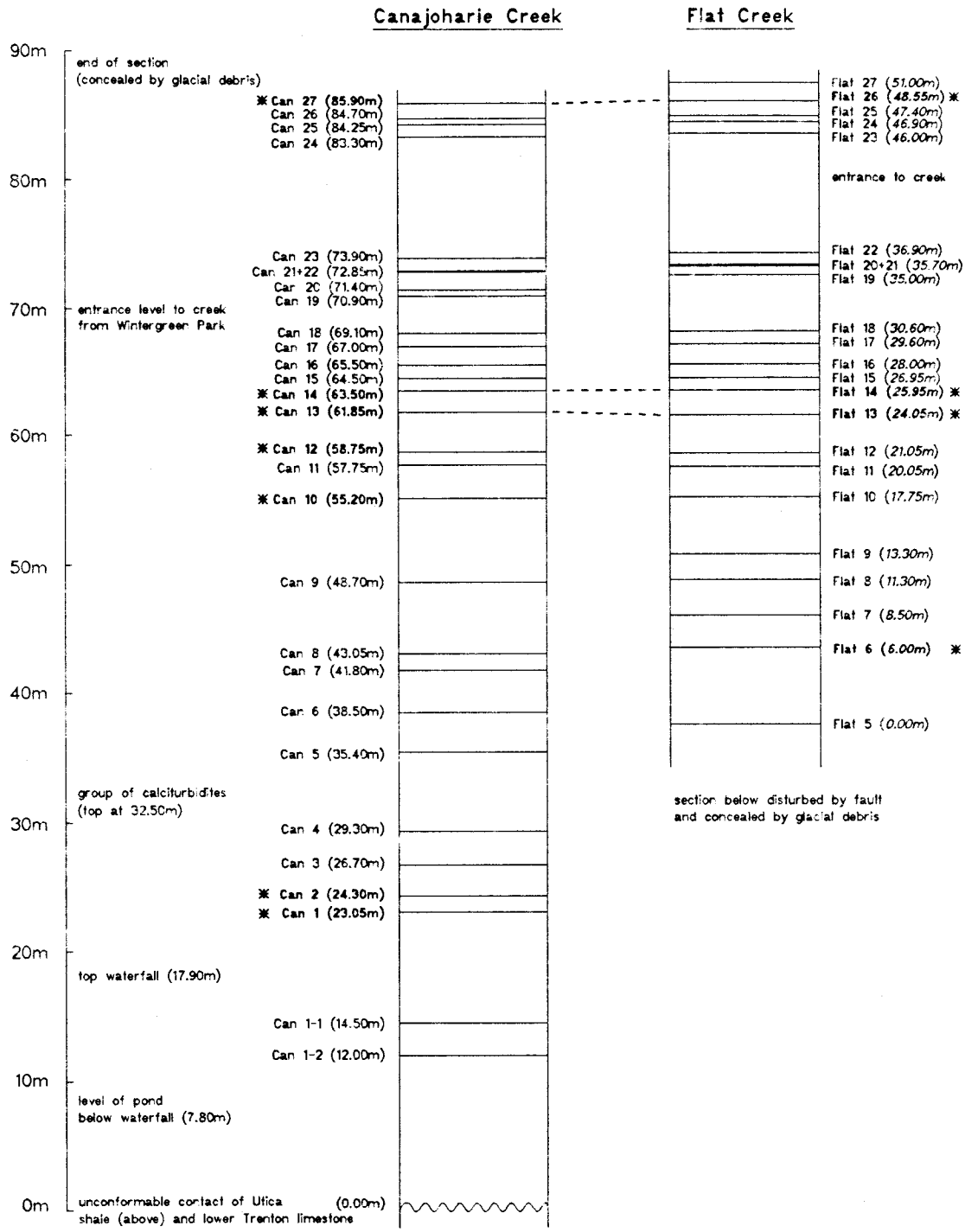

Figure 3: Measured sections of Utica shale in Canajoharie Creek, NY and Flat Creek. Exposed is a succession of about 30 K-bentonites, which have been numbered in ascending order. K-bentonites that were studied in detail are marked by an asterik. Stippled lines between the two sections indicate correlation based on geochemistry of melt inclusions (Chapter 2) and zircon morphology (Chapter 4). See Table I. for correlation of K-bentonite terminology used in present study with terminology of Cisne et al. (1982).

north of Guttenberg, IA. It is younger than the Millbrig and Dickeyville K-bentonites and exposed in carbonates of the Dunleith Formation (Shermanian stage) (Sloan, 1987).

The Middle Devonian Tioga-F K-bentonite occurs in shale of the Lower Marcellus Formation (Smith and Way, 1983). A sample of this altered ash, collected near Frankstown, PA, was provided by R.C. Smith to J.W. Delano.

1.5. Sample collection and preparation

Samples of K-bentonites were collected by either digging into the layers with a chisel or a steel rod, or, if possible, by removing the overlying strata. The samples were stored in new zip-lock plastic bags. Although sample masses of one to two kilograms were preferred, limited access to a few samples (i.e. Millbrig, Nasset, Hounsfield) yielded only a few hundred grams, which was nevertheless sufficient for the purpose of this study.

The sample-processing in the laboratory involved several steps in order to achieve the required separation of minerals from the clay-rich matrix. (1) All K-bentonite samples were split into size fractions by wet sieving through steel sieves of sizes 1000, 500, 250, 125, 63 and 45 microns. All steel sieves were carefully cleaned prior to preparation of a new sample in order to avoid cross contamination. (2) These fractions were ultrasonically cleaned for up to several hours to remove the clay adhering to the grains. Cleaned fractions were rinsed in acetone and dried under a red light to ensure removal of all moisture. (3) The minerals in the 500, 250, 125, 63 and 45 micron fractions were separated in two consecutive steps with heavy liquids (i.e., bromoform, density 2.85 g/cm^3; methylene iodide, density 3.32 g/cm^3). (4) For the present study, quartz and

zircons were each further concentrated according to their magnetic susceptibility by using a Frantz isodynamic magnetic separator (model L-1). The least magnetic fraction of the minerals having densities greater than 3.32 g/cm^3 (e.g. zircons) often contained large amounts of diagenetic pyrite and barite. These contaminants were dissolved in hot concentrated HNO_3 (dissolves pyrite) and H_2SO_4 (dissolves barite). Dissolution of zircons was not observed to have occurred for the duration (less than 5 minutes) of these acid treatments.

Chapter 2 "Melt inclusions"

2.1. Introduction

Interest in the study of melt inclusions seems to be increasing, due in part to the development of more sophisticated micro-analytical techniques (e.g. electron microprobe, infrared spectroscopy, ion microprobe). Since melt inclusions are samples of magma that became trapped in phenocrysts during growth in a large body of magma (Clocchiatti, 1975; Roedder, 1984) they are important geochemical recorders of a magmatic system (e.g. pre-eruptive volatile content, liquid line of descent).

Various mechanisms may lead to the formation of melt inclusions in magmatic phenocrysts during their growing from a melt. Deviation from euhedral crystal growth yields embayments in the surface of crystals in which liquid (e.g. melt) becomes trapped and subsequently sealed off due to the continued crystallization of the host phase. Magmatic corrosion may cause deep embayments that eventually become covered when crystal growth resumes leading to the entrapment of liquid as well. However, the most common trapping mechanism is believed to be rapid growth leading to skeletal crystal forms (Roedder, 1984).

Host phases to melt inclusions includes more-or-less the entire spectrum of magmatic liquidus phases (for summaries: Clocchiatti, 1975; Roedder, 1984), no matter if present as a major phase such as olivine, pyroxene, plagioclase, amphibole or quartz or as a minor phase like zircon, apatite, or Fe-Ti oxide.

However, the preservation of melt inclusions for geologically long time periods depends on presence or absence of certain mineral characteristics (i.e. cleavage in K-feldspar and biotite) that are protective against diagenesis. Quartz seems to be an ideal host for melt inclusions due to the absence of cleavage and

its resistance to weathering. These characteristics appear to be extremely helpful in the case of the Paleozoic K-bentonites, where the melt inclusions discovered in this present study are the only remnants of the once abundant volcanic glass, which has been extensively altered to clay during diagenesis. Due to the highly altered nature of the K-bentonites, little effort has previously been put into the geochemical investigation of their tectonic significance, despite their ubiquitous occurence.

The oldest recorded occurence of glassy melt inclusions in Paleozoic volcanics are of Carboniferous age (Belkin and Rice, 1990; Payette and Martin, 1986). Arndt et al. (1989), however, demonstrated that fresh glassy melt inclusions may occur in volcanics (i.e. komatiites) as old as 2.7 Ga. The present study presents the first recognition of glassy melt inclusions in quartz phenocrysts of Late Ordovician age from within the Utica Formation of New York State. The approach of studying K-bentonites of Paleozoic age via melt inclusions appears useful mainly for two reasons. First, as samples of the pre-eruptive magma, it is likely that the composition of melt inclusions represents the composition of the volcanic glass that was deposited to form the original ash, but which has subsequently been completely altered to a K-bentonite. Therefore, the composition of melt inclusions provides an ideal reference for evaluating the magnitude of elemental mobilities during diagenetic alteration processes. Second, the melt inclusions provide direct insight into the magmatic processes that occurred within a major volcanic arc about 450 million years ago.

2.2. Sample material

The starting materials for this study are Middle and Late Ordovician K-bentonites, as well as one Middle Devonian example. The K-bentonites chosen for separation of inclusion-bearing quartz and zircons were samples of which the morphology of their zircon populations had been studied. In addition, these K-bentonites could be correlated or distinguished by stratigraphy (Chapters 1 and 4). The samples in sequence of decreasing age are as follows: the Millbrig and Dickeyville K-bentonites (Wisconsin); Can 13, Can 14 and Flat 14 from Canajoharie Creek and Flat Creek (New York State); 89-050 from the West Canada Creek area and Can 27 from Canajoharie Creek (both New York State); and the Tioga-F ash bed (Pennsylvania). The reader is referred to Table I and Figures 1 and 3 in Chapter 1 for detailed information on sample localities, relative stratigraphic positions, and references.

2.2.1. Description of melt inclusions in quartz

The non-devitrified, glassy melt inclusions are clear in color, subspherical in shape, and invariably lack evidence of bubbles or any other voids caused by shrinkage upon cooling. They range in diameter from 10 to 100 microns. The average size is about 50 microns. Devitrified inclusions are opaque in transmitted light but appear white under reflected illumination, similar to the white spherules in perlites. They are most common among the largest inclusions, whereas the glassy inclusions are most common among the smaller sizes. Vitreous inclusions and devitrified ones commonly occur in the same grains. Physical defects in grains hosting devitrified inclusions (e.g. cracks) have not been evident at the micron

scale but can not be precluded at the sub-micron size. Anastomosing melt inclusions have not been observed in quartz hosts, although funnel shaped embayments that reach deep into the crystal and may once have been filled with melt were observed in several specimens (e.g. Figure 4).

The morphologies of quartz crystals that contain melt inclusions are variable. A first impression from the handpicking procedure suggests that there is a preferential occurence of melt inclusions in morphologically distinct quartz crystals. The distinct morphological features of quartz in the K-bentonites are euhedral to subhedral pseudohexagonal bipyramids (beta-quartz) or contrasting shard-shaped quartz fragments, which lack any evidence of crystal faces.

Figure 5 is a transmitted light photomicrograph showing several euhedral to subhedral quartz crystals and anhedral quartz fragments from one Late Ordovician K-bentonite hosting an assortment of glassy melt inclusions (clear), mineral inclusions (clear to black) and devitrified inclusions (black).

The number of melt inclusions hosted by a single quartz crystal varies from one inclusion up to sets of five, but rarely more. The proportion of quartz grains in a K-bentonite containing melt inclusions is highly variable from K-bentonite to K-bentonite. The Tioga-F ash bed and Can 14 and Flat 14 were samples which were overall very crystal rich and yielded the largest quantities of quartz crystals containing melt inclusions. K-bentonite Can 27 is the only sample examined that has yielded no quartz melt inclusions although twice the amount of sample material used for other samples has been processed (i.e. 2 kilograms).

Figure 4: Photomicrograph (transmitted light) of a quartz grain from K-bentonite Can 14. Various types of inclusions are present. Note the subspherical heterogeneous melt inclusion to the left of center, which is pictured as backscattered electron image in Figure 15. The unmixed domains are visible at 3 and 9 o'clock positions of that inclusion. A funnel-shaped inclusion, which is in part filled (black), opens towards the upper right rim of grain. Scale bar equals 200 microns.

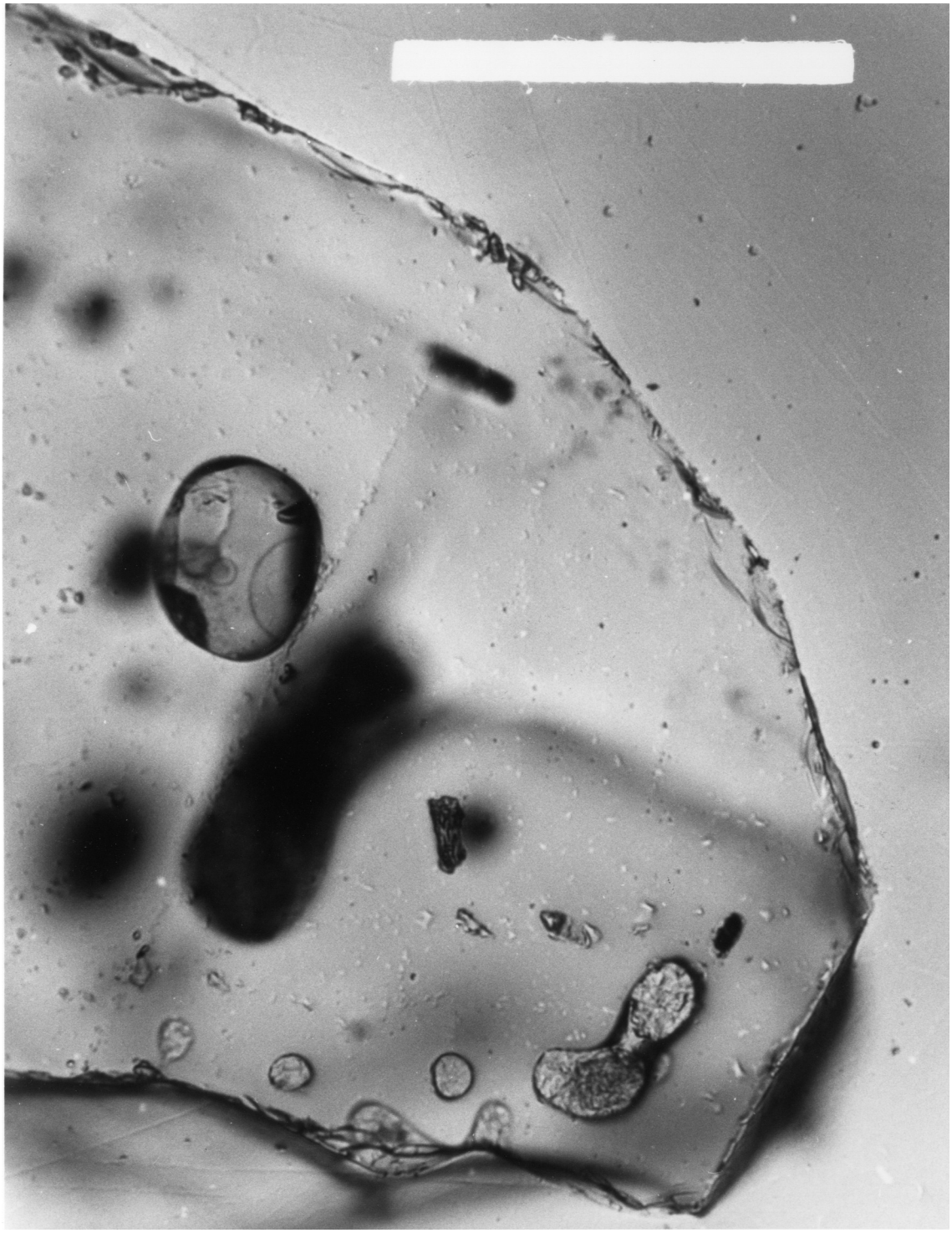

Figure 5: Quartz grains of various morphologies from K-bentonite Flat 14. Smaller grains are commonly present as subhedral, pseudohexagonal bipyramids (i.e. ß-quartz). Note, that glassy melt inclusions appear clear and lack shrinkage bubbles, whereas devitrified melt inclusions appear black. Scale bar equals 500 microns.

2.2.2. Description of melt inclusions in zircons

Most of the zircon phenocrysts containing melt inclusions are only slightly larger (up to 100 microns wide) than the average size of melt inclusions present in quartz (±50 microns across). Hence, the average size of melt inclusions trapped in zircons is comparatively smaller (i.e. average of <20 microns diameter).

Zircons contain clear glassy inclusions, as well as the devitrified variety. Melt inclusions in zircons are commonly subspherical in shape. Anastomosing inclusions are frequently observed in zircons in contrast to their virtual absence in quartz. The orientation of the inclusions often reflects their attachment to a former crystal face of the zircon, typically a pyramidal face (see Chapter 4 for detailed discussion of zircon morphology).

A quantitative description of the frequency at which melt inclusions occur in zircons is difficult because they are not as easily recognized as in quartz due to their small size. Furthermore, zircons are frequent hosts of other phases that strongly outnumber the melt inclusions. Such inclusions are mostly stubby or needle shaped apatites and Fe-Ti oxides, which very often hide melt inclusions.

2.3. Analytical techniques

2.3.1. Sample preparation

Crystalline phases were separated from K-bentonite samples and concentrated using heavy liquids (i.e. bromoform and methylene iodide) and isodynamic magnetic separation. Some of the inclusions in zircons from sample Can-14 were analyzed

within polished sections of bulk grain mounts, randomly arranged on 1-inch plexiglass disks. Inclusions in zircons from other samples (89-050 and Dickeyville) were analyzed in single-grain mounts on thin section glass slides.

Quartz grains were concentrated in the least magnetic fraction of the heavy liquid float (i.e., density less than bromoform) by isodynamic magnetic separation. They were then immersed in refraction oil and handpicked under the binocular according to the presence of melt inclusions. Selected quartz grains were mounted, ground and polished individually to assure that melt inclusions were sectioned in every grain.

2.3.2. Electron microprobe

All sample-mounts of inclusion-bearing quartz were carbon-coated and analysed for their major element composition (SiO_2, TiO_2, Al_2O_3, FeO, MnO, MgO, CaO, Na_2O, K_2O) with the electron microprobe located in the Department of Geology at the Rensselaer Polytechnic Institute. This instrument, a JEOL 733 Superprobe, uses five wavelength dispersive spectrometers with on-line data reduction using Bence-Albee matrix correction. Analyses were performed using an accelerating voltage of 15 kV, cup current of 8 nanoampere, and a broad beam (20 to 30 microns diameter) in order to avoid mobilization of Na during analysis. Counting-time was set to either 40 or 60 seconds at the peak position and half of that time at each background position on both sides of the peak. Backgrounds were routinely collected for each grain.

Backscattered electron images were collected at 15 kV accelerating voltage and 2 nanoampere beam-current and exposed onto Polaroid type-55 film at the slowest scan-speed possible. Typical scan-time for each exposure was about 8 minutes.

This setting is sufficient to reveal even slight differences in the average atomic mass of a sample (i.e. silicic glass).

Analytical accuracy was determined on the Rhyolite Glass Standard from Yellowstone National Park, (USNM 72854 VG-568). The average of repeated analyses of the Rhyolite Glass Standard during the microprobe sessions is listed in Table II.

2.3.3. Mobilization of sodium during analysis: Precautions and correction.

To avoid the severe problem of Na-mobilization during analysis, particularly in volatile-rich rhyolitic glasses (Nielsen and Sigurdsson, 1981; Rutherford et al., 1985), the diameter of the electron beam striking the sample surface was in most cases broadened to a diameter of twenty to thirty microns. Based on a test using the rhyolite glass standard (USNM 72854) and a large, homogeneous melt inclusion (sample Can 14) it was concluded that the loss of Na due to mobilization under the electron beam becomes negligible using the following conditions: (a) beam diameter greater than 20 microns; (b) accelerating voltage of 15 kV; (c) cup current of eight nanoamperes; and (d) counting-time of <60 seconds per element. In addition, the automated analyses were conducted in such way that the alkali elements (i.e. Na, K) were analyzed first.

In a few cases, the small size (<10 microns) of the melt inclusions required focusing of the electron beam to small beam diameters (<10 microns), that increased the amount of sodium lost during analysis. The following test was performed on a large melt inclusion (70 microns diameter) in order to quantify this problem of Na-loss. The conditions for this test were identical to the normal analytical procedures, except for the reduction of the beam-diameter. Counting-time was set to five seconds on the peak position and repeatedly performed until a cumulative

Table II.

Accuracy and precision of electron microprobe analysis based on average of 12 analyses of the Yellowstone Rhyolite Glass Standard USNM-72854.
Results are listed in weight percent ± one standard deviation.

	Glass standard USNM-72854	Average of 12 analyses	
		mean	±std.dev.
SiO_2	76.71	76.61	±0.29
TiO_2	0.12	0.08	±0.03
Al_2O_3	12.06	11.97	±0.09
FeO	1.23	1.11	±0.06
MnO	0.03	0.02	±0.02
MgO	0.00	0.03	±0.03
CaO	0.50	0.45	±0.02
Na_2O	3.75	3.69	±0.18
K_2O	4.89	4.90	±0.05
Total	99.41	98.87	±0.37

counting-time of 140 seconds was reached. The results are graphically displayed in Figure 6. The loss of sodium is most severe for a beam-size of one micron and is much less pronounced for a beam-size of approximately five to ten microns. Further tests performed at cumulative counting times of more than 15 minutes, reduced current (2-3 nanoampere) and 16 microns beam-diameter by J.W. Delano (1990, personal communication) revealed severe Na-loss even at these seemingly favorable analytical conditions (Figure 7). However, the loss of sodium occurred under these conditions at a slower rate compared to conditions of higher current (i.e. 8 nanoampere) and smaller beam-diameter (5-10 microns) (compare Figures 6 and 7). Similar tests performed by E.P. Vicenzi (1990, personal communication) confirmed the same significant problem of Na-loss in glasses of basaltic composition.

Analysis of quartz melt inclusions with a beam-diameter smaller than ten microns were consequently corrected based on the empirical test. The correction-factor was calculated as the true initial k-ratio of the analyzed quartz melt inclusion divided by the averaged k-ratios measured at 50, 55, 60, 65, and 70 seconds cumulative counting-time. However, only two analyses of quartz melt inclusions had to be corrected upward for Na_2O.

The small size (about 20 microns) of most melt inclusions within zircons required subnominal beam diameters for nearly all analyses, which caused measured Na_2O abundances to be too low. These analyses have been adjusted using a correction factor determined from the rhyolite glass standard using an identical beam diameter.

This correction scheme has been tested and was shown to be both valid and practical when compared to other techniques (Nielsen and Sigurdsson, 1981). This method yields more reliable results (Rutherford et al., 1985) than simply

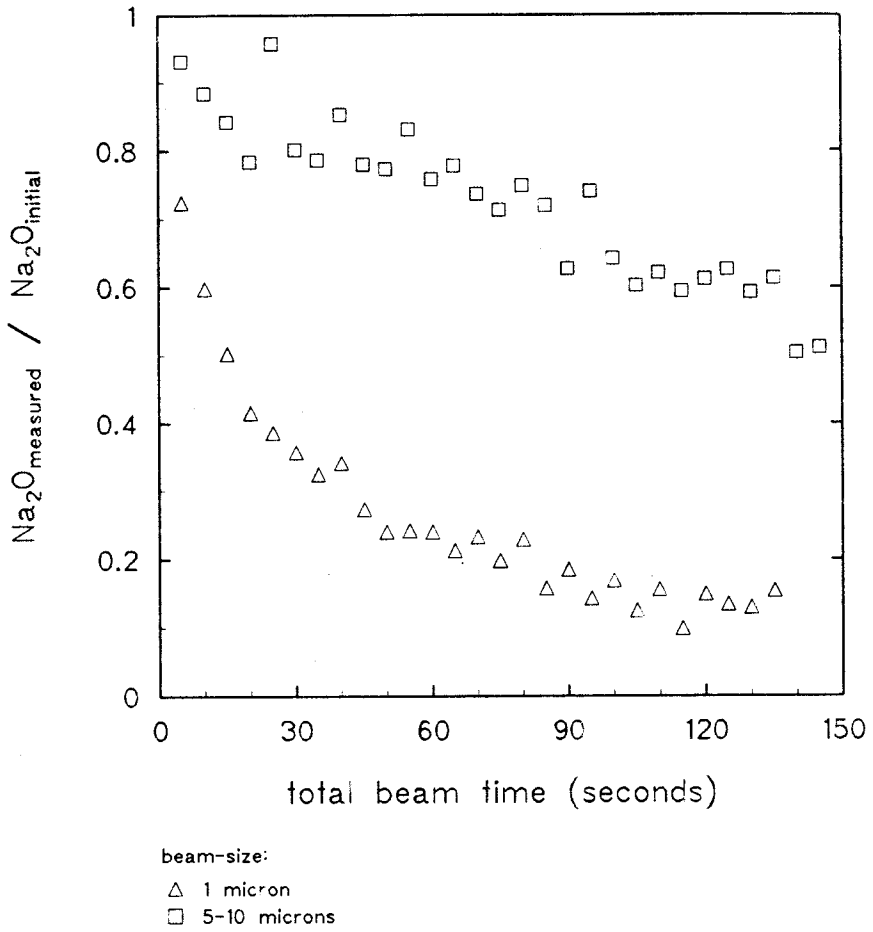

Figure 6: Successive loss of sodium in single melt inclusion during electron microprobe analysis. Plotted are the peak-counts of Na normalized to the initial (i.e. true) value versus the total beam-time for two different beam-diameters. Initial value was determined prior to test under non-mobilizing conditions (30 micron beam-diameter).

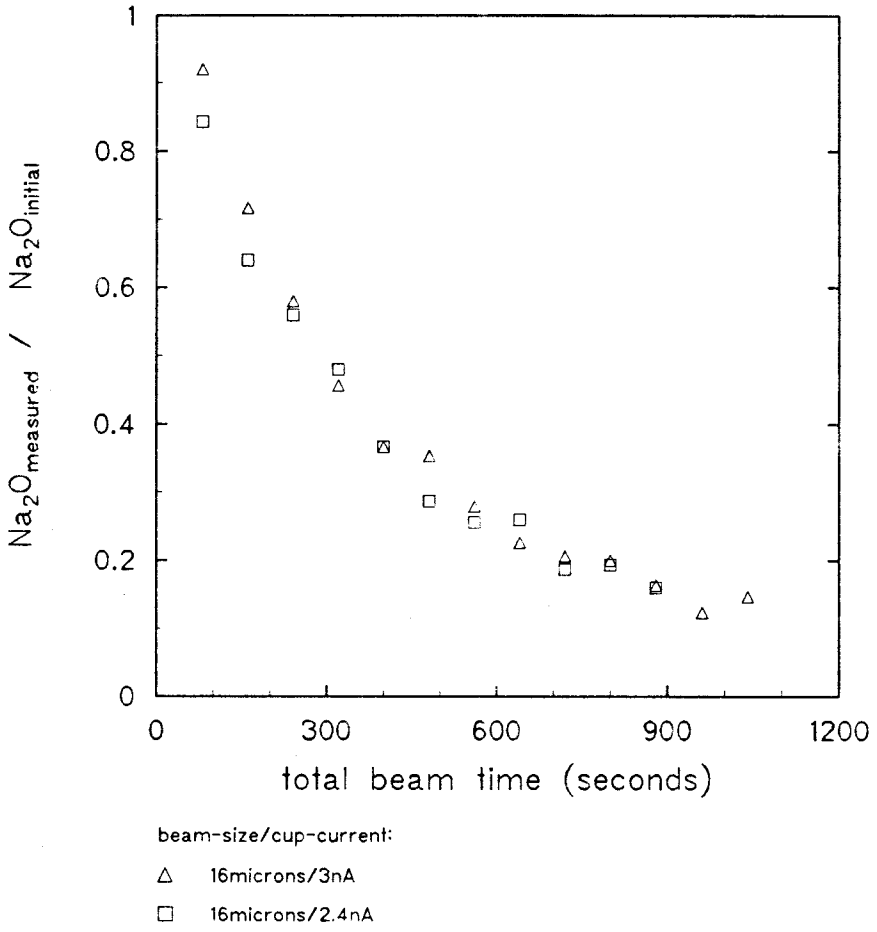

Figure 7: Loss of sodium under favorable analytical conditions (i.e., 16 microns beam-diameter, <3nA current) but total beam-times of more than 15 minutes. Plotted are quantities of Na_2O analyzed in two different melt inclusions normalized to the initial abundance (i.e. extrapolated) versus the total beam-time. (Analyses provided by J.W.Delano).

neglecting the effect of Na-mobilization by either (a) setting it to some constant value (e.g. 4.0 weight percent; Dunbar et al., 1989; Hervig et al., 1989), or (b) moving a small electron beam continuously across the sample (e.g. Melson, 1983).

Because the effect of Na-mobilization at low abundances (less than 1 weight percent) has not been tested to any extent, this correction was applied only to melt inclusions that contained Na_2O abundances comparable to that in the tested inclusion (i.e., about 3 to 4 weight percent).

2.4. Results

2.4.1. Homogeneous melt inclusions in quartz phenocrysts

Inclusions in quartz from six different samples were analyzed for their major-element compositions by electron microprobe. These samples are from the K-bentonites 89-050, Can 13, Can 14, Can 27, Flat 14 and the Tioga-F ash bed. Additional melt inclusion analyses from the Millbrig K-bentonite were provided by J.W. Delano.

The average compositions of melt inclusions from each sample and their standard deviations are shown in Table III. (see Appendix A for complete set of analyses). All of the vitreous melt inclusions analyzed in this study are highly silicic in composition (i.e. rhyolitic) and yield typical low oxide totals (i.e. 90 to 95 weight percent). The total alkali content (K_2O+Na_2O) is relatively uniform at 7 - 8 weight percent and the K_2O/Na_2O ratio, although somewhat variable, is greater than 1. CaO and FeO^* (total iron expressed as FeO) generally have abundances of less than one weight percent each, whereas TiO_2, MnO and MgO occur only in trace-quantities. Among the seven samples studied, Can 13 has the most distinctive melt inclusions. They are silicic (i.e. rhyolitic) but their total

Table III.

Average compositions from electron probe microanalysis and C.I.P.W. norms for homogeneous melt inclusions in quartz. All results are listed in weight percent. "Volatiles" were determined by difference-of-sum-method (see text for discussion).

	Can 13 n=3		Can 14 n=6		Flat 14 n=6	
	mean	±std.dev.	mean	±std.dev.	mean	±std.dev.
SiO_2	72.84	±1.42	72.73	±1.45	70.39	±2.39
TiO_2	0.22	±0.09	0.06	±0.04	0.04	±0.05
Al_2O_3	11.25	±0.14	11.57	±0.14	11.34	±0.29
FeO	0.93	±0.21	0.70	±0.27	0.80	±0.10
MnO	0.10	±0.04	0.06	±0.04	0.07	±0.03
MgO	0.20	±0.04	0.04	±0.03	0.02	±0.01
CaO	1.65	±0.06	0.74	±0.18	0.62	±0.09
Na_2O	3.08	±0.43	2.96	±0.26	2.97	±0.17
K_2O	1.92	±0.21	4.51	±0.16	4.33	±0.33
Total	92.17	±1.13	93.37	±1.58	90.59	±2.73
"volatiles"	7.83	±1.13	6.63	±1.58	9.41	±2.73
C.I.P.W. norm (volatile-free):						
Q	47.15		38.78		38.40	
or	12.27		28.57		28.27	
ab	28.28		26.78		27.76	
an	8.86		3.92		3.38	
C	1.21		0.51		0.71	
hy	1.27		1.05		0.94	
mt	0.54		0.26		0.47	
il	0.45		0.13		0.09	

Table III. continued

	89-050 n=10		Millbrig n=6		Tioga-F n=8	
	mean	±std.dev.	mean	±std.dev.	mean	±std.dev.
SiO_2	71.88	±1.35	72.04	±0.37	72.43	±0.58
TiO_2	0.08	±0.02	0.36	±0.12	0.10	±0.05
Al_2O_3	11.50	±0.22	12.00	±0.18	12.02	±0.07
FeO	0.81	±0.06	0.90	±0.14	0.79	±0.05
MnO	0.02	±0.02	0.15	±0.05	0.03	±0.01
MgO	0.07	±0.01	0.09	±0.03	0.11	±0.01
CaO	0.81	±0.05	0.95	±0.17	0.65	±0.05
Na_2O	2.36	±0.09	3.00	±0.00	2.77	±0.13
K_2O	5.28	±0.17	4.20	±0.39	4.71	±0.07
Total	92.82	±1.60	93.69	±0.58	93.61	±0.45
"volatiles"	7.18	±1.60	6.31	±0.58	6.39	±0.45

C.I.P.W. norm volatile-free:

Q	38.55	38.55	36.47
or	33.63	26.48	27.81
ab	21.57	27.08	23.43
an	4.32	5.06	3.22
C	0.46	0.83	1.19
hy	0.86	0.78	0.89
mt	0.47	0.52	0.42
il	0.17	0.74	0.20

alkali content is lower (5 weight percent) and the K_2O/Na_2O ratio less than 1. Although the FeO^* content is similar to the other K-bentonites (i.e. 1 weight percent), CaO is a factor of two greater in abundance than the other samples. Furthermore, the concentrations of TiO_2, MnO and MgO are significantly higher than in all other samples.

Compositional homogeneity within individual melt inclusions can be demonstrated by high-resolution backscattered electron images (Figures 8 and 9). The lighter brightness of the melt inclusions relative to their hosting quartz is caused by a higher average atomic weight of all elements present in the glass (e.g. 22 amu) compared to almost pure quartz (e.g. 20 amu). Although the boundary between host and inclusion is always sharp, it appears that the inclusions extend into the quartz host to form a halo of uniform width. Neither epitaxial growth of a crystalline phase nor dissolution of the host quartz is evidently present. What appears for example in Figure 9 like a fissure (i.e. black) between host quartz and inclusion and a halo surrounding this "fissure", seems morphology-related. That is illustrated in Figure 10, which is a secondary electron image of the same inclusion (Figure 9), in such way that it emphasizes surface relief between inclusion (i.e. low) and host quartz (i.e. high). The step morphology at the contact between inclusion and host is a result of the polishing preparation and reflects the different hardness of the two materials (i.e. quartz harder than glass). The relief causes the brightness difference in such way that the convex part of the step appears light and the concave part appears dark, suggesting a deep fissure, which is apparently not present (Figure 10). Note that the same light halo appears on the rim of several dark pits within the quartz host (Figures 9 and 10) as well.

Randomly distributed white speckles (i.e. high atomic weight) in backscattered electron images of melt inclusions from sample Can 13 have been observed (Figure 11). These speckles are present only in Can 13 inclusions and are also visible by

Figure 8: High-resolution backscattered electron image of homogeneous melt inclusion (light) within quartz host (dark) from K-bentonite 89-050. Note the halo (light) extending across "fissure" (black) into quartz host, which is caused by relief between melt inclusion (low) and quartz (high).

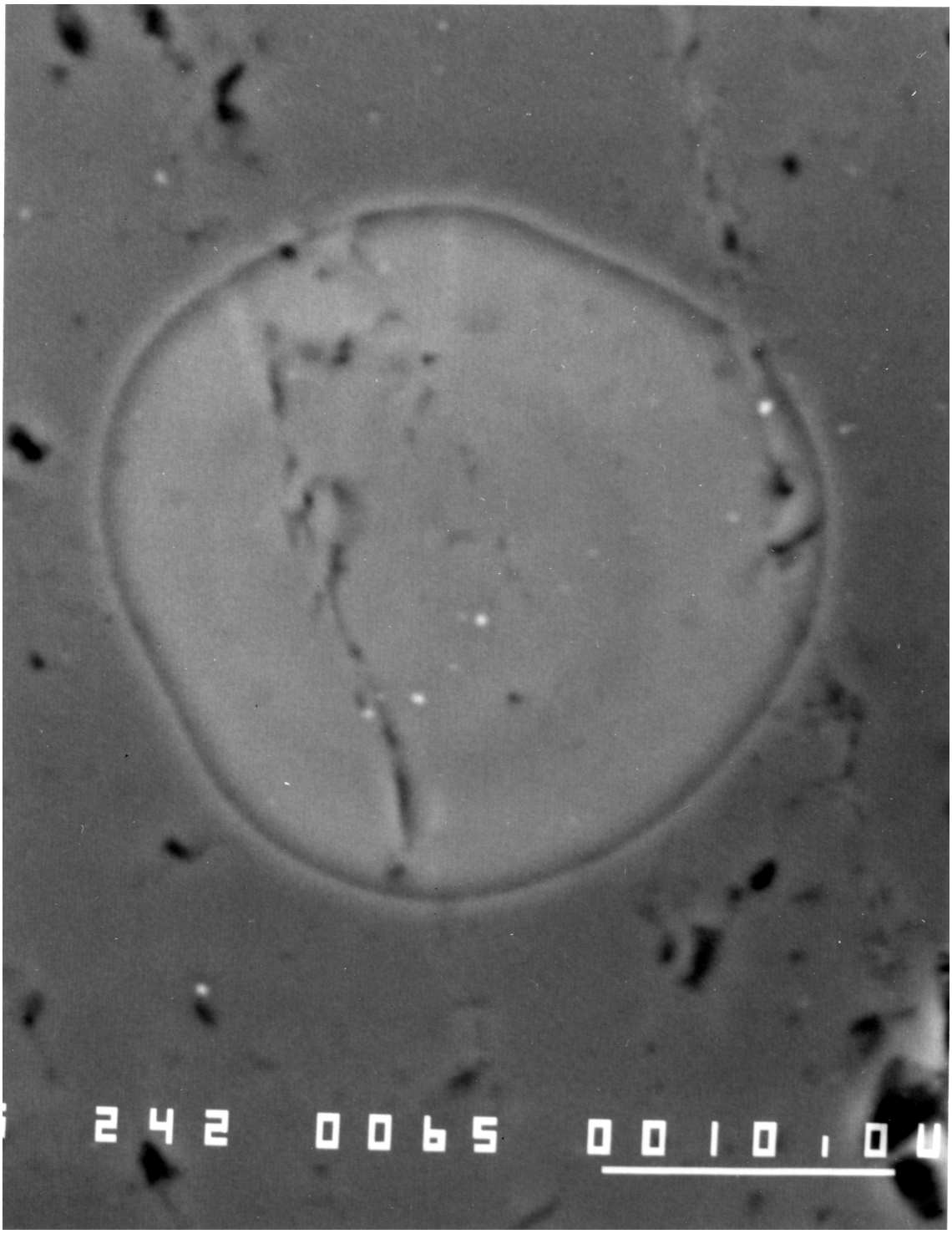
242 0065 0010,00

Figure 9: High-resolution backscattered electron image of homogeneous melt inclusion (light) within quartz host (dark) from K-bentonite Can 14. Note presence of light halo around melt inclusion and around several pits (black).

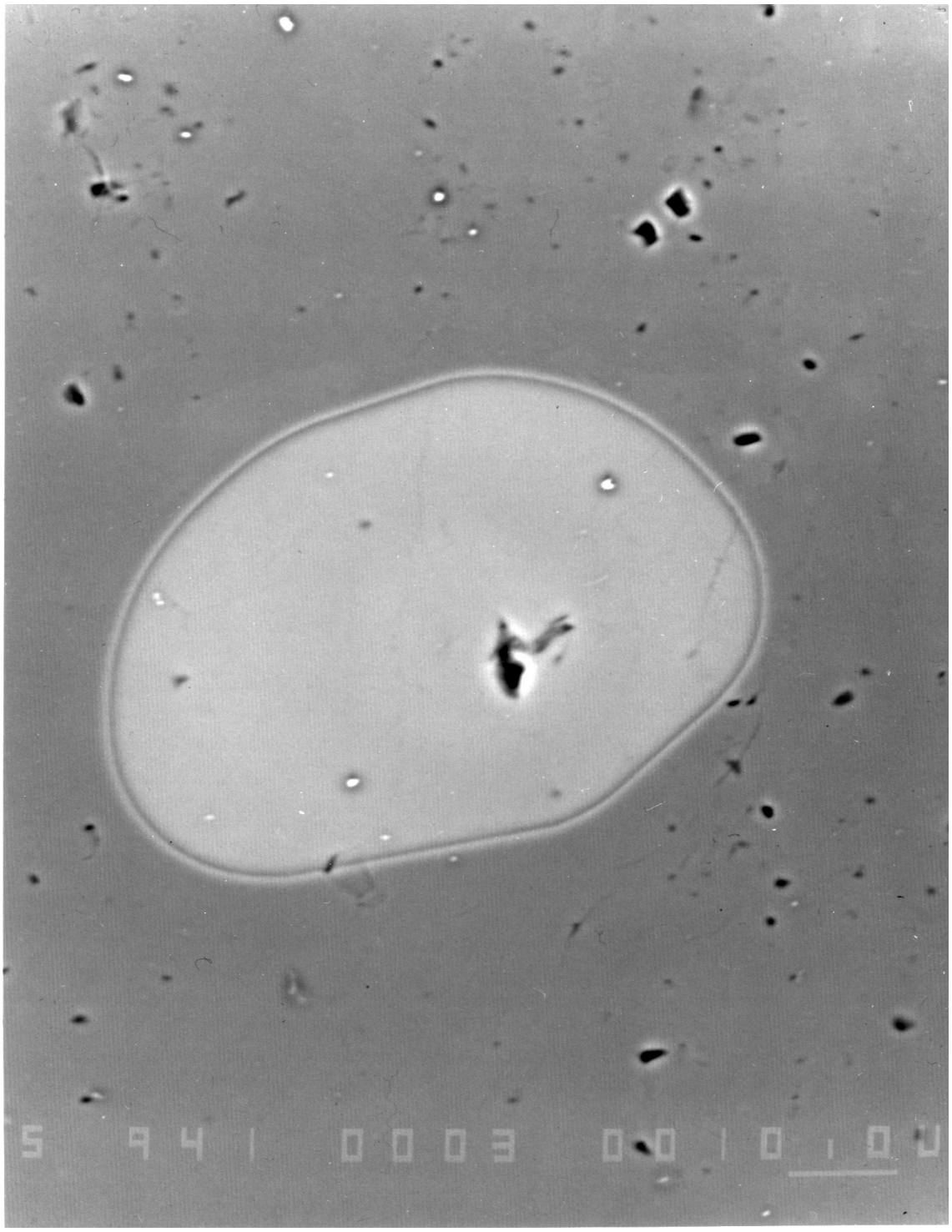
5 94 0003 00 0 0

Figure 10: Secondary electron image of the same melt inclusion that is shown in Figure 9. This picture emphasizes the relief between quartz host (high) and inclusion (low) that resulted from the sample preparation (i.e. polishing).

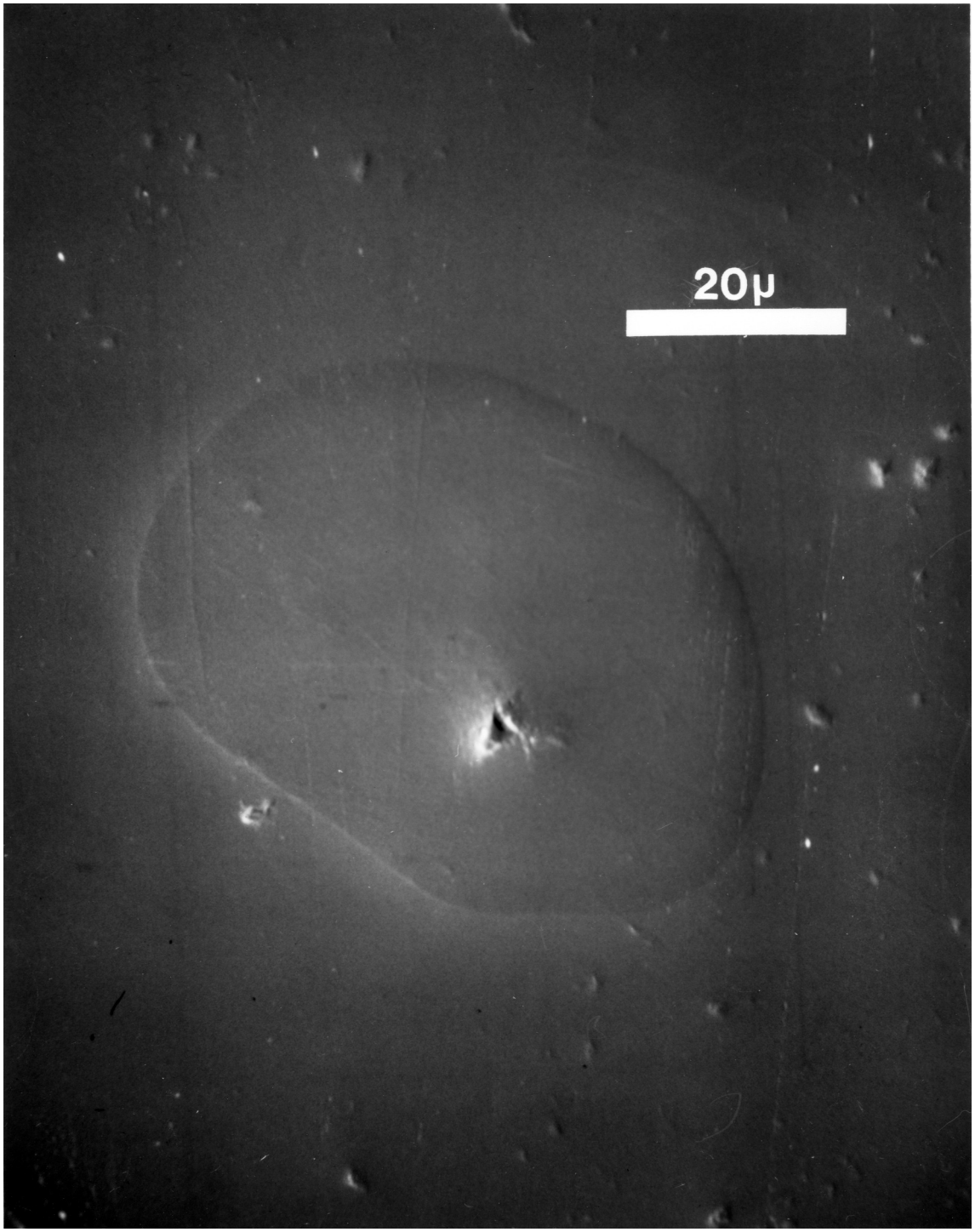
20μ

Figure 11: High-resolution backscattered electron image of melt inclusion from K-bentonite Can 13. White speckles (coarse) probably represent Fe-Ti oxides. They appear opaque in an otherwise clear inclusion when examined in transmitted light (Figure 12).

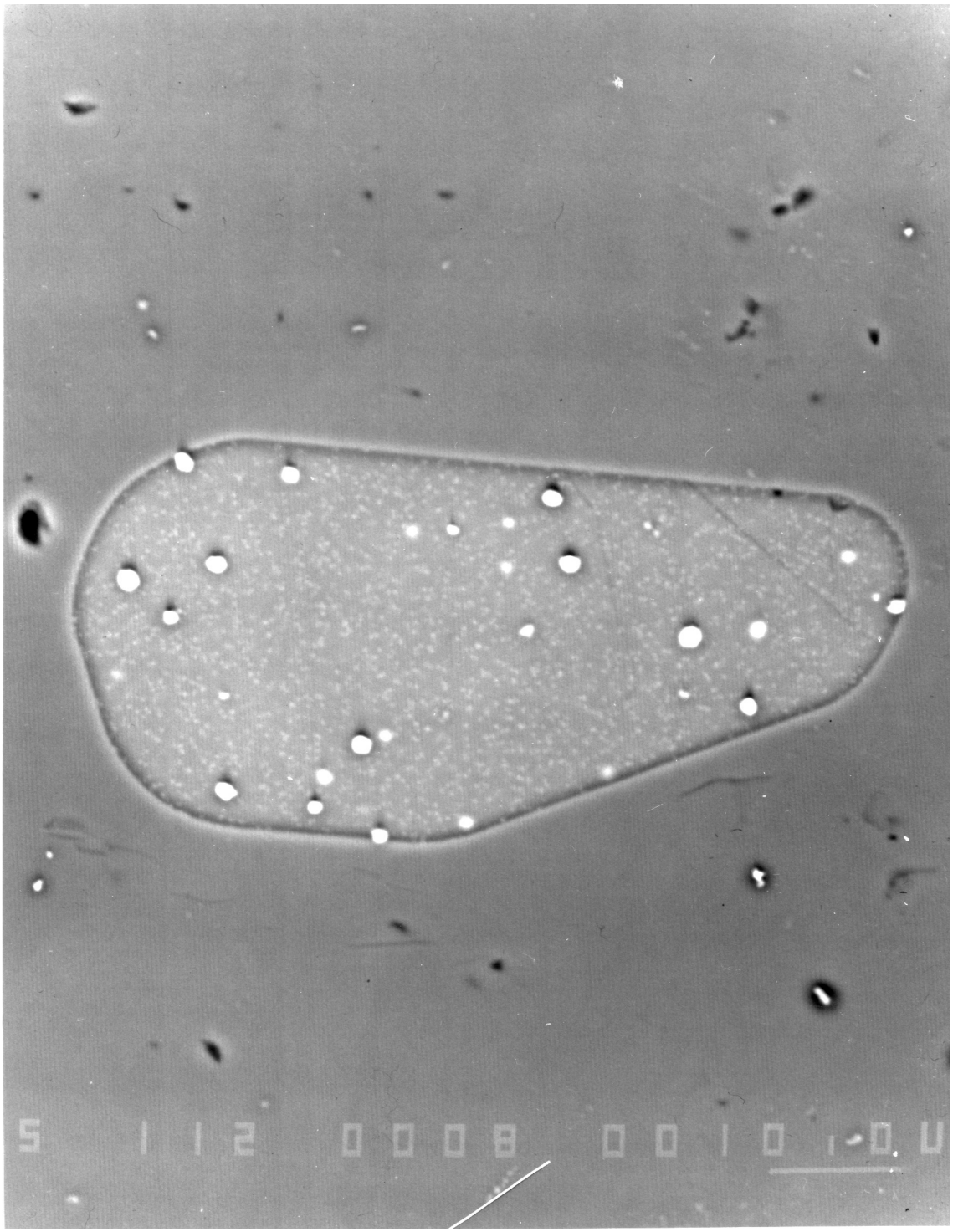

transmitted light microscopy as discrete, opaque grains (Figure 12). Note also that these opaque grains do not occur in the host quartz. It seems possible that these are small FeTi-oxides or Fe-sulfides that crystallized from the melts as discrete grains after entrapment in the quartz.

2.4.2. Heterogeneous melt inclusions in quartz phenocrysts

Some of the clear, non-devitrified melt inclusions in samples Can 14 and Flat 14 are heterogeneous in composition. The compositional heterogeneity is visible as different shades of grey in backscattered electron-images and is apparently not related to the occurrence of small grains within the melt inclusions of sample Can 13.

Increasing brightness in the backscattered electron images (Figure 13, 14, 15) corresponds to regions within these heterogeneous inclusions having concentrations of elements of higher average atomic weight. Each of the melt inclusions shown in Figures 13 - 15 appear to possess three compositionally distinct domains. Their arrangement relative to each other forms a consistent pattern. The largest domain of the melt inclusion is almost indistinguishable from the host quartz in backscattered electrons. The second domain is brighter in backscattered electrons and occurs as one or two separate hemispheres, each immediately adjacent to the wall of the hosting quartz (compare Figures 13 and 15, respectively). The boundary between these first two domains always appears diffuse (see Figures 13 and 15). A third type of domain is bright in backscattered electron image and has the smallest volume. It always occurs at a central position within the second domain, adjacent to the wall of the host quartz and seemingly as distant to the dark grey domain as possible. The shape of this third domain can occur either as an accumulation of

Figure 12: Photomicrograph of euhedral quartz crystal from K-bentonite Can 13 in transmitted light. Quartz grain contains several inclusions. Leftmost inclusion with opaque (black) speckles, which are most likely to represent Fe-Ti oxides, is pictured in Figure 11.

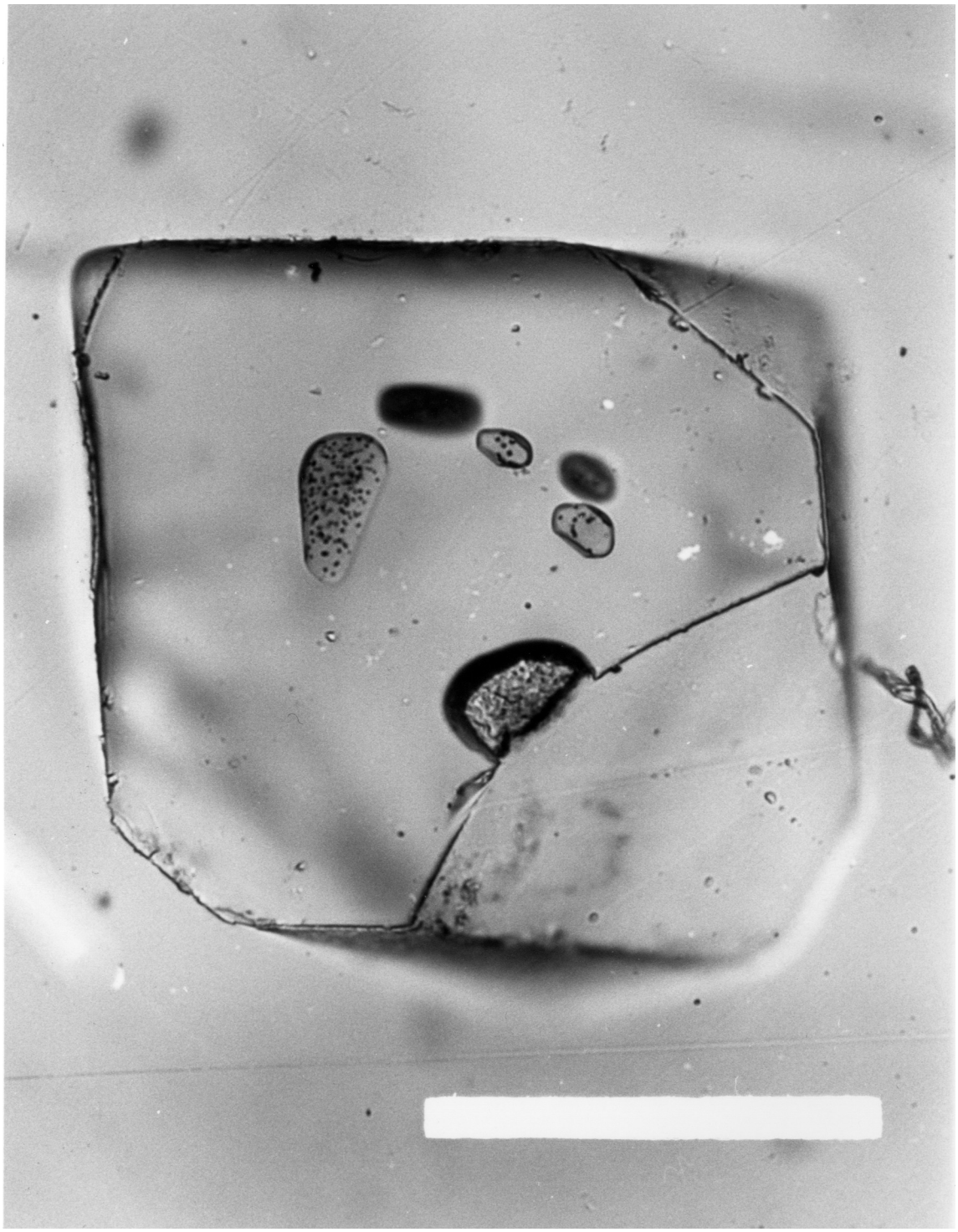

Figure 13: High-resolution backscattered electron image of heterogeneous melt inclusion in quartz from K-bentonite Can 14. Inclusion consists of three domains: dark grey, light grey and white. Note irregular, diffuse to flame-like pattern at boundary between dark and light grey domains compared to sharp boundary with quartz host.

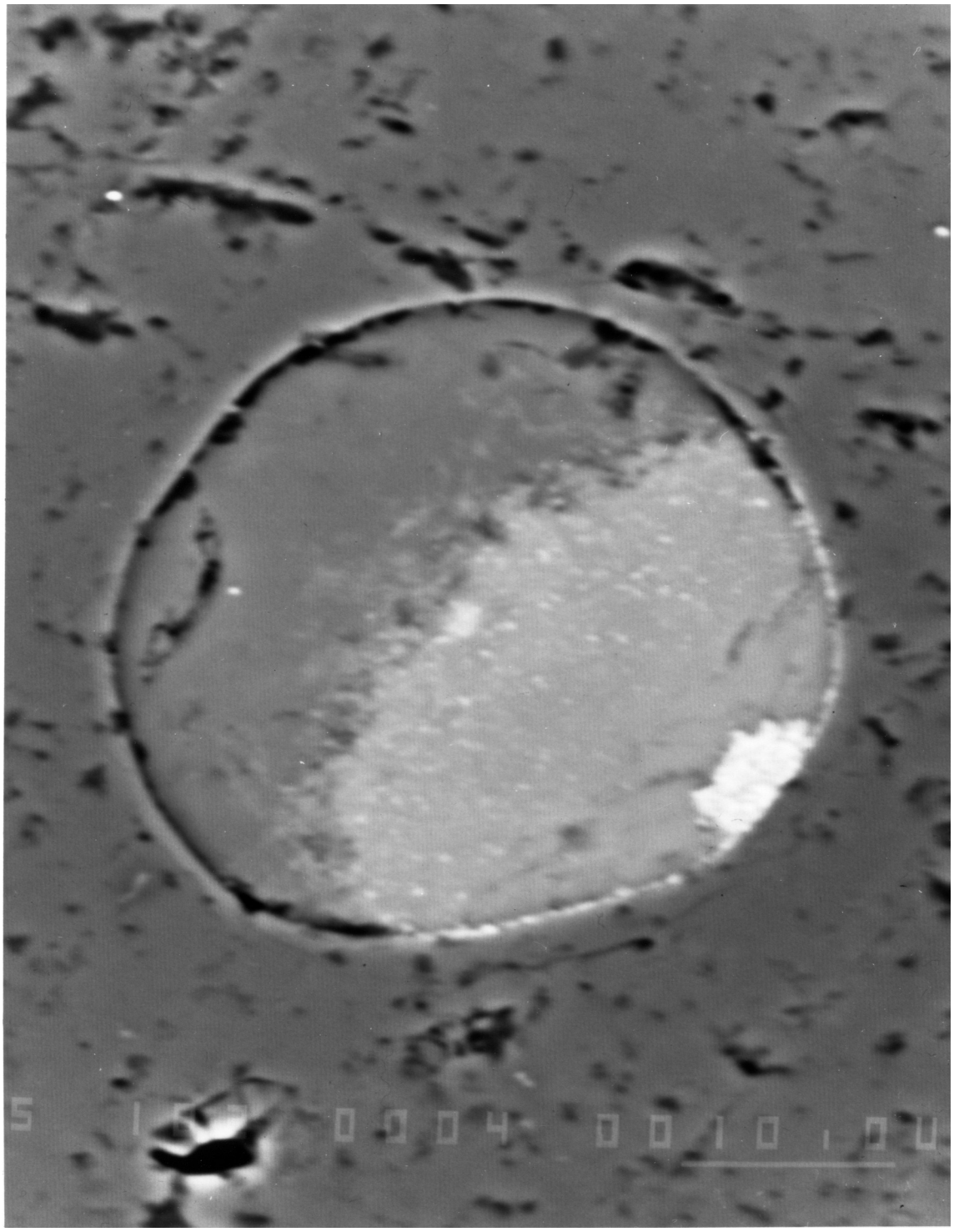

Figure 14: High-resolution backscattered electron image of heterogeneous melt inclusion in quartz from K-bentonite Flat 14. Inclusion (oval) comprises three different domains: dark grey, light grey (2) and white. Note the lath-shaped appearance of white area in contrast to aggregate-shape in Figures 13 and 15.

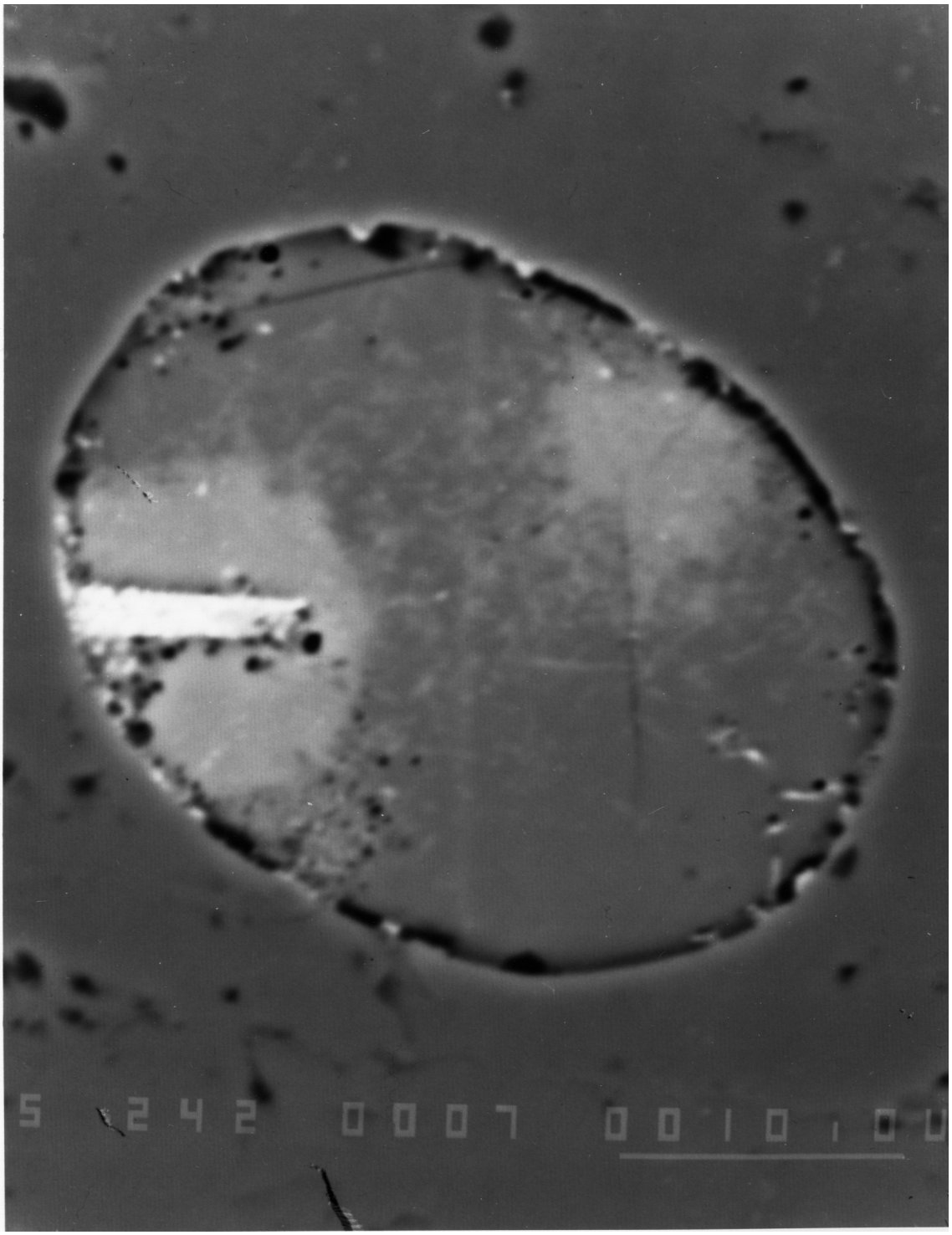
5 242 0007 0010.00

Figure 15: High-resolution backscattered electron image of heterogeneous melt inclusion in quartz from K-bentonite Can 14. Same inclusion is illustrated in Figure 4. Note the presence of two light grey domains besides dark grey, and small volume of white domain. Light circles (2) are traces caused by electron bombardment during microprobe analysis. Scale bar is 10 microns.

"aggregates" (Figure 13 and 15) or as a lath in Figure 14. In all instances, the boundaries of this third domain are sharp. In some cases these different domains may be visible even in transmitted light microscopy. For example, the inclusion shown in Figure 4 (transmitted light photomicrograph) is the same inclusion as in Figure 15 (backscattered electron image).

Average compositions for each of these three domains have been acquired by electron microprobe and are presented in Table IV. Although all domains are highly silicic, the three domains can be chemically distinguished by the relative abundances of Na_2O, K_2O, FeO, MgO and MnO. As inferred from the backscattered electron-images, the first (dark grey) domain is relatively rich in elements of low atomic numbers, particularly Na_2O and K_2O, with an average K_2O/Na_2O ratio less than 1. The second (light grey) domain represents a composition that is K_2O-rich and Na_2O-poor (K_2O/Na_2O ratio greater than 10), but is otherwise similar to the first (dark grey) domain. Enrichment in FeO^*, MgO and MnO by at least a factor of 10 relative to the other compositions causes the third domain to appear white in backscattered electron images. The concentrations of SiO_2 and Al_2O_3 are consistently highest in the first (dark grey) domain, intermediate in the second domain, and lowest in the third (white) domain.

The analytical results from these heterogeneous melt inclusions are plotted in Figures 16 and 17 to illustrate the compositional difference among the three domains. The corners of the ternary plots were chosen to represent combinations of elements that are geochemically correlated among the domains (i.e. Fe+Mg+Mn; K; Na+Ca). The tie-lines in Figures 16 and 17 connect coexisting domains within individual inclusions.

Table IV.

Average compositions from electron probe microanalysis and C.I.P.W. norms for each of the three domaines that occur in heterogeneous melt inclusions in quartz grains from K-bentonites Can 14 and Flat 14. All results are listed in weight percent. "Volatiles" were determined by difference-of-sum-method (see text for discussion).

	dark (n=20)		light (n=13)		white (n=3)	
	mean	±std.dev.	mean	±std.dev.	mean	±std.dev.
SiO_2	71.97	±1.31	70.48	±2.12	66.03	±2.68
TiO_2	0.03	±0.04	0.04	±0.03	0.03	±0.05
Al_2O_3	11.79	±0.20	11.63	±0.41	10.09	±0.56
FeO	0.46	±0.12	0.83	±0.37	13.68	±1.17
MnO	0.07	±0.03	0.05	±0.04	0.53	±0.10
MgO	0.01	±0.01	0.04	±0.02	0.69	±0.27
CaO	0.84	±0.09	0.19	±0.12	0.79	±0.55
Na_2O	3.47	±0.32	0.72	±0.33	0.21	±0.04
K_2O	3.29	±0.37	8.76	±0.89	2.58	±0.32
Total	91.93	±1.41	92.74	±2.37	94.64	±2.12
"volatiles"	8.07	±1.41	7.26	±2.37	5.36	±2.12

C.I.P.W. norm (volatile-free):

Q	40.37	34.38	44.39
or	21.16	55.85	16.07
ab	31.99	6.60	1.86
an	4.51	1.04	4.12
C	1.07	0.65	5.85
hy	0.58	0.96	25.54
mt	0.27	0.48	2.23
il	0.06	0.09	0.08

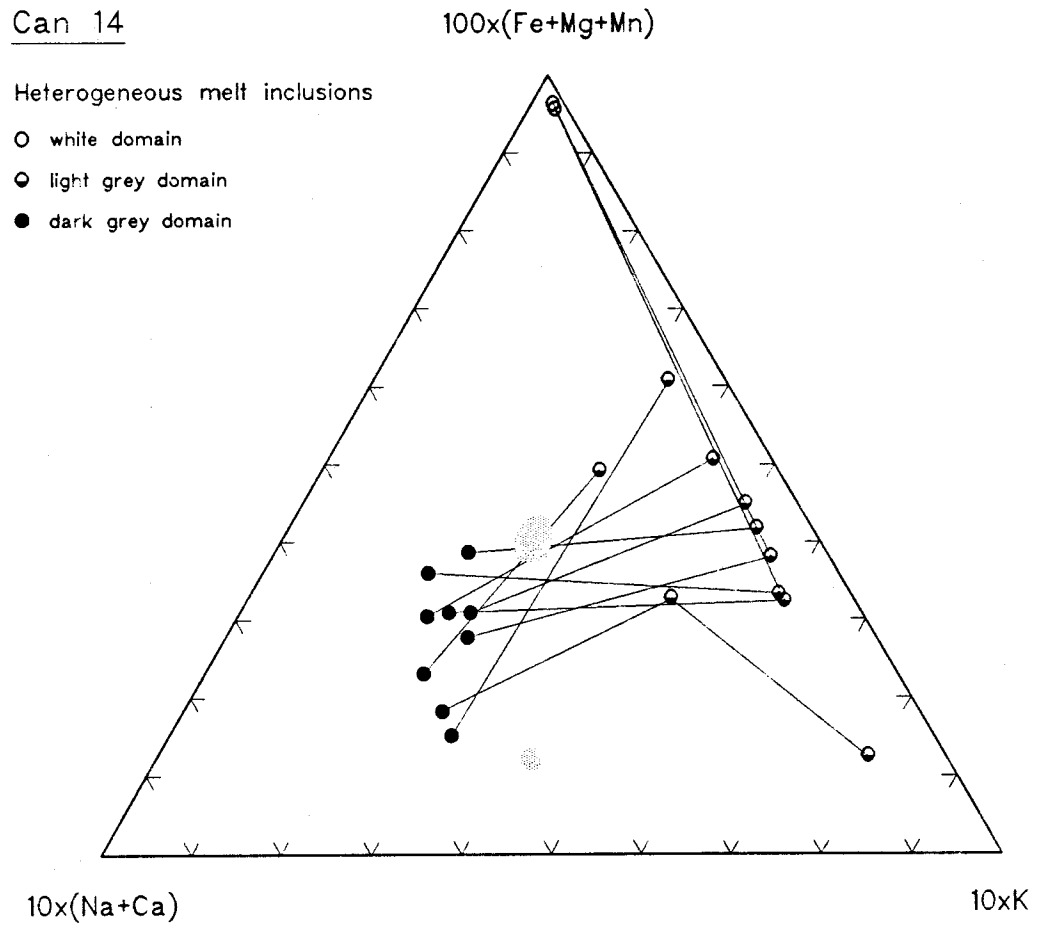

Figure 16: Ternary diagram illustrating the compositional difference of three distinct domains (i.e., white, light grey, and dark grey in backscattered electrons), which were observed in heterogeneous melt inclusions of K-bentonite Can 14. Chemical analyses are plotted according to element combinations (i.e., Fe+Mg+Mn, K, Na+Ca) that are correlated among the domains. Tie-lines connect coexisting domains within individual inclusions. The stippled areas represent analyses of homogeneous melt inclusions from the same K-bentonite.

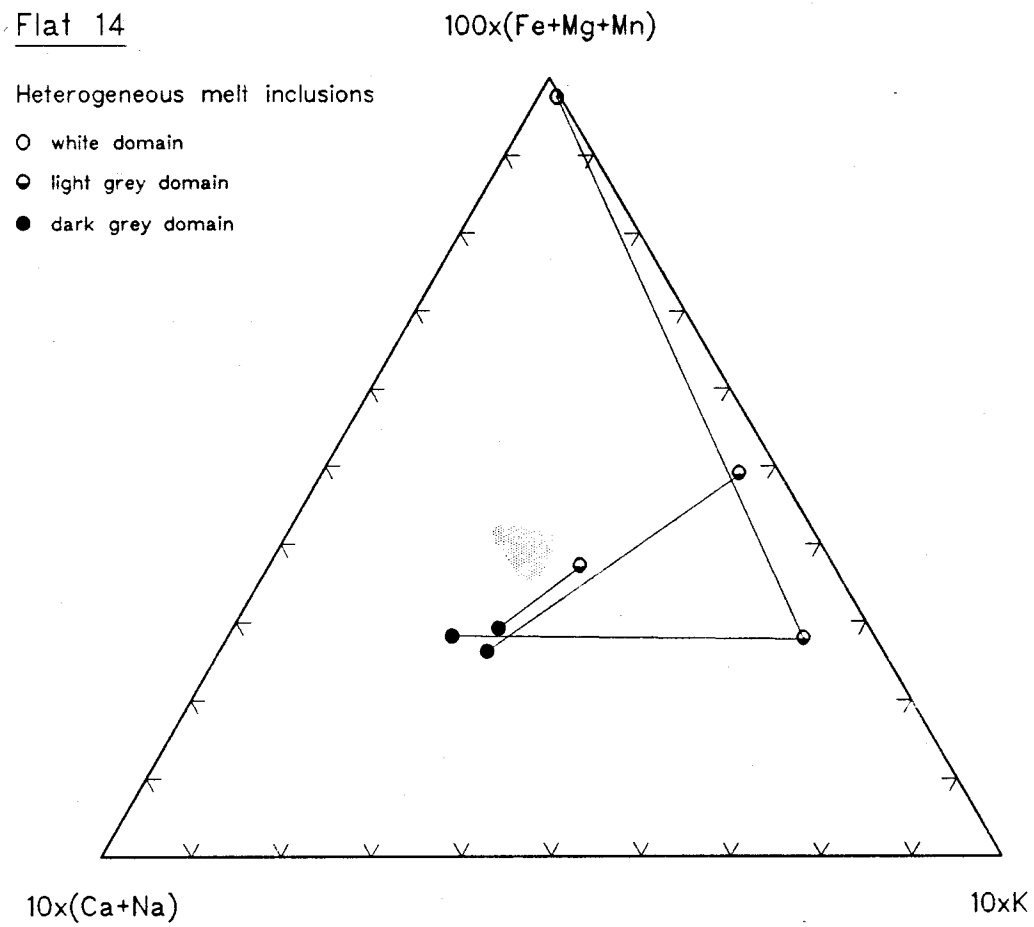

Figure 17: Ternary diagram illustrating the compositional difference of three distinct domains (i.e., white, light grey, and dark grey in backscattered electrons), which were observed in heterogeneous melt inclusions of K-bentonite Flat 14. Chemical analyses are plotted according to element combinations (i.e., Fe+Mg+Mn, K, Na+Ca) that are correlated among the domains. Tie-lines connect coexisting domains within individual inclusions. The stippled areas represent analyses of homogeneous melt inclusions from the same K-bentonite.

2.4.3. Melt inclusions in zircons

The first analyses of melt inclusions in zircons were of a reconnaissance nature and were conducted using analytical procedures suitable for detecting trace abundances of high atomic number elements in "stable" zircons but not for analysis of light elements in glasses (i.e., 20 kV, 20 nAmps, <20 micron beam-diameter). Melt inclusions in several zircons from the Can 14 sample analyzed with this procedure are now characterized by Na_2O-poor compositions due to Na-loss and variable K_2O contents. However, ratios of other elements present in detectable amounts such as iron and calcium, and of course silica and aluminum, should not have been affected. These circumstances limit the reliability of the analyses from zircon melt inclusions to these non-alkaline elements.

Although all of the glassy melt inclusions in zircons from samples Can 14, 89-050 and the Dickeyville are characterized by highly silicic composition, they are not as uniform as the melt inclusions hosted by quartz. In spite of that, a comparison of compositions for samples Can 14 and 89-050 on an anhydrous recalculated basis reveals that zircons consistently trapped melts which were within analytical uncertainties more-or-less equal in composition to those observed in quartz phenocrysts. This uncertainty is largest for the alkali elements sodium and potassium which do not compare very well for the Can 14 samples. The inclusions analyzed in zircons and quartz from the 89-050 sample are identical within analytical uncertainty, including for Na_2O and K_2O. One zircon melt inclusion from 89-050 is higher in FeO^* and TiO_2 caused by an Fe-Ti oxide present in the inclusion.

Figure 18 is a ternary diagram involving the components, quartz, orthoclase and plagioclase. All analyses of homogeneous melt inclusions are plotted in Figure 18 according to their CIPW-norms. This plot illustrates the scatter of data from

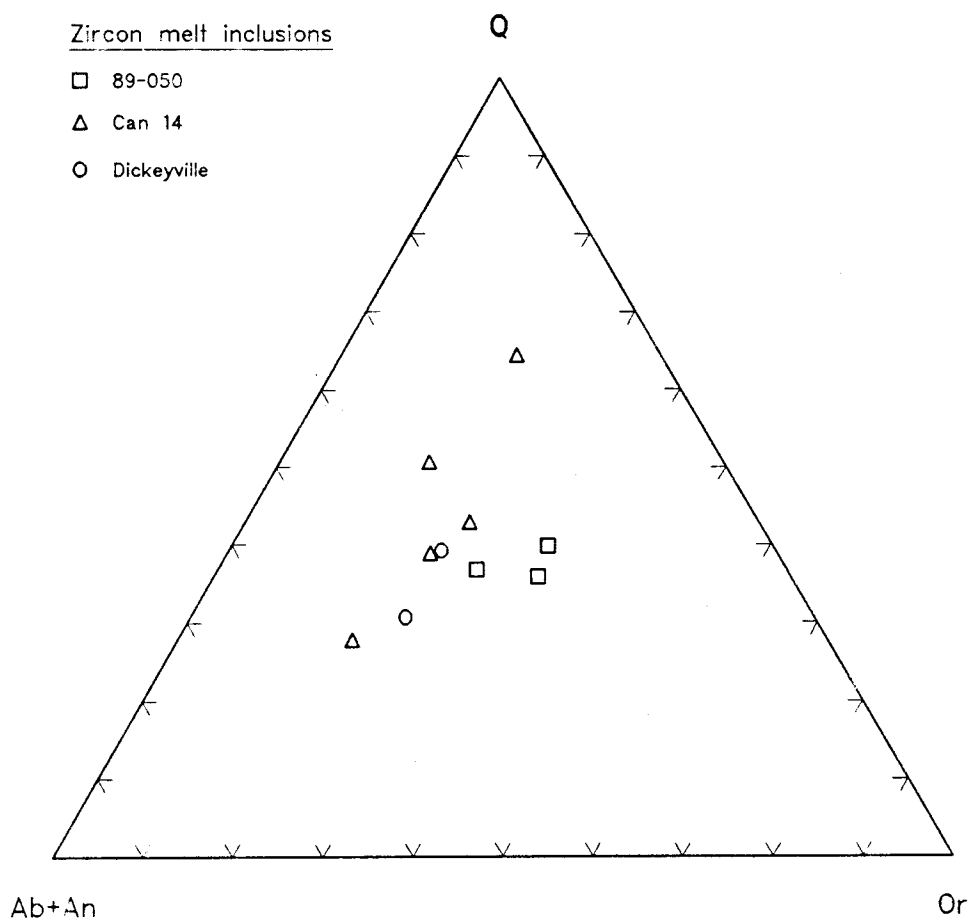

Figure 18: Plot of zircon melt inclusion analyses from three different K-bentonites according to their CIPW-norms involving the components quartz, orthoclase, and plagioclase.

Can 14 zircon melt inclusions, in part due to Na-loss, as well as some potential loss of potassium resulting from the "pre-analysis", in contrast to the compositional homogeneity of quartz melt inclusions (Figure 19). The inclusions in zircons from Can 14 scatter considerably compared to the equivalent quartz melt inclusions (Figure 20), whereas the inclusions in zircons and quartz from 89-050 agree well with each other (Figure 21).

Two melt inclusions in different zircon crystals of the Dickeyville sample represent the largest compositional difference yet observed among inclusions from a single K-bentonite. Since the observed differences are well-outside analytical uncertainties, the data appear to define two different melt compositions. The less evolved composition is clearly poorer in SiO_2 but richer in TiO_2, Al_2O_3, FeO^*, MgO, and CaO, as is expected for fractionation along a liquid line of descent.

2.5. Discussion

2.5.1. Do melt inclusions represent pre-eruptive melt?

Processes that may alter the original composition of a trapped liquid include (a) devitrification, (b) post-entrapment crystallization of the host phase on the inclusion wall, or (c) the boundary layer effect (Anderson, 1974a, 1967, 1976; Roedder, 1984; Watson, 1976). Whereas the latter process is difficult to evaluate, the first two processes may be assessed by optical inspection of the inclusions. If a boundary layer (Evans and Nash, 1979) were in effect and created compositional gradients adjacent to the crystallizing host phase, then this gradient should be preserved in the trapped melt composition (Anderson, 1974a). The largest compositional difference to the bulk melt would be expected to be preserved in the smallest inclusions, which would contain the largest volume of melt that is

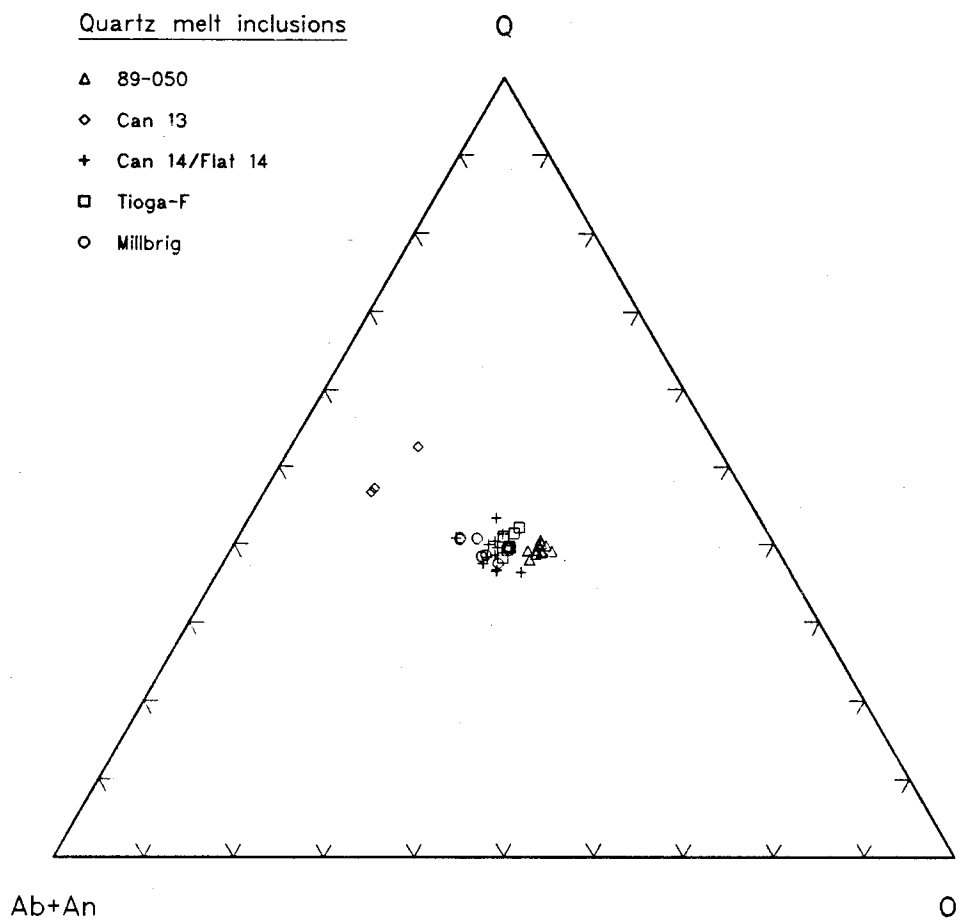

Figure 19: Plot of quartz melt inclusion analyses from five different K-bentonites according to their CIPW-norms involving the components quartz, orthoclase, and plagioclase.

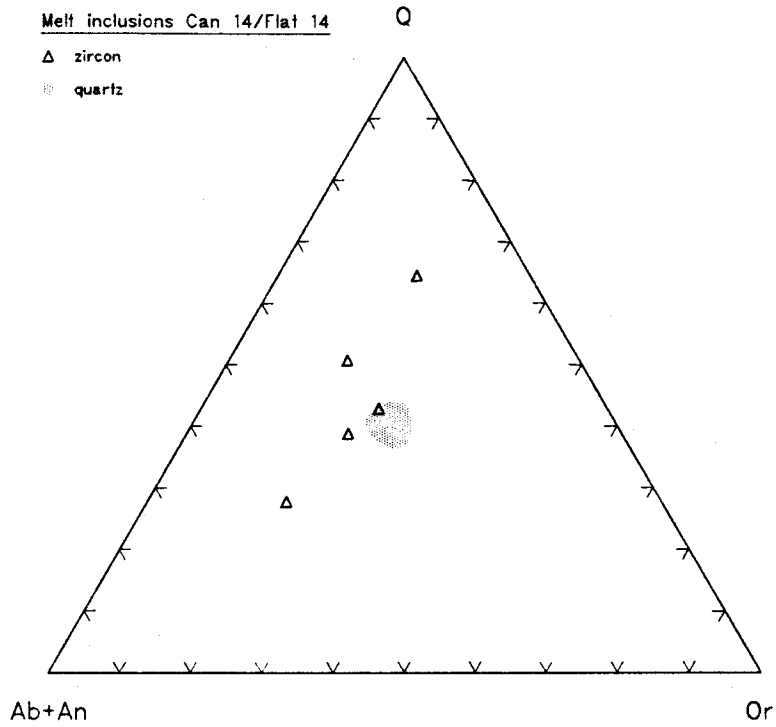

Figures 20 (above) and 21 (below): Geochemical comparison of zircon melt inclusions with quartz inclusions from single K-bentonites (89-050 and Can 14/Flat 14), according to their CIPW-norms involving the components quartz, orthoclase, and plagioclase. Quartz inclusions are outlined as fields whereas zircon inclusions are plotted individually.

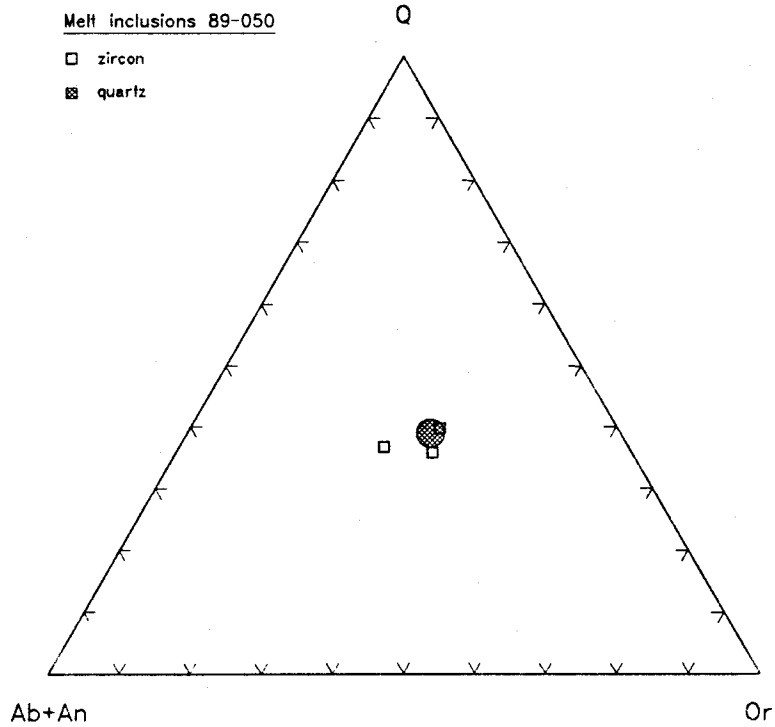

affected by the compositional gradient of the boundary layer (Roedder, 1984). Hence, this effect is noticeable by a size-dependence on the chemical compositions and can be modelled using the control line concept of Watson (1976). Alternatively, this effect can be avoided by not analyzing small inclusions (e.g. <25 microns; Anderson, 1974a).

This phenomen can be identified through a comparison of (a) the volatile-free composition in rhyolitic melt inclusions with (b) the coexisting bulk pumice and/or preserved matrix glass (e.g. Anderson et al., 1989; Beddoe-Stephens et al., 1983; Dunbar et al., 1989; Hervig et al., 1989; Rutherford et al., 1985; Rutherford and Devine, 1988; Sommer and Schramm, 1983). Close compositional agreement between (a) the melt inclusions and (b) matrix glasses and/or pumice could indicate that the melt inclusions have not been altered, and would therefore represent 'bona fide' samples of magma (Anderson et al., 1989; Beddoe-Stephens et al., 1983; Dunbar et al., 1989; Hervig et al., 1989; Rutherford et al., 1985; Rutherford and Devine, 1988; Sommer and Schramm, 1983). Although Melson (1983) and Rutherford et al. (1985, 1988) found that the anhydrous composition of melt inclusions contained within plagioclase was essentially identical to the rhyodacitic matrix glass produced by the May 18, Mount St. Helens eruptions, the pumice was considerably more mafic in composition (i.e. dacitic). This latter result is probably not too surprising since the pumice consists of up to about 40 percent by volume of crystalline phenocrysts that contribute to this more mafic composition of the bulk pumice. However, melt inclusions hosted by hornblendes were found to be slightly less evolved than those contained within plagioclases, in such way that they approximate the liquid line of descent of the May 1980 magma (Rutherford and Devine, 1988). Consequently, although melt inclusions may not be compositionally equivalent to a bulk rock, they generally preserve the composition of the liquid from which they were separated. It seems therefore reasonable to conclude that the

melt inclusions hosted by quartz and zircon phenocrysts from Paleozoic K-bentonites of New York State, Pennsylvania, and Iowa represent the pre-eruptive composition of rhyolitic liquid.

2.5.2. Geochemical classification

The total alkali versus silica (TAS) diagram (after LeBas et al., 1986 and LeMaitre, 1989) allows the chemical classification of the melt inclusions in terms of a volcanic rock type. A plot of all analyses from homogeneous quartz melt inclusions yields an almost uniform rhyolite composition (Figure 22). According to the K_2O versus SiO_2 diagram (LeMaitre, 1989) these rhyolitic compositions further qualify as being high K-types, except for the inclusions from sample Can 13, which qualify as medium-K type rhyolite (Figure 23). Since the K-bentonite Can 13 is directly overlain by Can 14 it seems possible that these altered volcanic ashes represent contemporary volcanic activity within distinct segments of a single arc or different arcs that contrast in tectonic setting and therefore geochemistry of the erupted volcanics.

The melt inclusion compositions for samples Can 14, Flat 14, 89-050 and the Millbrig are furthermore characteristic of I-type magmas (after Chappell and White, 1974) because (a) their molar $Al_2O_3/(Na_2O+K_2O+CaO)$ ratios are smaller than 1.1; (b) they are relatively high in sodium ($Na_2O>3$ weight percent; except 89-050); and (c) contain less than 1 percent normative corundum. The Tioga-F and Can 13 samples, however, show more affinity to S-types (i.e. molar $Al_2O_3/(Na_2O+K_2O+CaO) = 1.11$).

Although most of the zircon melt inclusion data for sample Can 14 should be regarded with caution due to K- and Na-mobility during analysis (e.g. note the wide range in Figure 20), the data from samples 89-050 and Dickeyville are reliable.

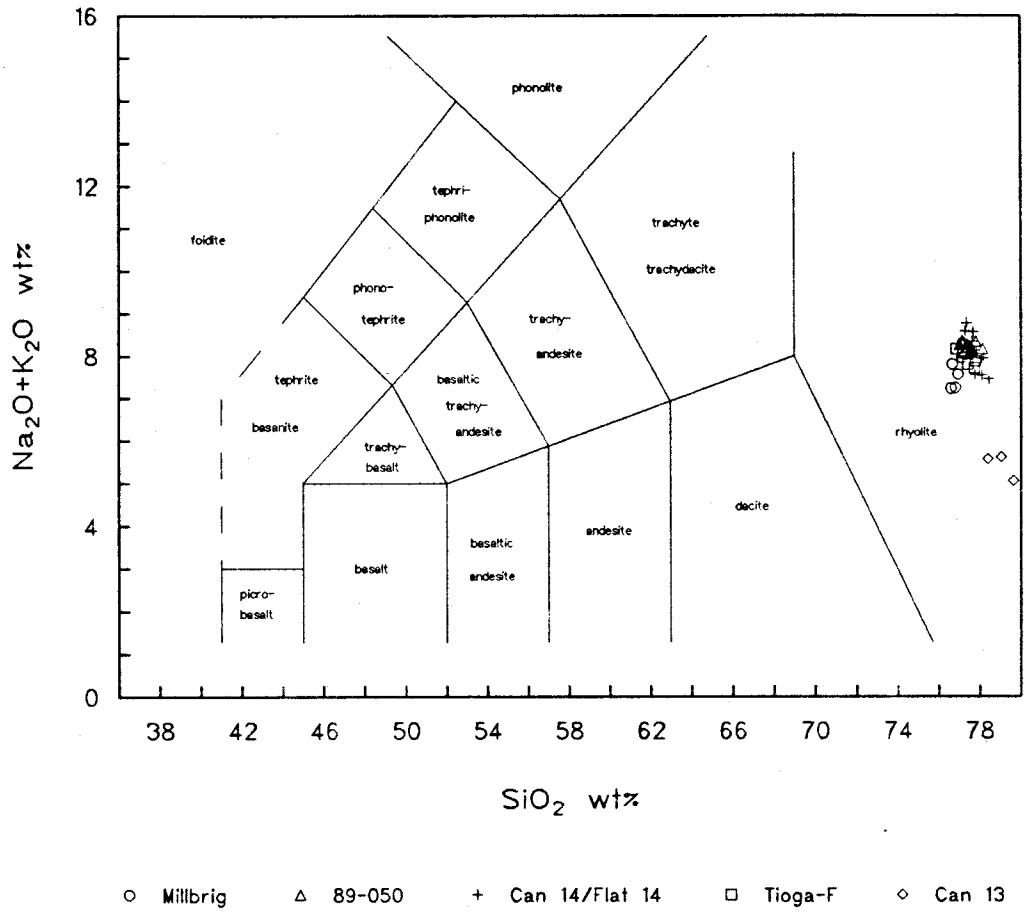

Figure 22: Geochemical classification of quartz melt inclusions from various K-bentonites. Analyses of inclusions (recalculated anhydrous to 100 weight percent) are plotted in the total alkali versus silica (TAS) diagram for volcanic rocks (after Le Maitre, 1989).

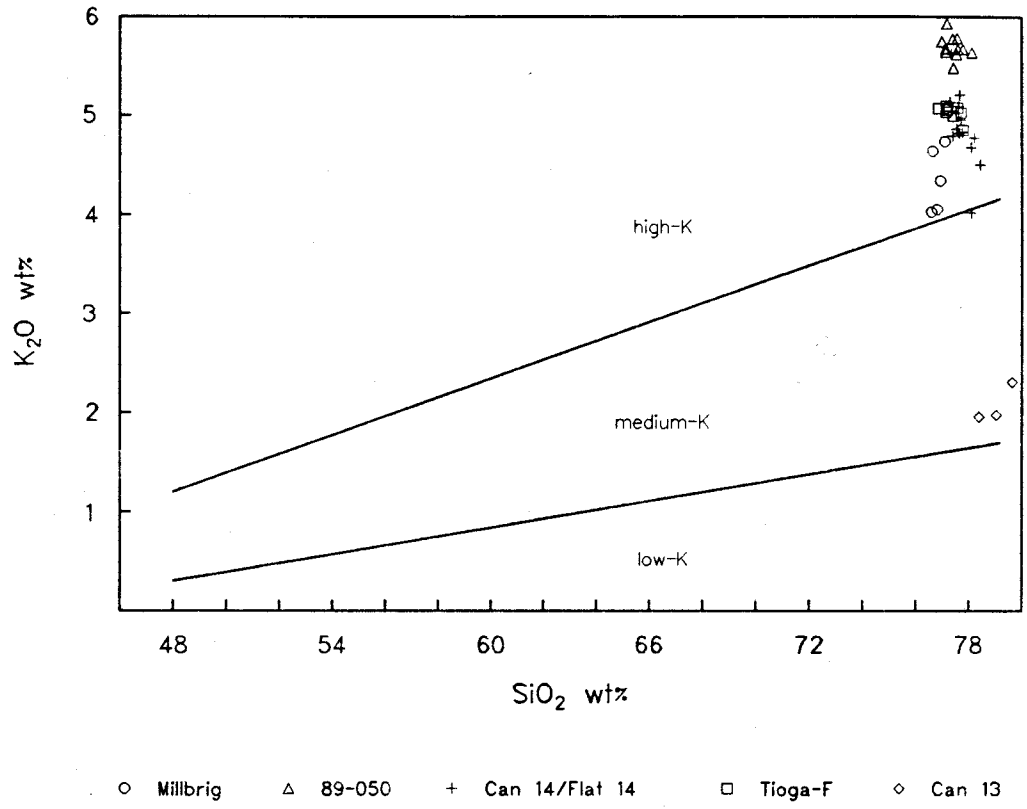

Figure 23: Geochemical division of quartz melt inclusions into high- and medium-K type according to a plot of their K_2O- versus silica-contents (recalculated anhydrous to 100 weight percent).

Despite this range, however, the zircon melt inclusions also represent rhyolitic compositions. This conclusion is reinforced by a ternary plot of the elements silicon, aluminum, and calcium in which melt inclusions from zircons and quartz compare closely (Figure 24). The Si/Al-ratios are identical and most variation is observed due to variable calcium-contents, with zircon melt inclusions tending to be richer in calcium. For comparison with the data shown in Figures 22 and 23, melt inclusions hosted by zircons are plotted in Figure 25 and 26. Note that they qualify as rhyolitic in composition although the scatter is so much greater compared to quartz melt inclusions.

Based on only two analyses it is impossible to determine whether the compositional variation recorded in the melt inclusions from the Dickeyville sample reflects either (a) fractional crystallization of a single magma or (b) compositionally distinct melts from two-or-more closely spaced eruptions. Clearly, more analyses of melt inclusions including some from other phenocryst phases, are needed. Nevertheless, this occurrence is worth mentioning because a similar observation has been made by J.W. Delano (1990, unpublished data) on melt inclusions contained within quartz phenocrysts from the Millbrig K-bentonite of Wisconsin. In addition to this compositional range of melt inclusions, the Millbrig and Dickeyville K-bentonites are characterized by the absence of a xenocrystic component (Kolata et al., 1986; Samson, 1986) that contrasts with younger (late Ordovician) K-bentonites of New York State, which contain (a) abundant xenocrysts (Delano et al., 1990) and (b) compositionally uniform melt inclusions.

The persistent rhyolitic compositions observed among all homogeneous melt inclusions conflicts with the trachyandesitic to rhyodacitic compositions (Delano et al., 1990; Huff and Türkmenoglu, 1981) inferred from allegedly diagnostic ratios of immobile trace elements (i.e. Nb, Y, Ti, Zr) for the K-bentonites (Winchester

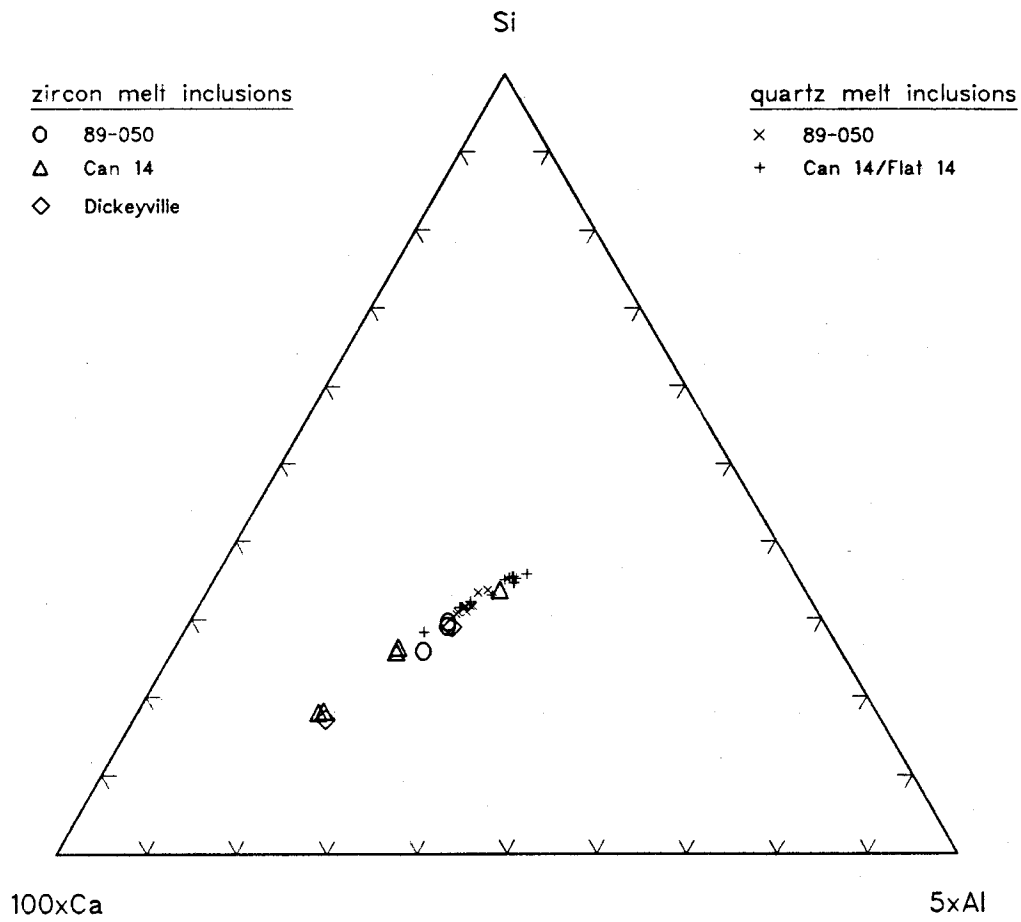

Figure 24: Geochemical comparison of zircon melt inclusions with quartz inclusions in a ternary diagram involving the atomic proportions of silica, aluminum and calcium.

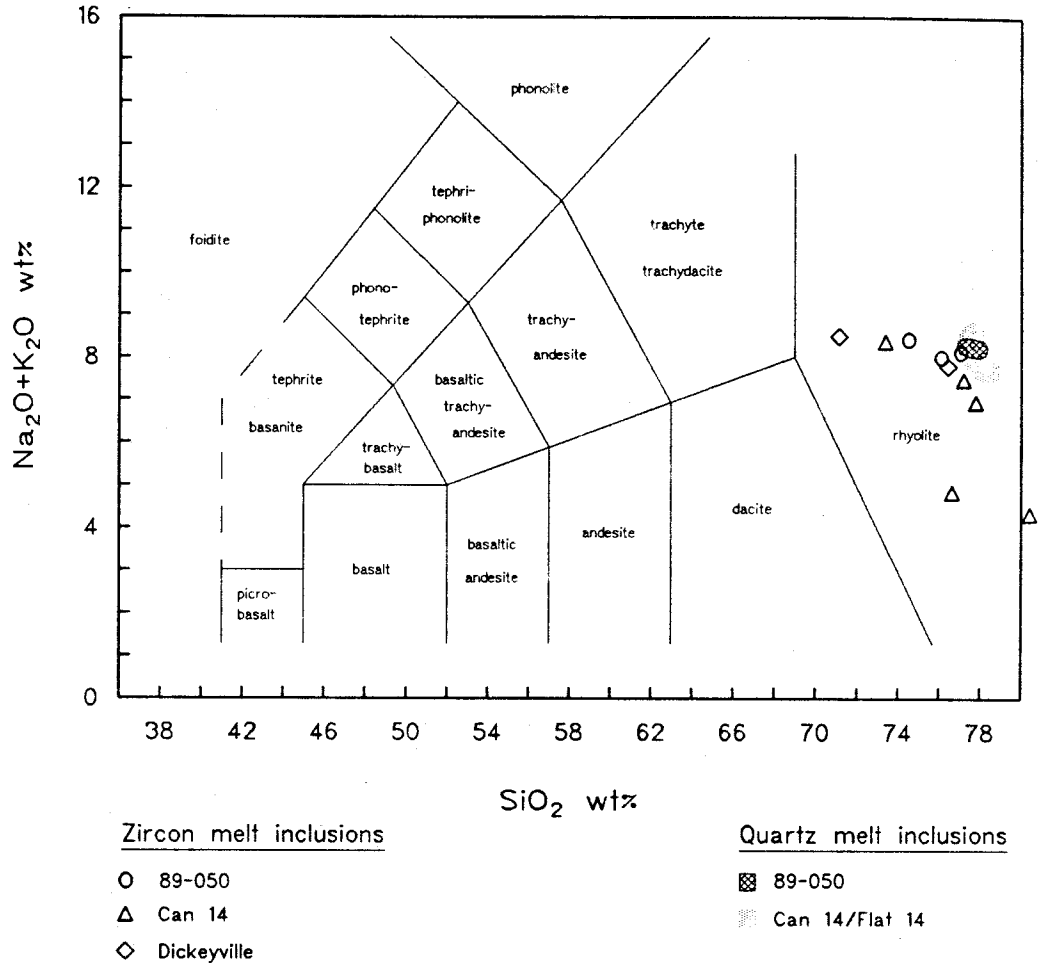

Figure 25: Geochemical classification of zircon melt inclusions from three K-bentonites according to the TAS diagram (after Le Maitre, 1989). Quartz melt inclusions are plotted as fields for comparison.

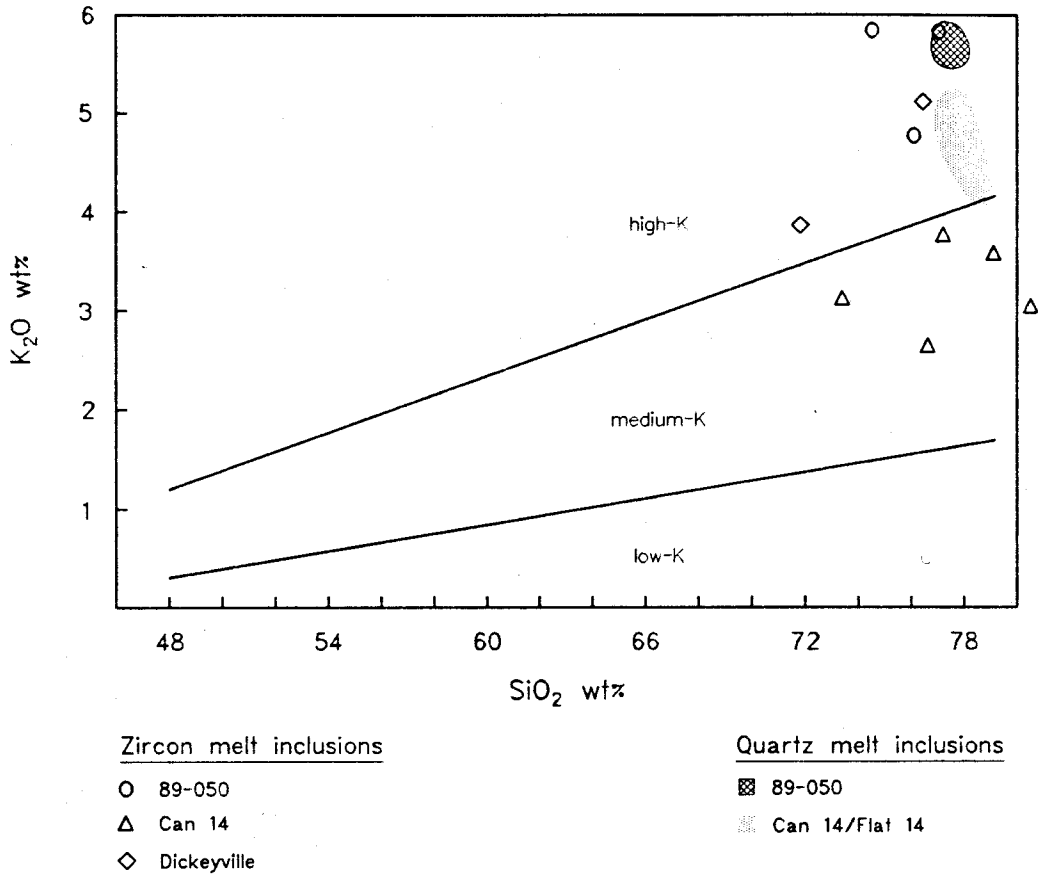

Figure 26: Geochemical division of zircon melt inclusions from three K-bentonites in high- and medium K-type rhyolites according to the plot of their K_2O- versus silica contents. Outlined are the fields defined by quartz melt inclusions for comparison.

and Floyd, 1977). Several possibilities exist to account for the discrepancy. For example, if one-or-more of these elements had been mobile during diagenesis of the K-bentonites (Delano et al., 1990; Zielinski, 1982) misleading relationships would have resulted. Alternatively, the melt inclusions might represent an evolved melt composition derived by fractionation from a more mafic parental magma. However, the absence of any difference between the immobile trace element ratios among the different size fractions of the K-bentonites (Delano et al., 1990) suggests that bulk eruptive rock and melt were essentially identical and only subsequently altered by extensive diagenesis. A difference would be expected for the case where the altered glass, which is presumably represented now by the finest sample fraction (<45 microns), was highly evolved in its composition but contrasts with the bulk rock composition when the coarse sample fraction (>45 microns), representing phenocrysts ± xenocrysts, is included (e.g. Rutherford et al., 1985).

The phenocryst assemblages, especially the host phases of melt inclusions, provide further evidence in support of a rhyolitic bulk composition of these volcanic eruptives. Quartz is an abundant phenocryst phase in the K-bentonites and is also common host of melt inclusions. Other phases (i.e., zircon; apatite) have been positively identified as phenocrysts in most of the K-bentonites. Although plagioclase and K-feldspar are often present, they have been identified, at least in some samples (e.g., Flat 14), as xenocrystic in origin (Delano et al., 1990) and do not contain melt inclusions. Ferromagnesian phases are commonly present in many of the Late Ordovician K-bentonites (e.g. garnet, clinopyroxene, orthopyroxene, hornblende and Fe-Ti oxides), but most of them are interpreted as xenocrystic in origin (Delano et al., 1990), and thus cannot account for any melt fractionation. Plagioclase (An 29%-38%), alkali feldspar (Or 38%-91%), and biotite occur as inclusions in quartz phenocrysts. This phenocryst assemblage supports the view of a highly evolved, rhyolitic, bulk volcanic rock.

When a compilation of rhyolites and granites from published chemical analyses are plotted in the discriminant diagram devised by Winchester and Floyd (1977), the rhyolite field expands into the trachyandesite field towards lower Zr/TiO_2 ratios. However, the K-bentonite values for this ratio are still lower than the proposed field extension (Figure 27). This suggests that original volcanic ash composition of K-bentonites determined with diagnostic trace elements should be regarded with caution. The acquisition of trace element data for melt inclusions could be achieved using an ion microprobe and would certainly help to evaluate this discrepancy and its ultimate causes.

2.5.3. Volatile contents of the melt inclusions

Volatiles are recognized as an important magmatic constituent composed mostly of H_2O and minor amounts of CO_2 and other volatiles (Burnham, 1979; Clemens, 1984; Holloway, 1976; Holloway and Jacobsson, 1986; Newman et al., 1988). Since they influence the geochemical and petrologic evolution of a magma, data on the nature of magmatic volatiles place constraints on the history of a magmatic system.

Although it is not clear to what extent the pre-eruptive volatile content of a magma determines the eruption style of a magma (Fisher and Schmincke, 1984), several apparent correlations have been observed. There is the general tendency that melt inclusions contained within ash fall deposits of highly explosive, plinian eruptions contain high (i.e. several weight percent) concentrations of volatiles, mostly water. The volatile content of melt inclusions that occur within ashflow deposits and ignimbrites is observed to be lower (Anderson et al., 1989; Newman et al., 1988; Self et al., 1983; Sommer and Schramm, 1983). Anderson et al. (1989) and Sommer and Schramm (1983) analyzed the Bishop and Bandelier Tuffs,

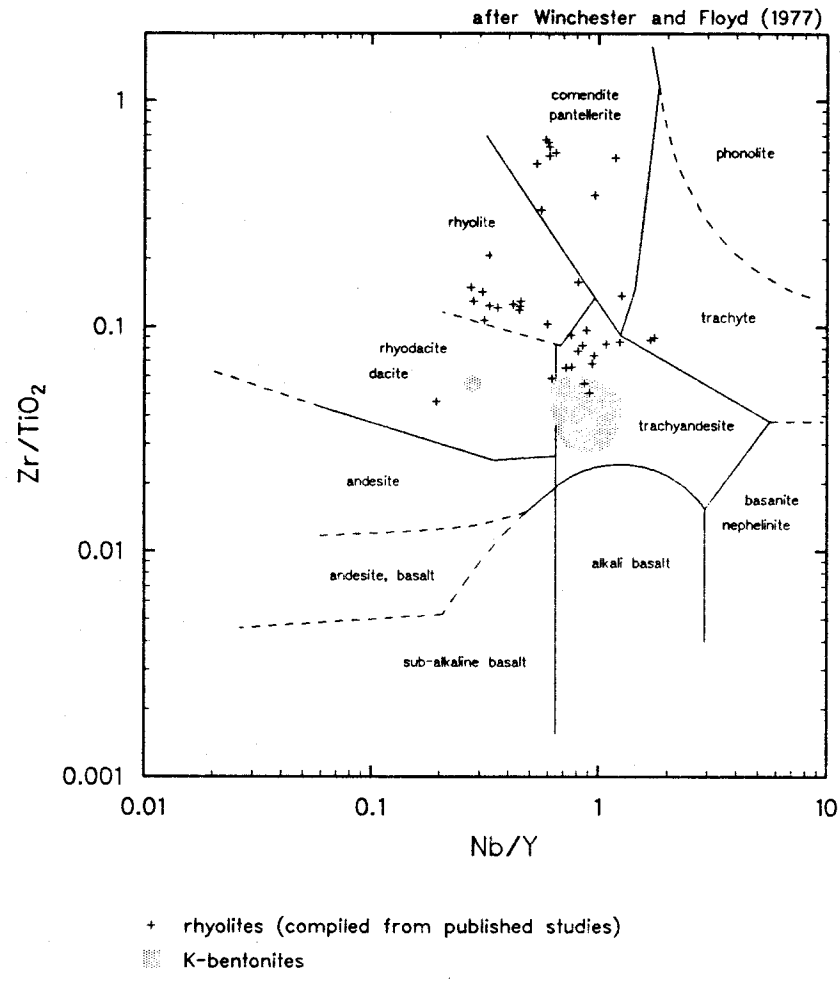

Figure 27: Analyses of rhyolites from various localities were compiled and plotted in this diagram after Winchester and Floyd (1977), which is based on ratios of diagnostic elements that are considered relatively immobile. The data suggest that the rhyolite field devised by Winchester and Floyd (1977) should be expanded towards lower Zr/TiO_2 ratios. The field defined by K-bentonite analyses is shown for comparison.

respectively, and found evidence for volatile zonation in the magma chambers (i.e., enriched in H_2O upwards, along with a decrease in CO_2 content).

Several methods have been devised for the direct measurement of the volatiles (e.g. H_2O and CO_2) in melt inclusions (Stolper, 1982; Hervig et al., 1989; Dunbar et al., 1989; Newman et al., 1986; Harris, 1981; Yonover et al., 1989). An indirect, widely used approach is the difference-of-sum method for electron microprobe analyses (e.g. Anderson, 1973, 1974b; Beddoe-Stephens et al., 1983; Carron, 1961; Chaigneau et al., 1980; Melson, 1983; Rutherford et al., 1985, 1988; Sommer, 1977). This method is based on the assumption that the difference of the sum of all major-element weight percentages from one hundred percent corresponds to the volatile content, which can not be analyzed directly with the electron microprobe. Although the uncertainties of this method are large (e.g., $\pm$1.4 weight percent; Anderson, 1974b), they are comparable with those associated with some direct measuring methods. For example, the analytical uncertainty for measurements of H_2O with the ion microprobe can be larger than $\pm$1 weight percent (Dunbar et al., 1989; Hervig et al., 1989) and therefore yields quantitative results no better than those obtained from electron microprobe analyses. In order to obtain a first approximation of a melt's volatile content, it seems reasonable to apply the difference-of-sum method. Care must however be exercised during microprobe analysis to avoid the mobilization of Na that would yield artificially low totals, and hence excessive estimates for the volatile abundance.

The pre-eruptive volatile contents for the melt inclusions of the present study range between 6 and 9 weight percent based on the difference-of-sum method. Average values are listed in Table III. for all samples. Only one sample (Flat 14) yields a higher average value of 9.4 weight percent "volatiles" due to the presence of two melt inclusions with very low totals around 87 weight percent.

Under the assumptions that (a) water is the only volatile constituent and (b) the temperature of melt entrapment was 850°C, the inferred saturation pressures would be about 2000 bars for 6 weight percent and about 3000 bars for 9 weight percent dissolved water (after Silver et al. 1990). With regard to the large uncertainties involved in the estimates of the water content in the melt inclusions, such as temperature and CO_2 content which are both unknowns, it is unjustified at present to estimate the pressures any more closely. Instead, the pressures of 2 - 3 kilobars represent minimum values because (a) the state of saturation (or undersaturation respectively) is not known, and (b) increasing CO_2-concentrations dissolved in the melt increase the saturation pressure of H_2O (Anderson et al., 1989; Newman et al., 1988). That implies that the melts represented by the melt inclusions in these Ordovician K-bentonites had resided at depths of at least 6 to 9 kilometers during crystallization of quartz and zircon phenocrysts prior to explosive eruption.

2.5.4. Source and origin of the volcanic ashes

From the preceding discussion, it is concluded that the K-bentonites are products of explosive rhyolitic volcanism. In the following section, constraints on the source and origin of the volcanics are discussed.

Isotopic (Samson et al., 1989) and petrologic (Delano et al., 1990) constraints have been acquired on the nature of the presumed volcanic arc that generated the K-bentonites. These data require that the volcanic arc was constructed on Proterozoic continental crust. Not only was this continental crust involved in the anatexis that produced these silicic magmas (Samson, et al., 1989), but also it constituted the country rock at shallow levels through which the

volcanic vent passed (Delano et al., 1990). A broadly similar scenario, in which silicic magmas produced at a convergent tectonic margin pass through a thick sequence of Precambrian continental crust, presently occurs in the Central Volcanic Zone (CVZ) of the South American Andes (Thorpe et al., 1982). Although the compositions of the CVZ volcanic rocks range from basalt to rhyolite, andesites and dacites are dominant (Harmon et al., 1984). The limited range of volcanic compositions among the Paleozoic K-bentonites (i.e., high-K rhyolites), however, is not surprising because highly explosive, plinian style volcanic eruptions are most often associated with rhyolites (Fisher and Schmincke, 1984). It is likely that mafic volcanics associated with the eruption of the rhyolitic ashes (i.e. K-bentonites) were erupted less violently and are not represented among distant airfall deposits (i.e. K-bentonites).

The geochemical similarity of the K-bentonites (i.e. high-K type rhyolites) with volcanics erupted in continental volcanic arcs (e.g. volcanics of the CVZ) supports the isotopic and petrologic constraints (Delano et al., 1990; Samson et al., 1989) which indicate that the volcanic arc was built on Proterozoic continental crust (Delano et al., 1990; Samson et al., 1989).

2.5.5. Correlation of K-bentonites based on melt inclusions

Although the rhyolitic melt inclusions from all of the K-bentonite samples analyzed in this study are chemically similar (Figures 19, 21) they are not identical. Small, but analytically significant, differences in composition exist among suites of inclusions from different K-bentonite samples. For example, sample 89-050 contains homogeneous melt inclusions that are demonstrably richer in K_2O and poorer in Na_2O than melt inclusions from other K-bentonites. On the other hand,

samples Can 14 and Flat 14, which have been independently correlated using stratigraphic relationships, contain melt inclusions with striking similarities. Both samples have provided a unique assemblage of quartz phenocrysts containing homogeneous, as well as heterogeneous, melt inclusions. The chemical compositions of both types of inclusions are without exception identical (Figures 16, 17), and thereby reinforce the inference made from field-stratigraphic evidence that Can 14 and Flat 14 are from a single K-bentonite bed.

The compositional difference between homogeneous melt inclusions of samples 89-050 and Can 14 and Flat 14 is illustrated in Figures 19 and 26. The K-bentonite bed of sample 89-050 corresponds to the M37 bed of Cisne et al. (1982) in the West Canada Creek south of Middleville, NY, and was correlated with a group of four bentonites in Canajoharie Creek and Flat Creek about 40 km further east. The apparent split from one bed (89-050) into four beds (Can 14,15,16,17) occurs between sections 15 and 20 in the cross-section of Cisne et al. (1982). The lowermost of these four K-bentonites in Canajoharie Creek and Flat Creek is identical with Can 14 and Flat 14 (this study). The correlation of Cisne et al. (1982) implies that sample 89-050 is identical, at least in part, with samples Can 14 and Flat 14. However, the evidence from melt inclusions presented above contradicts this view. Can 14 and Flat 14 are (a) identical and correlative and (b) are unquestionably distinct from sample 89-050. If this new interpretation is correct, then sample 89-050, the M37 bed west of section 15 (Cisne et al. 1982), can be assigned to the K-bentonite bed of sample Can 27 in Canajoharie Creek and Flat 26 in Flat Creek (this study; see also Figure 3 for stratigraphy). In addition, this new correlation is supported by (a) the unusual thickness (about 7 cm) and outcrop appearance and (b) the similar morphology of zircon populations (see also Chapter 4). Unfortunately, since no melt inclusions have yet been found in sample Can 27 this proposal has not been confirmed.

Although only three melt inclusions have been analyzed from K-bentonite bed 13 in Canajoharie Creek (Can 13), they are compositionally distinct from those in the adjacent overlying K-bentonite (Can 14), as well as from all other melt inclusions (Figure 19). The compositional similarity between homogeneous inclusions from samples Can 14, Flat 14 and Tioga-F is striking but not unsurmountable. A small but analytically significant difference exists in the higher MgO abundance throughout the Tioga-F melt inclusions compared to Can 14 and Flat 14. The low abundance of MgO emphasizes the need for high precision analysis at enhanced conditions (e.g. lower detection limit), especially for elements occurring in minor-to-trace amounts (e.g. Ti, Mg, Mn). These elements may often provide the critical distinction between volcanic ash layers. The large number of K-bentonites (e.g. about 30 in Canajoharie Creek), however, may require analysis of additional trace elements (e.g., Rb, Sr, Ba, Zr, Th, REE), in order to discriminate these altered ashes by their original glass composition (i.e. melt inclusions) (e.g. Sarna-Wojcicki et al., 1984).

The limited number of reliable analyses from melt inclusions within zircons is indicative of the fact that these inclusions require stringent analytical procedures to avoid element-mobilization. Despite this, the results obtained so far do not preclude their applicability for correlation of K-bentonite beds based on compositional differences among melt inclusions. However, the combination of greater abundance and relative ease of preparation and analysis makes quartz melt inclusions superior to zircon melt inclusions as a correlation tool.

2.6. Conclusions

1. Non-devitrified silicate melt inclusions have been identified in quartz and zircon phenocrysts contained within Late Ordovician and Middle Devonian K-bentonites.

2. The chemical composition of these melt inclusions constrains the origin of the K-bentonites to be in highly explosive eruptions of high-K type rhyolitic magmas.

3. The geochemistry of the melt inclusions supports isotopic and petrological data suggesting that the volcanic arc was built on mature and old continental crust.

4. The pre-eruptive volatile content of the melts inferred by the difference-of-sum method generally varies between 6 to 9 weight percent. In order to dissolve these large amounts of water, a pressure of at least 2000 to 3000 bars would be required. Therefore, the magma resided at minimum depths of 6 to 9 kilometers during crystallization of the melt inclusion hosts.

5. Since quartz melt inclusions are compositionally uniform within a single K-bentonite but distinct in composition between K-bentonites, they can be used as an important new correlation tool for Paleozoic samples.

Chapter 3 "Geochemistry of ash-to-K-bentonite alteration"

3.1. Introduction

The current model of K-bentonite formation is that a bentonite, which is dominated by clay minerals of the smectite group, forms from silicic volcanic ashes by alteration under subaqueous conditions (Altaner et al., 1984; Hein and Scholl, 1978). The vitric shards in the ash become fragmented under the burial load of overlying sediments and alter to clay, predominantly smectite (Hein and Scholl, 1978). The conversion of bentonites into K-bentonites progresses with increasing burial metamorphism as potassium-poor clay minerals (smectites) in the bentonite change successively to potassium-rich mixed-layer smectite/illite (Hower et al., 1976). This model requires, however, that potassium is provided from breakdown of potassium-bearing phases (e.g. K-feldspar, muscovite) in the surrounding sediment, and that time and temperature are appropriate (Hower et al., 1976).

The compositional difference between clay minerals (i.e. smectites, illites, chlorites) and unaltered volcanic ashes (i.e. rhyolites) implies that significant geochemical changes occur due to the diagenetic alteration and mineralization (Henderson et al., 1971; Kiersch and Keller, 1955; Ross, 1928). The magnitude and pattern of these changes is of interest as it is a contribution to the understanding of diagenetic processes. Furthermore, there is a need to identify elements that are resistant to diagenetic alteration (e.g. immobile: Ti, Nb, Zr, Y, Th) and that perhaps can be used as reliable indicators of the original composition of altered volcanic rocks (e.g. Winchester and Floyd, 1977).

In order to determine the amount and pattern of chemical changes, it is necessary to compare the composition of the final product (i.e. bentonite or K-bentonite) with its original unaltered parent (i.e. volcanic ash). In ideal

occasions altered and unaltered ash are juxtaposed in a single outcrop (e.g. Zielinski, 1982) or lateral correlation of altered ashes with fresh volcanics is possible (Zielinski, 1985). However, the occurence of unaltered volcanic ashes of Paleozoic age is not to be expected because glass is thermodynamically unstable (Fisher and Schmincke, 1984) and can not survive hydrous conditions without devitrification and decomposition. This apparent shortcoming is now overcome with the analysis of melt inclusions (i.e. glass) that geochemically represent the unaltered volcanic ash (Chapter 2).

The direction and magnitude of geochemical changes that led to the present compositions of some K-bentonites of Late Ordovician to Middle Devonian age have been investigated. The effect of ash alteration on the geochemistry of the adjacent shales was also investigated for the particular case of a K-bentonite from the Utica Formation (K-bentonite Can 27).

3.2. Sample description and analytical techniques

The discussion is based on chemical analyses of (a) melt inclusions and bulk samples from K-bentonites, (b) shales, and (c) turbidites. Melt inclusions were analysed by electron microprobe for their major-element composition (SiO_2, TiO_2, Al_2O_3, FeO, MnO, MnO, CaO, Na_2O, K_2O) (see Chapter 2 for details). The bulk chemical compositions of K-bentonites, shales, and turbidites were determined by X-ray fluorescence at the geochemical laboratory located at McGill University. The results of these analyses are from Delano et al. (1990) and Delano et al. (in preparation). The bulk sample of the Tioga-F ash bed was analyzed by Smith and Way (1983).

The comparison of the bulk K-bentonite Can 27 with the melt inclusions from sample 89-050 relies on the correlation of the two K-bentonites, as discussed in Chapters 2 and 4. All other individual pairs of melt inclusion and K-bentonite were taken from the same bulk sample.

Sixty-three (63) samples of black shale were used to define the average shale composition. These samples have been collected at several localities in the Upper Mohawk Valley and cover the entire stratigraphic section of the Late Ordovician Utica Formation. Samples of shale and flysch turbidites were collected from the Frankfort/Schenectady Formation that overlies the Utica Formation in the same geographic area (see Chapter 1 for overview of the study area).

Figure 28 pictures the relative stratigraphic positions of the shale samples on top and below K-bentonite Can 27. Analyses of these samples, as well as the terminology adopted by the present study, are derived in part from Delano et al. (1990).

The "brown phase" is abundant in all grain size fractions of K-bentonites Can 14 and Flat 14. It has been most prominently observed also in sample Can 27 and 89-050, but occurs in several other K-bentonites of the Utica Formation as well. This phase is a soft, brownish to blackish colored, aggregate of micaceous minerals that neither swells upon soaking in water nor dissaggregates upon extended ultrasonic treatment (i.e. several hours). Furthermore, it is distinct from discrete, white, mica-like grains found in the Tioga-F ash bed. Fifteen grains of the brown phase were handpicked from K-bentonite Flat 14 and analyzed by electron microprobe for their major-element composition (SiO_2, TiO_2, Al_2O_3, FeO, MgO, MnO, CaO, Na_2O, K_2O) (analyzed by J.W. Delano).

The major element compositions and standard deviations for compiled averages are listed in Table V. and Table VI. For analytical results of the melt inclusions refer to Chapter 2.

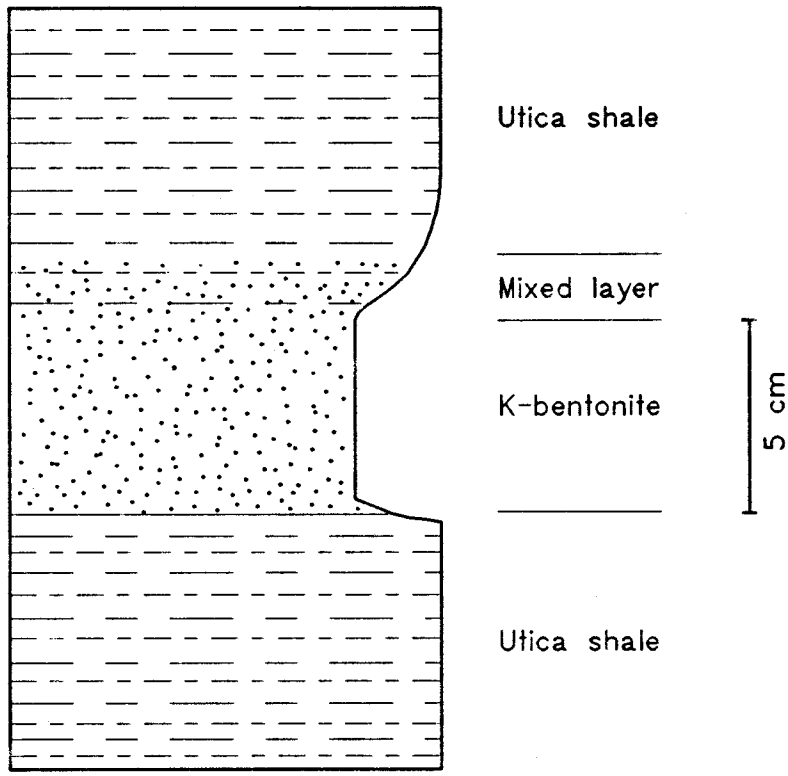

Figure 28: Schematic illustration of the stratigraphic relation of K-bentonite (Can 27) and the adjacent shale of the Utica Formation. Note the sharp contact at the bottom in contrast to the mixed layer of shale and K-bentonite on top of the layer. Nomenclature is adopted from Delano et al. (1990).

Table V.

Major element compositions of K-bentonite (Can 27), melt inclusions (89-050; i.e. glass), brown phase (Flat 14), and average composition of Utica shale, shale at the lower contact with K-bentonite Can 27, and the overlying mixed layer. Listed are averages ±2 sigma. All analyses are recalculated LOI- and CaO-free to 100 weight percent.

	K-bentonite average (n=4)		glass	brown phase average (n=15)	
SiO_2	54.71	±2.59	78.05	55.65	±1.28
TiO_2	0.60	±0.08	0.09	0.07	±0.06
Al_2O_3	31.66	±2.18	12.49	33.67	±1.36
Fe_2O_3	4.16	±4.53	0.98	1.04	±0.39
MnO	0.00	±0.01	0.02	0.01	±0.02
MgO	2.21	±0.09	0.08	2.03	±0.43
Na_2O	0.21	±0 05	2.56	0.14	±0.05
K_2O	6.44	±0.60	5.73	7.28	±0.52

	Utica shale average (n=63)		shale lower contact	mixed layer average (n=3)	
SiO_2	66.46	±7.05	75.50	63.28	±3.27
TiO_2	0.84	±0.21	0.62	0.72	±0.21
Al_2O_3	16.66	±3.16	13.43	24.18	±3.49
Fe_2O_3	7.39	±4.11	3.65	3.58	±0.58
MnO	0.10	±0.09	0.06	0.03	±0.02
MgO	3.94	±4.30	2.84	2.41	±0.18
Na_2O	0.83	±0.68	1.02	0.79	±0.34
K_2O	3.79	±0.86	2.88	5.01	±0.71

Table VI.

Major element compositions (averages) of the siliceous shales close to K-bentonites in the Utica Formation, and turbidites and shales from the Frankfort/Schenectady Formation. Listed are averages ±2 sigma. All analyses are recalculated LOI- and CaO-free to 100 weight percent.

	siliceous shale average (n=20)		turbiditic flysch average (n=3)		shaly flysch average (n=20)	
SiO_2	73.75	±3.26	71.76	±0.97	61.16	±3.72
TiO_2	0.72	±0.13	0.93	±0.05	1.04	±0.07
Al_2O_3	13.15	±1.76	13.94	±1.09	20.73	±2.86
Fe_2O_3	4.46	±1.04	6.82	±0.87	8.30	±0.88
MnO	0.08	±0.02	0.13	±0.10	0.08	±0.04
MgO	3.94	±1.05	2.49	±0.82	3.08	±0.33
Na_2O	1.12	±0.28	1.48	±0.49	0.92	±0.30
K_2O	2.78	±0.34	2.44	±0.13	4.68	±0.65

3.3. Discussion

3.3.1. The geochemical changes

All geochemical comparisons are made under the assumption that the composition of glassy melt inclusions represents the composition of the original unaltered volcanic ash. It is discussed and concluded in Chapter 2 that this assumption is justified.

The different geochemical compositions of altered K-bentonites and unaltered volcanic ashes are illustrated in Figure 29. All analyses were recalculated LOI- and CaO-free to 100 weight percent. CaO was omitted because it occurs in variable amounts as carbonate in the K-bentonites. The comparison is based on ratios of the major-element composition from the K-bentonites (in weight percent) normalized to the composition of the equivalent melt inclusion. All ratios that are greater than one indicate that the element is enriched in the altered K-bentonite, whereas ratios less than one indicate depletion. The punctuated horizontal line at a ratio of 3 is the postulated upper limit of enrichment in an insoluble residuum. This postulation is similar to that introduced by Zielinski (1982) and its magnitude was determined under the following consideration. The decomposition of volcanic ash involves major losses of SiO_2, Na_2O and K_2O (Henderson et al., 1971; Kiersch and Keller, 1955; Ross, 1928), which will hence cause a weight percent gain of the remaining oxides proportional to the total losses. The upper limit is the factor (i.e. 2.8 for Can 27), by which the remaining oxides are multiplied when the original ash composition is recalculated with smaller SiO_2-, K_2O-, Na_2O- quantities analyzed in the K-bentonite, simulating the loss of these elements (Table VII.). About 60 percent of the original SiO_2 present in the silicic ash was lost. That

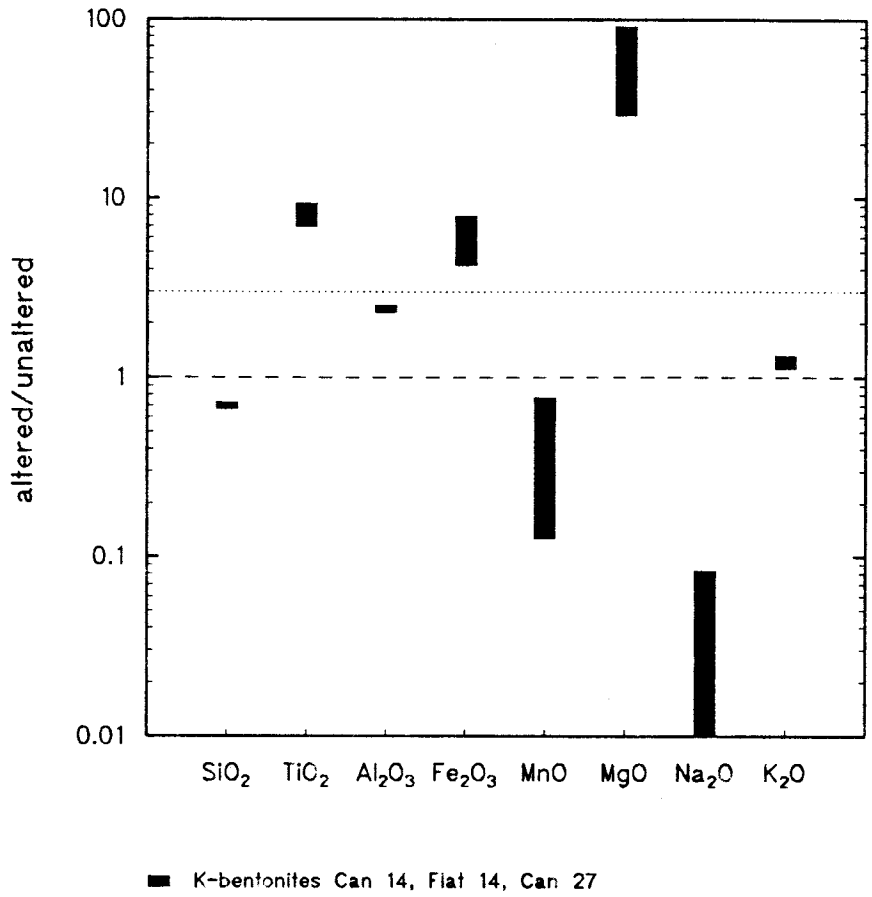

Figure 29: Enrichment or depletion of elements due to diagenetic alteration is illustrated in this graph by normalization of K-bentonite compositions (i.e. altered ash) to the composition of vitreous melt inclusions (i.e. unaltered ash). The punctuated line at a ratio of 3 is the postulated upper limit of enrichment in an insoluble residuum (see text for discussion). All analyses were recalculated anhydrous and CaO-free to 100 weight percent.

Table VII.

Modelled conversion of glass (i.e. melt inclusions) into altered ash (i.e. K-bentonite) composition for Can 27, assuming mobilization and migration of SiO_2 from the ash into underlying shale (compare Table I.), and significant losses of Na_2O and K_2O. SiO_2, Na_2O and K_2O concentrations are preset to values analyzed in the K-bentonite (marked by asterik). All other oxides are correspondingly recalculated. Results are listed in weight percent. See Appendix B for recalculation procedure.

	glass	calculated composition	K-bentonite	
SiO_2*	77.96	54.71	54.71	±2.59
TiO_2	0.09	0.25	0.60	±0.08
Al_2O_3	12.48	35.05	31.66	±2.18
Fe_2O_3	1.09	3.06	4.16	±4.53
MnO	0.02	0.06	0.00	±0.01
MgO	0.08	0.22	2.21	±0.09
Na_2O*	2.56	0.21	0.21	±0.05
K_2O*	5.72	6.44	6.44	±0.60

implies that silicic volcanic ashes suffer substantial amounts of mass loss, which is released dominantly as SiO_2 into the surrounding sediment.

The actual enrichment pattern in the K-bentonites is different from that expected from the recalculation, since all oxides that experienced gains would be expected to be enriched by the same calculated factor, which is close to the postulated upper limit. It is evident (Figure 29) that only Al_2O_3 and K_2O are enriched within the postulated limit, whereas TiO_2, Fe_2O_3 and MgO have experienced larger, variable enrichments. Note that Al_2O_3 is the only oxide enriched close to the postulated limit. SiO_2, Na_2O, and MnO are depleted in the K-bentonites.

This comparison of weight percentages can lead to a circumstance where an element may appear to be enriched, whereas in fact it has been lost (e.g. K_2O in Figures 29 and 30). A different, and preferable, form of comparison whereby two compositions are each normalized to a single element that is known to be immobile, would more realistically illustrate enrichment or depletion. Al_2O_3 is known to be immobile during diagenesis due to its negligible solubility under most Eh, pH conditions (Kiersch and Keller, 1955; Kronberg et al., 1979; Zielinski, 1982) and is consequently used as reference in the present study. Furthermore, this normalization is independent of variable amounts of carbonates and other authigenic phases (e.g. pyrite) that are present in the K-bentonites. Ratios that are greater than one indicate enrichment in the K-bentonite and ratios smaller than one depletion, respectively. Although Figure 30 exhibits the general pattern as in Figure 29, K_2O now clearly emerges as being depleted in the K-bentonites relative to the original unaltered ash.

The range of enrichment/depletion patterns widens when additional K-bentonites and bentonites from different localities are considered (Figure 31). Elements having low concentrations and relatively large analytical uncertainties (e.g. Mn, Mg, Na) in the K-bentonites or the melt inclusions are characterized by large

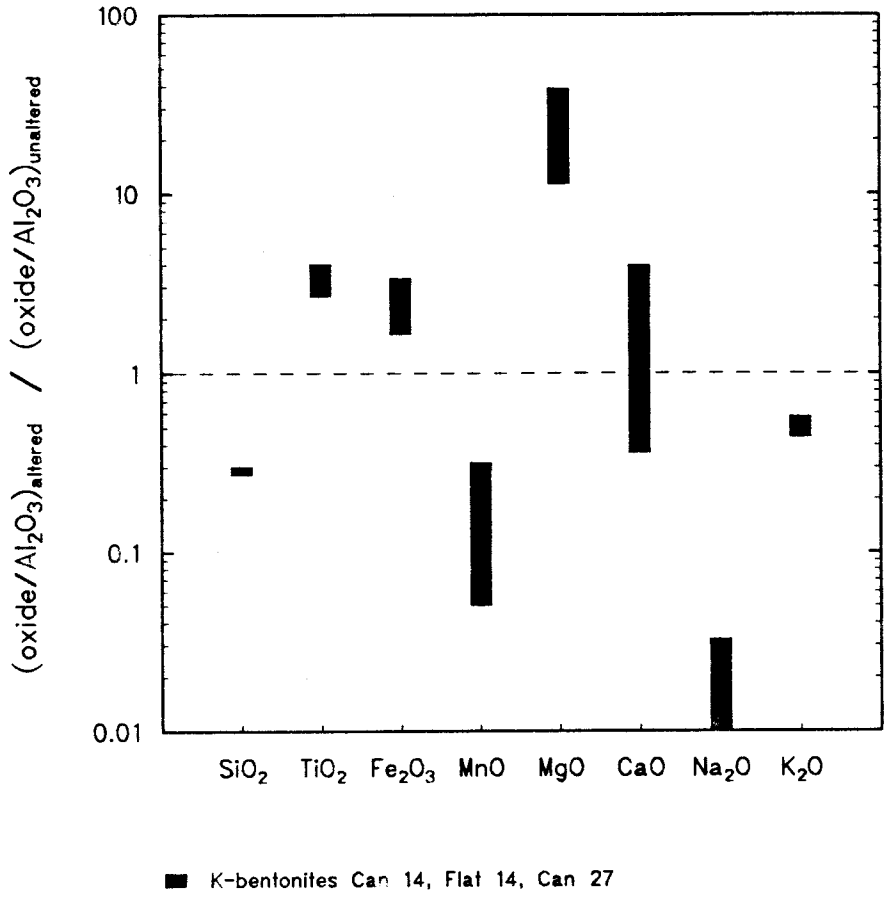

Figure 30: This diagram illustrates depletion or enrichment of elements in K-bentonites (i.e. altered ash) relative to melt inclusions (i.e. unaltered ash) for the same samples as displayed in Figure 29 but on the basis of Al_2O_3-normalized compositions.

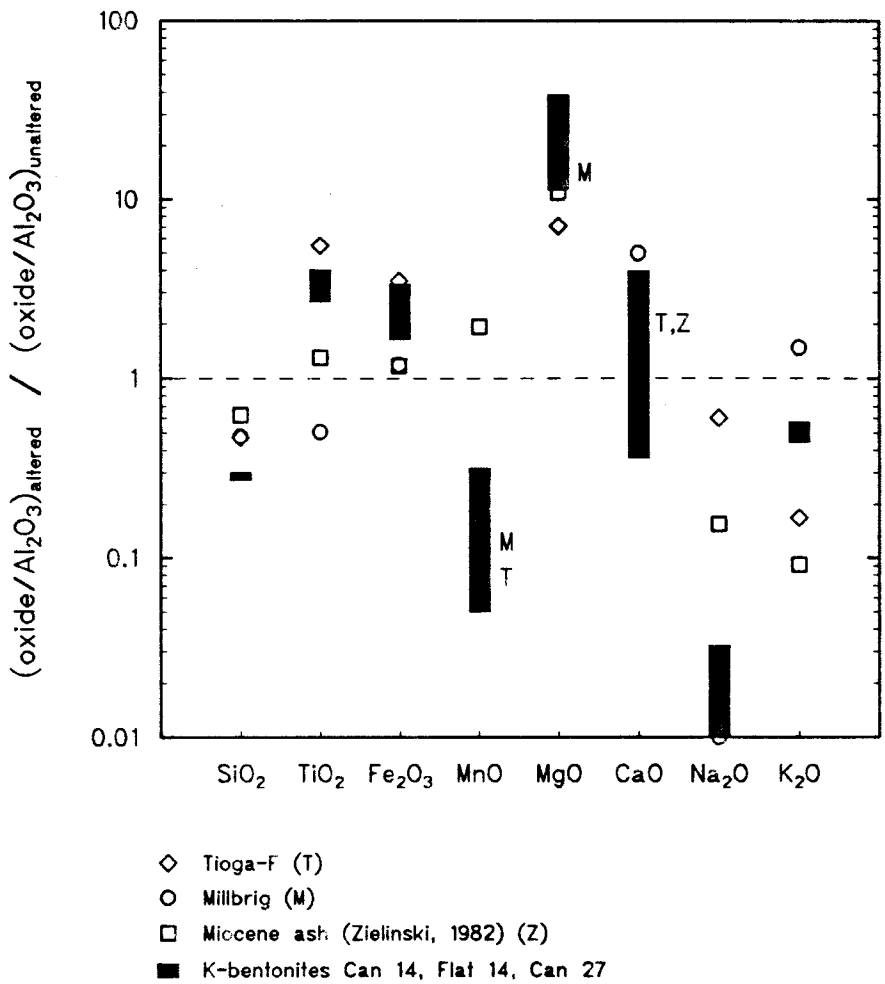

Figure 31: Illustration of enrichment and depletion pattern for samples of altered K-bentonites compared to unaltered ash (i.e. melt inclusions) (Al_2O_3-normalized) from different localities. The ranges observed for K-bentonites from the Utica shale (Figure 30) are plotted for comparison.

ranges in Figures 29 - 31. The apparent mixed behavior of CaO, whereby it is enriched in some samples but depleted in others, is likely to reflect variable amounts of carbonate observed in K-bentonites. Iron is variably enriched (Figure 31) and is often observed to be correlated with the abundance of diagenetic pyrite (present study; Delano et al., 1990; Samson, 1986; Smith and Way, 1983). Specifically, iron apparently migrated into the K-bentonites from the adjacent shales during diagenesis. In most K-bentonites, MgO is enriched by at least a factor of 10. Magnesium substitutes for aluminum in clay minerals (Weaver, 1989) and is known to occur in significant quantities (2 to 4 weight percent) in smectite/illite of some K-bentonites (Srodon et al., 1986). Since magnesium also occurs in similar quantities (about 2 weight percent) in the "brown phase" (Section 3.3.3.), it seems likely that MgO-enrichment in the K-bentonites is controlled by its incorporation into smectite/illite clay minerals. In contrast, Na_2O is known to be highly soluble and mobile during glass alteration (Noble, 1976), so its depletion in all K-bentonites is not surprising (Figure 31). K_2O is depleted relative to Al_2O_3 in all K-bentonites except the Millbrig, where it is enriched by a factor of 1.5. This enrichment may be associated with the presence of authigenic feldspar (Kolata et al., 1986), which is manifest in the $^{40}Ar/^{39}Ar$ age spectrum of a K-feldspar aliquot of the Millbrig sample (unpublished data of J.W.Delano). The magnitude of K_2O-depletion in all other K-bentonites on the other hand seems to be correlated with the amount of illite present and hence the degree of diagenetic illite growth (Altaner et al., 1984). For example, a Miocene ash having a large K_2O-depletion is known to contain abundant potassium-poor montmorillonite (Zielinski, 1982) and no illite. Similarly, the Tioga-F ash bed lacks significant amounts of potassium bearing clay minerals (e.g. mixed layer smectite/illite; Smith and Way, 1983), which is reflected in the magnitude of K_2O-depletion (Figure 31). The K-bentonites from the Utica Formation have suffered the least amount of overall

losses of K_2O, indicating the presence of potassium-bearing clay minerals such as mixed layer smectite/illite. This interpretation is supported by X-ray diffraction data (Trippi, 1986) showing mixed layer smectite/illite with 88 percent illite as clay minerals in the K-bentonite Can 14 for example.

The general depletion of potassium in the K-bentonites bears an important implication for the conversion of smectites into illites. The current model of K-bentonite formation (e.g. Altaner et al., 1984) requires decomposition of K-bearing minerals (e.g. K-feldspar, muscovite) in the surrounding sediment in order to provide the necessary potassium for the conversion. However, the overall loss of K_2O, even in illite-rich K-bentonites (e.g. Can 14, Flat 14, Can 27) implies that potassium was once present in quantities in excess of that consumed by the conversion of smectite into illite. If then the alteration of the volcanic ash proceeded in a closed system at least until completion of this conversion, no breakdown of K-bearing phases in the embedding sediment would be required. Although the closed system behavior of potassium is not indicated (e.g. loss of K_2O), further investigation into the self-supply of potassium in illite-rich K-bentonites seems justified.

3.3.2. The titanium-dilemma

It was indicated in Figure 30 that no other major or minor element besides aluminum appeared immobile in the volcanic ash during diagenetic alteration of the K-bentonites Can 14, Flat 14 and Can 27. This is surprising because TiO_2 is also considered to be an immobile element and has been used as one of the discriminating elements for the identification of altered volcanic rocks (Winchester and Floyd, 1977). However, all these K-bentonites (i.e. Can 14, Flat 14, Can 27) are enriched

in TiO_2 by a factor of 3 to 4 relative to Al_2O_3 (Figure 30). Hence, titanium must either (a) have been present in the ashes in quantities and in phases that are not represented by the melt inclusions or (b) have been added to the K-bentonites during diagenesis.

A Ti-enrichment of the magnitude observed in K-bentonites was not evident in either a comparison of coexisting glassy and bulk volcanic rocks (Lipman, 1965) or in any of several melt inclusion studies (Beddoe-Stephens et al., 1983; Dunbar et al., 1989; Hervig et al., 1989; Rutherford et al., 1985; Rutherford and Devine, 1988; Sommer and Schramm, 1983). In addition, even an example from the May, 18, Mount St. Helens eruptions with pronounced chemical differences between bulk ash and highly evolved melt inclusions and matrix glass exhibits only a 1.5x-enrichment of TiO_2 in the bulk pumice (i.e. dacitic) relative to the rhyolitic matrix glass and the rhyolitic melt inclusions (Rutherford et al., 1985). In the light of these studies it appears unlikely that the TiO_2-enrichment observed in the Paleozoic K-bentonites was a primary feature of the original parent ashes.

It is possible that the enrichment of TiO2 relative to Al_2O_3 in the bulk K-bentonite compared to the melt inclusions was caused by either (a) Ti-bearing phases of xenocrystic origin (Delano et al., 1990) or (b) detrital contamination. Analyses (Delano et al., 1990; Samson, 1986) have shown that there is no preferred concentration of TiO_2 (Al_2O_3-normalized) in any particular size-fraction of K-bentonites (Table VIII.). This lack of TiO_2-enrichment in the coarser grain size-fractions, as well as the geochemical similarity (i.e. major elements) of all fractions to the finest fraction (i.e. clay minerals), indicates that titanium does not occur as a coarse clastic component in the K-bentonites (e.g. xenocrysts; detrital grains). Instead, it seems to be associated with the clay minerals. The possibility exists that the TiO_2-enrichment in the K-bentonites is a result of contamination from minute clay minerals of the Utica shale. Titanium could be

Table VIII.

TiO_2/Al_2O_3 ratios for different size fractions of K-bentonites Can 14, Flat 14 and Can 12 (Delano et al., 1990; Delano, unpublished analyses), and SK89-02 and S85-01 (Samson, 1986). Note, that analyses of the fractions from K-bentonites Can 14, Flat 14 and Can 12 involve all material that is smaller than the grain size indicated (i.e. cumulative), whereas K-bentonites SK-86-02 and S85-01 were split into different size fractions. Ratios were calculated from weight percent.

	grain size (microns):					
	bulk	-500	-250	-125	-63	-45
sample:						
Can 14	0.0147	0.0153	0.0167	0.0166	0.0160	0.0169
Flat 14	0.0126					0.0142
Can 12	0.0334	0.0347	0.0349	0.0354	0.0358	0.0346

	bulk	-250+91	-91+38	-38+25	-25
SK86-02	0.0115	0.0118	0.0125	0.0121	0.0109

	bulk	-250+74	-74+38	-38+25	-25
S85-01	0.0204	0.0209	0.0222		0.0200

either incorporated into the structure of these clay minerals or it could occur as particles of anatase (TiO_2-pellets; 0.05-0.1 microns in diameter) adhering to the clay particles (e.g. in kaolinites; Weaver, 1976). However, such occurrences have not been reported yet for illites, which are the dominant clay minerals in shales and K-bentonites of the Utica Formation (Trippi, 1986).

At present, the author's preferred explanation involves contamination of the volcanic ash shortly after deposition by the finest clay detritus (i.e. hemipelagic) that settled into the voids between glass shards and pumice of the unaltered ash. The major-element composition of the contaminated K-bentonite would not be dramatically changed because the composition of shale and K-bentonite are chemically similar owing to the dominance of the same type of clay minerals (i.e. illites). However, significant amounts of TiO_2 either structurally incorporated or as TiO_2-pellets attached to the clay particles of the hemipelagic clay could have raised the TiO_2/Al_2O_3 ratio in the unaltered ash to those observed in the K-bentonites.

The TiO_2/Al_2O_3 ratio of the contaminating clay particles can be estimated based on the sorting trend of clastic sediments in which the proportion of TiO_2 minerals relative to the clay minerals (i.e. TiO_2/Al_2O_3 ratio) is positively correlated with the amount of siliciclastic component (i.e. quartz) (Spears and Kanaris-Sotiriou, 1976). Although the quartz content per se was not determined in the present study, it is assumed that SiO_2/Al_2O_3 ratios greater than that of clay (e.g. >1.61 for 100% illite; Weaver, 1989) are indicative of free quartz (i.e. SiO_2) besides the clay minerals (i.e. Al_2O_3). The TiO_2/Al_2O_3 ratio of the clay particles can be estimated by extrapolation of the sorting trend (Figure 32) to SiO_2/Al_2O_3 = 1.61 for 100 % illite. The TiO_2/Al_2O_3 ratio for the clay that occurs in flysch sediments is about 0.04 (Figure 32) and indicates the maximum of titanium incorporated into the clay minerals and/or adhering to them (Spears and

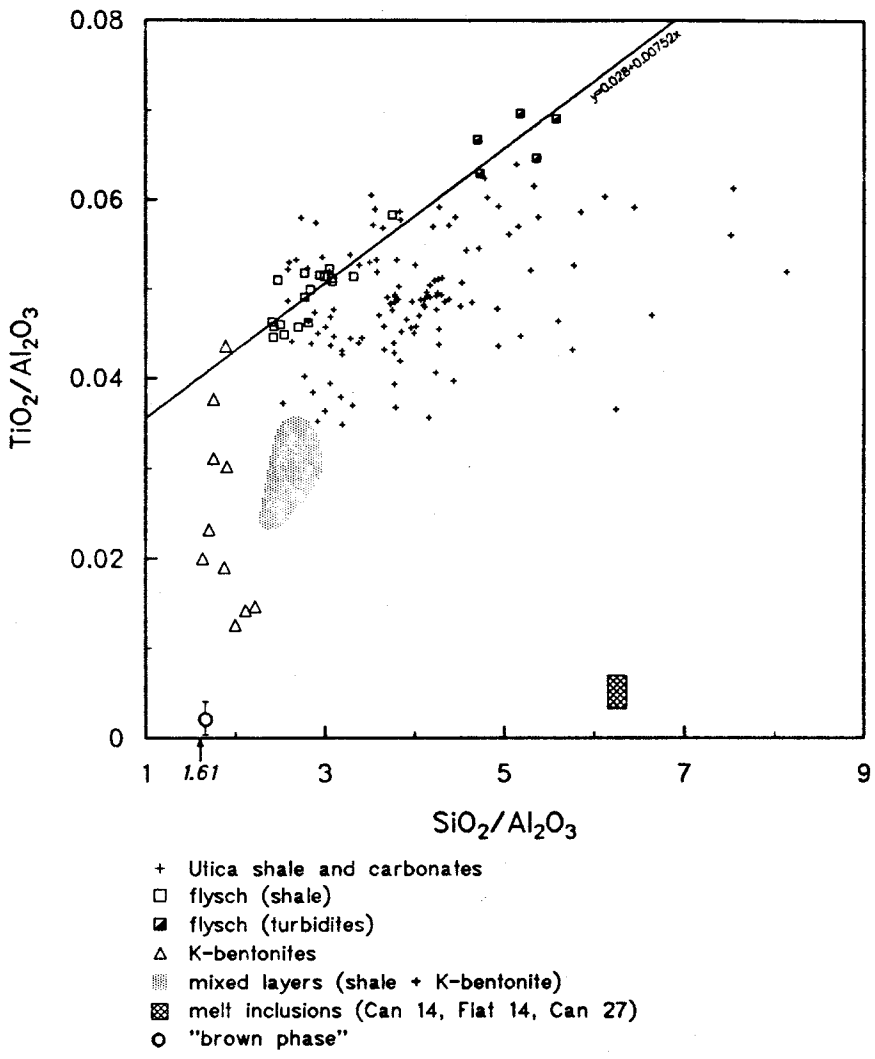

Figure 32: Plot of K-bentonites, shale samples and various lithologies of the flysch, illustrating the possible contamination of K-bentonites with TiO_2-rich (Al_2O_3-normalized) mud particles of shale or flysch. Mixed layers of K-bentonite and shale are plotted for comparison. The line indicates the sorting trend of flysch sediments, such that TiO_2 increases relative to Al_2O_3 with increasing siliciclastic component (i.e. SiO_2/Al_2O_3 ratio).

Kanaris-Sotiriou, 1976). Shale and carbonates (e.g. calciturbidites) of the Utica Formation and Trenton Group plot along a trend subparallel to the flysch at lower TiO_2/Al_2O_3 ratios, which extrapolates to a ratio of about 0.03 for that clay.

The K-bentonites plot along a trend at a constant SiO_2/Al_2O_3 ratio (about 1.8) that is characteristic of quartz-free clay. The TiO_2/Al_2O_3 ratios vary within the range that is confined by the clay-fraction of the flysch (TiO_2/Al_2O_3 <0.042) and the original ash (TiO_2/Al_2O_3 >0.005) (Figure 32). The addition of contaminants from the adjacent muds may have been restricted to the finest, TiO_2-rich clays (leaving the SiO_2/Al_2O_3 ratio in the altered K-bentonite largely unchanged) because the structure of the ash could have acted as a filter that kept out the coarse-grained siliciclastic detritus having higher SiO_2/Al_2O_3 ratios (e.g. >2.5) (Figure 32). This trend among K-bentonites should therefore not be confused with physical mixtures of shale + K-bentonites (mixed layer in Figure 32), which are often present at the upper contact of K-bentonites (Figure 28).

All of the K-bentonites having TiO_2/Al_2O_3 ratios >0.03 occur within shales of the Utica Formation that belong chemically to the flysch trend and hence could have caused the TiO_2/Al_2O_3 ratios to be greater than 0.03 (Figure 32).

Owing to the lack of chemical analyses from the overlying sediments it is not possible to verify whether the enrichment of TiO_2 that is observed in the Tioga-F ash bed (Figure 31) results from this same contamination process. However, the Miocene ash of Zielinski (1982) is the least enriched in TiO_2 due largely to its considerable thickness (25 to 50 cm). In particular, the altered part of the ash may have been 'protected' from contamination by overlying, unaltered ash. This would suggest that the magnitude of TiO_2-enrichment should be inversely correlated with the thickness of the K-bentonites. The depletion of TiO_2 that is observed in

the Millbrig K-bentonite may have been caused by the same process, different only in such way that the TiO_2/Al_2O_3 ratio of the contaminating particles from the overlying sediment was less than that of the K-bentonite.

In summary, it appears that the contamination of volcanic ashes with clay of detrital origin (i.e. shale) is a likely cause for the TiO_2-enrichment observed in K-bentonites. This interpretation is consistent with the observed geochemical patterns and stratigraphic relations of K-bentonites and their hosting shales. It may be worthwhile to investigate in detail the nature of the TiO_2 in K-bentonites and whether the inferred association with clay particles in the overlying shale and the altered ash actually exists.

3.3.3. The "brown phase"

It is likely that the most abundant phases in a K-bentonite, which are the clay minerals (Weaver, 1953), control the geochemistry (i.e. chemical fingerprint; Samson, 1986). Although clay is generally fine grained (<20 microns; Weaver, 1989), at least some of the K-bentonites (Can 14, Flat 14, Can 27) contain grains of soft, brownish to blackish, fine-grained material that is not identifiable with common petrological methods. These grains are referred to as "brown phase" (present study) and may represent macroscopic aggregates of clay minerals. Several individual aggregates, each approximately 200 microns in diameter from the K-bentonite Flat 14 were analyzed by electron microprobe (Table V.). The same phase was found to be present as inclusions in quartz and zircons that were open to the external environment. This is interpreted as evidence that the brown phase is the alteration product of glass, originally present in both the bulk ash and in inclusions. Although X-ray diffraction data are not available, it seems likely

that the brown phase is an aggregate of mixed layer illite/smectite (I/S). Its major element composition is uniform (Table V.) and is compositionally similar to I/S clay minerals found in other K-bentonites (Srodon et al., 1986). In addition, the similarity of the brown phase compositions compared with the bulk K-bentonites (Table V.) is striking. This is illustrated in Figure 33, where the major element composition of the K-bentonites (Can 14, Flat 14, Can 27) are Al_2O_3-normalized and compared with the brown phase. SiO_2, MgO and K_2O, which are major cations in illite clay minerals (Weaver, 1989), are (relative to Al_2O_3) identical in the K-bentonites and the brown phase. MnO and Na_2O are variable due to their low concentrations in the brown phase. CaO is enriched and observed as carbonate in K-bentonites. Fe_2O_3 occurs as ferrous iron in diagenetically produced pyrite that causes its enrichment in the K-bentonites.

3.3.4. Geochemistry of shale adjacent to a K-bentonite

It has been shown that volcanic ashes release substantial amounts of SiO_2 (about 50 weight percent) and minor amounts of Na_2O and K_2O during alteration to a K-bentonite. The surrounding shale, particularly, may be a 'sink' for the released SiO_2 and hence be enriched in SiO_2. Brusewitz (1986), for example, noted silicification at the lower contact of a flat-lying K-bentonite that is most likely related to the release of silica from the volcanic ash during alteration. Although the shale at the lower contact with K-bentonite Can 27 is not visibly silicified, its geochemical composition, when compared to average Utica shale, shows it to be enriched in SiO_2 and depleted in most other major elements (Table V.). Despite the fact that Utica shale is variable in its chemical composition, the lower contact shale does not overlap with the standard deviation (2 sigma) of the average shale

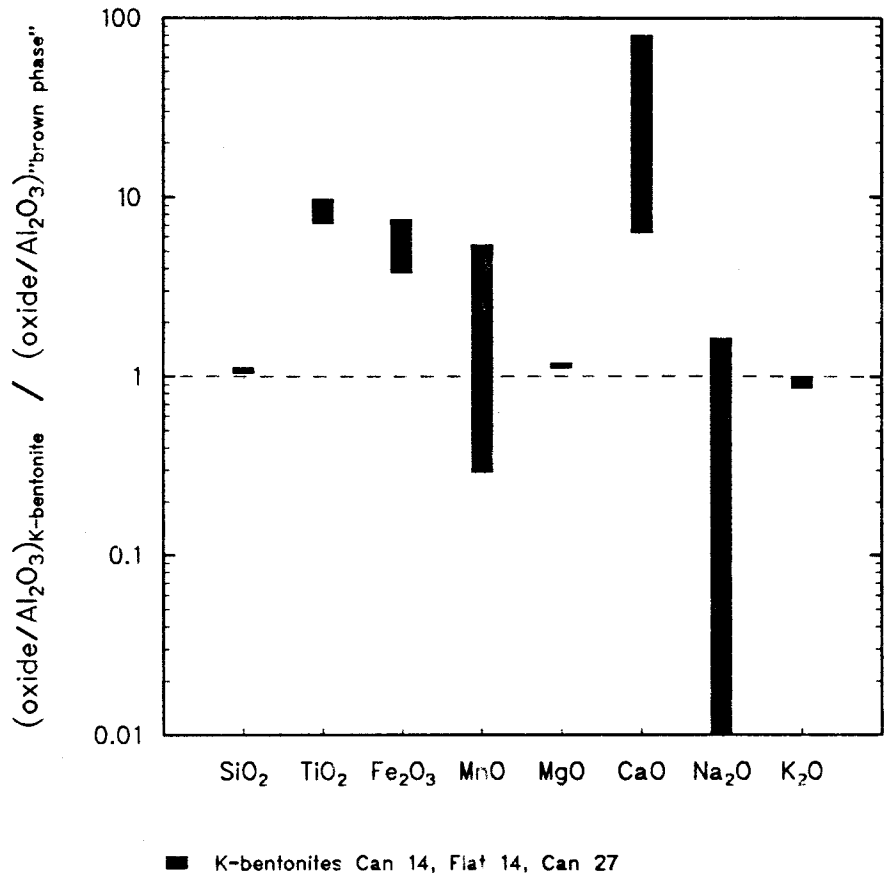

Figure 33: Comparison of Al_2O_3-normalized K-bentonite compositions with the brown phase, illustrating their geochemical similarity with regard to SiO_2, Al_2O_3, MgO, and K_2O, which are major cations in clay minerals.

(Table V.). Specifically, Figure 34 illustrates that relative to aluminum only SiO_2 is clearly enriched in the lower contact compared to the average shale, whereas all other elements vary within the standard deviation. The unusual composition at the lower contact with K-bentonite Can 27 is likely to be a shale of average composition that experienced an addition of SiO_2 that had been diagenetically released from the overlying volcanic ash.

Shale samples located less than one meter stratigraphically from a K-bentonite were found to be enriched in SiO_2 relative to Al_2O_3 (Si/Al > 4). Those samples were omitted from the calculation of an average shale composition because that enrichment appears to be caused by SiO_2 migration from the K-bentonites into the over- and underlying shale (Figure 34). The average composition of siliceous Utica shale was calculated using samples (n=20) that had been omitted from compilation of the "normal" shale average (n=63) using the following criteria: (a) located stratigraphically within a meter of K-bentonites; (b) their Si/Al-ratio is greater than 4; and (c) they contain commonly more than 70 weight percent SiO_2 (recalculated LOI- and CaO-free). The averaged major-element composition of these siliceous shales is indistinguishable from the "normal" average shale within the standard deviation except for SiO_2 which is enriched relative to Al_2O_3 by the same factor as the lower contact shale (Figure 36).

As an alternative to this view of shale silicification, at least two other sources of SiO_2 are conceivable. For example, the excess silica may be of either biogenic (e.g. Henderson et al., 1971) or siliciclastic origin. However, since there is no published evidence for silicic fossils (e.g. radiolarian ooze, diatoms) in the Utica Formation, this seems unlikely as a source. In contrast, since siliciclastic turbidites overly the Utica shale as flysch in the Frankfort and Schenectady Formations, it is conceivable that precursors of this sediment-type might have appeared sporadically during the time of Utica shale deposition. Figure

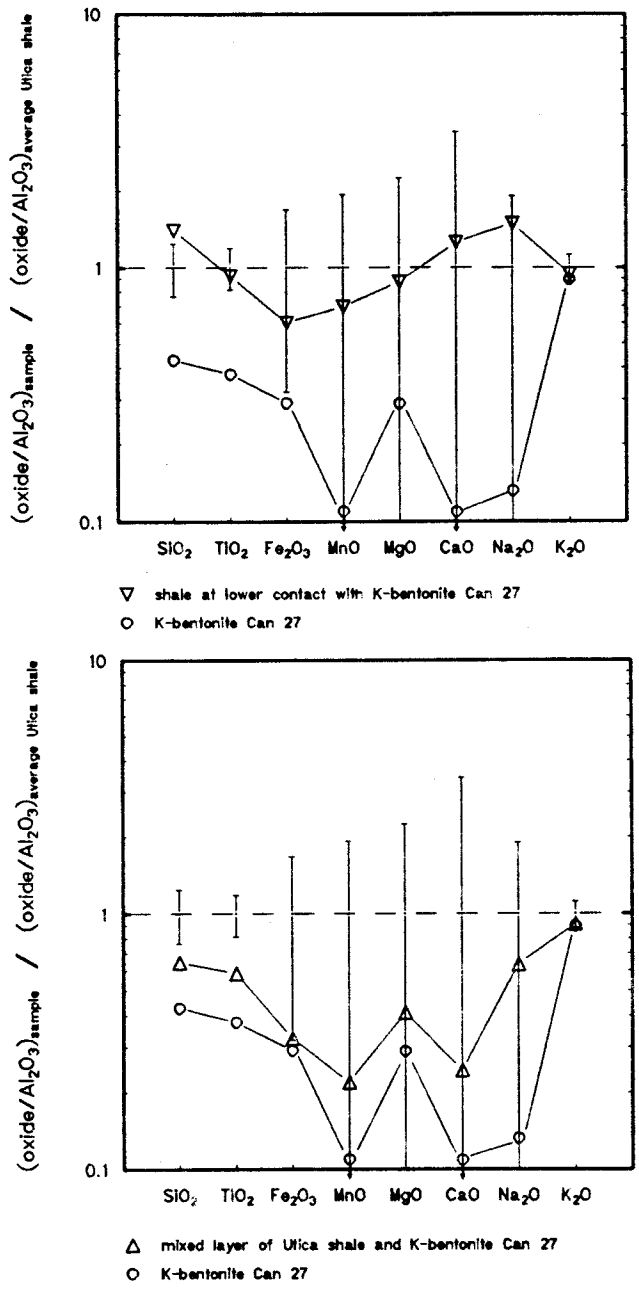

Figure 34 (upper): Plot of shale composition (lower contact with K-bentonite Can 27), illustrating the SiO_2-enrichment relative to average Utica shale composition. K-bentonite Can 27 is plotted for comparison.
Figure 35 (lower): Plot of mixed layer composition relative to average Utica shale, illustrating a pattern that is similar to the K-bentonite pattern.
Error bars indicate $\pm$2sigma standard deviation of average Utica shale composition.

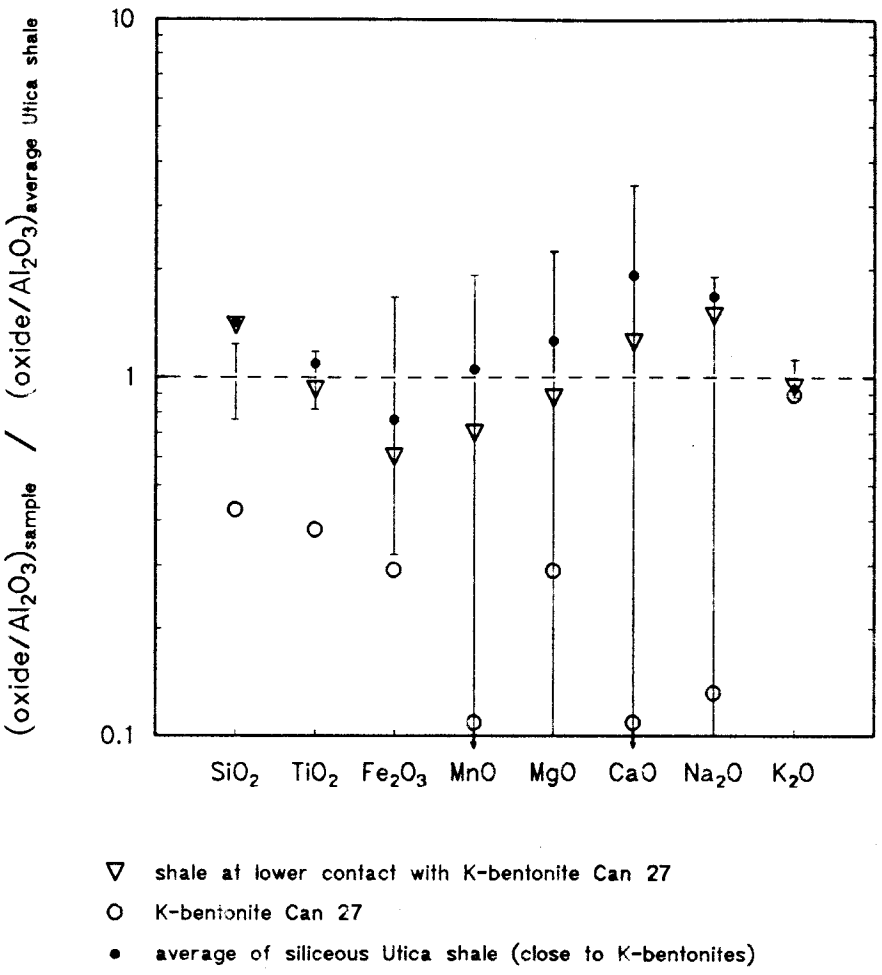

Figure 36: Illustration of similar SiO_2-enrichment in shale at lower contact with K-bentonite and siliceous shales relative to average Utica shale composition. Error bars indicate $\pm$2sigma standard deviation of the average Utica shale composition.

37 compares the fine-grained (i.e. shale) and the coarse-grained (i.e. turbidites) lithologies from the flysch relative to the siliceous shale of the Utica Formation. The fine-grained flysch material is depleted in SiO_2 relative to Al_2O_3 and could not, therefore, be related to the siliceous shale. Although the coarse-grained turbidites are SiO_2-enriched (Figure 37), the magnitude is less than that observed in the siliceous shale. In addition, if turbidites had contributed, a textural coarsening of the siliceous shale would be expected, but is not observed in the siliceous shale samples. Furthermore, the TiO_2-enrichment in the coarse fraction of the flysch is not observed in the siliceous shales (Figure 37). Since it appears unlikely that either biogenic or flysch material have contributed SiO_2 to the shale, the alteration of the volcanic ashes with subsequent release and migration of SiO_2 into the surrounding shale is the preferred mechanism for producing the observed compositions of shales and K-bentonites.

The "mixed layer" on top of K-bentonite Can 27, which resembles a reworked zone (e.g., by bioturbation and/or bottom currents) (Delano et al., 1990), is chemically distinct from the lower contact shale (Table V., Figure 35). Its major element chemistry, when normalized to Al_2O_3 and compared with average Utica shale (Figure 35), is depleted in all major elements and mimics the pattern exhibited by the K-bentonite. This pattern suggests that the mixed layer is a blend of K-bentonite and average shale (Delano et al., 1990). On the other hand, the REE-pattern of the mixed layer indicates a more complex relation than simple blending of the two components K-bentonite and shale. Diagenetic mobilization of the REE out of K-bentonites into the surrounding shales (Delano et al., 1990; Zielinski, 1982) apparently overprinted a simple mixture of shale and K-bentonite.

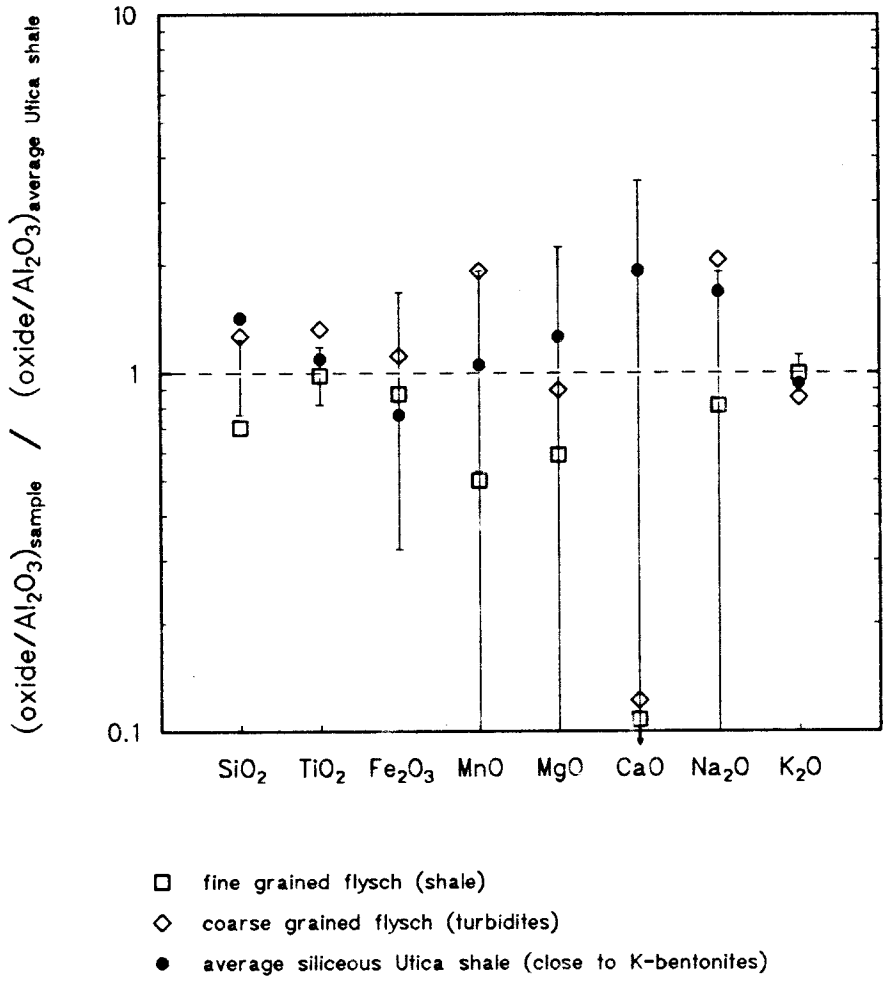

Figure 37: Al_2O_3-normalized compositions relative to average Utica shale for fine and coarse grained flysch lithologies are compared with siliceous Utica shales. Error bars indicate ±2sigma standard deviation of the average Utica shale composition.

3.4. Conclusions

The bulk compositions of several late Ordovician and middle Devonian K-bentonites were compared to their original parental compositions based on melt inclusions in phenocrysts. The geochemical changes inferred from this comparison are consistent with current models and observations concerning the diagenetic alteration of silicic volcanic ashes to K-bentonites. The observations made in the present study are:

1. The volcanic ashes have lost large quantities (about 50 weight percent) of SiO_2. This SiO_2 migrated out of the ashes into the over- and underlying shale causing an observed enrichment in the adjacent sediment.
2. Compared to "normal" average Utica shale, the siliceous shales have the following characteristics: (a) elevated Si/Al ratios greater than 4; (b) high concentrations of SiO_2 (>70 weight percent; recalculated LOI- and CaO-free); and (c) occurrence stratigraphically within a meter of K-bentonites.
3. Most of the Na_2O that was originally present in the volcanic ash has been lost.
4. K_2O-loss is indicated for all K-bentonites that contain only clay minerals. Formation of authigenic K-feldspar may have caused the apparent K_2O-enrichment in the Millbrig K-bentonite .
5. MgO was gained in all K-bentonites, which is most likely related to the newly formed clay minerals into which MgO is incorporated.
6. Titanium is either enriched or depleted in the K-bentonites relative to aluminum. The settling of detrital TiO_2-rich clay particles into voids within the original volcanic ash may have caused the TiO_2-enrichment. This detrital

contamination suggests that titanium is not reliable as a discriminating trace element, in combination with other immobile trace elements (e.g. Zr, Nb, Y), for estimating the original composition of K-bentonites.

Chapter 4 "Zircon morphology"

4.1. Introduction

Several Middle- and Late-Ordovician K-bentonites in eastern North America have been successfully correlated over distances of up to 900 km using the method of chemical fingerprinting of the bulk composition of altered ashes (Cullen-Lollis and Huff, 1986; Huff, 1983; Kolata et al., 1986, 1987). This is an extension of the method of correlating unaltered volcanic ashes based on the geochemical composition of glasses (e.g. Borchardt et al., 1971; Borchardt et al., 1973; Smith and Nash, 1976). The general applicability of 'chemical fingerprinting' to correlation of altered volcanic ashes (i.e. K-bentonites), however, is not without problems (Samson, 1986). For example, it is not yet completely understood why elements identified as being most discriminating in one correlation experiment are found to be non-discriminating in other instances (i.e., Na, K, Rb, Cs, Ga, Cr, Yb, As, Sb: Huff, 1983; Kolata et al., 1986), even though both experiments included the same K-bentonite (i.e. Deicke K-bentonite; Samson et al., 1988). Further difficulties concerning chemical fingerprinting may be encountered in (a) possible occurrence of xenocrystic components (Delano et al., 1990), (b) sample contamination (Kolata et al., 1986), and (c) insufficient discrimination of large numbers of different K-bentonites (e.g. minimum of 30 beds in New York State).

Samson et al. (1988) demonstrated that the chemical composition (i.e. REE) of apatite phenocrysts, which are not affected by diagenetic alteration (Samson et al., 1989), can be used as an alternative correlation tool. Possible limitations implied in this method, however, may be the overlap of element concentrations and

-ratios among apatites separated from various K-bentonites. It is therefore reasonable to investigate additional methods that can be used in tandem for the reliable characterization of individual K-bentonites.

The morphology of zircons is considered another potential correlation tool for the following reasons: (a) zircon is a common, well-preserved accessory phase in most silicic volcanic rocks and occurs throughout the Ordovician K-bentonites owing to the mineral's resistance to weathering and diagenesis; (b) the morphology of zircons systematically vary over a wide range depending on physico-chemical conditions in the magma during zircon crystallization (Pupin and Turco, 1975). It is therefore likely that the morphology of a zircon population in a K-bentonite records the individual conditions that prevailed in the pre-eruptive magma chamber shortly before the explosion and distribution of the volcanic ash. In fact, individual layers of altered volcanic ashes can be identified and correlated using the systematic morphology of their zircon populations (Kowallis and Christiansen, 1990; Winter, 1981, 1984).

In this chapter, it is demonstrated that (a) individual layers of the Ordovician K-bentonites in eastern North America can be distinguished and correlated, and (b) inferences can be made about the petrogenesis of those altered volcanic ashes based on the morphology of their zircon populations.

4.2. Sample preparation and techniques

Zircons are most abundant in the sieve fractions that range in size from 125 microns to 45 microns, from which they were separated following the mineral separation procedure (i.e. densimetric and electromagnetic) as described in Chapter 1. Initially, from each sample, a few hundred grains of the zircon-concentrate were

sprinkled onto a glue patch fixed to an aluminum stamp, which holds the sample in the scanning electron microscope. However, sprinkle mounts were abandoned at an early stage of this study. Subsequently, zircon grains were arranged in 10-by-10 grids by handpicking under the binocular (40x magnification) to assure that (a) repeated counting during the morphology determination would be avoided and (b) a particular zircon grain could be identified for subsequent chemical analysis by electron microprobe.

Grain mounts were coated with gold-palladium or gold in a sputter coater (Technics, Hummer-V) for study in a scanning electron microscope (ISI Super MINI-SEM; 20 kV; 23 mm working distance), which is located at the Department of Biological Sciences of the State University of New York at Albany. The scanning electron microscope was preferred over the light microscope because it offers (a) the possibility of viewing individual grains from various perspectives in order to avoid ambiguities with regard to the morphology-type and (b) higher resolution of the surface of crystals that can provide supplementary data in distinguishing individual zircon populations.

4.3. The morphology of zircons

Although the general prismatic habit of zircon is controlled by its tetragonal structure (space group $I4_1/amd$), the actual morphology is determined by the combination and development (i.e. relative proportions) of its prismatic and pyramidal crystal faces (Sunagawa, 1987). The most common of those faces are of the {100} and {110} prisms and the {101} and {211} pyramids (Pupin and Turco, 1972b). Each of the prism forms {100} and {110} and the pyramid form {101} is constituted by four equivalent crystal faces, whereas the {211} pyramid form

comprises eight crystal faces. The proportions of those faces, and therefore the morphology, depend on the relative growth rates of these individual forms (Sunagawa, 1987). Figure 38 illustrates the development of a zircon morphology depending on the growth rates of prism and pyramid forms: the faster a particular prism or pyramid subform grows relative to another subform, the smaller appear the crystal faces of the faster growing subform in the morphology relative to the dominating faces of the slower growing subform. Furthermore, the relative growth rates apparently depend on the conditions that prevail in the magma from which a crystal grows. Temperature and composition of the melt (i.e. agpaicity) have been identified as particularly important in the case of zircon (Pupin and Turco, 1975). Those parameters influence the zircon morphology in such a way that preferred development of the {100} prism relative to {110} is correlated with increasing temperature. The development of the {211} pyramid is correlated with more aluminous melt compositions compared to the dominance of {101} pyramids in more alkaline melts (Pupin and Turco, 1975) (Figure 38).

Pupin and Turco (1972b) proposed a classification scheme for zircons that recognizes the various combinations of the prism and pyramid forms as morphology types (Figure 39). This scheme was also used for the present study in order to morphologically classify the zircon populations of the Ordovician K-bentonites. It should be pointed out that Pupin and Turco (1972b) used indices for the crystal faces, proposed by Caruba and Turco (1971), which are different from the Miller (hkl)-indices (see Figure 39 for translation). For the application of the classification scheme, the proportions of the prism faces relative to each other ranging from 1:1 to 4:1 were considered as (110)>(100) or (110)<(100) respectively; proportions ranging from 4:1 to 10:1 as (110)>>(100) or (110)<<(100); and proportions 10:1 and more were considered as single prism ((110) or (100) only). The classification of the pyramid faces ((211) and (101)) was made following the

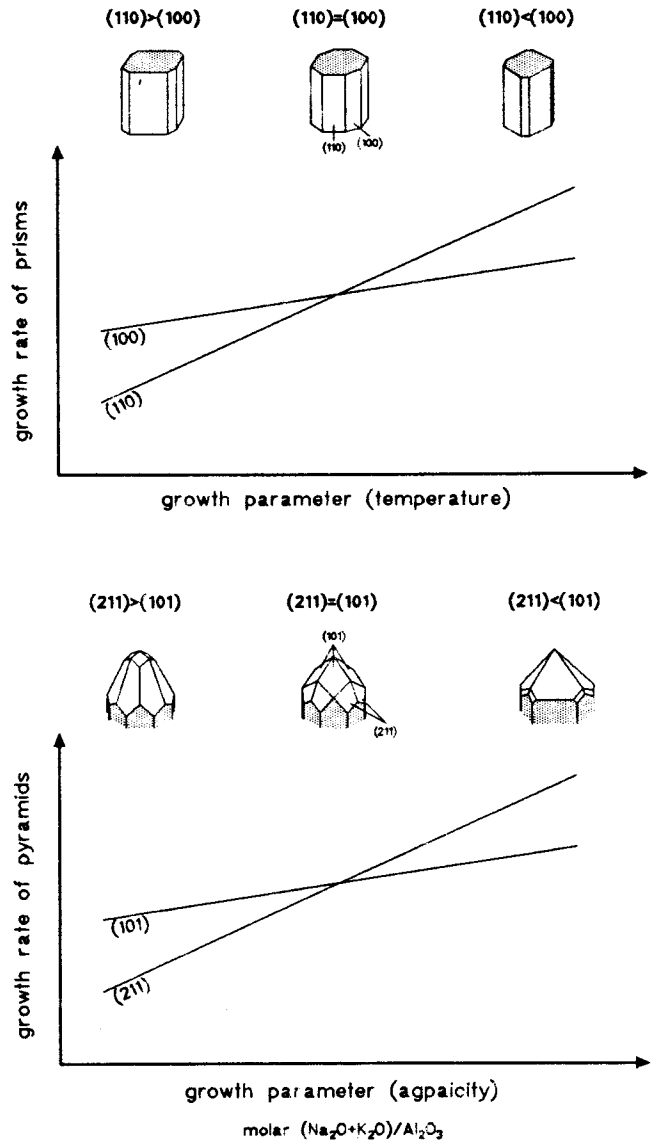

Figure 38: Development of zircon morphology depends on the relative growth rates of the prism (upper diagram) and pyramid forms (lower diagram). The diagrams illustrate, how the growth rates of the individual subforms, and hence the morphology (i.e. (100) and (110) prisms; (101) and (211) pyramids), change relative to each other with change of the respective growth parameter temperature or agpaicity. (After Sunagawa, 1987; Pupin and Turco, 1975).

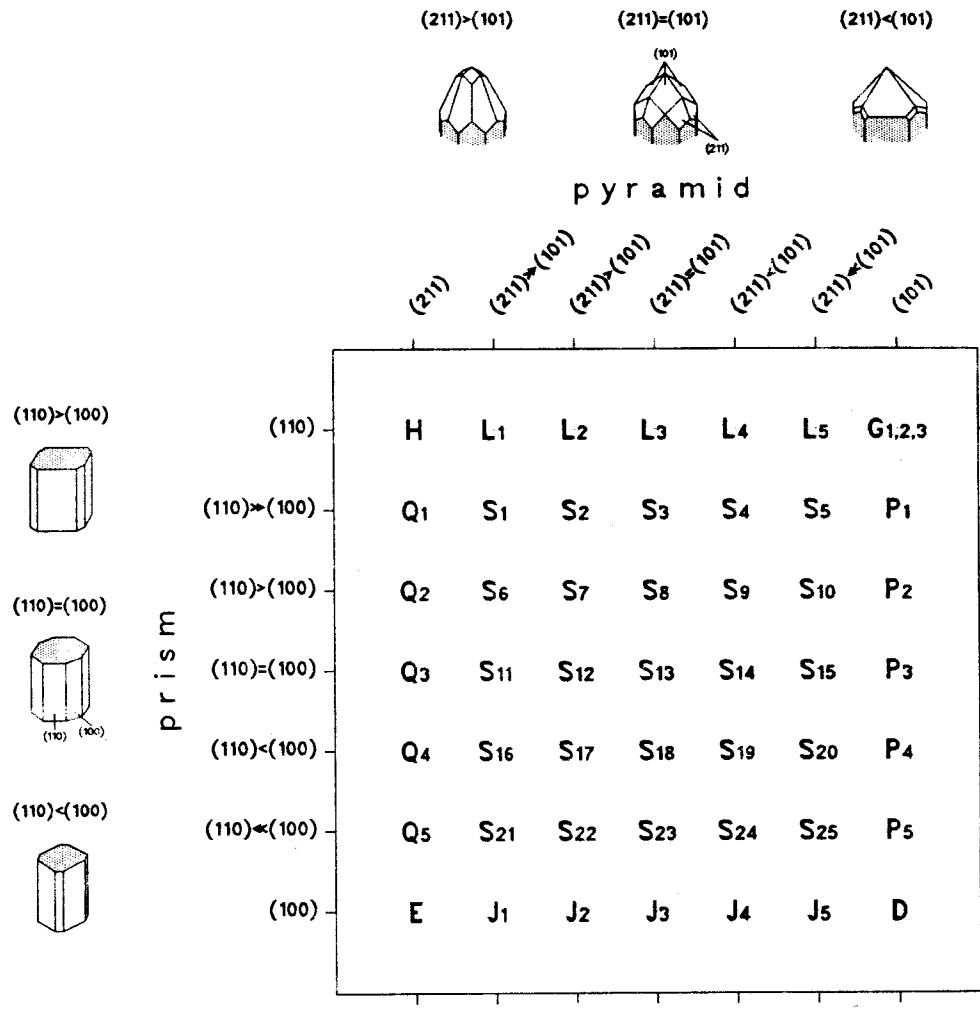

Indices (present study)	(hkl)-indices (Miller)
(100)	(110)
(110)	(100)
(101)	(111)
(211)	(311)

Figure 39: The classification scheme of zircon morphology (after Pupin and Turco, 1972b). Displayed are only the combinations of the two prism forms {100} and {110} with the pyramid forms {101} and {211}, which were observed among the zircon populations in the present study. The translation of the indices used for this scheme (after Caruba and Turco, 1971) to Miller (hkl)-indices is listed in the table.

same relative proportions (Figure 39). Additional morphology types that include supplementary pyramid forms (e.g. {301}, {112}, {321}, {311}, {511} and {001}) have been defined (Pupin and Turco, 1972b; Pupin, 1980) but were not observed in the present study and hence omitted from Figure 39.

Several euhedral zircon crystals are pictured in Figures 40 thru 44 and have been morphologically classified in order to illustrate this scheme. Figure 40 shows a zircon of P1 morphology possessing the following characteristics: (a) the terminal pyramids each comprise the four faces of the simple {101} pyramid; (b) faces of the {211} pyramid are not present; and (c) the faces of the {100} prism are much less developed than the {110} prism faces. Note, that this crystal, which is slightly asymmetric, exhibits no cracks or indentations on its surface. In contrast, the zircon shown in Figure 41 is distinguished by a different morphology and a more-or-less regular pattern of cracks on its surface. These cracks may have resulted from strain between adjacent layers of metamict and crystalline zircon. The metamict layers would be enriched in radioactive elements (e.g. U and Th) and experienced greater expansion relative to the crystalline layers due to alpha-decay induced damage of the crystal lattice (Chakoumakos et al., 1987; Holland and Gottfried, 1955). The morphology of this zircon is a S8 type whereby (a) the {211} and {101} pyramid faces are equal in size, whereas (b) the {100} prism faces of the prism are smaller than the {110} faces. Figure 42 illustrates a zircon crystal representing a S22 morphology type in which (a) the faces of the {211} pyramids are always larger than the {101} faces, and (b) the {100} prism is much larger relative to the {110} prism. In contrast to it is the S25 morphology type, where the prism is similarly developed (i.e. (100)>>(110)) but faces of the {101} pyramid dominate over faces of the {211} pyramid (Figure 43).

Anisotropic growth of equivalent faces results in an asymmetric morphology as illustrated in Figure 44: the {100} prism is generally larger than the {110},

Figure 40: SEM photomicrograph of euhedral zircon crystal exhibiting a P1 morphology.

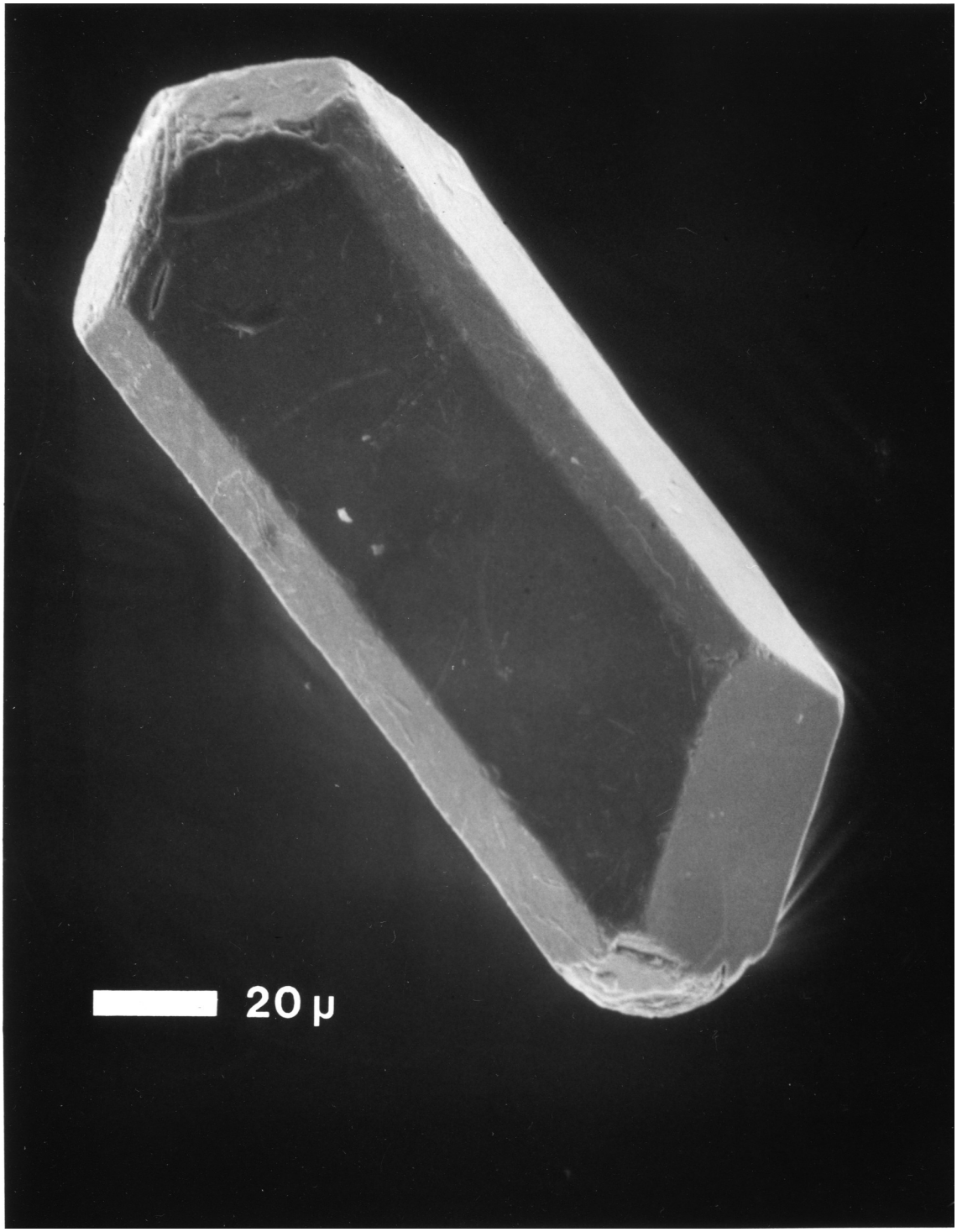
20 µ

Figure 41: SEM photomicrograph of euhedral zircon crystal exhibiting a S7 morphology. Note the crack pattern on the surface of the crystal; the cracks are oriented either parallel or perpendicular to the long axis of the zircon (i.e. c-axis)

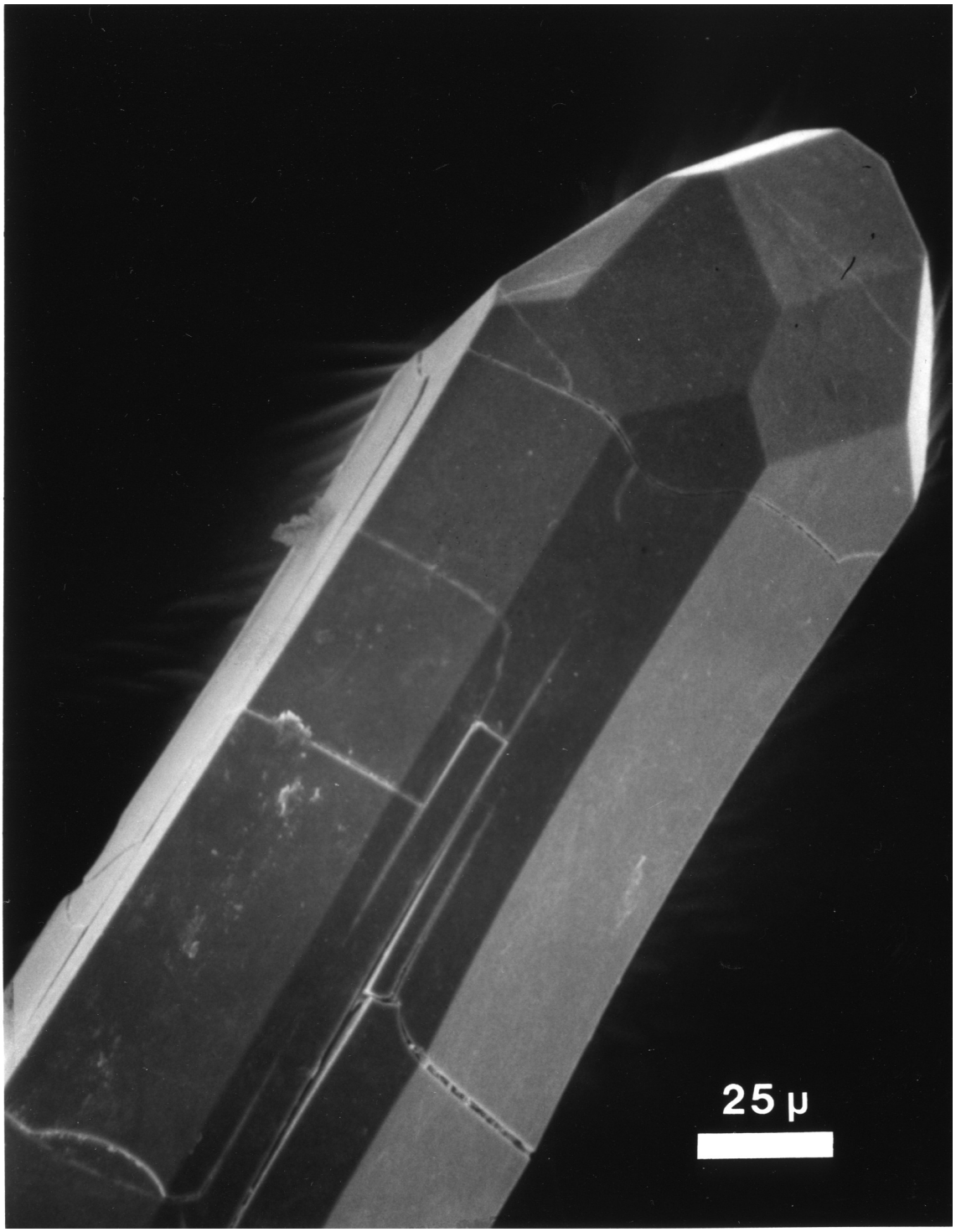
25 μ

Figure 42: SEM photomicrograph of euhedral zircon crystal exhibiting a S22 morphology.

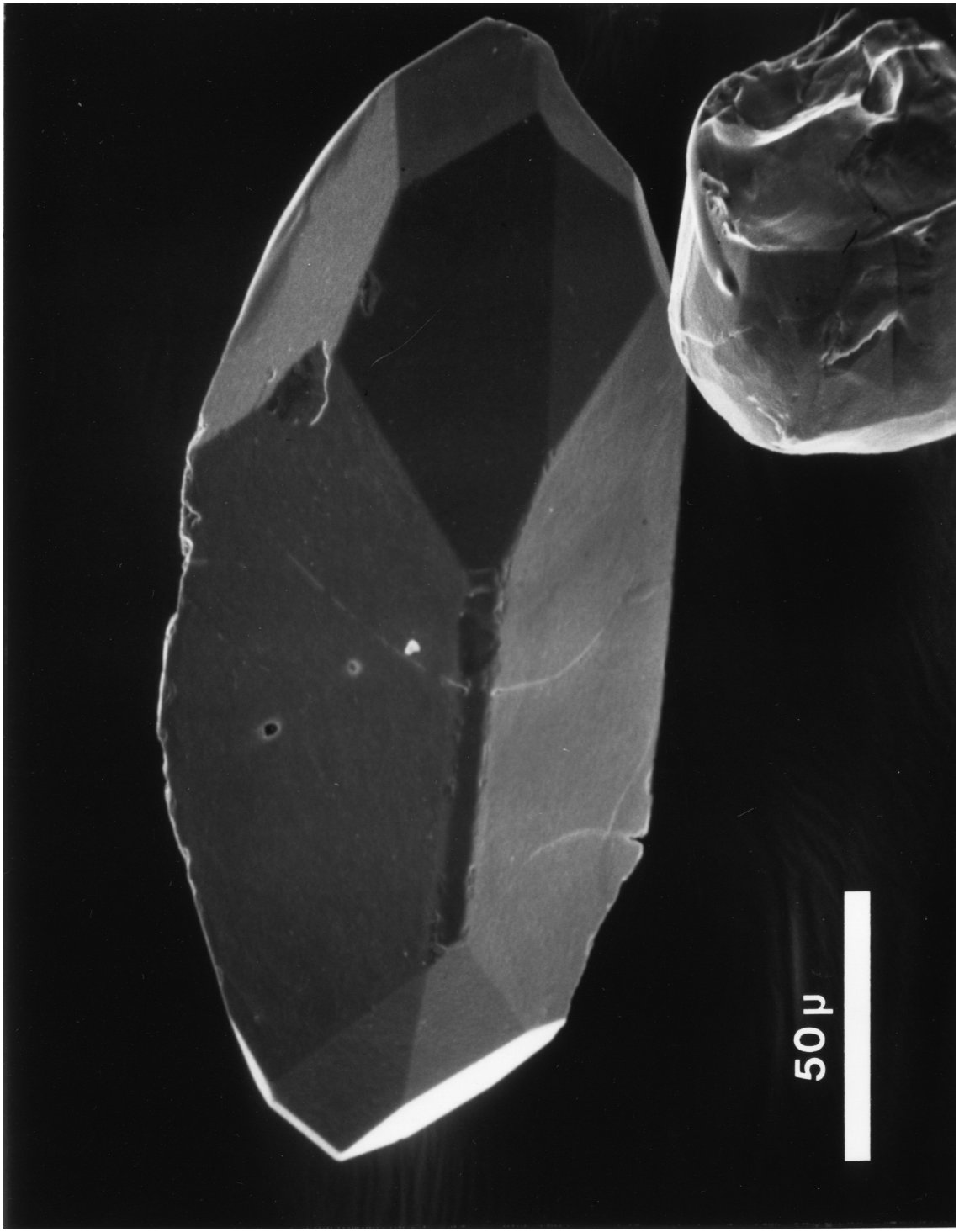
50 μ

Figure 43: SEM photomicrograph of euhedral zircon crystal exhibiting a S25 morphology.

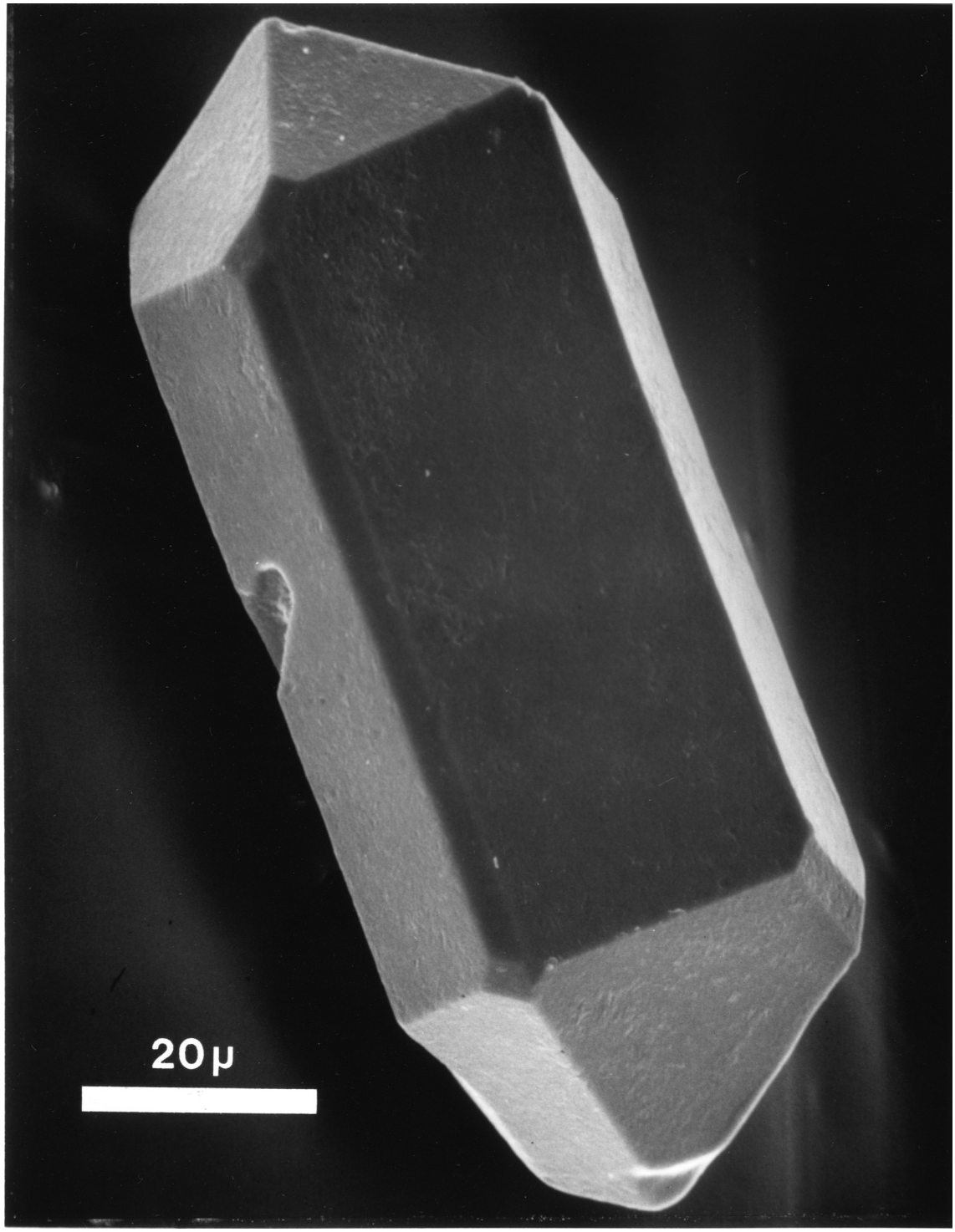
20μ

Figure 44: SEM photomicrograph of euhedral zircon crystal that has developed an asymmetric morphology. Each tip exhibits a combination of S17 and S19 morphology, which is considered an averaged S18 morphology.

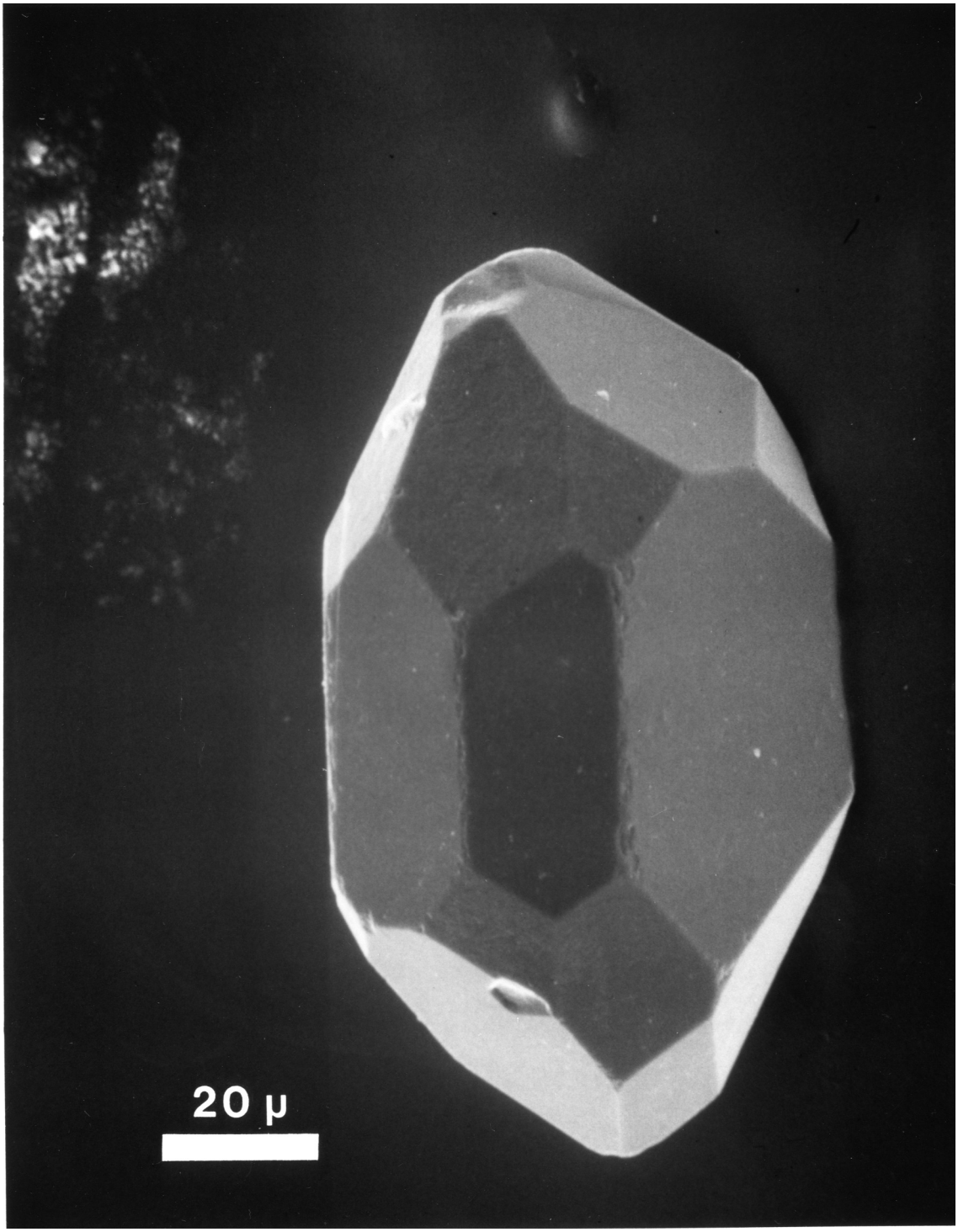
20 µ

whereas the faces of both terminating pyramids vary in their proportions relative to each other, such that one side of each tip is dominated by {211} faces in contrast with the dominance of the {101} face relative to the {211} faces on the side 90° next to it. Asymmetries of this kind were often encountered during this study and either an average of the exhibited morphologies determined or different morphology types were noted in case of two distinct tips on a single crystal.

Although they were not used for discrimination of K-bentonites, morphological features (e.g. surface relief, crack patterns and indents; Figure 45) are noteworthy because they apparently represent distinct morphological features of individual zircon populations.

More than 80 percent of the crystals among the zircon populations studied were found to be euhedral with length/width ratios ranging from 2 to >7 (e.g., Figures 46, 47). The dimensions of the zircons were not investigated further because bias was expected from sieving into various size-fractions and from long crystals that were broken during the sample preparation (e.g. sieving).

4.4. Results and discussion

The results of this typological study are presented in histograms and are based on the classification scheme discussed in the previous section (Figure 39). Every morphologic type occurring in a population is represented by a marker, of which the size corresponds to its relative abundance (see Appendix C for results).

The accuracy of the morphologic classification was tested with a second student on a subset of 150 grains from a well-studied sample (i.e., 89-050). The results (Figure 48) indicate that the differences between the classifications performed by different students (A and B) are insignificant compared with the

Figure 45: SEM photomicrograph of euhedral zircon crystal, displaying a variety of morphological features on the surface of the crystal: (1) a pattern of cracks, which are oriented either parallel or perpendicular to the long axis of the zircon (i.e. c-axis) and (2) flat or deep indentations on the surface that reflect the shape of some crystal, which obstructed the growth of the zircon (i.e. negative form).

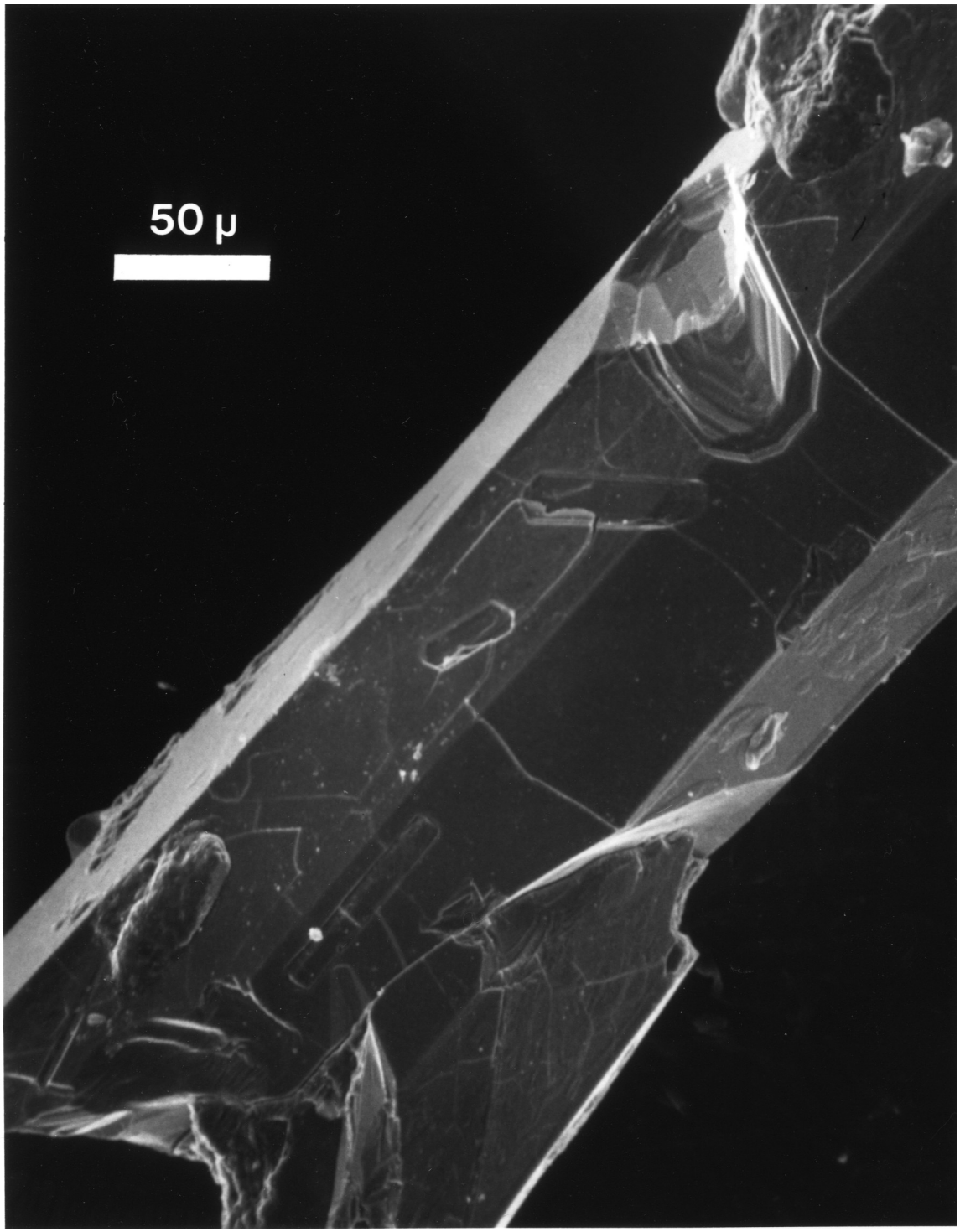
50 μ

Figure 46: SEM photomicrograph of very short, euhedral zircon crystal, which has developed an asymmetric combination of S7 and S8 morphologies. Compare with the length of zircon crystal pictured in Figure 47.

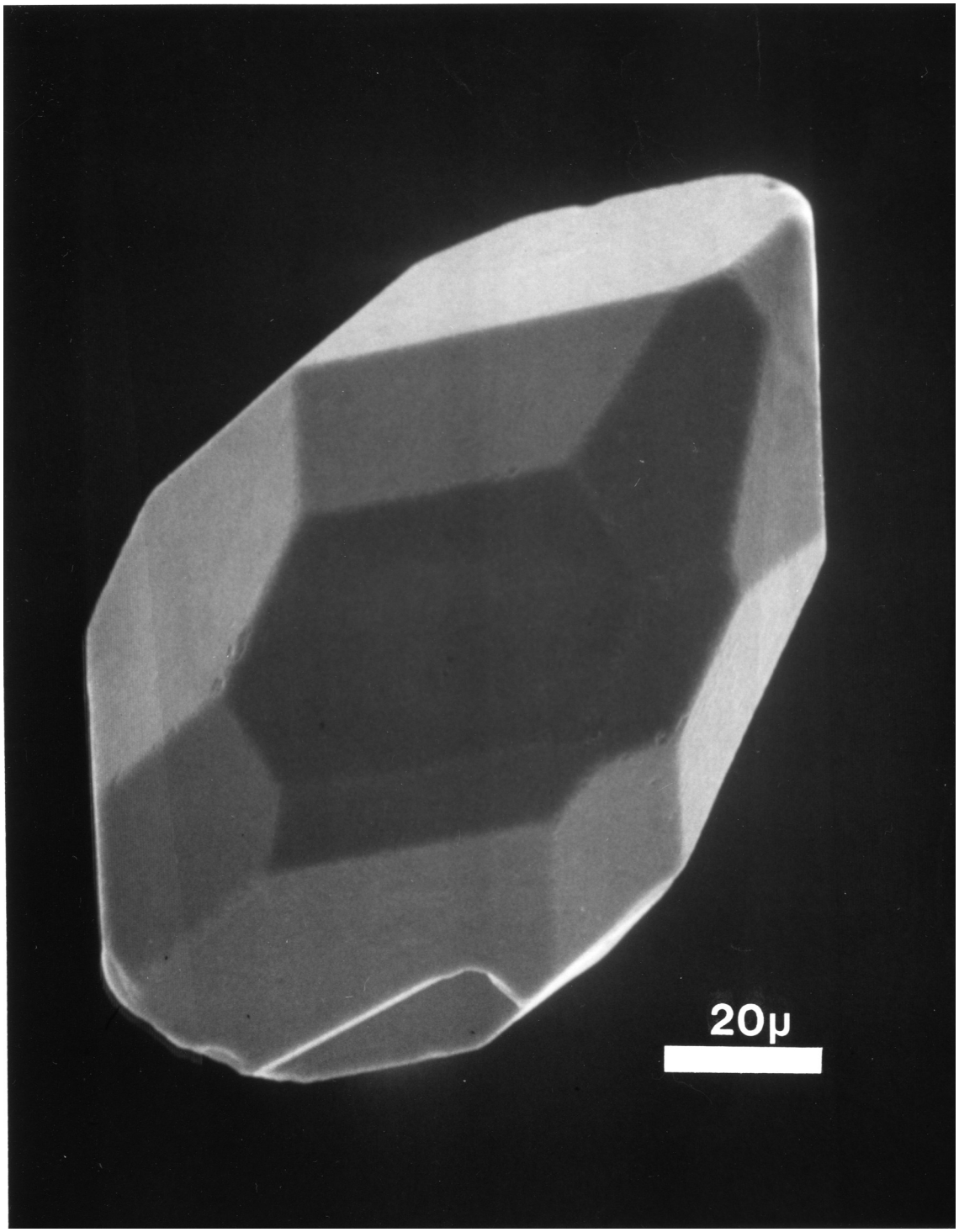
20μ

Figure 47: SEM photomicrograph of very long, euhedral zircon crystal, exhibiting a combination of S17 to S20 morphologies. Compare with short zircon crystal pictured in Figure 46.

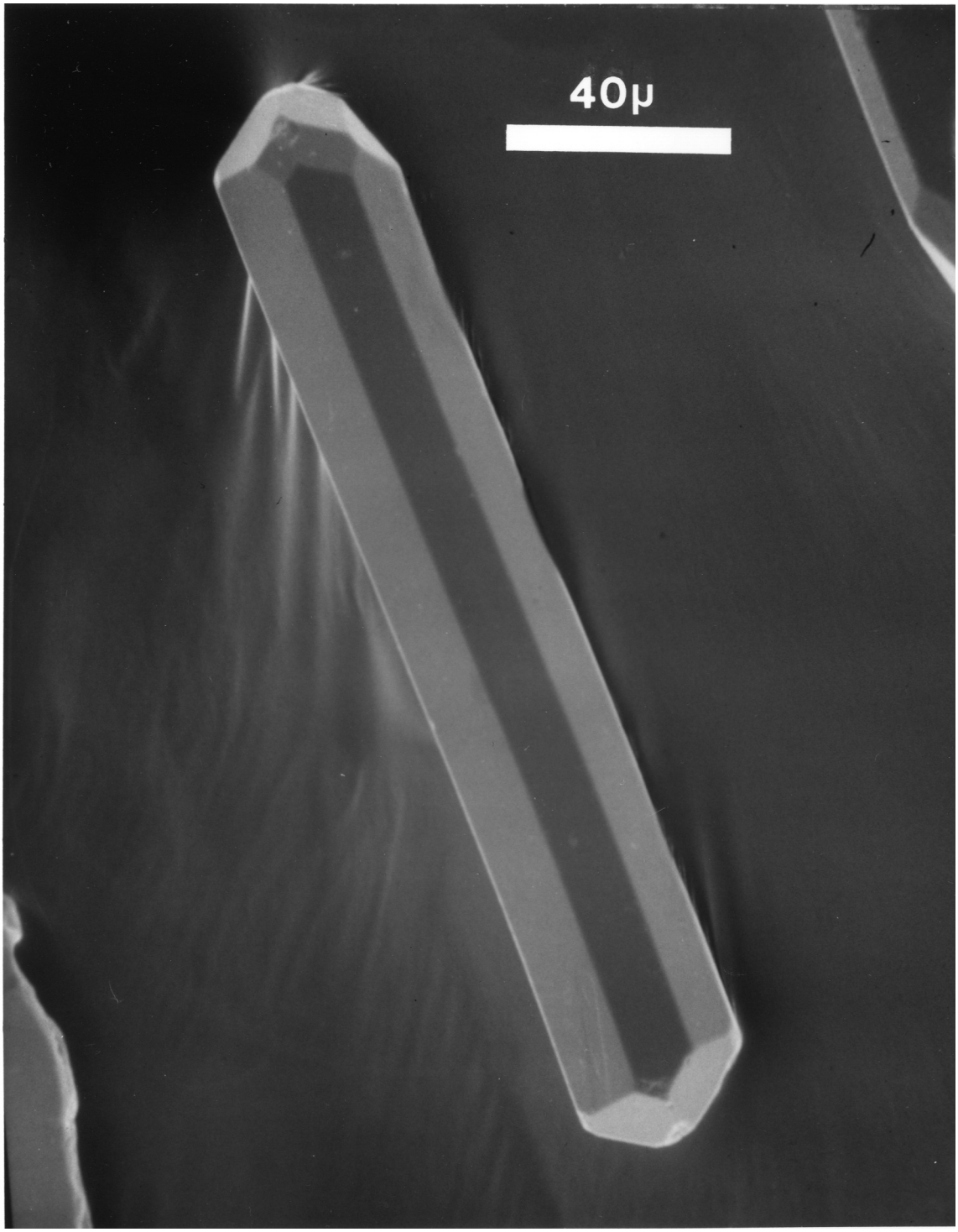
40μ

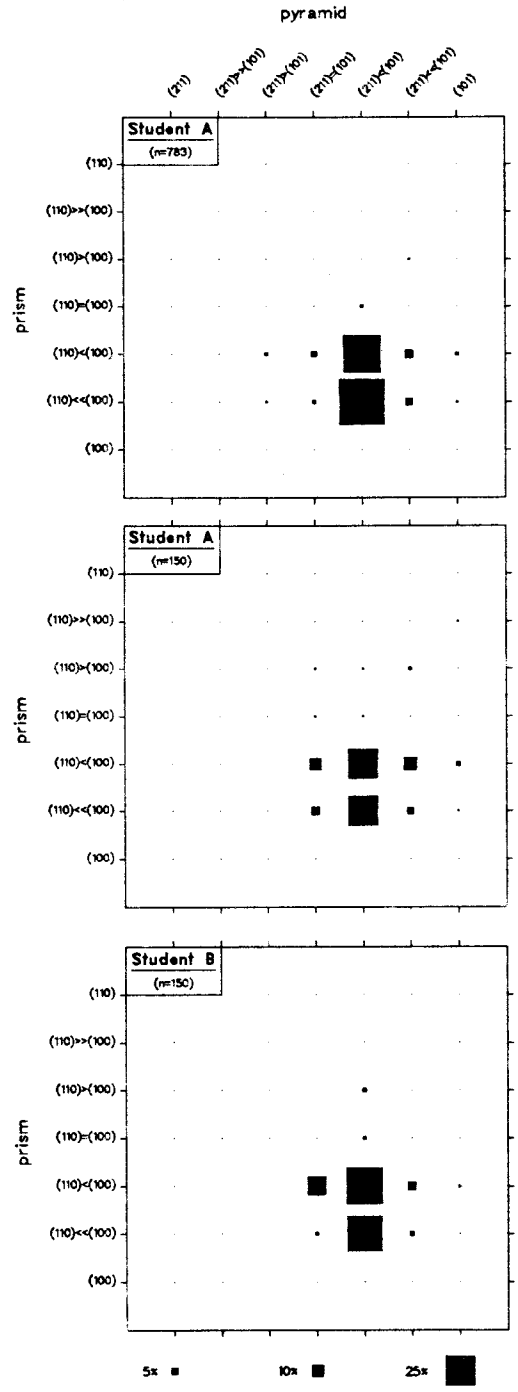

Figure 48: Comparison of the histograms that display the results of the morphology classification of 783 zircon grains from sample 89-050 by student A (upper diagram), and the classification of a subset (150 grains) from sample 89-050 by student A (middle diagram) and a second student B (lower diagram). See text for discussion.

differences relative to zircon populations from other K-bentonites. A sample-set containing fewer grains may, however, yield results that are slightly different from a study of a large sample set (150 versus 783 grains; Figure 48). The morphologic type was therefore determined for at least a total of 300 grains per sample. In order to avoid bias from broken grains in the typological study, each crystal tip was counted individually (i.e. two counts for whole grains).

4.4.1. Petrogenetic implications of zircon morphology

In order to make inferences about the petrogenesis of these altered volcanic ashes (i.e. K-bentonites) using zircon morphology, it is necessary to assume that the zircons are of phenocrystic origin. This assumption seems justified because (a) of the common occurrence of zircons that contain melt inclusions of rhyolitic composition (Chapter 2) and (b) the euhedral shape of the majority of zircon grains, which lack any sign of sedimentary transport (i.e. abrasion).

Mean points (Pupin and Turco, 1972c) were calculated for the zircon populations of the 16 Ordovician K-bentonites studied in order to interpret their morphologies with regard to the influence of temperature and chemical composition on zircon morphology (Pupin and Turco, 1975; Pupin, 1980) (Figure 49). The mean points align along two trends (Trenton-1 to Flat 6; and Can 27 to Can 14) indicative of zircon crystallization in I-type magmas (i.e. calc-alkaline series) (Pupin, 1980). Whereas populations that plot along the trend between the Trenton-1 and Flat 6 K-bentonites (Figure 49) may have crystallized in slightly more aluminous melts, those along the trend between Can 27 and Can 14 (Figure 49) indicate more alkaline melt compositions. However, whether these trends represent distinct differentiation series, and possibly different source-volcanoes, remains

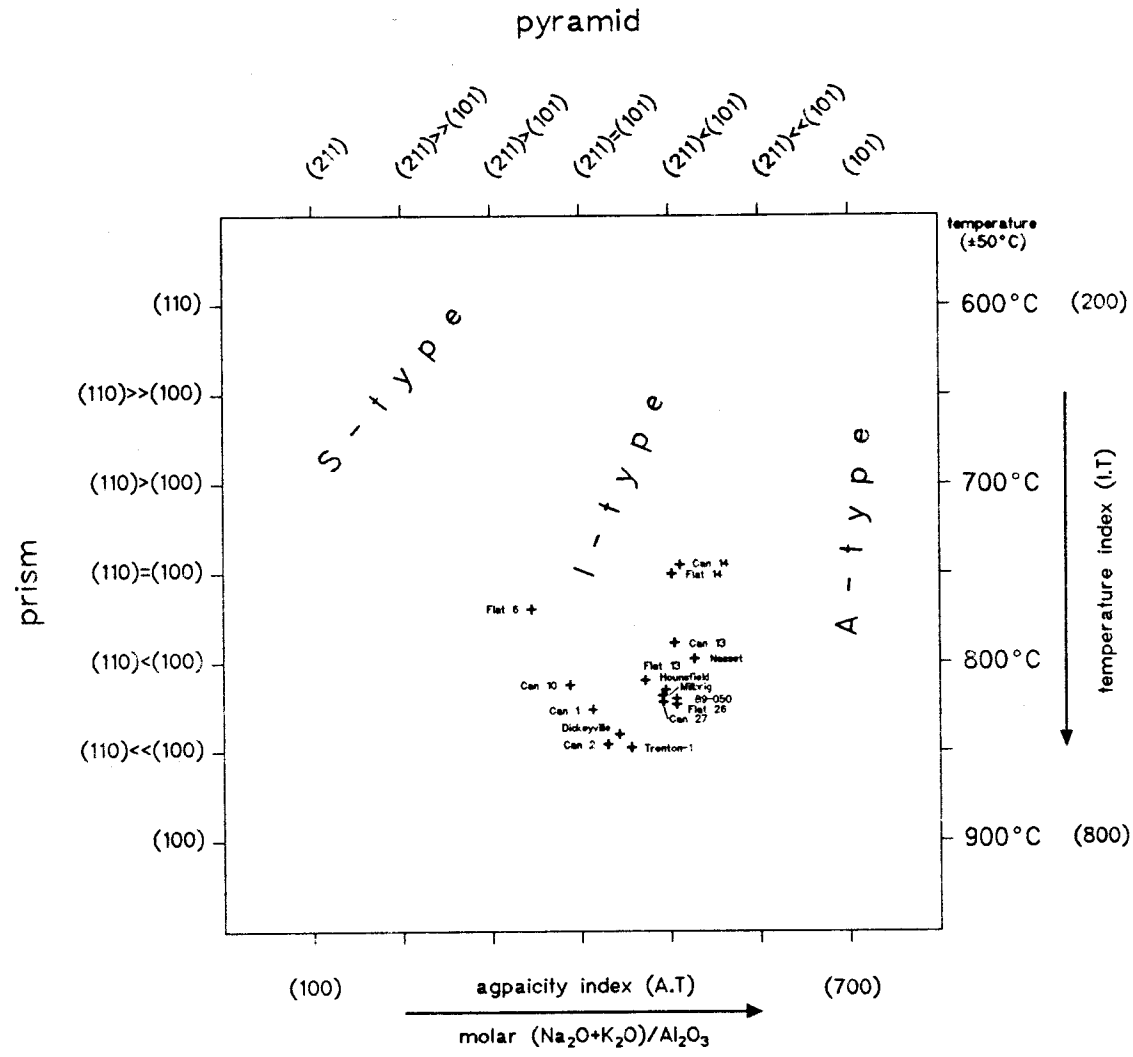

Figure 49: A plot of the mean points for the zircon populations of Ordovician K-bentonites in comparison with the distribution of mean points observed for zircon populations that crystallized in magmas of the indicated S-, I- or A-type (after Pupin, 1980). Mean point coordinates were calculated after Pupin and Turco (1972c).

unknown at this stage. Chemical analyses of associated melt inclusions and isotopic studies on phenocrysts (e.g. Rb-Sr, Sm-Nd), however, may help to solve these questions.

The temperature indices of the mean points (Figure 49) indicate zircon crystallization in the range from 750° to 850°C (Pupin, 1980). The error of these estimates (±50°C), however, is fairly large because the temperature scale was calibrated against crystallization temperatures of volcanic and plutonic rocks (Pupin and Turco, 1972a). Although these temperatures are only approximations, they are consistent with the interpretation that the zircons, and hence the K-bentonites, are of volcanic origin. This is furthermore supported by relatively small variations in proportions of the prisms {100} and {110} within each zircon population, which is explained as a result of interrupted zircon crystallization upon rapid cooling of erupted volcanics (Pupin, 1980).

The interpretation of zircon morphology as a petrogenetic indicator supports the evidence from the melt inclusion study (Chapter 2) that the Ordovician K-bentonites were produced by volcanic eruptions of silicic I-type magmas in an active continental margin.

4.4.2. Correlation of K-bentonites based on zircon morphology

Most of the samples in the present study were selected from the succession of K-bentonites in Canajoharie Creek and Flat Creek (New York State) because their stratigraphic relations are known from measured sections, which can be correlated from one locality to another (see Figure 3). Thus, the applicability of zircon morphology as a correlation tool could be tested on samples from K-bentonites that are known to be correlated (i.e., Can 27 with Flat 26; Can 14 with Flat 14; Can 13

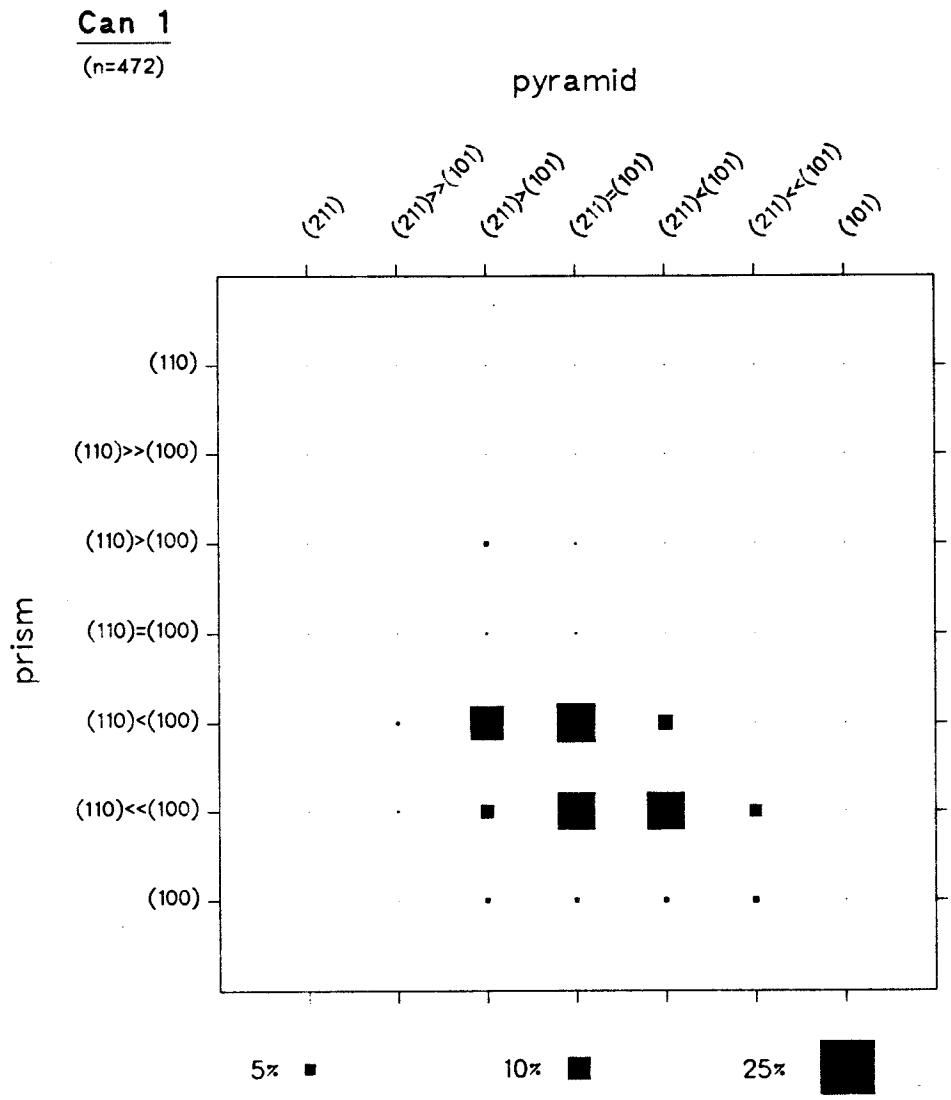

Figure 50: Histogram displaying the relative abundances of zircon morphologies from K-bentonite Can 1. Dominant morphologies are the S17, S18, S23, and S24 types.

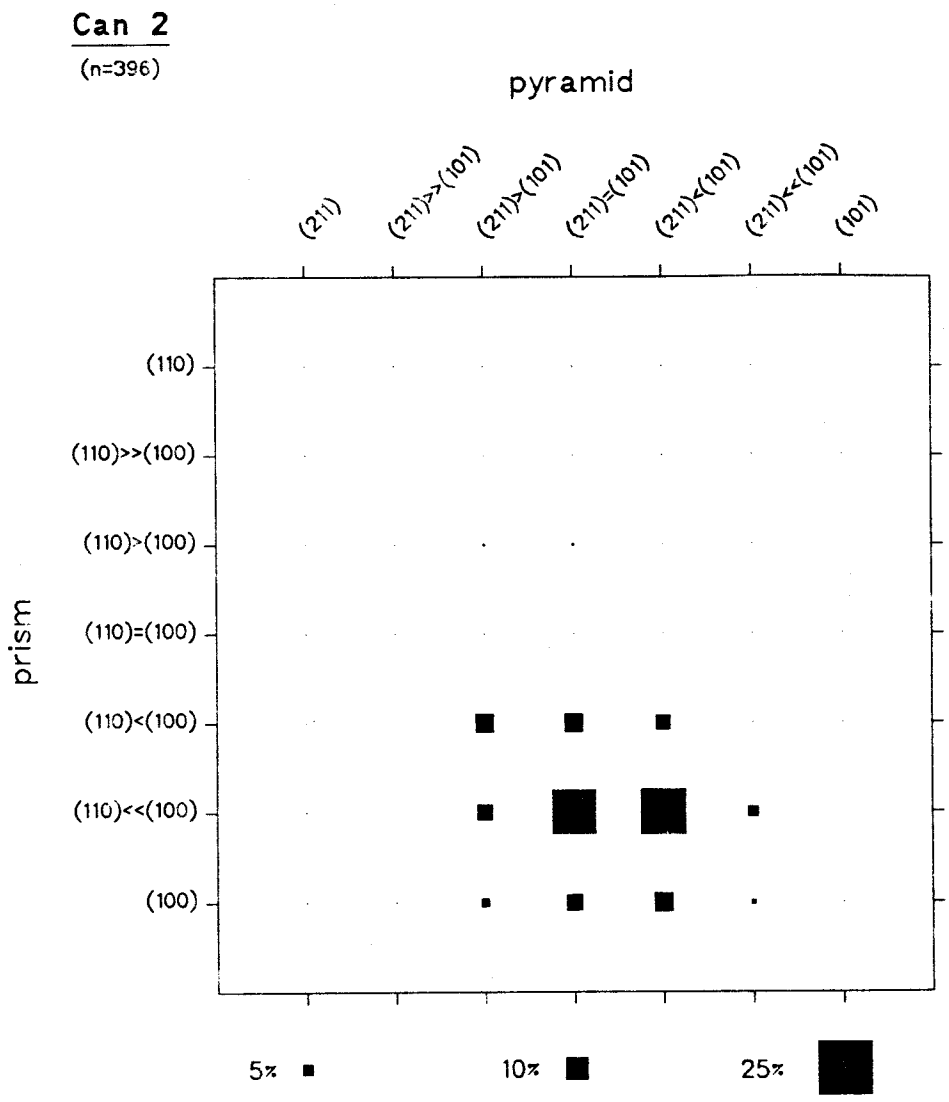

Figure 51: Histogram displaying the relative abundances of zircon morphologies from K-bentonite Can 2. Dominant morphologies are the S23 and S24 types.

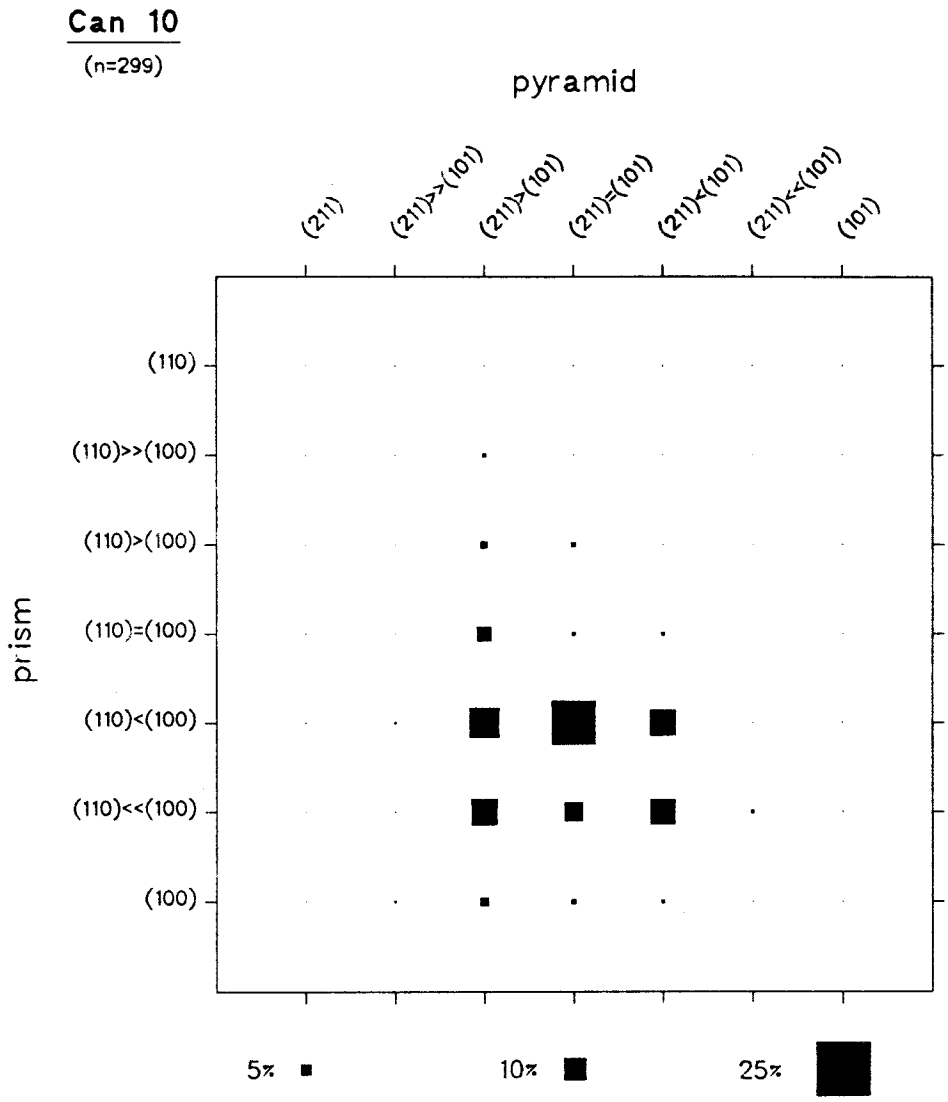

Figure 52: Histogram displaying the relative abundances of zircon morphologies from K-bentonite Can 10. Similarly abundant are the S18 and related morphology types (i.e. S17, S19, S22, S23, and S24).

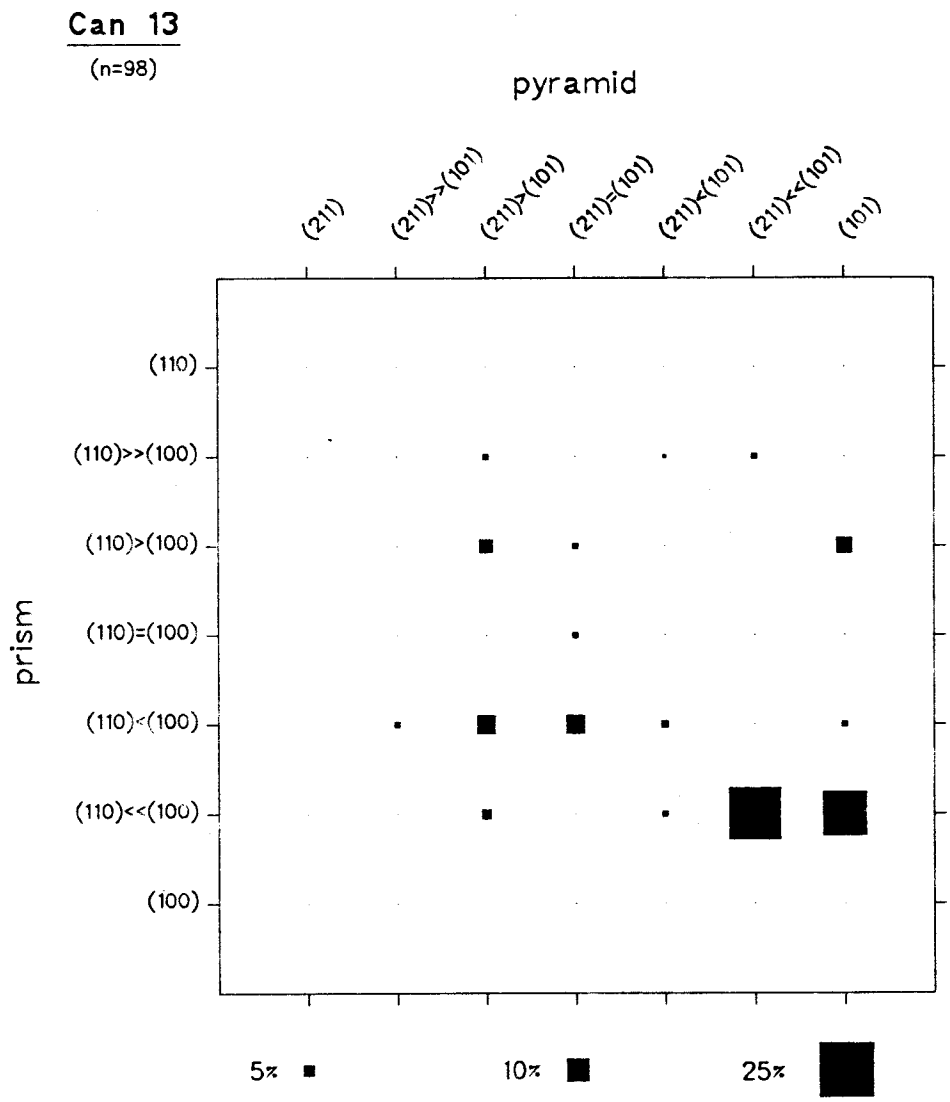

Figure 53: Histogram displaying the relative abundances of zircon morphologies from K-bentonite Can 13. Although the S25 and P5 morphology types seem to prevail, they are not considered representative of the zircon population because of the small number of euhedral zircons. Zircons of this K-bentonite are dominantly anhedral, rounded grains (see Figure 60).

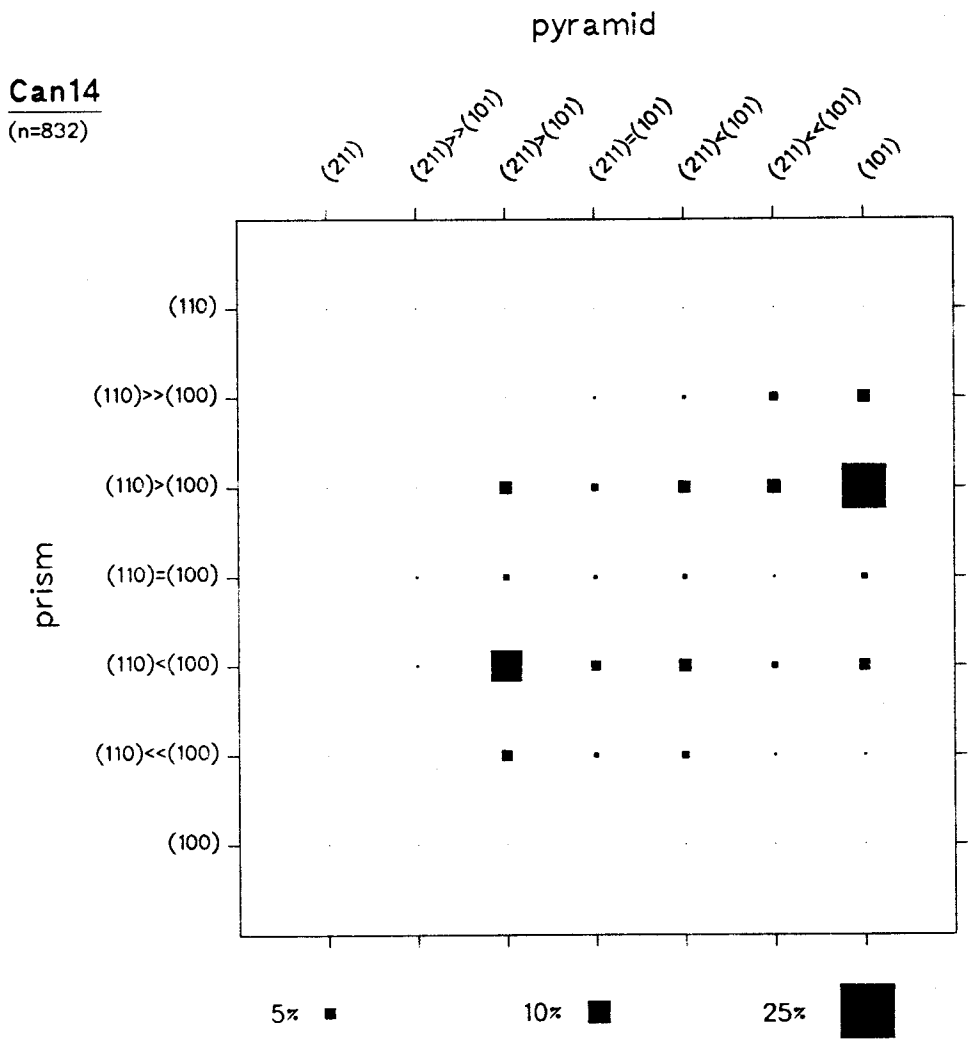

Figure 54: Histogram displaying the relative abundances of zircon morphologies from K-bentonite Can 14. Dominant are the contrasting S17 and P2 morphology types.

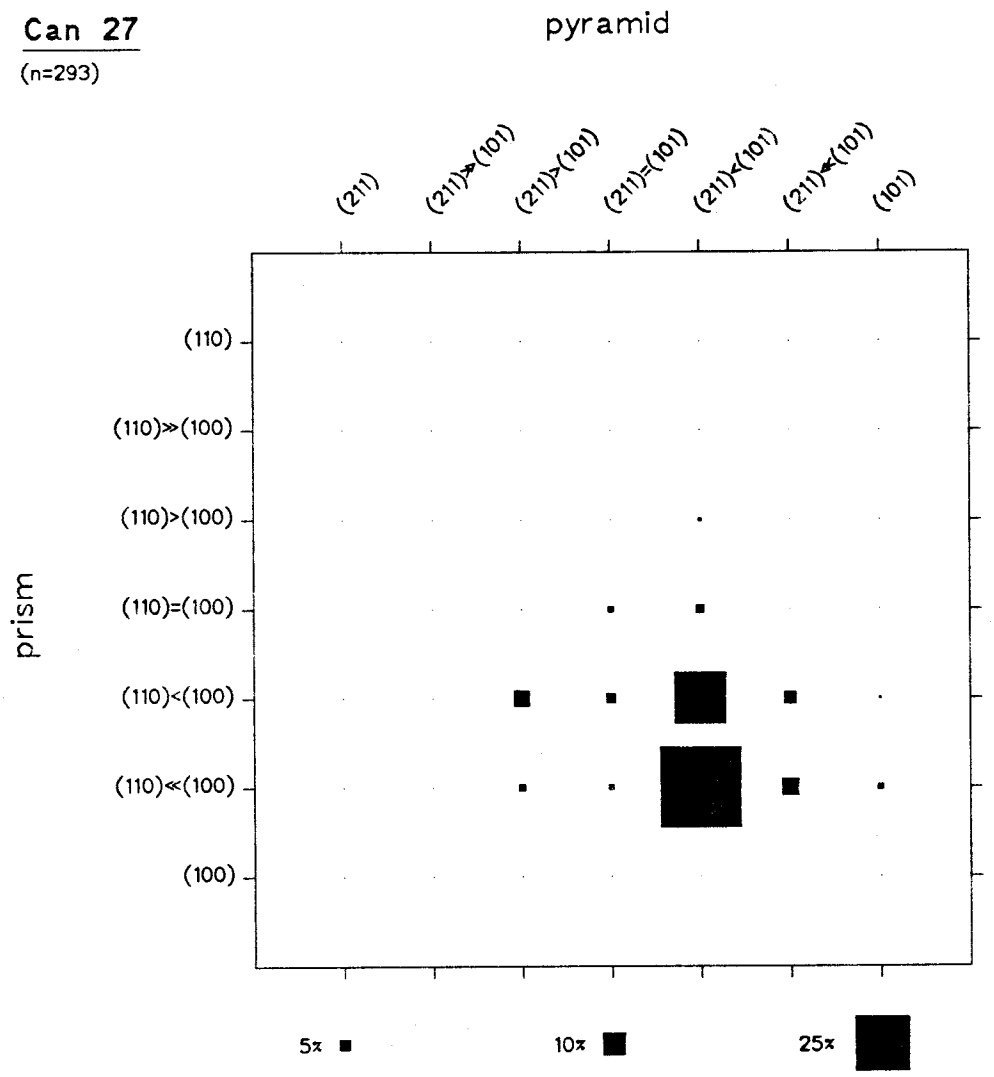

Figure 55: Histogram displaying the relative abundances of zircon morphologies from K-bentonite Can 27. Dominant morphologies are the S24 and S19 types.

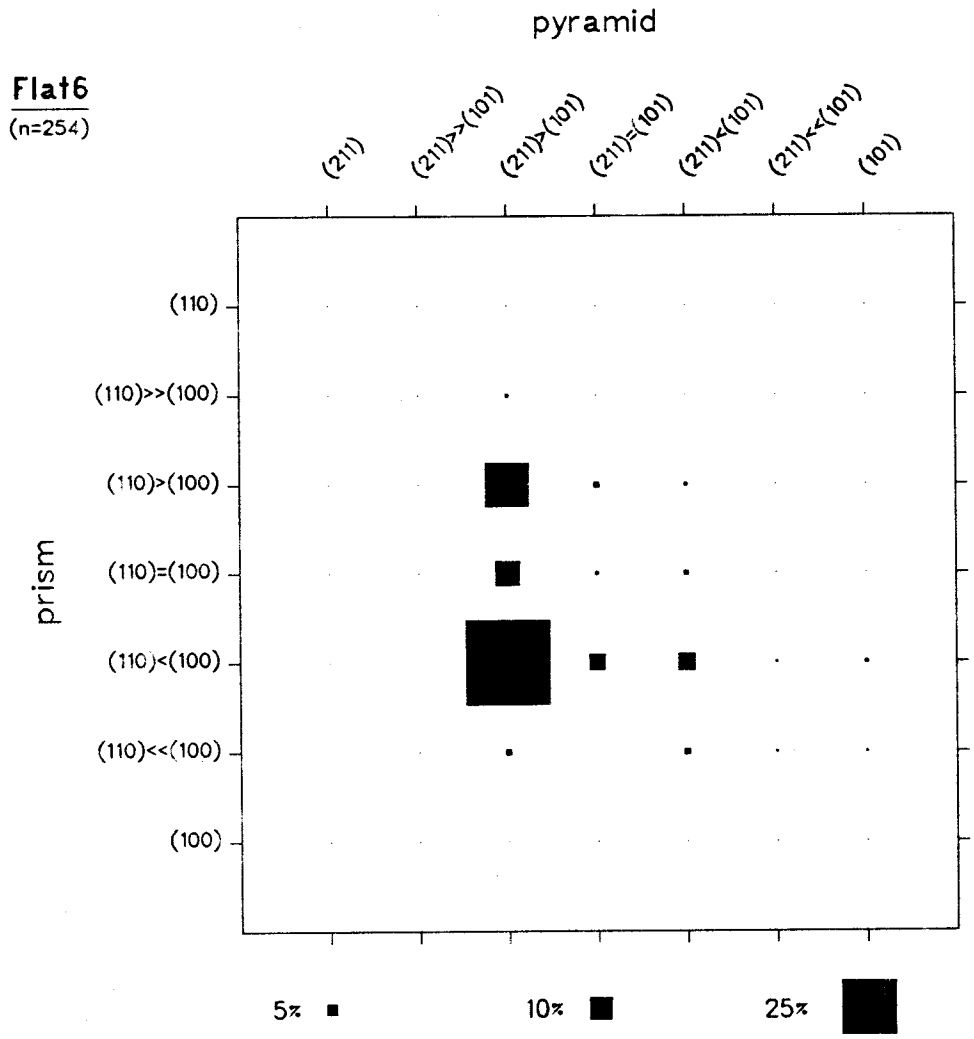

Figure 56: Histogram displaying the relative abundances of zircon morphologies from K-bentonite Flat 6. Dominant morphologies are the S17, S12 and S7 types.

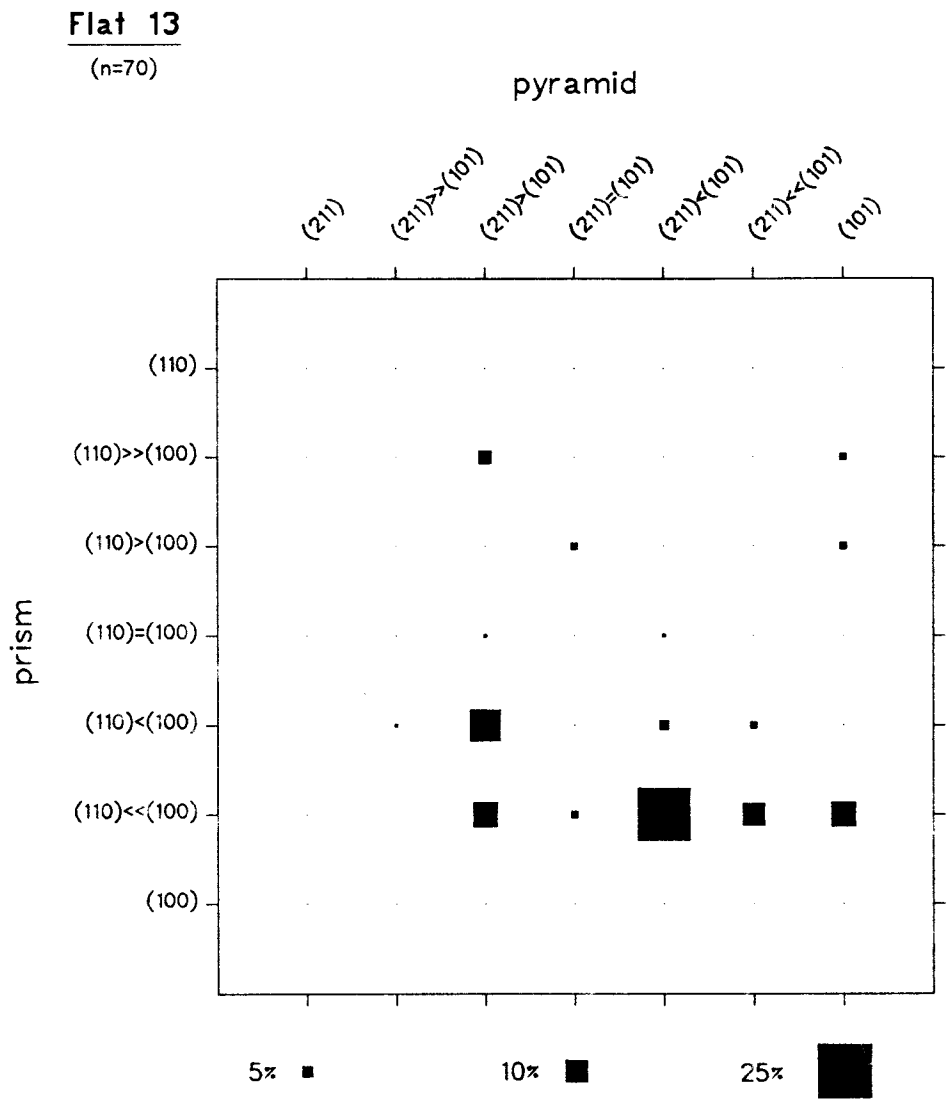

Figure 57: Histogram displaying the relative abundances of zircon morphologies from K-bentonite Flat 13. Similar to Can 13 (Figure 53), the prevalence of S24 and related morphology types is not considered representative due to the small number of euhedral crystals (see text for discussion). Zircons of anhedral, rounded morphology (see Figure 60) are dominant.

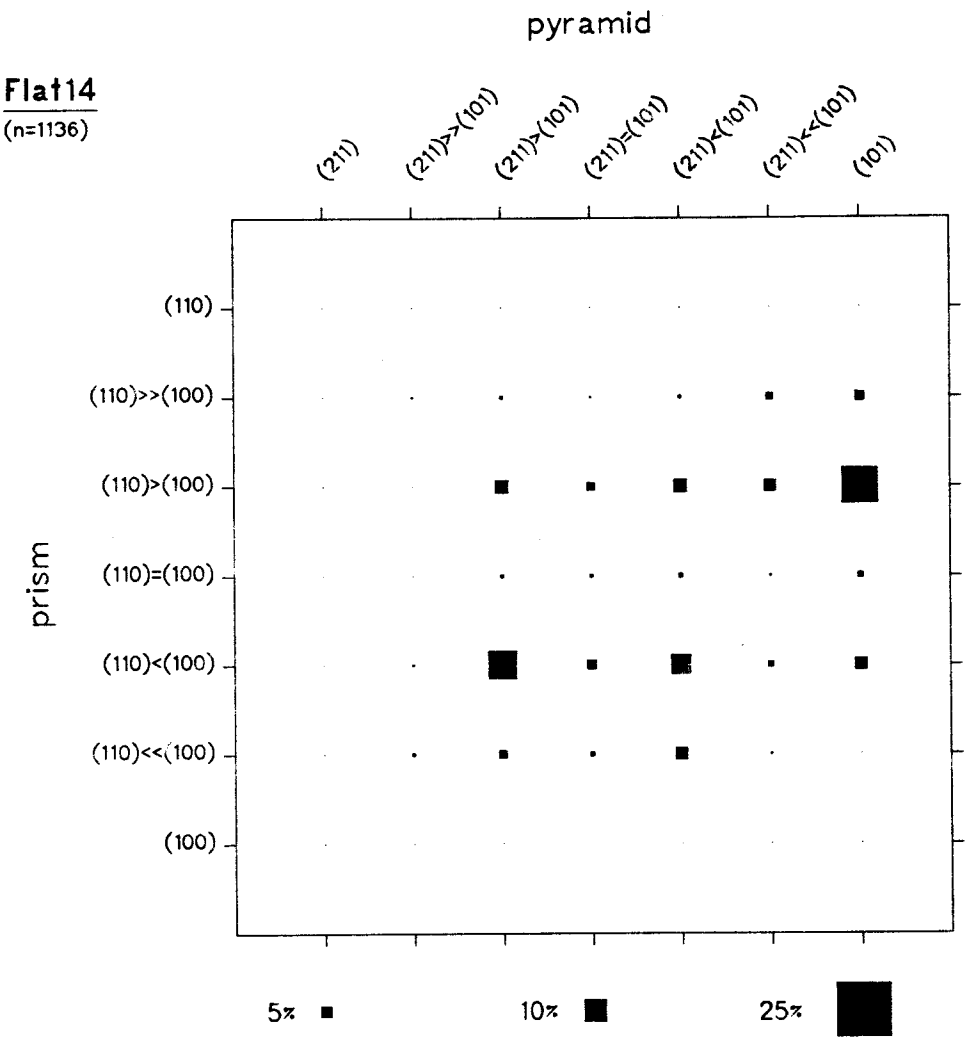

Figure 58: Histogram displaying the relative abundances of zircon morphologies from K-bentonite Flat 14. Dominant are the contrasting S17 and P2 morphology types.

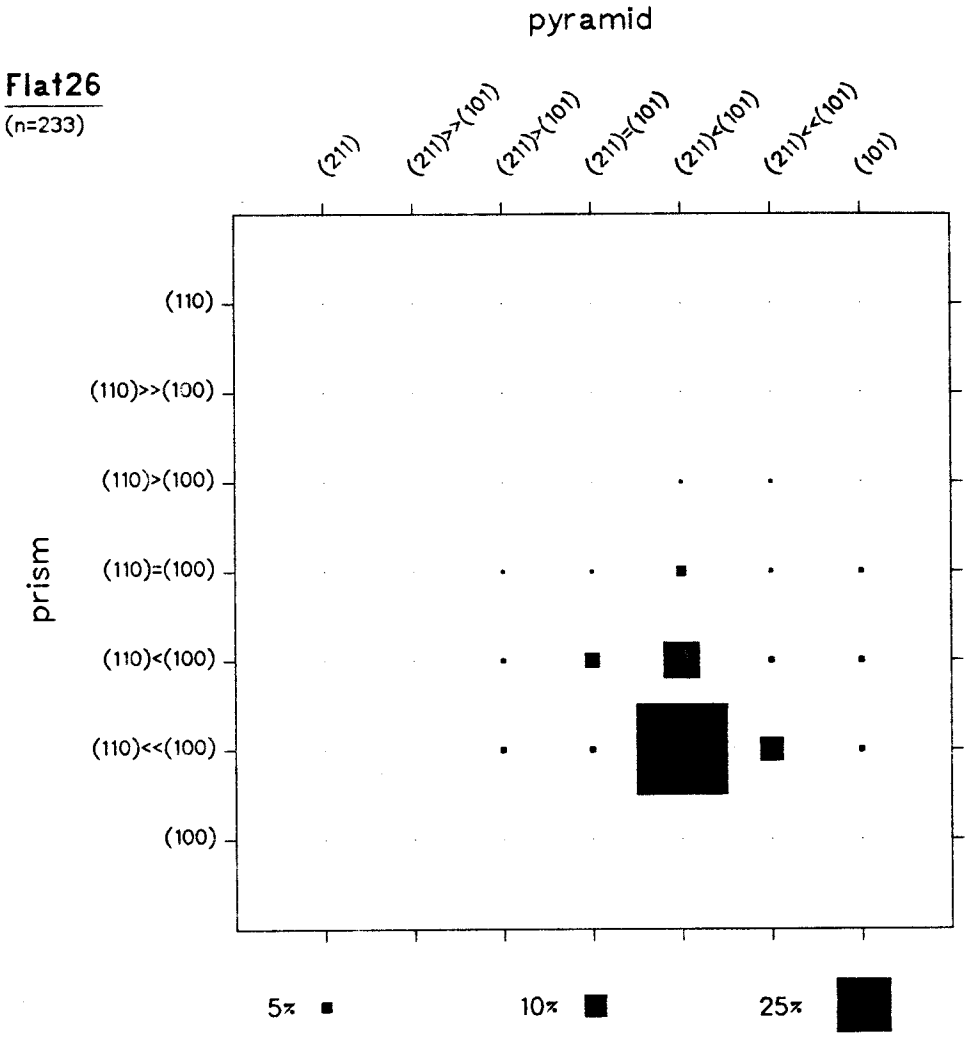

Figure 59: Histogram displaying the relative abundances of zircon morphologies from K-bentonite Flat 26. Dominant morphologies are the S24 and S19 types.

Figure 60: This SEM photomicrograph pictures a zircon grain that is representative of the prevalent morphology among the zircon populations in samples Can 13 and Flat 13. Note the anhedral shape of the grain, which exhibits a smooth surface without sign of abrasion due to sedimentary transport. Cracks on the surface of those grains were not observed.


20 µ

with Flat 13). Additional samples of K-bentonites (i.e., Can 1; Can 2; Can 10; Flat 6) from those sections were examined to see whether they contain zircon populations that are sufficiently distinct from another.

Figures 50 thru 56 illustrate that different K-bentonites (e.g., Can 1; Can 2; Flat 6; Can 10; Can 13; Can 14; Can 27) (Figure 3) indeed contain morphologically distinct zircon populations. Although the majority of the zircon populations exhibits a distribution of related morphologies around a central type, individual populations have developed distinctive variations either among the prisms (e.g. Can 27, Flat 6; Figures 55, 56) or among the pyramids (e.g. Can 1, Can 2; Figures 50, 51). More diverse, and hence characteristic, populations showing for example development of two contrasting morphologic types (e.g. Can 14; Figure 56) were also observed.

The histograms in Figures 56 and 58, as well as those in Figures 55 and 59, illustrate that samples from correlated K-bentonites, which were collected at different localities (e.g. Can 14 and Flat 14; Can 27 and Flat 26; compare Figure 3), yield zircon populations that are morphologically indistinguishable from another. Samples Can 13 and Flat 13 (Figures 53 and 57), on the other hand, represent a single K-bentonite that could not be correlated based on the morphology of euhedral zircons, which comprise less than 15 percent of each population. However, a correlation is possible because the majority of the zircons in both samples consists of anhedral, rounded grains with a characteristic smooth surface (Figure 60), in contrast to the surface of grains that were rounded due to abrasion during sediment transport (Figure 67).

The results of this local correlation experiment indicate that the morphology of zircon populations, which may contain euhedral as well as anhedral grains, can be used for correlation of Late Ordovician K-bentonites. Hence, the zircon populations of several other K-bentonites were studied, for which longer-distance

correlation had been independently suggested (e.g. by stratigraphy). The samples that were selected for this purpose are the Hounsfield, Trenton-1, and 89-050 K-bentonites from New York State and the Millbrig, Dickeyville, and Nasset K-bentonites from the upper Mississippi Valley.

The K-bentonite 89-050 (West Canada Creek area south of Middleville, NY.) is identical to the M37 bed of Cisne et al. (1982), which those authors correlated with a set of four K-bentonites in Canajoharie Creek and Flat Creek. These four K-bentonites correspond to Can 14, Can 15, Can 16 and Can 17 in Canajoharie Creek and the respective K-bentonites in Flat Creek (Cisne, personal communication, 1989; Table I.). However, upon comparing Figures 54, 58, and 61 it is readily apparent that (a) Can 14 and Flat 14 represent a single K-bentonite, but (b) 89-050 contains a zircon population that is morphologically distinct. This latter view is also consistent with the evidence from melt inclusions (Chapter 2). However, the K-bentonite represented by samples Can 27 (Canajoharie Creek) and Flat 26 (Flat Creek), which are about 20 meters stratigraphically above Can 14 and Flat 14 (Figure 3), contain a zircon population (Figures 55 and 58) that is morphologically indistinguishable from that of K-bentonite 89-050 (Figure 61). This is interpreted to mean that the K-bentonite 89-050 is correlated with a single bed represented by Can 27 and Flat 26, rather than the set of four K-bentonites proposed by Cisne et al. (1982).

Based on morphologically identical zircon populations, it is now possible to correlate two different K-bentonites between the upper Mississippi Valley and New York State. Figures 62 and 63 support the suggestion of Kay (1931) that the Hounsfield K-bentonite is identical with the Millbrig K-bentonite, whereas Figures 64 and 65 indicate that the Dickeyville K-bentonite is correlated with the Trenton-1 K-bentonite. The Nasset K-bentonite (Figure 66), however, could not be correlated with any of the K-bentonites from New York State that have been studied

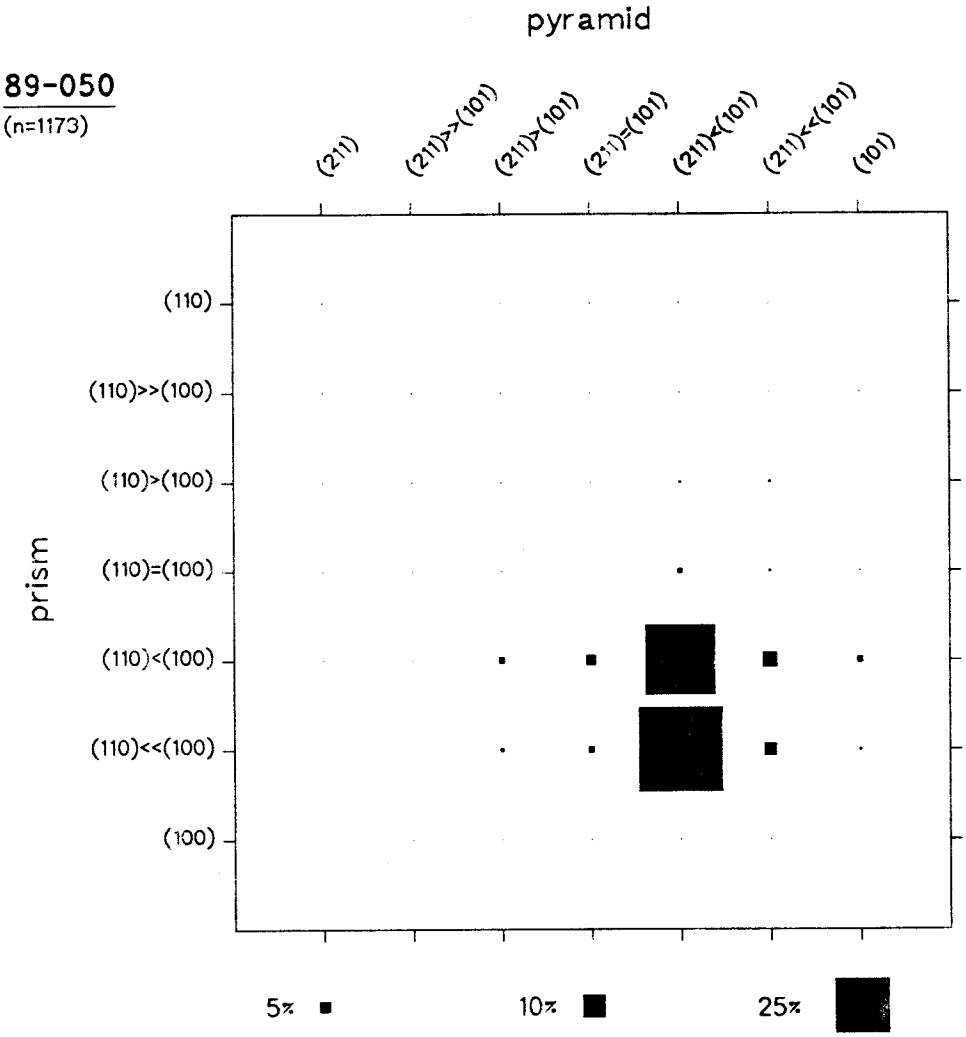

Figure 61: Histogram displaying the relative abundances of zircon morphologies from K-bentonite 89-050. Dominant morphologies are the S24 and S19 types.

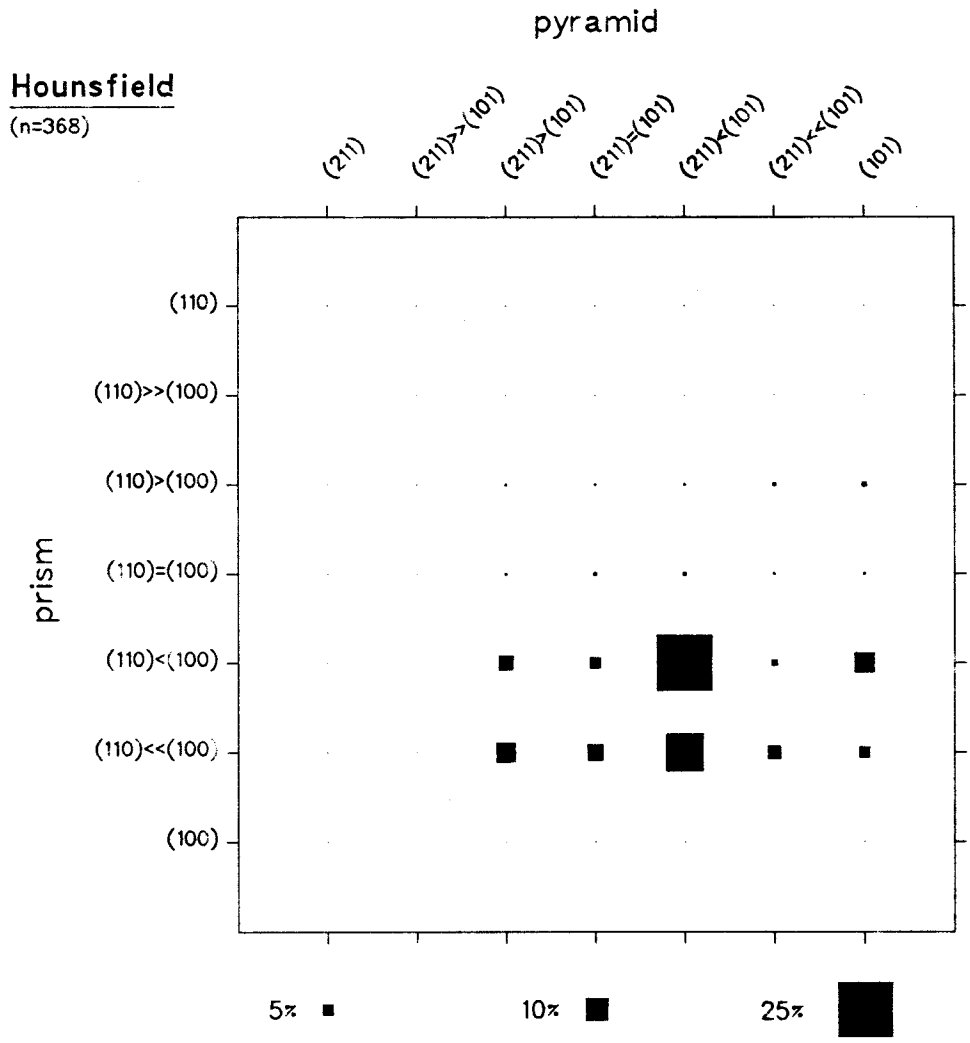

Figure 62: Histogram displaying the relative abundances of zircon morphologies from the Hounsfield K-bentonite. Dominant morphologies are the S19 and S24 types.

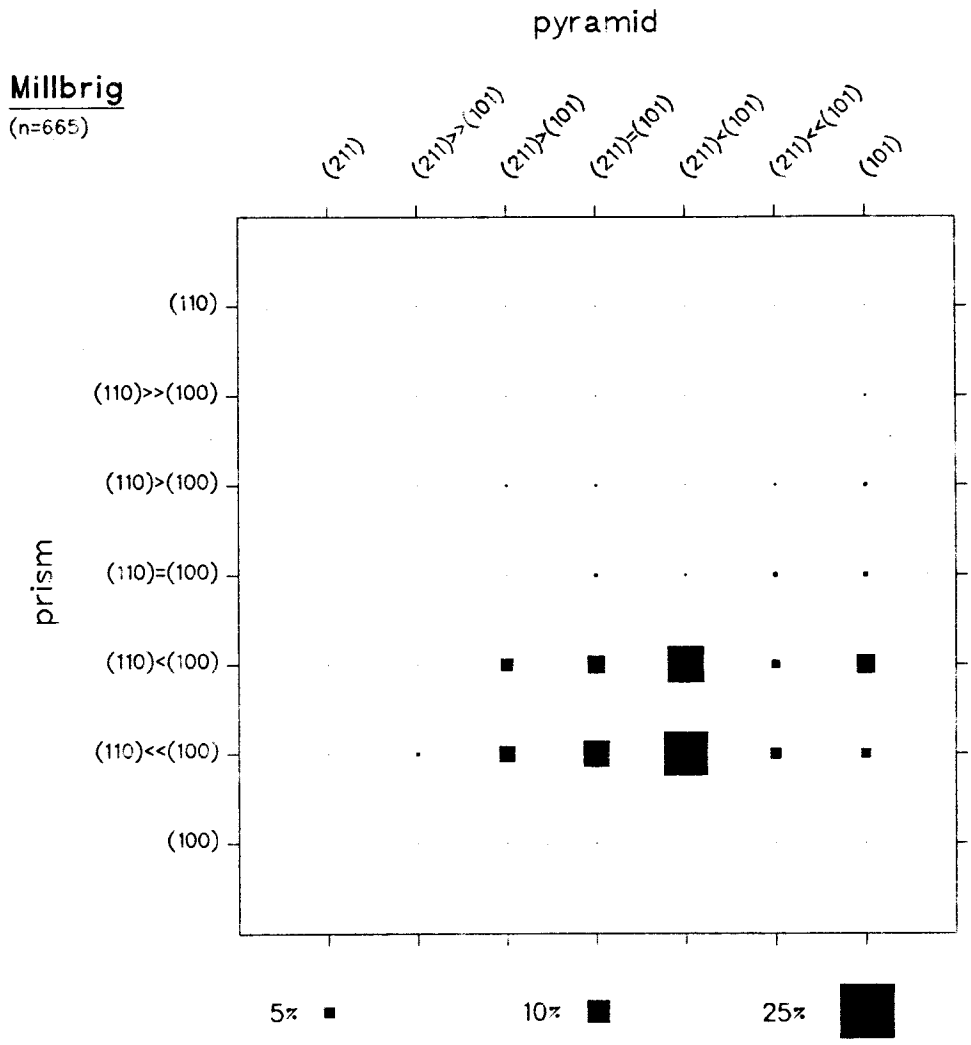

Figure 63: Histogram displaying the relative abundances of zircon morphologies from the Millbrig K-bentonite. Dominant morphologies are the S24 and S19 types.

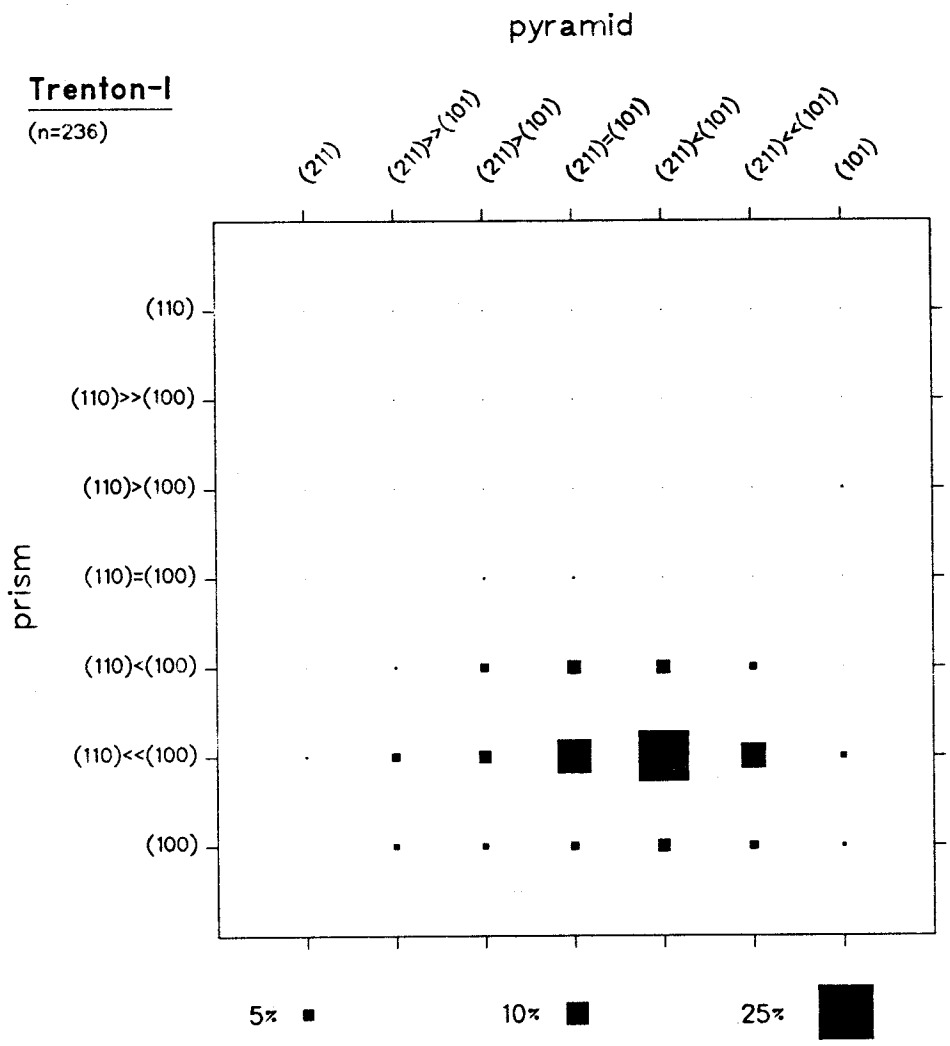

Figure 64: Histogram displaying the relative abundances of zircon morphologies from the Trenton-1 K-bentonite. Dominant morphologies are the S24 and S23 types.

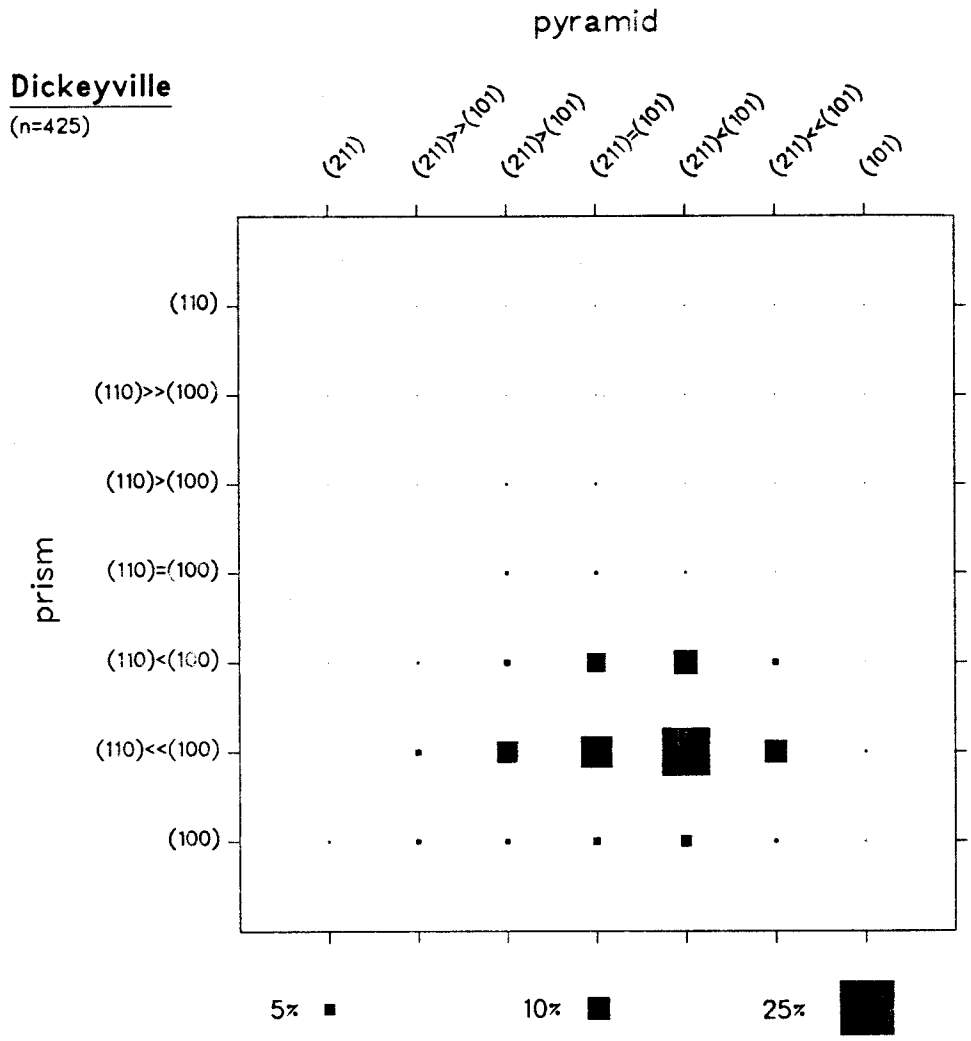

Figure 65: Histogram displaying the relative abundances of zircon morphologies from the Dickeyville K-bentonite. Dominant morphologies are the S24 and S23 types.

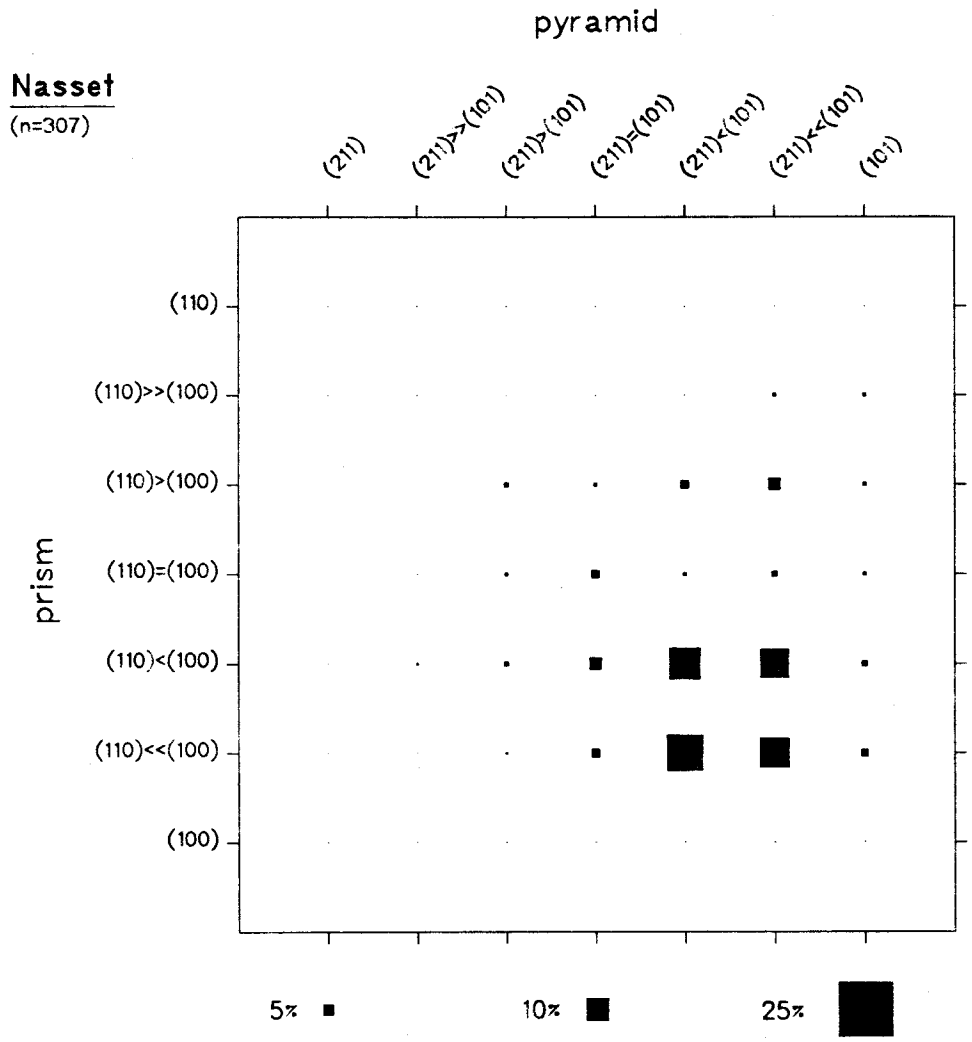

Figure 66: Histogram displaying the relative abundances of zircon morphologies from the Nasset K-bentonite. The dominating S24, S25, and S19 and S20 morphology types are approximately equally abundant.

so far, although Templeton and Willman (1963) suggested its correlation with a K-bentonite at the top of the Poland Formation in the Trenton Falls section, NY (Kay, 1943). The stratigraphic position of that K-bentonite is between the Trenton-1 and the 89-050 K-bentonites (Kay, 1943), which is equivalent to the stratigraphic interval that comprises all K-bentonites in Canajoharie Creek (Figure 1), implying that the Nasset, if present in New York State, is likely to be correlated with one of the unstudied K-bentonites within this stratigraphic interval.

The successful correlation of the Hounsfield and Millbrig K-bentonites demonstrates the advantage of using zircon morphology for correlation purposes because the small amount of material (about 200 grams) from the Hounsfield was contaminated with soil and could not have been used for methods such as chemical fingerprinting. Zircons, however, that are derived from soil, can be clearly distinguished from zircon phenocrysts based on their morphology. A morphological study of a soil sample revealed a zircon population (130 grains) that consists entirely of abraded, anhedral or fragmented zircon grains (Figures 67, 68, 69). Whereas the majority of the zircons (65 percent) in the Hounsfield sample consists of euhedral crystals, the remaining grains exhibit morphologies indicative of soil contamination. Although samples of K-bentonites should, nevertheless, be collected with great care, these results demonstrate that even extremely thin layers (less than 5 mm) of K-bentonites (e.g. Hounsfield), which are susceptible to contamination, can be correlated using zircon morphology.

All K-bentonites were included in the calculation of a morphology-based correlation matrix, for which similarity coefficients (Borchardt et al., 1972) were calculated for all combinations of K-bentonites. The similarity coefficient is an average of ratios of the relative abundances of morphology types in two zircon populations (i.e. K-bentonites). The ratios are calculated for each morphologic

Figure 67: SEM photomicrograph illustrating a completely rounded zircon from a soil sample. Rounded shape and surface texture indicate aeolian transport (after Krinsley and Doornkamp, 1973).


20 µ

Figure 68: SEM photomicrograph of an anhedral zircon with smooth surface from a soil sample. Surface of the grain is smooth, although exhibiting network of extensive cracks.

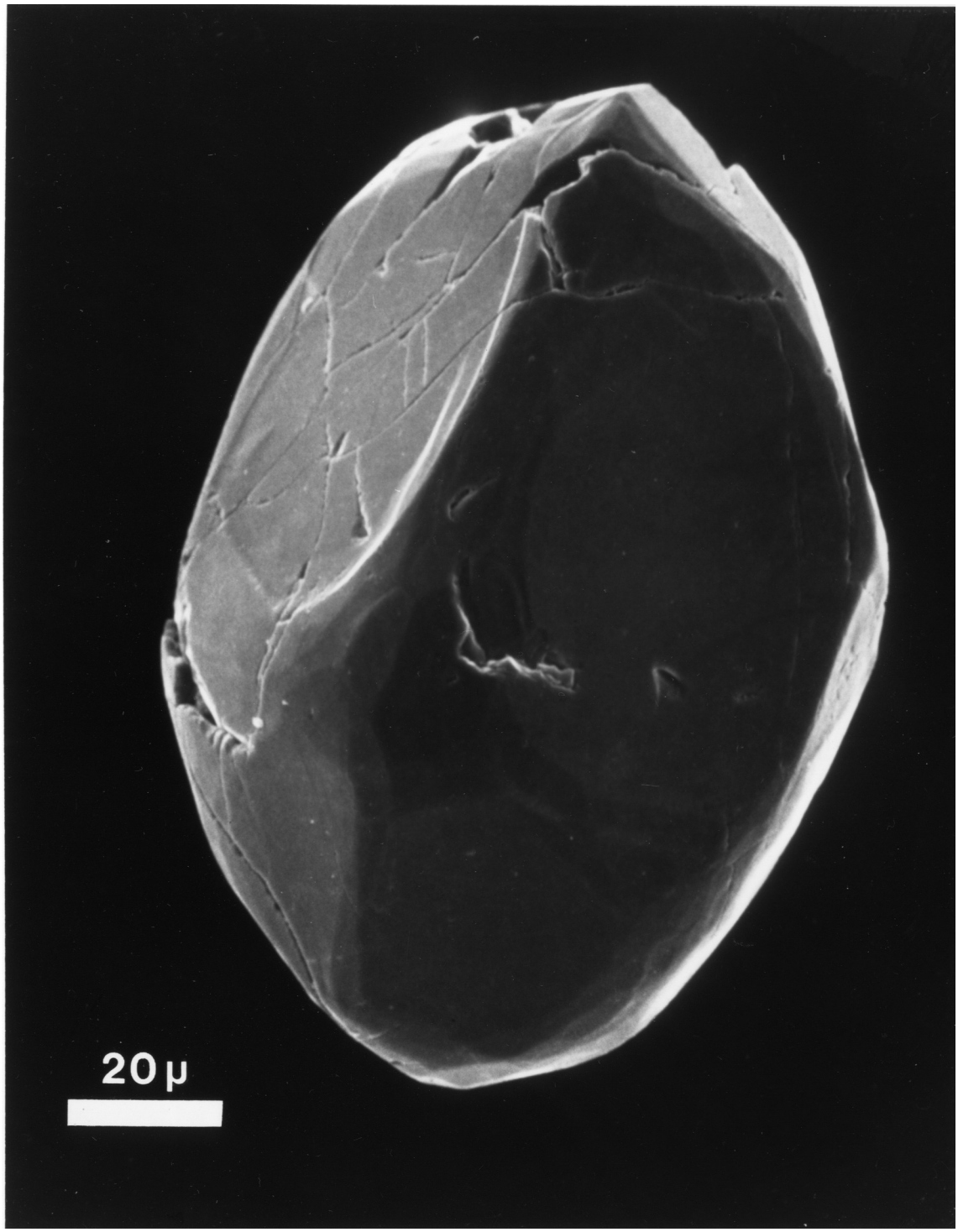
20 µ

Figure 69: SEM photomicrograph of an angular zircon grain from a soil sample that exhibits conchoidal fractures and sharp edges without any sign of rounding, which is characteristic for grains of glacial sediments (after Krinsley and Doornkamp, 1973).

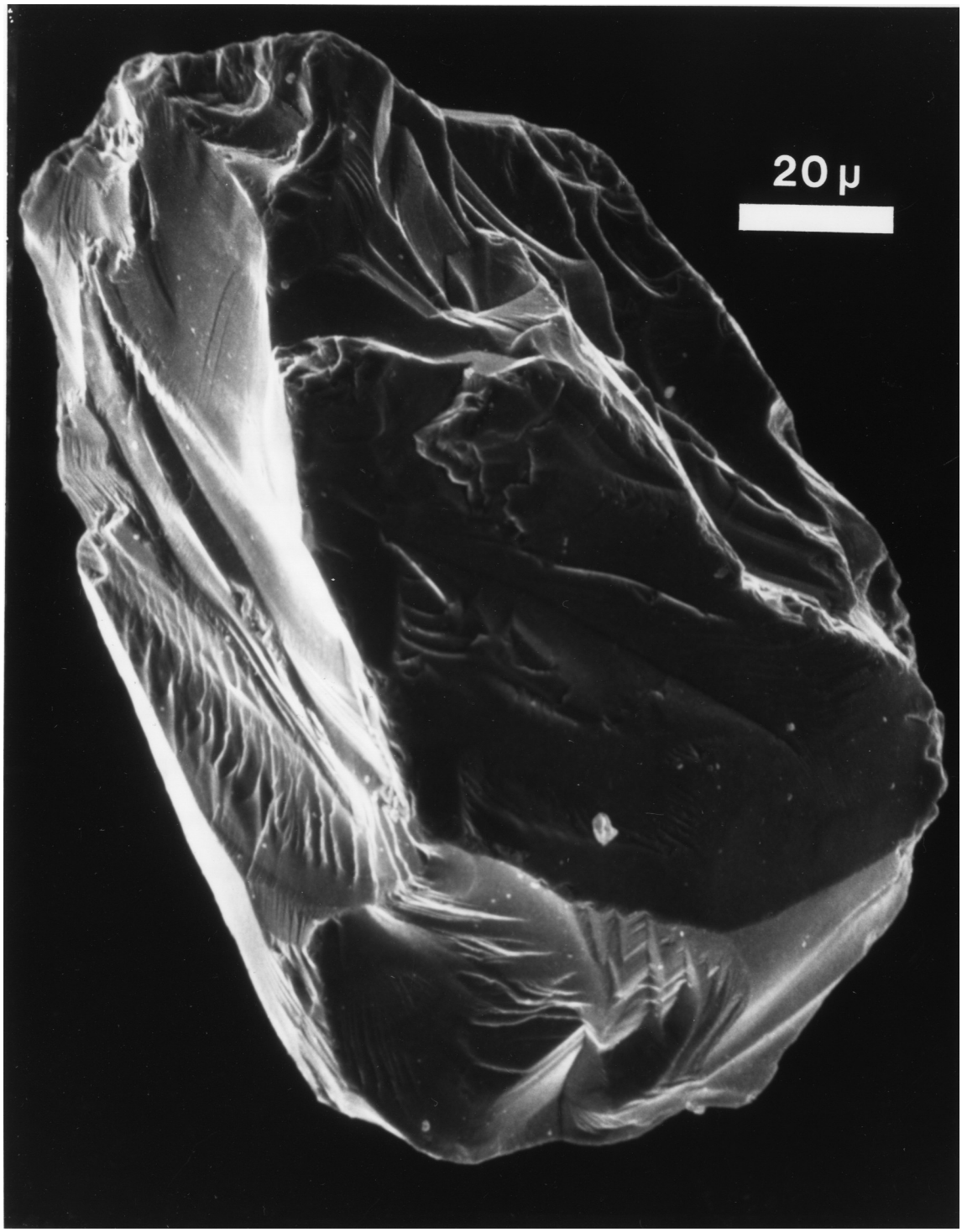
20 µ

type by dividing the smaller relative abundance in one sample by the higher relative abundance in another sample, such that the ratio is always less than one. Relative abundances of less than one percent were considered not present and therefore set to zero. In the ideal case of identical samples, the average ratio (i.e. similarity coefficient) would be unity. In practice, however, the similarity coefficients of samples that are known to be identical (e.g. 89-050) range from 0.75 to 0.91 (Table IX.). The smaller, non-ideal values for the similarity coefficients are due to the fact that the sample sizes examined by students A and B contained too few grains to be representative of the zircon population. However, similarity coefficients among samples known to be representative (i.e. stamps 1, 2 and 3; Table IX.) yield coefficients that range from 0.85 to 0.91.

Similarity coefficients of zircon populations from pairs of uncorrelated K-bentonites yield values that are lower (0.48 to 0.84; Table X.) than those expected for identical samples (i.e. >0.85). An exception is the similarity coefficient of 0.88 for K-bentonites Can 1 and Can 2, which are known to be different layers (Figure 3) and that contain distinct zircon populations according to the histograms (compare Figures 50 and 51).

The K-bentonites known to be correlated yield similarity coefficients (0.82 to 0.91) that are always highest among the combinations with other samples (Table X.) and close to the values expected from identical samples (i.e. >0.85). The only exception is the low coefficient for Can 13 and Flat 13 (0.67), which is due to the small abundance of euhedral zircons in these samples.

These results indicate that although a matrix yields the same correlations as suggested by individual morphology histograms, possible ambiguities among the similarity coefficients limit its reliability. This apparent limitation may eventually be avoided by using digital image processing for the morphologic classification, which would dramatically enhance the resolution of this method.

Table IX.: Correlation matrix for morphologic classification of zircon populations from K-bentonite 89-050, studied on several stamps (1;2;3), and by different students (A and B).

	stamp 1	stamp 2	stamp 3	Student A	Student B
stamp 1	-	0.85	0.91	0.75	0.90
	stamp 2	-	0.85	0.82	0.84
		stamp 3	-	0.76	0.87
			Student A	-	0.83

Table X.: Correlation matrix for morphologic classification of zircon populations from different Paleozoic K-bentonites.

	Can 2	Can 10	Can 13	Can 14	Can 27	Flat 6	Flat 13	Flat 14	Flat 26	89-050	Hounsfield	Trenton-I	Millbrig	Dickeyville	Nasset
Can 1	0.88	0.78	0.64	0.58	0.69	0.64	0.66	0.54	0.64	0.81	0.67	0.77	0.66	0.78	0.60
Can 2		0.75	0.64	0.61	0.74	0.66	0.66	0.55	0.69	0.76	0.72	0.82	0.72	0.84	0.60
Can 10			0.68	0.62	0.68	0.75	0.68	0.65	0.64	0.72	0.68	0.69	0.64	0.74	0.62
Can 13				0.63	0.66	0.73	0.67	0.65	0.62	0.65	0.67	0.55	0.65	0.58	0.62
Can 14					0.66	0.70	0.69	0.91	0.68	0.69	0.67	0.53	0.62	0.53	0.68
Can 27						0.73	0.72	0.66	0.82	0.86	0.82	0.71	0.76	0.72	0.75
Flat 6							0.66	0.72	0.68	0.72	0.68	0.56	0.63	0.61	0.67
Flat 13								0.67	0.72	0.72	0.73	0.62	0.66	0.62	0.63
Flat 14									0.66	0.67	0.69	0.48	0.62	0.53	0.68
Flat 26										0.84	0.76	0.69	0.79	0.67	0.78
89-050											0.81	0.70	0.75	0.72	0.77
Hounsfield												0.68	0.86	0.72	0.74
Trenton-I													0.70	0.87	0.58
Millbrig														0.73	0.69
Dickeyville															0.60

4.5. Conclusions

1. Based on the identical morphology of their zircon populations, a correlation of the Hounsfield K-bentonite (New York State) with the Millbrig K-bentonite (upper Mississippi Valley) seems assured.

2. This correlation (Hounsfield and Millbrig) indicates that individual volcanic layers were deposited and preserved over the entire area of K-bentonite occurrences in eastern North America (between the Mississippi Valley and northeastern United States) covering an area of more than 1,200,000 km^2.

3. Identical morphologies of zircon populations indicate that the lower of two K-bentonites (i.e. Trenton-1) in the Kings Falls limestone east of Middleville, NY is correlated with the Dickeyville K-bentonite in the upper Mississippi Valley.

4. Data on zircon populations do not support the correlation of K-bentonite 89-050 south of Middleville, NY (M37 bed of Cisne et al., 1982) with a set of four K-bentonites (Can 14 thru 17) in Canajoharie Creek, NY and Flat Creek (Flat 14 thru 17).

5. Alternatively, identical zircon morphologies suggest that the 89-050 K-bentonite is correlated with a single K-bentonite in Canajoharie Creek and Flat Creek, which has been identified in the present study as the single bed represented by samples Can 27 and Flat 26 respectively.

6. The petrogenetic interpretation of zircon morphologies indicates that the zircons crystallized in I-type magmas at temperatures common for silicic volcanic rocks (i.e. $>750\pm50^{o}C$) and supports the evidence from melt inclusions that those K-bentonites were generated by volcanic eruptions in a continental volcanic arc.

Chapter 5 "Zircon chemistry"

5.1. Introduction

The investigation into the geochemistry of zircons was complementary to the morphologic study in order to examine (a) the applicability of zircon chemistry as a correlation tool and (b) to study previously observed correlations between trace element abundances (particularly Y and Ce) in silicic rocks and the morphology of zircons (Brotzen, 1952; Pupin, 1985).

Although it has been demonstrated that, in contrast to apatite phenocrysts, the geochemistry of bulk zircon concentrates can not be used for correlation of Ordovician K-bentonites (Samson, 1986; Samson et al., 1988), it seemed worthwhile to attempt a different geochemical approach by avoiding the geochemistry of bulk samples and rather analyze individual grains. The analysis of bulk zircon samples may not have yielded the required discrimination because the chemical fingerprint of the zircons contained within those K-bentonites is possibly influenced by the presence of inherited zircon cores of Proterozoic age (Samson et al., 1988, 1989). Furthermore, unusually high and variable abundances of barium for example (ranging from not detectable to 15000 ppm within a single K-bentonite), seem to indicate contamination of the zircon separates (e.g. barite) (Samson, 1986). It therefore appears unlikely one can obtain a characteristic chemical fingerprint by analyzing bulk concentrates of zircons.

In the present study, the apparent limitations of analyzing bulk mineral separates were considered and alternatively it was attempted to characterize the geochemistry of individual zircon populations by analyzing multiple spots on single grains with the electron microprobe. Following this approach it is possible to distinguish the composition of inherited cores that may be chemically different

from the magmatic overgrowth. In such case one may even take advantage of those patterns that may be characteristic of individual zircon populations. The overgrowth onto inherited zircons, on the other hand, is expected to reflect the geochemical composition of the melt from which the zircon continued to crystallize prior to the volcanic eruption and by which different K-bentonites could hence be identified.

As this investigation into the geochemistry of zircons was supplementary to the morphologic study, it was intended to analyze zircons of various morphologies in order to study whether the relation between Ce and Y contents in silicic rocks and the morphology of zircons (Brotzen, 1952; Pupin, 1985) is reflected by the composition of individual zircons as well. According to these authors, an increase in yttrium content (in the bulk rock) is correlated with the prefered development of the {110} prism (see Figure 39) whereas the dominance of the {100} prism increases with the Ce-content of the rock. In the present study it was therefore intended to analyze the Y and Ce abundances, besides other trace elements, and to compare them with the morphology of the particular zircon.

5.2. Analytical techniques

Only zircons, of which the morphology had been determined, were used for chemical analysis with the electron microprobe. Hence, selected zircon mounts that had been prepared and studied in the morphologic study using the SEM (see Chapter 4), were transferred from the aluminum stamps onto 1-inch acrylic disks and fixed with epoxy glue, keeping the original arrangement of the grains, which allows the correlation of geochemistry and morphology. The crystals were mounted either flat-lying, yielding polished sections parallel to the long axis of the grains

(i.e. c-axis), or in an erected orientation, yielding polished sections perpendicular to the long axis of the grains. This second approach was undertaken in order to investigate compositional zonation in the zircons that might coincide with the variable development of the two distinct prism forms {100} and {110} from core to rim.

The sample mounts were carbon coated for analysis with the electron microprobe (JEOL 733 Superprobe), which is located in the Department of Geology at the Rensselaer Polytechnic Institute. This instrument uses five wavelength dispersive spectrometers with on-line data reduction using ZAF matrix correction instead of the Bence-Albee matrix correction, which could not be used for the combination of elements analyzed in the present study. All zircons were analyzed for ZrO_2, SiO_2, HfO_2, Ti, P, Y, Yb, Ce, U and Th using a special setup (i.e. column automation), which allows analysis of individual spots at low currents (i.e. 25 nA cup current) for the major elements ZrO_2 and SiO_2 in the first part, and with high currents (i.e. 400 nA cup current) for Hf, Ti, P, Y, Yb, Ce, U and Th in the second part of each analysis. The accelerating voltage was set to 20 kV and a beam diameter of approximately 5 microns used for analysis. The high currents (400 nA) and long counting times (50 seconds; 150 seconds for Ce) yield detection limits of approximately 100 ppm for the trace elements (i.e. Hf, Ti, P, Y, Yb, Ce, U, Th), of which each was analyzed by collecting peak counts as well as background counts for each analysis in order to minimize analytical uncertainties. Backgrounds were also routinely collected for Zr and Si.

Zr and Si were calibrated on the Mud Tank Zircon standard; Hf on pure hafnium metal; Ti on rutile; P on the Durango Apatite standard; U and Th on the RPR Monazite standard; Y, Ce and Yb on Drake and Weill Glass standards No. 2 and No. 3. The analytical uncertainties were estimated from repeated analyses of the Mud Tank Zircon and standards, for which individual zircons of the present study were used.

The analytical error (2 sigma) for ZrO_2, SiO_2, and HfO_2 is less than 5 percent based on repeated analyses of the Mud Tank Zircon. Although the analyses of Ti, P, Y, Yb, and U are reproduceable within 5 percent (2 sigma error), the analytical uncertainty for comparing analyses from different dates is estimated at 30 percent, which is believed to result from the heterogeneity of the zircons that had to be used as standards because the abundances of these elements in the Mud Tank Zircon are below the detection limit. The uncertainties for thorium and cerium could not be estimated owing to abundances below the detection limit in all standards.

5.3. Discussion

Zircons from 7 samples, which represent three different K-bentonites (i.e. Can 13 and Flat 13; Can 14 and Flat 14; Can 27, Flat 27, and 89-050; see also Figure 3, Chapters 2 and 4), were selected for chemical analysis. The choice of these samples provided a similar controlled experiment as for the morphologic study because the stratigraphic relations of these K-bentonites are well known (see Figure 3). Hence, it could be tested whether the zircons contained within different samples of the same K-bentonite are chemically indistinguishable from another but distinct from zircons contained within other K-bentonites.

However, Figure 70 illustrates the trace element variation that may be encountered in single zircon grains. The relative abundances of HfO_2, P_2O_5, and Y_2O_3, which were analyzed in 20 points across a zircon grain that is pictured in Figure 71, illustrate the contrasting compositions of the center of this grain and its adjacent zones. The center, which appears light in Figure 71, contains only about 1 weight percent HfO_2 compared to more than 1.5 weight percent HfO_2 in the darker, surrounding zones, whereas P_2O_5 and Y_2O_3 are much more abundant (2 to 3

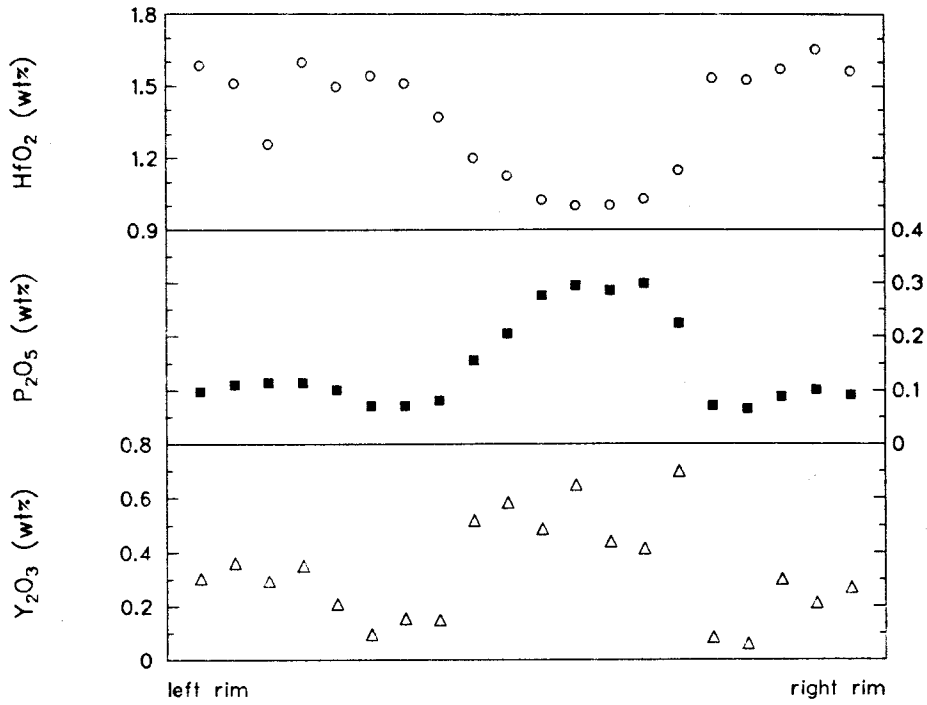

Figure 70: Compositional variation of HfO_2, P_2O_5, and Y_2O_3 along a traverse across a single zircon crystal (pictured in Figure 71). The left side of the diagram corresponds to a point at the left rim of the zircon (Figure 71) approximately 20 microns below the elongate, black inclusion near the middle of the grain. The traverse crosses the grain perpendicular to the long axis towards the right rim.

Figure 71: High-resolution backscattered electron image of a zircon crystal sectioned parallel to the c-axis. Note the zonation of the crystal which reflects compositional variations illustrated in Figure 70. The black inclusions at each tip of the elongate, light zone in the center of the crystal represent melt inclusions of rhyolitic composition.

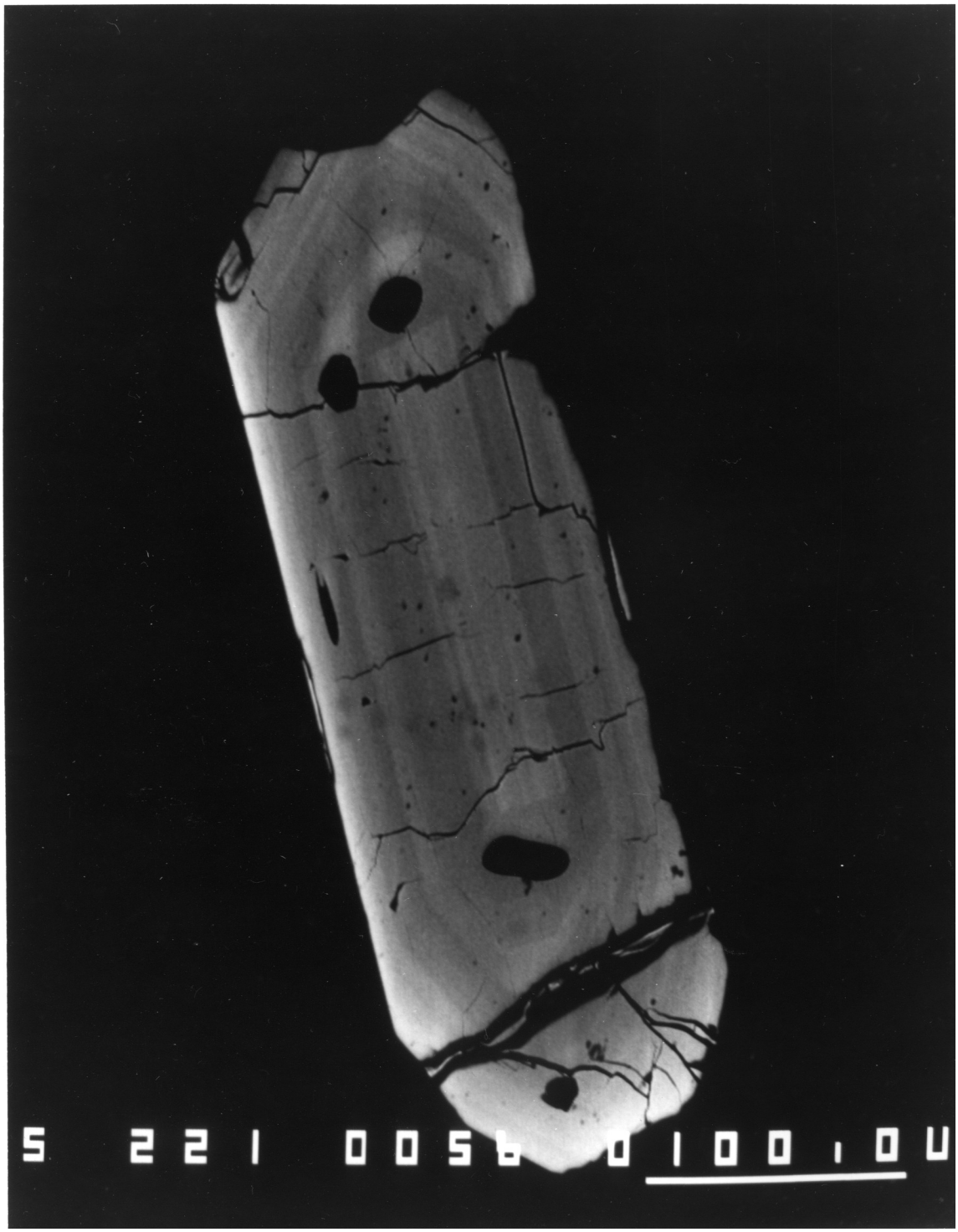
5 221 0056 0100 U

times) in the center than in the adjacent zones (Figure 70). These contrasting compositions between the core and rim of single grains, however, are not apparent from the analyses of 33 grains from the same sample (i.e. Can 14). Figures 72 and 74 illustrate that the core and rim compositions of zircons contained within K-bentonite Can 14 are indistinguishable with regard to hafnium, phosphorous and yttrium and the compositional range of these elements (i.e. Hf, P, Y) within individual grains, is as large as the ranges observed within the entire sample (compare Figures 72, 73, 74, and 75). Similar variations and indistinguishable compositions (i.e. core vs. rim) are also evident from zircons of a different K-bentonite (i.e. 89-050) (compare Figures 76, 77, 78, and 79). These results already indicate that a zircon population can not be characterized in a simple way by analyzing single grains at known positions (i.e. core or rim; internal zonation) owing to the large variations and overlap of the trace element abundances among different grains.

Plotting the results of the chemical analyses, which include compositions of zircons from three different K-bentonites, in various element combinations (Figures 80 thru 83), further illustrates that the zircons from those K-bentonites can not be distinguished one from another based on the analyses of individual grains. No single zircon population exhibits a distinct trace element content or a characteristic correlation of two elements.

A correlation of the trace element abundances of Y or Ce with the morphology of individual crystals could not be detected either, probably because the large variations that are commonly observed within single grains conceal any systematic variation of Ce- and Y-contents in the zircons. The high-resolution backscattered electron image of this zircon, which is sectioned perpendicular to its c-axis, suggests that the change of the relative proportions of the prisms {110} and {100} from a single prism (i.e. {100}) in the core to a surface morphology of the prisms,

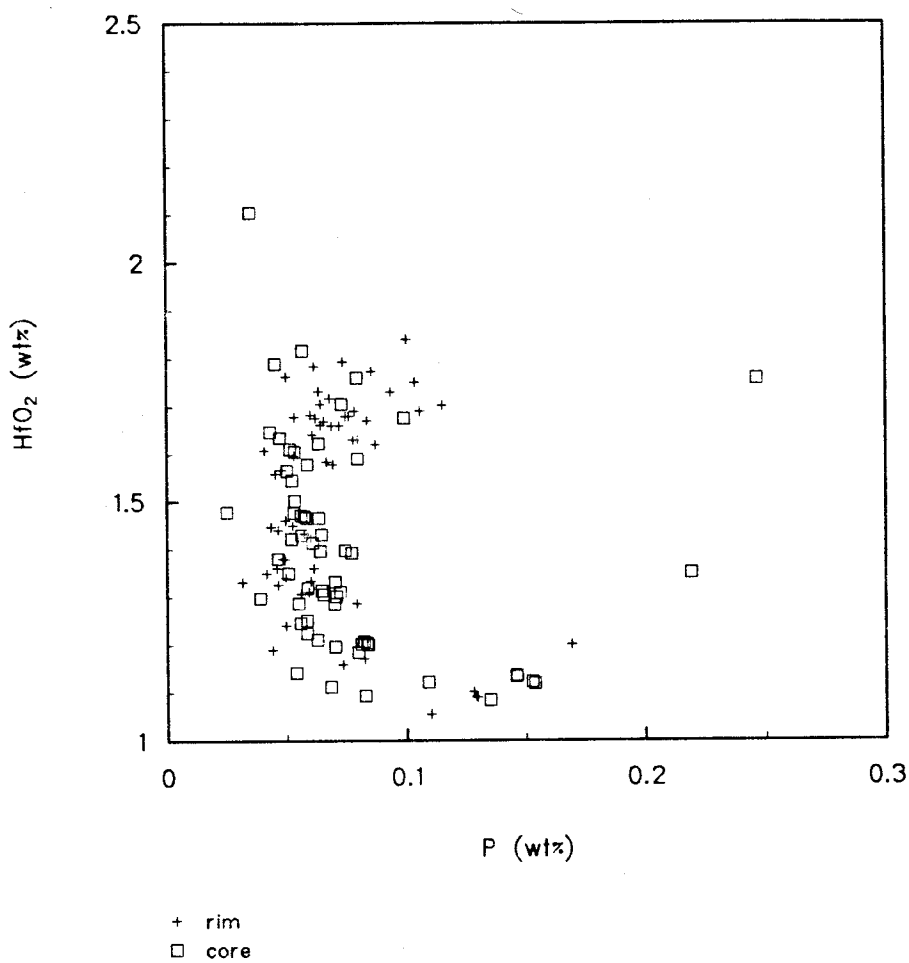

Figure 72: The variation of HfO_2- and P-abundances among zircons from K-bentonite Can 14. Analyses of cores are distinguished from analyses of the grain rims by different symbols. Note, however, the complete overlap of core and rim compositions.

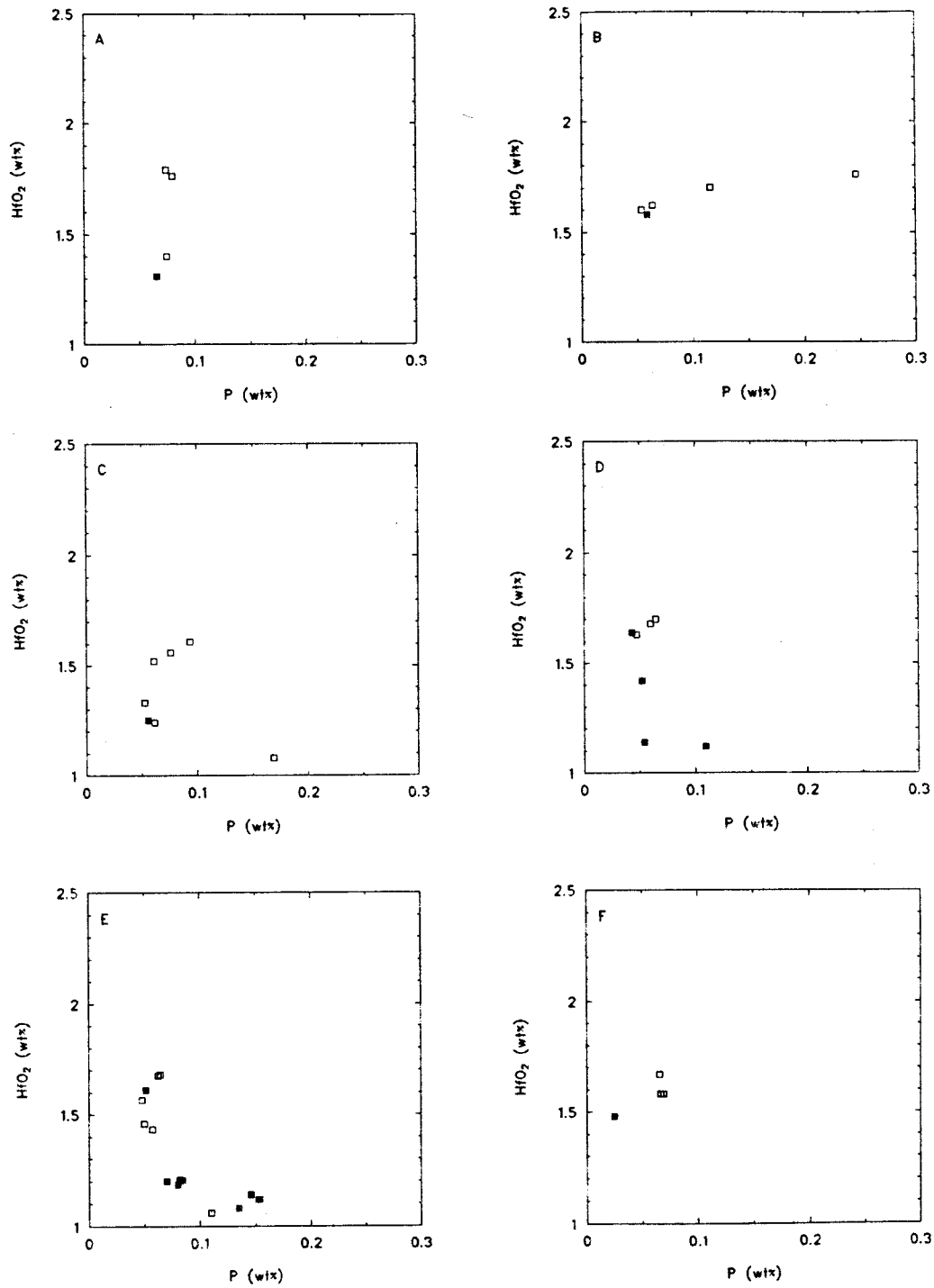

Figure 73: The variation of HfO_2- and P-abundances within six individual grains from K-bentonite Can 14 (included in Figure 72). Analyses of cores are represented by filled boxes compared with open squares for rim analyses.

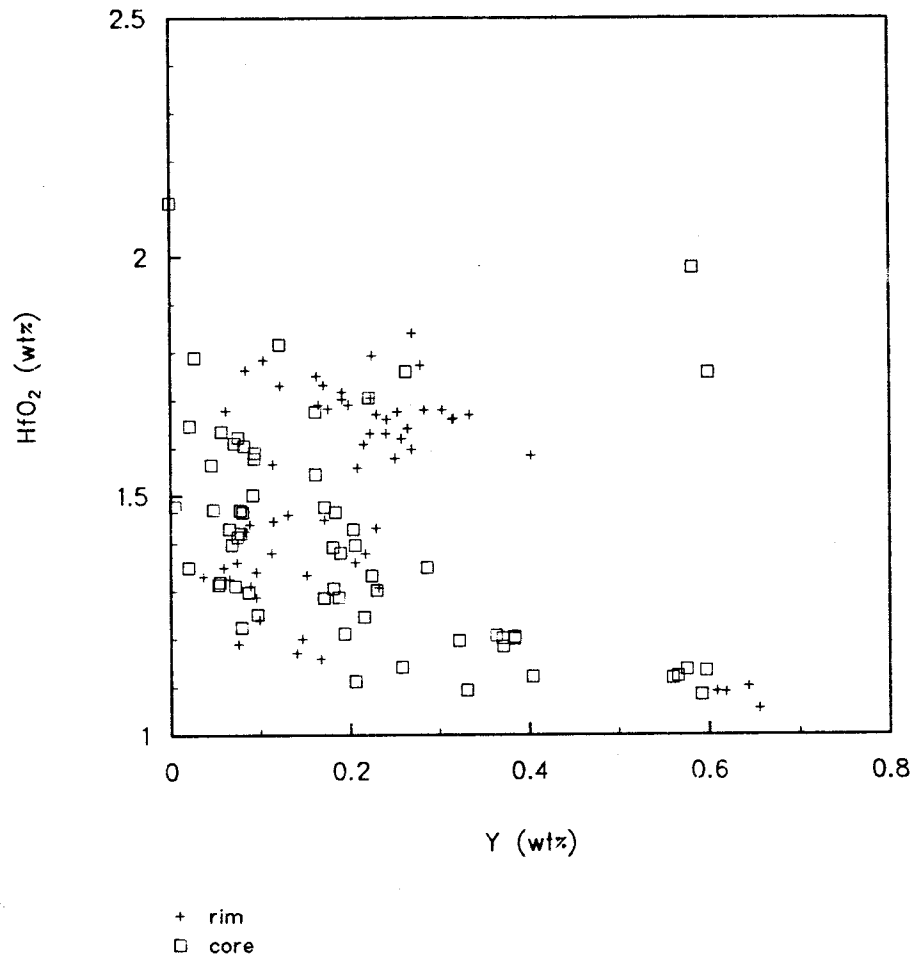

Figure 74: The variation of HfO_2- and Y-abundances among zircons from K-bentonite Can 14. Note the overlap of the analyses from cores and rims that are distinguished by different symbols.

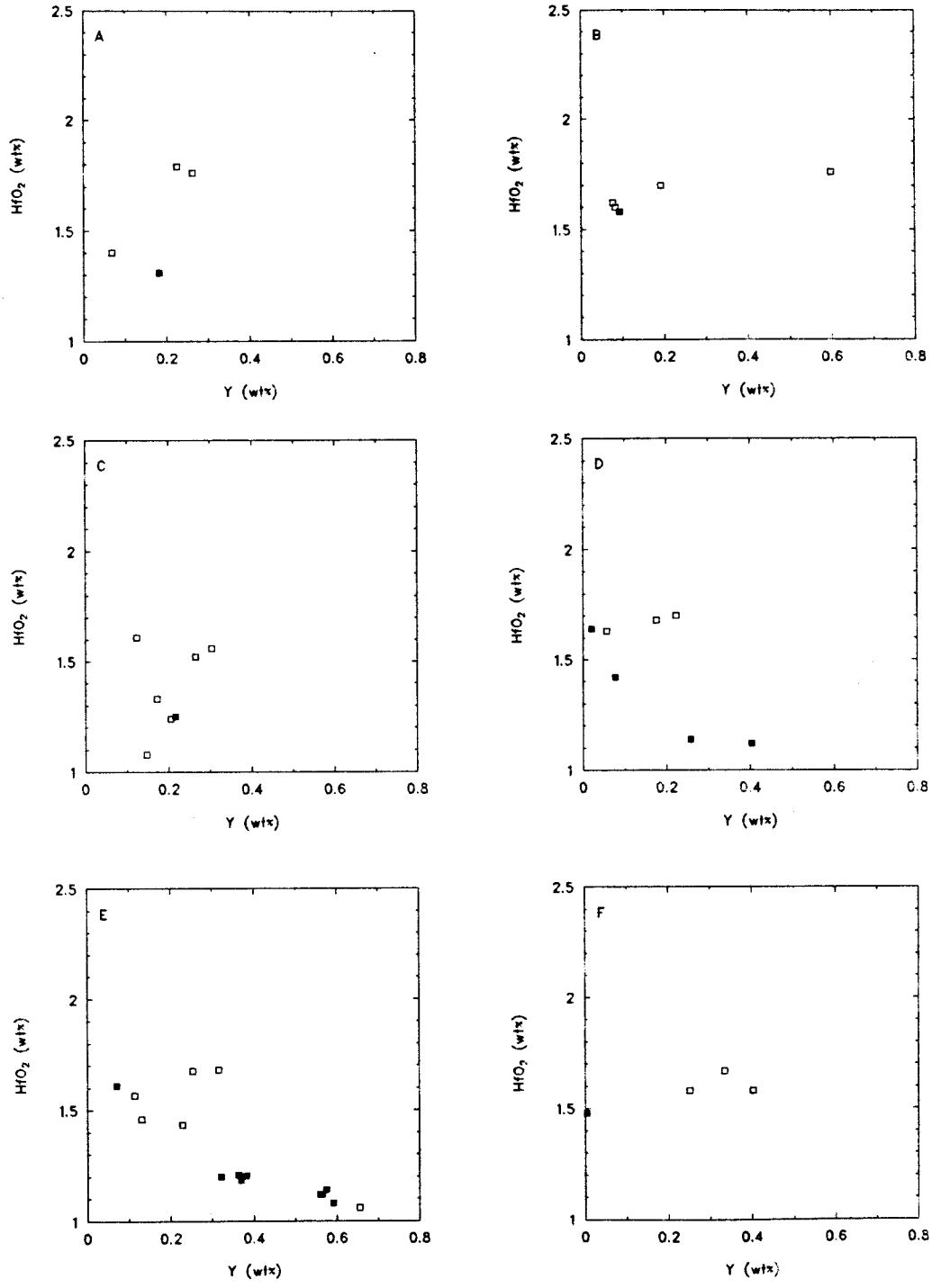

Figure 75: The variation of HfO_2- and Y-abundances within six individual grains from K-bentonite Can 14 (same grains as in Figure 73). Analyses of cores are represented by filled boxes compared with open squares for rim analyses.

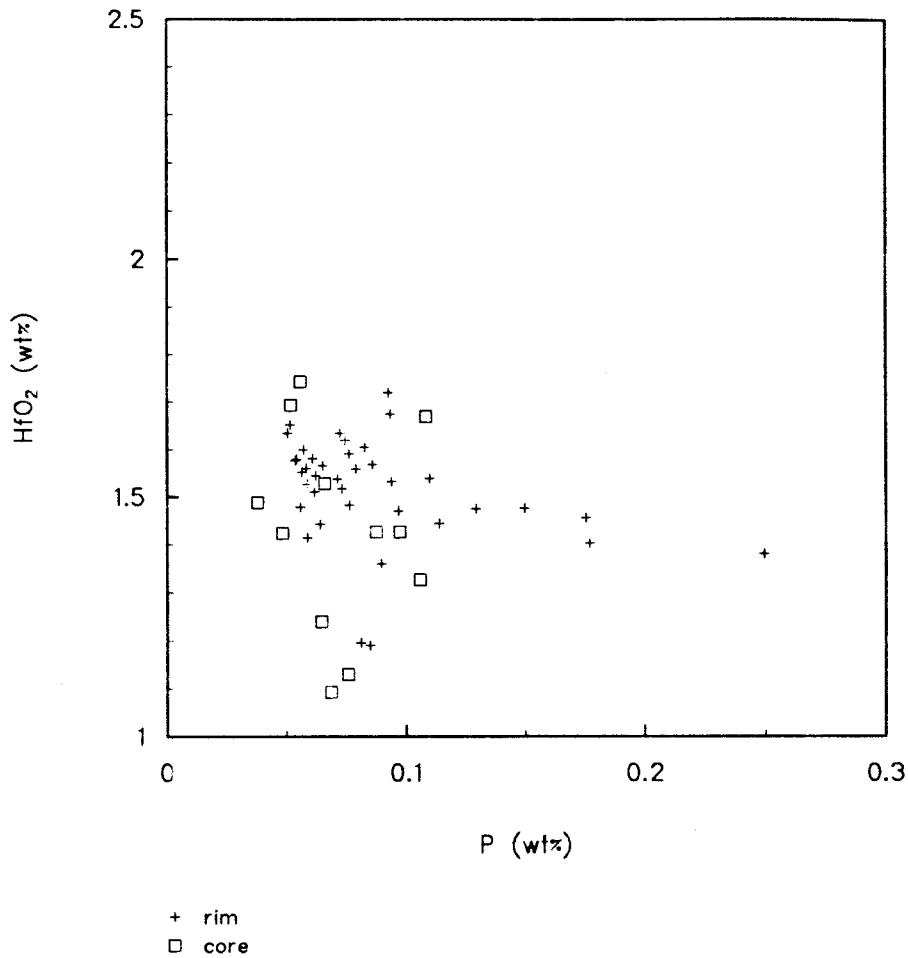

Figure 76: The variation of HfO_2- and P-abundances among zircons from K-bentonite 89-050. Note the overlap of the analyses from cores and rims, which is similar to the pattern observed in K-bentonite Can 14 (Figure 72).

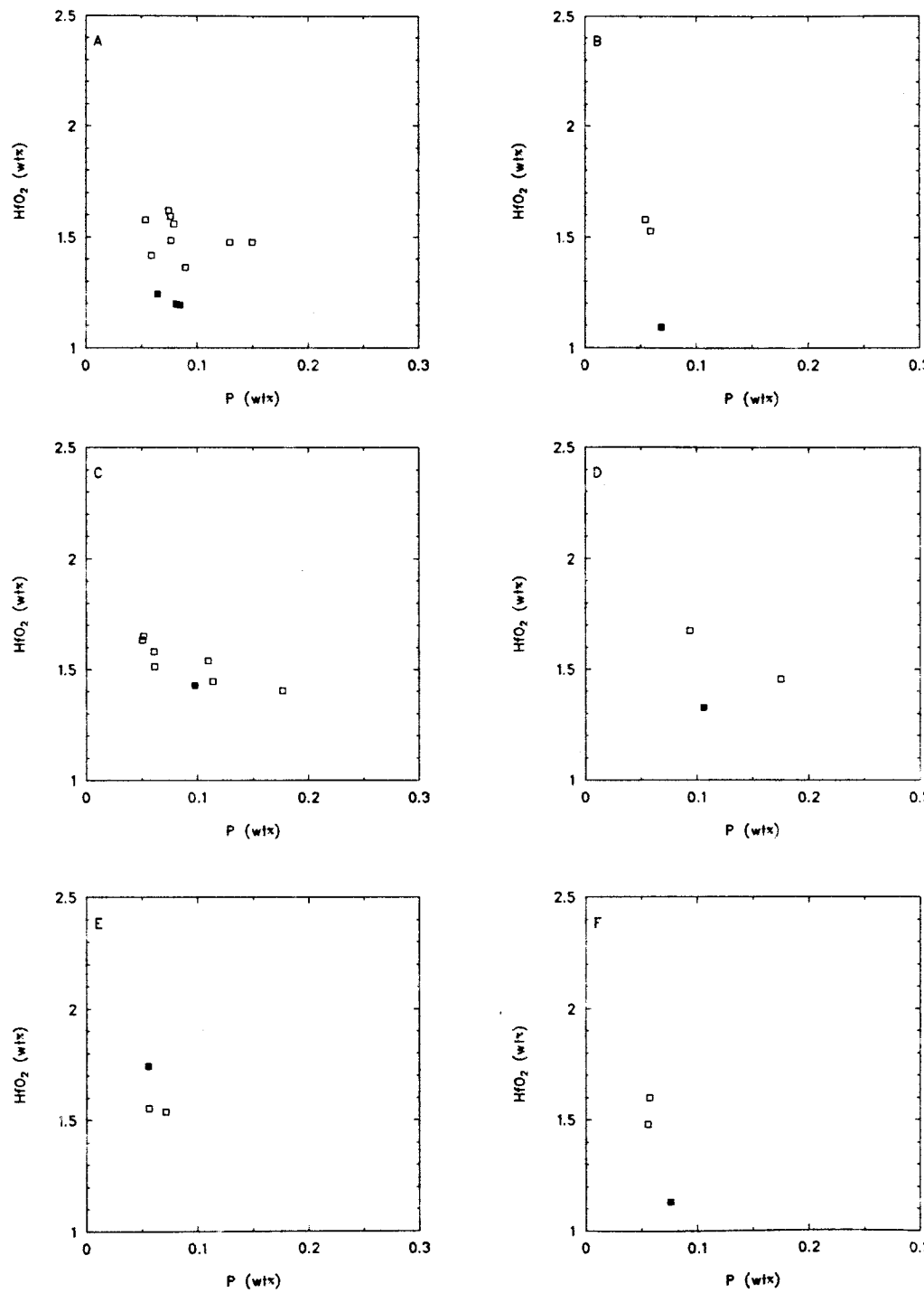

Figure 77: The variation of HfO_2- and P-abundances within six individual grains from K-bentonite 89-050 (included in Figure 76). Analyses of cores are represented by filled boxes compared with open squares for rim analyses.

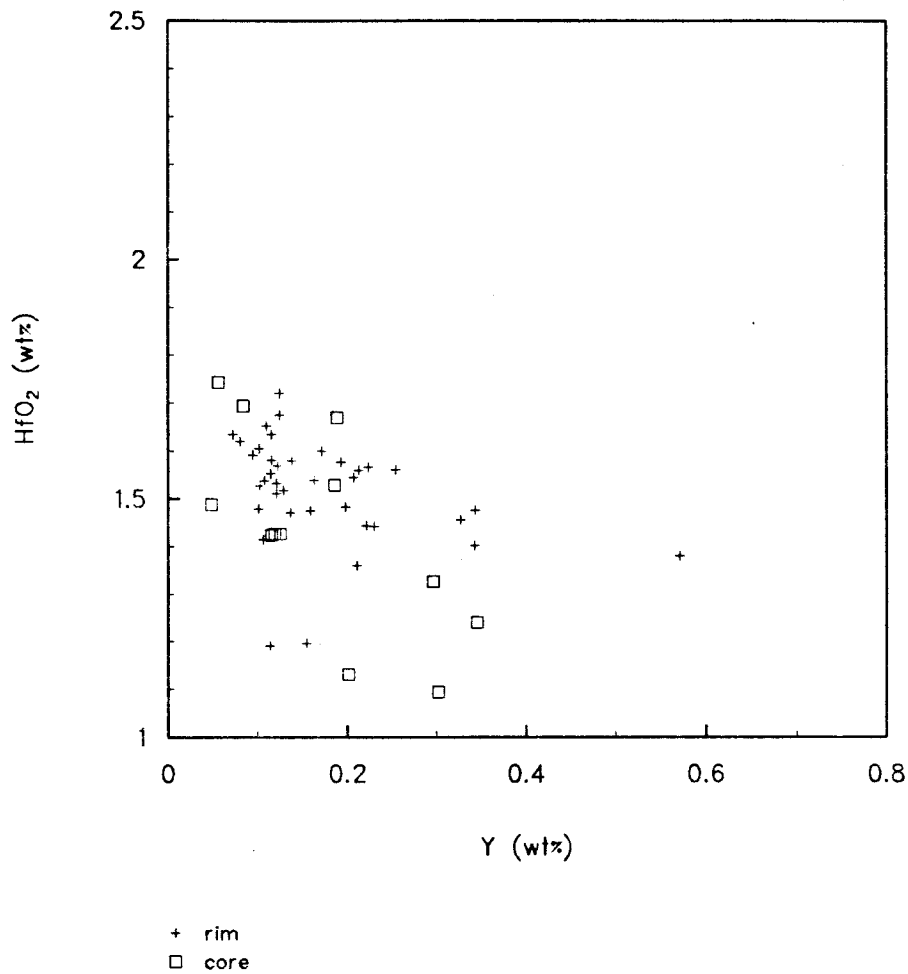

Figure 78: The variation of HfO_2- and Y-abundances among zircons from K-bentonite 89-050. Note again the overlap of the analyses from cores and rims, which is similar to the pattern observed in K-bentonite Can 14 (Figure 74).

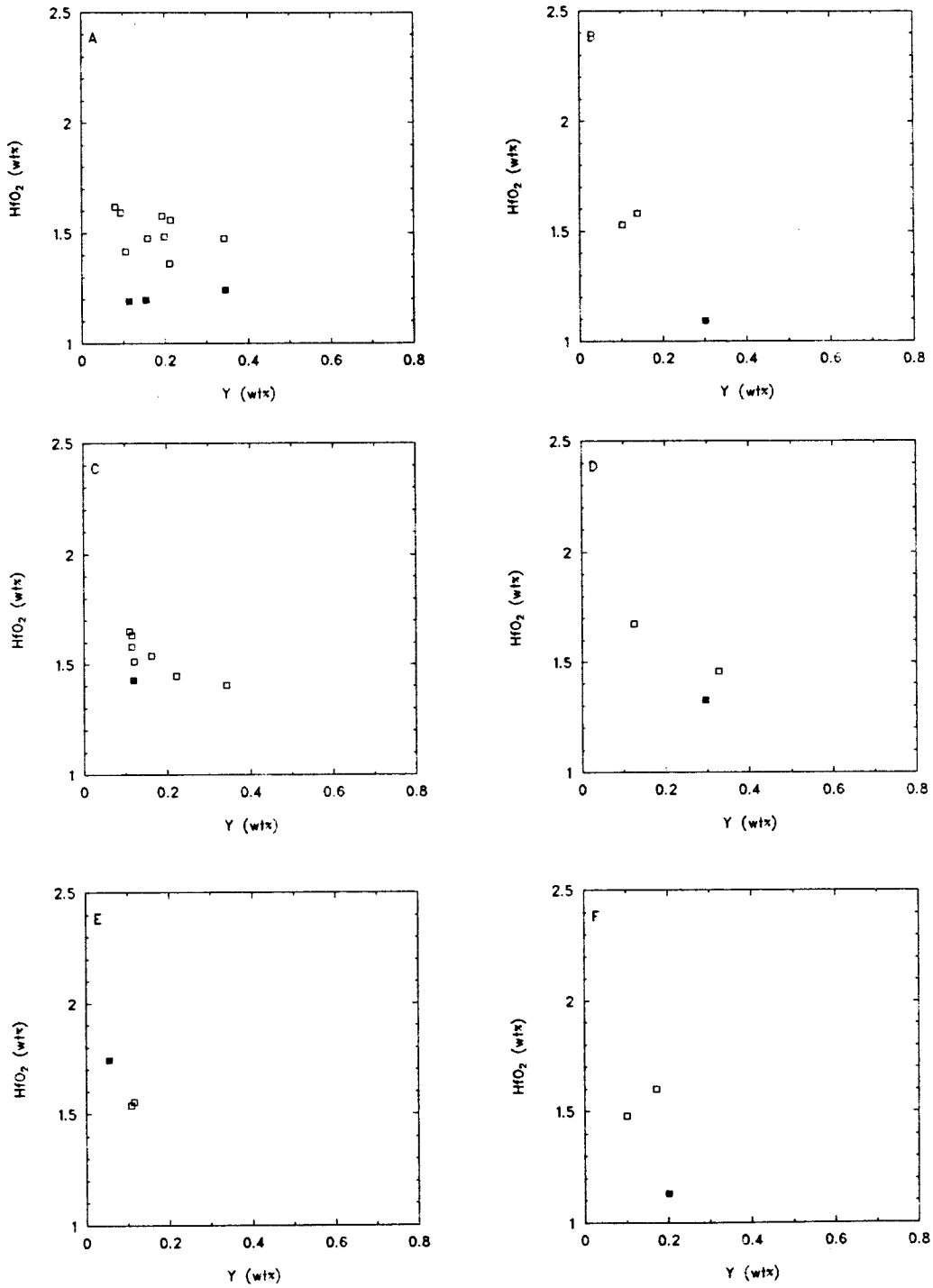

Figure 79: The variation of HfO_2- and Y-abundances within six individual grains from K-bentonite 89-050 (same grains as in Figure 77). Analyses of cores are represented by filled boxes compared with open squares for rim analyses.

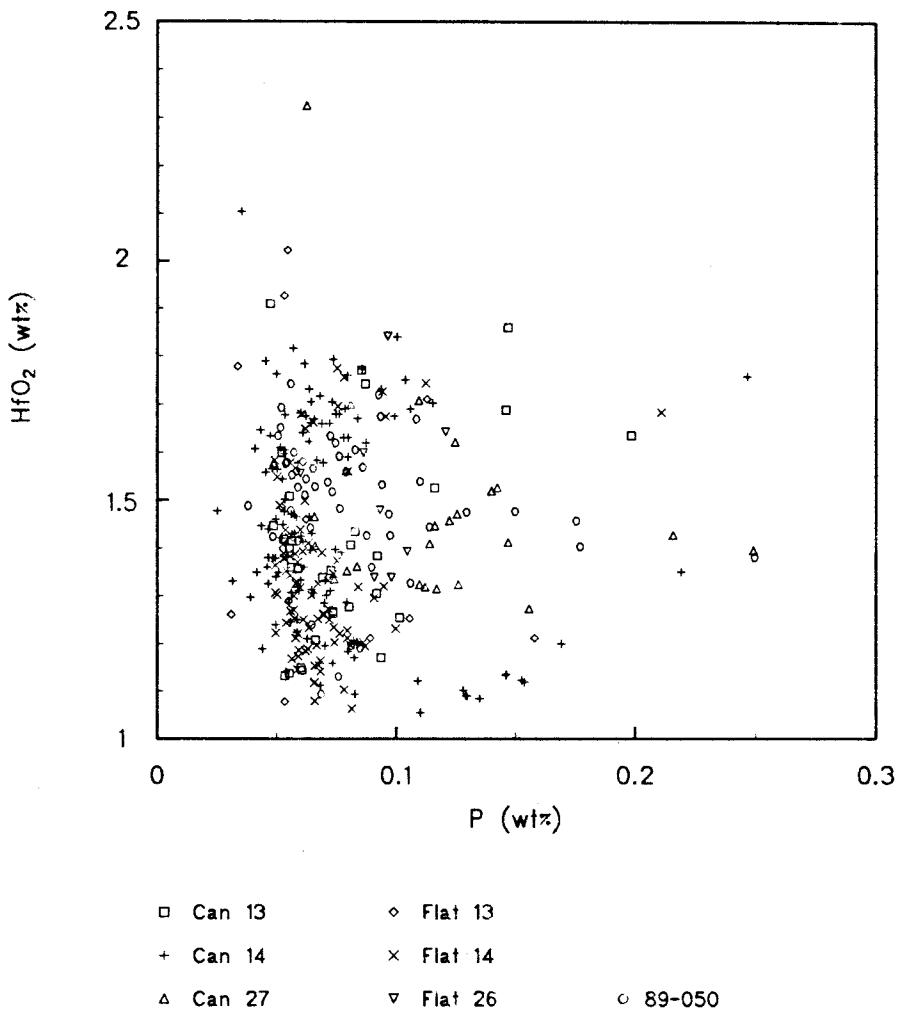

Figure 80: Illustration of the compositional heterogeneity of zircons from various K-bentonites, which are indistinguishable one from another. Note that the variation observed in single grains (Figures 73, 75, 77, 79) is about as great as the variation observed among all zircons from different samples.

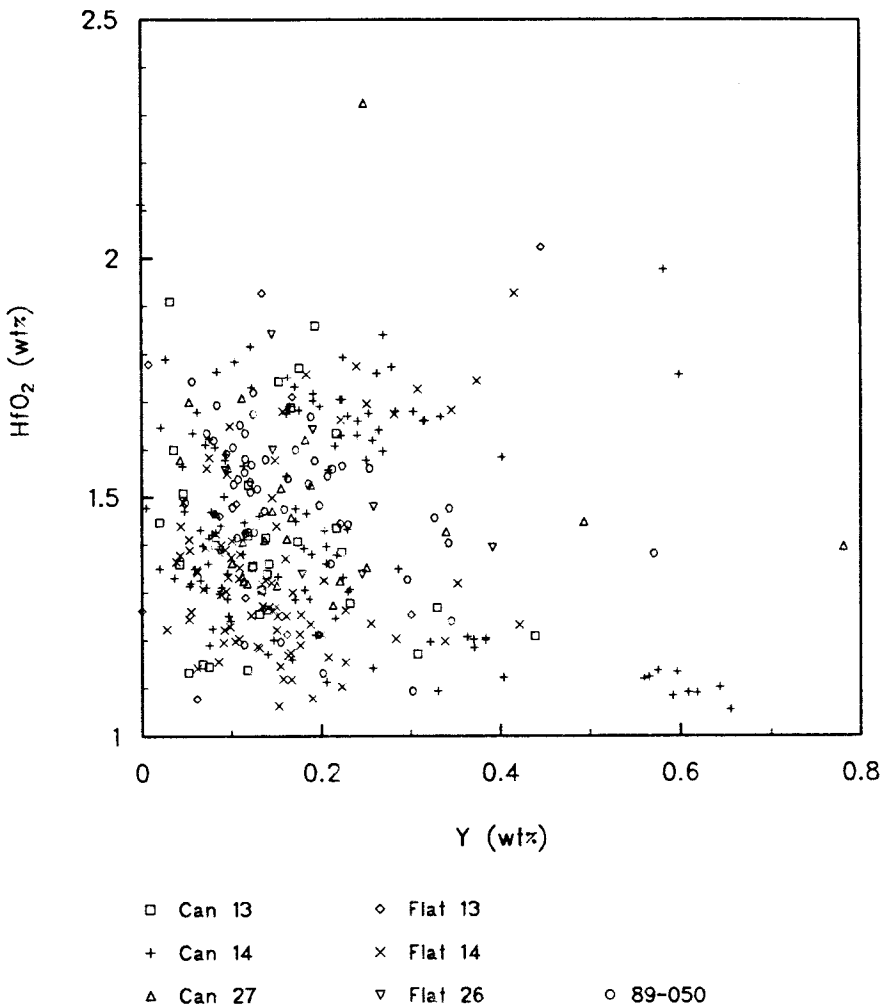

Figure 81: Similar illustration as Figure 80, which demonstrates the heterogeneity of individual zircon populations that are hence indistinguishable.

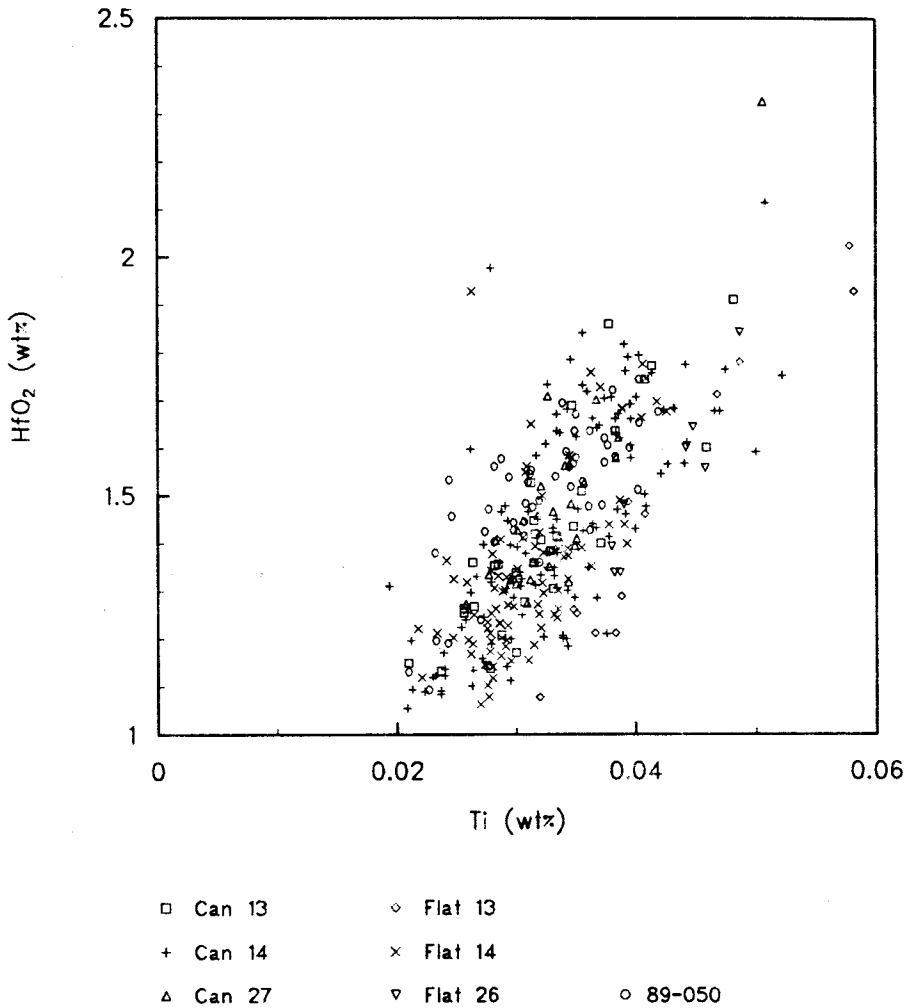

Figure 82: A plot of HfO_2- versus Ti-abundances in zircons illustrates the positive correlation of these elements due to their similar chemical behaviour. There is, however, no discrimination among zircons from different K-bentonites.

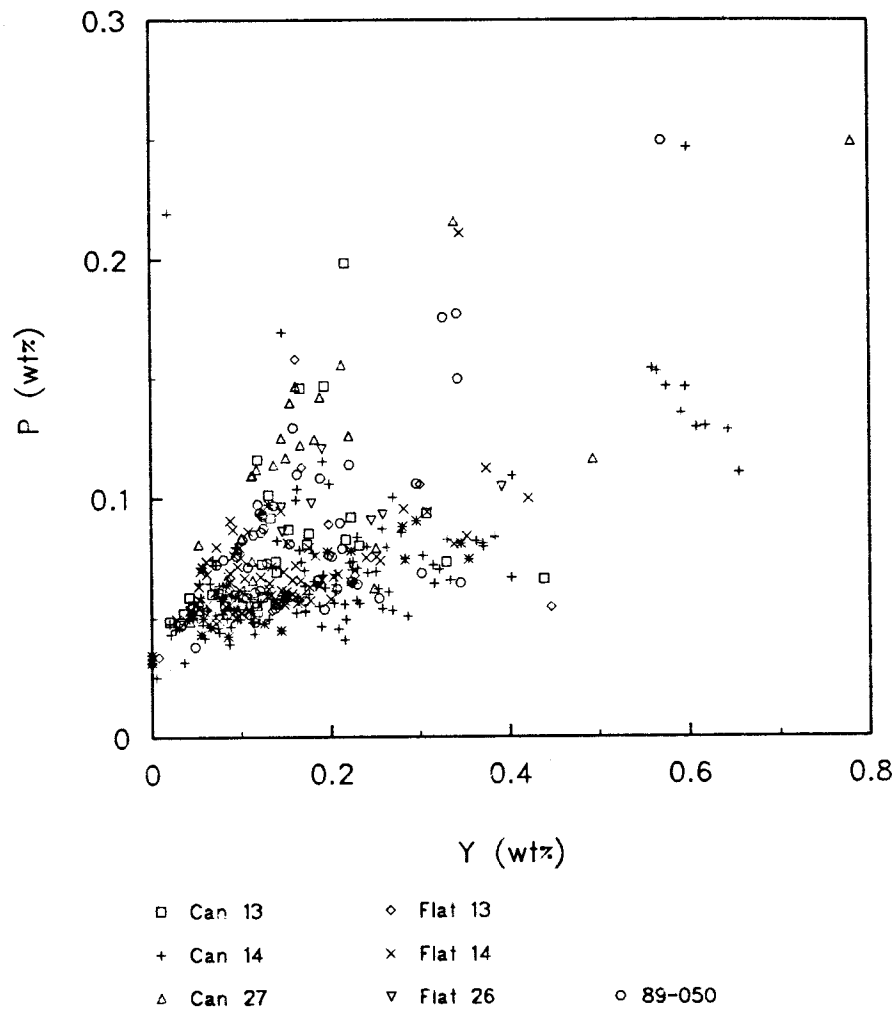

Figure 83: A discrimination of zircons from different K-bentonites is not apparent from a plot of the P- versus Y-abundances despite the variations by a factor of up to four and greater (e.g. Y).

Figure 84: High-resolution backscattered electron image of a zircon crystal that is sectioned perpendicular to its c-axis. The surface morphology was determined in the morphologic study as (100)>>(110). The light-dark zonation of the crystal, which reflects compositional variations, however, indicates a morphology at an earlier stage of crystallization (now overgrown), at which only the {100} prism was developed (compare zonation at center of crystal with overall shape).

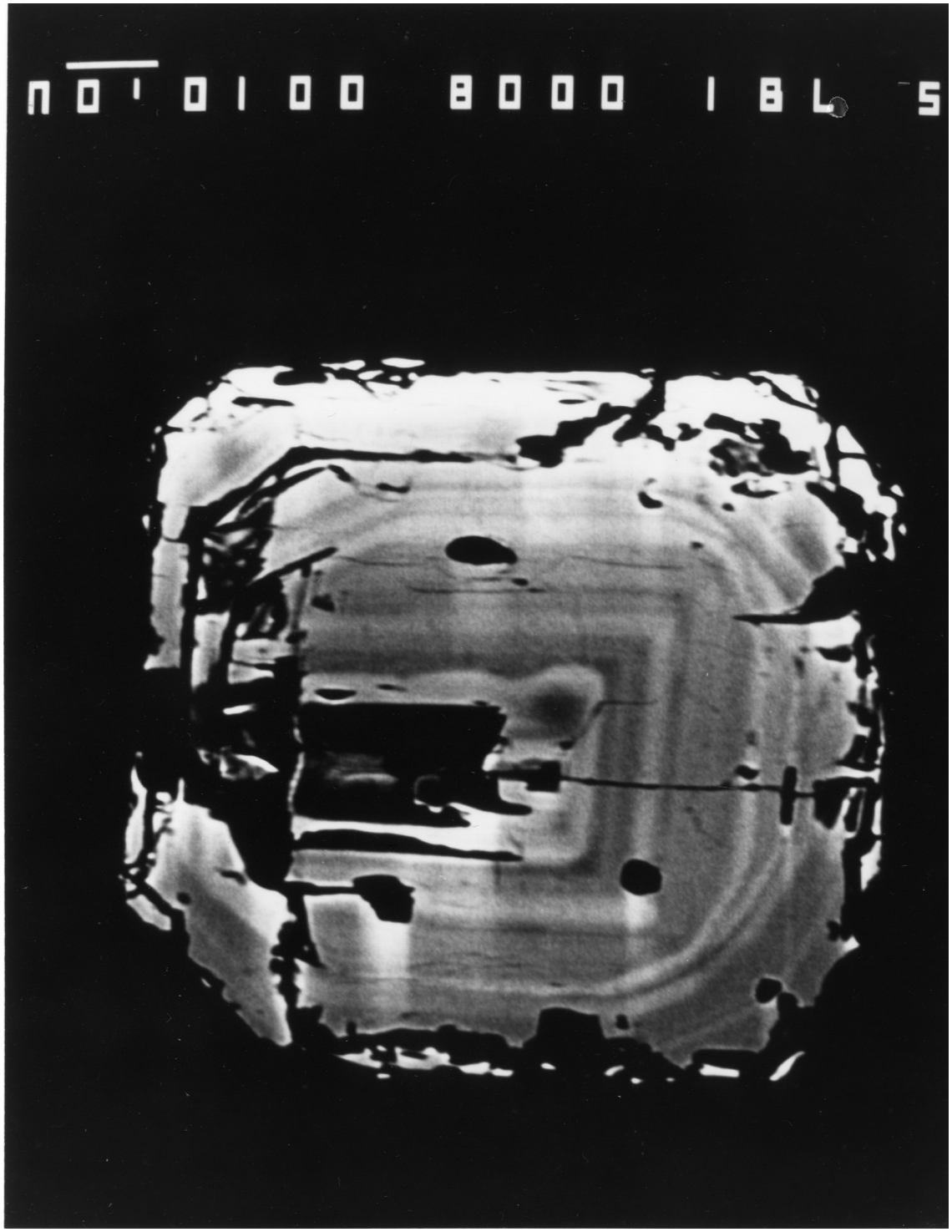

where (100)>>(110), is not correlated with the compositional zonation reflected by the alternating grey shades (Figure 84). This lack of correlation may indicate that the geochemical composition of a zircon is very sensitive to parameters that have no influence on the morphology (e.g. diffusivity of trace elements in the boundary layer versus rate of crystal growth) and hence further complicate the attempt to characterize K-bentonites based on the geochemistry of zircons.

5.4. Conclusions

1. In summary, it has to be concluded that at the present stage it is not possible to use the trace element composition of individual zircons for correlation of Ordovician K-bentonites owing to their geochemical heterogeneity.
2. A correlation of the Y- and Ce-content with the morphology of individual zircon crystals could not be tested owing to the compositional heterogeneity of single zircons, which is suspected to conceal any systematic variation.

Bibliography

Allen, V.T., 1929, Altered tuffs in the Ordovician of Minnesota., Journal of Geology, 37, p.239-248.

Allen, V.T., 1932, Ordovician altered volcanic material in Iowa, Wisconsin, and Missouri., Journal of Geology, 40, p.259-269.

Altaner, S.P., Hower, J., Whitney, G., and Aronson, J.L., 1984, Model for K-bentonite formation: Evidence from zoned K-bentonites in the disturbed belt, Montana., Geology, 12, p.412-415.

Anderson, A.T., 1967, Possible consequences of composition gradients in basalt glass adjacent to olivine phenocrysts., (abstr.), American Geophysical Union Transactions, 48, p.227.

Anderson, A.T., 1973, The before-eruption water contents of some high-alumina magmas., Bulletin volcanologique, 37, p.530-552.

Anderson, A.T., 1974a, Evidence for a picritic, volatile-rich magma beneath Mt. Shasta, California., Journal of Petrology, 15, p.243-267.

Anderson, A.T., 1974b, Chlorine, sulfur and water in magmas and oceans., Geological Society of America Bulletin, 85, p.1485-1492.

Anderson, A.T., 1976, Magma mixing: petrological process and volcanological tool., Journal of Volcanology and Geothermal Research., 1, p.3-33.

Anderson, Jr., A.T., Newman, S., Williams, S.W., Druitt, T.H., Skirius, C., and Stolper, E., 1989, H_2O, CO_2, Cl, and gas in Plinian and ash-flow Bishop rhyolite., Geology, 17, p.221-225.

Arndt, N.T, Nisbet, E.G. and Cameron, W.G., 1989, Geochemistry of extremely fresh komatiites from the Belingwe Belt, Zimbabwe., Chemical Geology, 70, p.140 (abstract).

Beddoe-Stephens, B., Aspden, J.A., Shepherd, T.J., 1983, Glass inclusions and melt compositions of the Toba tuffs, Northern Sumatra., Contributions to Mineralogy and Petrology, 83, p.278-287.

Belkin, H.E., and Rice, C.L., 1990, The origin of some Flint clays in the central Appalachian Basin: evidence from silicate-melt inclusions., PACROFI III, vol. 3, Program and Abstracts, Univ. of Toronto, May 20-22, 1990, p.15.

Bergström, S.M., 1983, Trans-Iapetus significance of Ordovician bentonite bed complexes., Geological Society of America Abstracts with program., 15, p.255.

Bock, B., 1990, Geochemistry of garnet xenocrysts and garnet-bearing xenoliths in Ordovician bentonites., M.S. thesis, State University of New York at Albany, 113pp.

Borchardt, G.A., Harward, M.E., and Schmitt, R.A., 1971, Correlation of volcanic ash deposits by activation analysis of glass separates., Quaternary Research, 1, p.247-260.

Borchardt, G.A., Aruscavage, P.J., and Millard, H.T.,Jr., 1972, Correlation of the Bishop Ash, a Pleistocene marker bed, using instrumental neutron activation analysis., Journal of Sedimentary Petrology, 42, p.301-306.

Borchardt, G.A., Norgren, J.A., and Harward, M.E., 1973, Correlation of ash layers in peat bogs of eastern Oregon., Geological Society of America Bulletin, 84, p.3101-3108.

Brotzen, O., 1952, Die zonaren Zirkone des Ramberggranites., Geologiska Föreningen: Förhandlingar, 74(2), p.173-184.

Brun, J., and Chagnon, A., 1979, Rock stratigraphy and clay mineralogy of volcanic ash beds from the Black River and Trenton Groups of southern Quebec., Canadian Journal of Earth Science, 16, p.1499-1507.

Brusewitz, A.M., 1986, Chemical and physical properties of Paleozoic potassium bentonites from Kinnekulle, Sweden., Clays and Clay Minerals, 34, p.442-454.

Burnham, C.W., 1979, The importance of volatile constituents., in: The evolution of igneous rocks., Fiftieth Anniversary Perspective, Yoder, H.S.,(ed), Princeton University Press, p.439-479.

Cameron, B., and Kamal, R.A., 1977, Paleoecology and stratigraphy of the Ordovician Black River Group Limestones: central Mohawk Valley., in: Wilson, P.C.,(ed), Guidebook to field excursions, 49th Annual Meeting New York State Geological Association 1977, A-8, p.1-28.

Carron, J.-P., 1961, Prèmieres données sur la composition chimique de certains reliquats magmatiques., Comptes rendus de l'Académie des Sciences, Paris, 253, p.3016-3018.

Caruba, R. and Turco, G., 1971, Mise au point sur la notation des faces du zircon. Élaboration d'une méthode d'indexation rapide des faces des zircons accessoires des roches par utilisation d'abaques., Bulletin Société Française de Minéralogie et de Cristallographie, 94, 427-436.

Chaigneau, M., Massare, D., and Clocchiatti, R., 1980, Contribution à l'étude des inclusions vitreuses et des éléments volatils contenus dans les phénocristaux de quartz de roches volcaniques acides., Bulletin of Volcanology, 43, p.233-240.

Chakoumakos, B.C., Murakami, T., Lumpkin, G.R. and Ewing, R.C., 1987, Alpha-decay-induced fracturing in zircon: the transition from the crystalline to the metamict state., Science, 236, p.1556-1559.

Chappell, B.W., and White, A.J.R., 1974, Two contrasting granite types., Pacific Geology, 8, p.173-174.

Cisne, J.L., and Rabe, B.D., 1978, Coeonocorrelation: gradient analysis of fossil communities and its applications in stratigraphy., Lethaia, 11, p.341-364.

Cisne, J.L., Karig, D.E., Rabe, B.D., and Hay, B.J., 1982, Topography and tectonics of the Taconic outer trench slope as revealed through gradient analysis of fossil assemblages., Lethaia, 15, p.229-246.

Cisne, J.L., Gildner, R.F., and Rabe, B.D., 1984, Epeiric sedimentation and sea level: Synthetic ecostratigraphy., Lethaia, 17, p.267-288.

Clemens, J.D., 1984, Water contents of silicic to intermediate magmas., Lithos, 17, p.273-287.

Clocchiatti, R., 1975, Les inclusions vitreuses des cristaux de quartz. Etude optique, thermo-optique et chimique. Applications geologiques., Societe Geologique de France, Memoires No. 122, 113pp.

Cullen-Lollis, J., and Huff, W.D., 1986, Correlation of Champlainian (Middle Ordovician) K-bentonite beds in central Pennsylvania based on chemical fingerprinting., Journal of Geology, 94, p.865-874.

Delano, J.W., Schirnick, C., Bock, B., Kidd, W.S.F., Heizler, M.T., Putman, G.W., DeLong, S.E., and Ohr, M., 1990, Petrology and geochemistry of Ordovician K-bentonites in New York State: constraints on the nature of a volcanic arc., Journal of Geology, 98, p.157-170.

Delano, J.W., Kidd, W.S.F., Schirnick, C., and Bock, B., Geochemistry of Ordovician flysch, black shales, and calciturbidites from New York State (USA) and Quebec (Canada): Tectonic implications., in preparation.

Dunbar, N.W., Hervig, R.L., and Kyle, P.R., 1989, Determination of pre-eruptive H_2O, F an Cl contents of silicic magmas using melt inclusions: examples from Taupo volcanic center, New Zealand., Bulletin of Volcanology, 51, p.177-184.

Evans, S.H.,Jr., and Nash, W.P., 1979, Diffusion gradients in natural silicic liquids., EOS, 60, p.402.

Fisher, D.W., Correlation of the Hadrynian, Cambrian and Ordovician rocks in New York State., New York State Museum Map and Chart Series, 25, 75pp.

Fisher, R.V., and Schmincke, H.-U., 1984, Pyroclastic rocks., Springer-Verlag, Berlin Heidelberg New York Tokyo, 472pp.

Forsman, N.F., 1984, Misuse of the term "bentonite" for ash beds of Devonian age in the Appalachian basin: Discussion and Reply. Discussion., Geological Society of America Bulletin, 95, p.124

Harmon, R.S., Barreiro, B.A., Moorbath, S., Hoefs, J., Francis, P.W., Thorpe, R.S., Deruelle, B., McHugh, J., and Viglino, J.A., 1984, Regional O-, Sr- and Pb isotope relationships in late Cenozoic calc-alkaline lavas of the Andean Cordillera., Journal Geological Society London, 141, p.803-822.

Harris, C.M., 1981, The microdetermination of H_2O, CO_2 and SO_2 in glass using a 1280°C microscope heating stage, cryopumping, and vapor pressure measurements from 77 to 273 K. Geochimica et Cosmochimica Acta, 45, p.2023-2036.

Hay, B.J., and Cisne, J.L., 1988, Deposition in the oxygen-deficient Taconic Foreland Basin, Late Ordovician., in: Keith, B.D.,(ed), The Trenton Group (Upper Ordovician Series) of Eastern North America. Deposition, Diagenesis, and Petroleum., AAPG Studies in Geology, 29, AAPG, Tulsa, Oklahoma., p.113-134.

Hein, J.R., and Scholl, D.W., 1978, Diagenesis and distribution of late Cenozoic volcanic sediment in the southern Bering Sea., Geological Society of America Bulletin, 89, p.197-210.

Henderson, J.H., Jackson, M.L., Syers, J.K., Clayton, R.N., and Rex, R.W., 1971, Cristobalite authigenic origin in relation to montmorillonite and quartz origin in bentonites., Clays and Clay Minerals, 19, p.229-238.

Hervig, R.L., Dunbar, N., Westrich, H.R., and Kyle, P.R., 1989, Pre-eruptive water content of rhyolitic magmas as determined by ion microprobe analyses of melt inclusions in phenocrysts., Journal of Volcanology and Geothermal Research, 36, p.293-302.

Hildreth, W., 1979, The Bishop Tuff: Evidence for the origin of compositional zonation in silicic magma chambers., in: Chapin, C.E., and Elston, W.E., eds., Ash flow tuffs., Geological Society of America, Special Paper, 180, p.43-75.

Holland, H.D., and Gottfried, D., 1955, The effect of nuclear radiation on the structure of zircon., Acta Crystallographica, 8, p.291-300.

Holloway, J.R., 1976, Fluids in the evolution of granitic magmas: consequences of finite CO_2 solubility., Geological Society of America Bulletin, 87, p.1513-1264.

Holloway, J.R., and Jakobsson, S., 1986, Volatile solubilities in magmas: transpot of volatiles from mantles to planet surfaces., Journal of Geophysical Research, 91, p.D505-D508.

Hower, J., Eslinger, E.V., Hower, M.E., Perry, E.A., Mechanism of burial metamorphism of argillaceous sediment: 1. Mineralogical and chemical evidence., Geological Society of America Bulletin, 87, p.725-737.

Huff, W.D., 1983, Correlation of Middle Ordovician K-bentonites based on chemical fingerprinting., Journal of Geology, 91, p.657-669.

Huff, W.D., 1983, Misuse of the term "bentonite" for ash beds of Devonian age in the Appalachian basin: Discussion and Reply. Discussion., Geological Society of America Bulletin, 94, 681-682.

Huff, W.D., and Türkmenoglu, A.G., 1981, Chemical characteristics and origin of Ordovician K-bentonites along the Cincinnati Arch., Clays and Clay Minerals, 29, p.113-123.

Huff, W.D., Anderson, T.B., and Morgan, D.J., 1988, Immobile trace element chemistry of Llandovery (Silurian) K-bentonites in the United Kingdom: Implications for tectonic setting., Geological Society of America Abstracts with Programs, 20, p.350.

Kay, G.M., 1930, Age of the Hounsfield bentonite., Science, 72, p.365.

Kay, G.M., 1931, Stratigraphy of the Ordovician Hounsfield metabentonite., Journal of Geology, 39, p.361-376.

Kay, G.M., 1935, Distribution of Ordovician altered volcanic materials and related clays., Geological Society of America Bulletin, 46, p.226-231.

Kay, G.M., 1943, Mohawkian Series on West Canada Creek, New York., American Journal of Science, 241, p.597-606.

Kiersch, G.A., and Keller, W.D., 1955, Bleaching clay deposits, Sanders-Defiance Plateau District, Navajo country, Arizona., Economic Geology, 50, p.469-494.

Kolata, D.R., Frost, J.K., and Huff, W.D., 1986, K-bentonites of the Ordovician Decorah Subgroup, Upper Mississippi Valley: correlation by chemical fingerprinting., Illinois Department of Energy and Natural Resources, State Geological Survey Division, Circular 537, 30pp.

Kolata, D.R., Frost, J.K., and Huff, W.D., 1987, Chemical correlation of K-bentonite beds in the Middle Ordovician Decorah Subgroup, upper Mississippi Valley., Geology, 15, p.208-211.

Kowallis, B.J., and Christiansen, E.H., 1990, Applications of zircon morphology: Correlation of pyroclastic rocks and petrogenetic inferences., in: Field Conference and Workshop on Tephrochronology Abstracts, INQUA Inter-Congress Committee on Tephrochronology, Mammoth Hot Springs, Yellowstone National Park, 17-26th June, 1990, p.25.

Krinsley, D.H., and Doornkamp, J.C., 1973, Atlas of quartz sand surface textures., Cambridge University Press, Cambridge, 91pp.

Kronberg, B.I., Couston, J.F., Stilianidi Filho, B., Fyfe, W.S., Nash, R.A., and Sugde, D., 1979, Minor element geochemistry of the Paragominas bauxite, Brazil., Economic Geology, 74, p.1869-1875.

Kunk, M.J., and Sutter, J.F., 1984, $^{40}Ar/^{39}Ar$ age spectrum dating of biotite from Middle Ordovician bentonites, eastern North America., in: Bruton, D.L.,(ed), Aspects of the Ordovician System., Paleontological Contributions from the University of Oslo, No. 295, Universitetsforlaget., p.11-22.

LeBas, M.J., LeMaitre, R.W., Streckeisen, A., and Zanettin, B., 1986, A chemical classification of volcanic rocks based on the Total Alkali-Silica diagram., Journal of Petrology, 27, p.745-750.

LeMaitre, R.W.,(editor), 1989, A classification of igneous rocks and glossary of terms., Blackwell Scientific Publications, Oxford, 193pp.

Lipman, P.W., 1965, Chemical comparison of glassy and crystalline volcanic rocks., U.S. Geological Survey Bulletin, 1201-D, p.D1-D24.

Maaloe, S., and Wyllie, P.J., 1975, Water content of a granite magma deduced from the sequence of crystallization determined experimentally with water-undersaturated conditions., Contributions to Mineralogy and Petrology, 52, p.175-191.

Mahood, G., and Hildreth, W., 1983, Large partition coefficients for trace elements in high-silica rhyolites., Geochimica et Cosmochimica Acta, 47, p.11-30.

Melson, W.G., 1983, Monitoring the 1980-1982 eruptions of Mount St. Helens: compositions and abundances of glass., Science, 221, p.1387-1391.

Merriman, R.J., and Roberts, B., 1990, Metabentonites in the Moffat Shale Group, Southern Uplands of Scotland: Geochemical evidence of ensialic marginal basin volcanism., Geological Magazine, 127, p.259-271.

Mossler, J.H., and Hayes, J.B., 1966, Ordovician potassium bentonites of Iowa., Journal of Sedimentary Petrology, 36, p.414-421.

Nadeau, P.H., Wilson, M.J., McHardy, W.J., and Tait, J.M., 1984, Interstratified clays as fundamental particles., Science, 225, p.923-925.

Nadeau, P.H., Wilson, M.J., McHardy, W.J., and Tait, J.M., 1985, The conversion of smectite to illite during diagenesis: evidence from some illitic clays from bentonites and sandstone., Mineralogical Magazine, 49, p.393-400.

Nelson, W.A., 1922, Volcanic ash bed in the Ordovician of Tennessee, Kentucky, and Alabama., Geological Society of America Bulletin, 33, p.605-615.

Newman, S., Stolper, E.M., and Epstein, S., 1986, Measurement of water in rhyolitic glasses: calibration of an infrared spectroscopic technique., American Mineralogist, 71, p.1527-1541.

Newman, S., Epstein, S., and Stolper, E.M., 1988, Water, carbon dioxide, and hydrogen isotopes in glasses from the ca. 1340 A.D. eruption of the Mono Craters, California: constraints on degassing phenomena and initial volatile content., Journal of Volcanology and Geothermal Research, 35, p.75-96.

Nielsen, C.H., and Sigurdsson, H., 1981, Quantitative methods for electron microprobe analysis of sodium in natural and synthetic glasses., American Mineralogist, 66, p.547-552.

Noble, D.C., 1967, Sodium, potassium, and ferrous iron contents of some secondarily hydrated natural silicic glasses., American Mineralogist., 52, p.280-286.

Payette, C. and Martin, R. F., 1986, The Harvey Volcanic Suite, New Brunswick. I. Inclusions of magma in quartz phenocrysts., Canadian Mineralogist, 24, p.557-570.

Pupin, J.P., 1980, Zircon and granite petrology., Contributions to Mineralogy and Petrology, 73, p.207-220.

Pupin, J.P., 1985, Magmatic zoning of Hercynian granitoids in France based on zircon typology., Schweizerische mineralogische und petrographische Mitteilungen, 65, 29-56.

Pupin, J.P., and Turco, G., 1972a, Le zircon accessoire en géothermométrie., Comptes rendus de l'Académie des Sciences, Paris., 274, p.2121-2124.

Pupin, J.P. and Turco, G., 1972b, Une typologie originale du zircon accessoire., Bull. Soc. franc. Minéral. Cristallogr., 95, p.348-359.

Pupin, J.P. and Turco, G., 1972c, Application des données morphologiques du zircon accessoire en petrologie endogène., Comptes rendus de l'Académie des Sciences, Paris., 275, p.799-802.

Pupin, J.P. and Turco, G., 1975, Typologie du zircon accessoire dans le roches plutoniques dioritiques, granititique et syenitiques. Facteurs essentiels déterminant les variations typologiques., Pétrologie, 2, p.139-156

Rickard, L.V., 1973, Stratigraphy and structure of the subsurface Cambrian and Ordovician carbonates of New York., New York State Museum Map and Chart Series, 18, 26pp.

Roberts, B., and Merriman, R.J., 1990, Cambrian and Ordovician metabentonites and their relevance to the origins of associated mudrocks in the northern sector of the Lower Palaeozoic Welsh marginal basin., Geological Magazine, 127, p.31-43.

Roedder, E., 1984, Fluid inclusions., Ribbe, P.H.,(ed), Reviews in Mineralogy, Mineralogical Society of America., 644pp.

Roen, J.B., and Hosterman, J.W., 1982, Misuse of the term "bentonite" for ash beds of Devonian age in the Appalachian basin., Geological Society of America Bulletin, 93, p.921-925.

Roen, J.B., and Hosterman, J.W., 1983, Misuse of the term "bentonite" for ash beds of Devonian age in the Appalachian basin: Discussion and reply. Reply., Geological Society of America Bulletin, 94, p.682-683.

Roen, J.B., and Hosterman, J.W., 1984, Misuse of the term "bentonite" for ash beds of Devonian age in the Appalachian basin: Discussion and reply. Reply., Geological Society of America Bulletin, 95, p.125.

Rosenkrans, R.R., 1934, Correlation studies of the central and south central Pennsylvania bentonite occurrences., American Journal of Science, 27, p.113-134.

Ross, C.S., 1928, Altered Paleozoic volcanic materials and their recognition., American Association of Petroleum Geologists Bulletin, 12, p.143-164.

Rowley, D.B., and Kidd, W.S.F., 1981, Stratigraphic relationships and detrital composition of the medial Ordovician flysch of western New England: implications for the tectonic evolution of the Taconic Orogeny., Journal of Geology, 89, p.199-218.

Ruedemann, R., and Chadwick, G.H., 1935, Ordovician black shales of New York., Science, 81, p.400.

Rutherford, M.J., Sigurdsson, H., Carey, S., and Davis, A., 1985, The May 18, 1980, eruption of Mount St. Helens, 1, Melt composition and experimental phase equilibria., Journal of Geophysical Research, 90, p.2929-2947.

Rutherford, M.J., and Devine, J.D., 1988, The May 18, 1980, eruption of Mount St. Helens, 3, Stability and chemistry of amphibole in the magma chamber., Journal of Geophysical Research, 93, p.11949-11959.

Samson, S.D., 1986, Chemistry, mineralogy, and correlation of Ordovician bentonites. M.S. thesis, Minneapolis, Minnesota, University of Minnesota, 128 pp.

Samson, S.D., Kyle, P.R., and Alexander, E.C.,Jr., 1988, Correlation of North American Ordovician bentonites by using apatite chemistry., Geology, 6, p.444-447.

Samson, S.D., Patchett, P.J., Roddick, J.C., and Parrish, R.R., 1989, Origin and tectonic setting of Ordovician bentonites in North America: Isotopic and age constraints., Geological Society of America Bulletin, 101, p.1175-1181.

Sarna-Wojcicki, A.M., Bowman, H.R., Meyer, C.E., Russell, P.C., Woodward, M.J., McCoy, G., Rowe, J.J.Jr., Baedecker, P.A., Asara, F., and Michael, H., 1984, Chemical analyses, correlations, and ages of Upper Pliocene and Pleistocene ash layers of East-Central and Southern California., U.S. Geological Survey Professional Paper, 1293, 40pp.

Self, S., Sommer, M.A.,II, and Schramm, L.S., 1983, Controls on the collapse of plinian eruption columns: water in the Bandelier Tuff magma., EOS, 64, p.341.

Silver, L.A., Ihinger, P.D., and Stolper, E., 1990, The influence of bulk composition on the speciation of water in silicate glasses., Contributions to Mineralogy and Petrology, 104, p.142-162.

Sloan, R.E.,(ed), 1987, Middle and Late Ordovician lithostratigraphy and biostratigraphy of the upper Misissippi Valley., Minnesota Geological Survey Report of Investigations, 35, p.7-20.

Smith, R.C., and Way, J.H., 1983, The Tioga ash beds at Selinsgrove Junction., in: Nickelsen, R.P., and Cotter, E.,(eds.), Guidebook for the 48th Annual Field Conference of Pennsylvania Geologists, p.74-88.

Smith, R.C.,II., Berkheiser, S.W.,Jr., and Way, J.H., 1988, The Bald Hill bentonite beds: a Lower Devonian pyroclastic-bearing unit in the northern Appalachians., Northeastern Geology, 10, p.216-230.

Smith, R.P., and Nash, W.P., 1976, Chemical correlation of volcanic ash deposits in the Salt Lake Group, Utah, Idaho and Nevada., Journal of Sedimentary Petrology, 46, p.930-939.

Sommer, M.A., 1977, Volatiles H_2O, CO_2 and CO in silicate melt inclusions in quartz phenocrysts from the rhyolitic Bandelier air-fall and ash-flow tuff, New Mexico., Journal of Geology, 85, p.423-432.

Sommer, M.A., and Schramm, L.S., 1983, An analysis of the water concentrations in silicate melt inclusions in quartz phenocrysts from the Bandelier Tuff, Jemez Mts., New Mexico., Bulletin volcanologique, 46, p.300-320.

Spears, D.A., and Kanaris-Sotiriou, R., 1976, Titanium in some Carboniferous sediments from Great Britain., Geochimica et Cosmochimica Acta., 40, p.345-351.

Srodon, J., Morgan, D.J., Eslinger, E.V., Eberl, D.D., and Karlinger, M.R., 1986, Chemistry of illite/smectite and end-member illite., Clays and Clay Minerals, 34, p.368-378.

Stolper, E.M., 1982, Water in silicate glasses: an infrared spectroscopic study. Contributions to Mineralogy and Petrology, 81, p.1-17.

Stolper, E., Fine, G., Johnson, T., and Newman, S., 1987, The solubility of carbon dioxide in albitic melt., American Mineralogist, 72, p.1071-1085.

Sunagawa, J., 1987, Morphology of minerals., in: Sunagawa, J.,(ed), Morphology of crystals., TERRAPUB, Tokyo., p.509-587.

Takenouchi, S.,and Imai, H., 1975, Glass and fluid inclusions in acidic igneous rocks from some mining areas in Japan., Economic Geololgy, 70, p.750-769.

Templeton, J.S., and Willman, H.B., 1963, Champlainian Series (Middle Ordovician) in Illinois., Iilinois State Geological Survey Bulletin, 89, 260pp.

Thorpe, R.S., Francis, P.W., Hamill, M., and Baker, M.C.W., 1982, The Andes., in: Thorpe, R.S.,(ed), Andesites: orogenic andesites and related rocks., J.Wiley & Son, p.187-205.

Trippi, M.H., 1986, Chemical fingerprinting, clay mineralogy and heavy minerals of several Champlainian K-bentonites of North-central and eastern New York., M.S. Thesis, University of Cinncinatti, 157pp.

Tuttle, O.F., and Bowen, N.L., 1958, Origin of granite in the light of experimental studies in the system $NaAlSi_3O_8$-$KAlSi_3O_8$-SiO_2-H_2O., Geological Society of America; Memoir, 74, 153pp.

Velde, B., and Brusewitz, A.M., 1982, Metasomatic and non-metasomatic low-grade metamorphism of Ordovician meta-bentonites in Sweden., Geochimica et Cosmochimica Acta, 46, p.447-452.

Watson, E.B., 1976, Glass inclusions as samples of early magmatic liquid: determinative method and application to a South Atlantic basalt., Journal of Volcanology and Geothermal Research, 1, p.73-84.

Way, J.H., Smith, R.C,II., and Roden, M., Detailed correlations across 175 miles of the Valley and Ridge of Pennsylvania using 7 ash beds in the Tioga zone., in: Sevon, W.D.,(ed), Guidebook for 51st Annual Field Conference of Pennsylvania Geologists, p.55-72.

Weaver, C.E., 1953, Mineralogy and petrology of some Ordovician K-bentonites and related bentonites., Geological Society of America Bulletin, 64, p.921-944.

Weaver, C.E., 1976, The nature of TiO_2 in kaolin., Clays and Clay Minerals, 24, p.215-218.

Weaver, C.E., 1989, Clays, muds, and shales., Developments in sedimentology, 44. Elsevier, New York, 819pp.

Weaver, C.E., and Bates, T.F., 1951, Mineralogy and petrology of the Ordovician K-bentonites and related limestones., Geological Society of America Bulletin, 62, p.1488.

Willman, H.B., and Kolata, D.R., 1978, The Platteville and Galena Groups in northern Illinois., Illinois State Geological Survey Circular, 502, 75pp.

Winchester, J.A., and Floyd, P.A., 1977, Geochemical discrimination of different magma series and their differentiation products using immobile elements., Chemical Geology, 20, p.325-343.

Winter, J., 1981, Exakte tephrostratigraphische Korrelation mit morphologisch differenzierten Zirkonpopulationen (Grenzbereich Unter-/Mitteldevon, Eifel-Ardennen)., Neues Jahrbuch für Geologie und Paläontologie; Abhandlungen, 162, p.97-136.

Winter, J., 1984, Identifizierung von Keratophyr-Horizonten durch Tracht und Habitus ihrer Zirkone (Unterdevon, Rheinisches Schiefergebirge)., Zeitschrift der deutschen geologischen Gesellschaft, 135, p.501-527.

Yonover, R.N., Sinton, J.M., Sommer, M.A., and Gibson, E.K., 1989, C-O-H ratios of silicate melt inclusions in basalts from the Galapagos Spreading Center near 95°W: A laser decrepitation mass spectrometry study., Geochimica et Cosmochimica Acta, 53, p.3145-3154.

Zielinski, R. A., 1982, The mobility of Uranium and other elements during alteration of rhyolite ash to Montmorillonite: a case study in the Troublesome Formation, Colorado, U.S.A., Chemical Geology, 35, p.185-204.

Zielinski, R.A., 1985, Element mobility during alteration of silicic ash to kaolinite - a study of tonstein., Sedimentology, 32, p.567-579.

Appendix A

Composition of homogeneous quartz melt inclusions from various K-bentonites. Analyses were performed by electron microprobe and are listed in weight percent.

sample:	89-050	89-050	89-050	89-050	89-050	89-050	89-050	89-050
inclusion:	#50	G-39	G-28	G-40	A-48	G-29	#30	G-28
spot:			A-I		A			A-II
beam-size: (microns)	20	20	30	20	20	15	20	20
SiO2:	68.47	70.71	71.74	71.79	71.83	72.09	72.49	72.60
TiO2:	0.06	0.09	0.09	0.11	0.10	0.11	0.05	0.07
Al2O3:	11.05	11.69	11.47	11.61	11.72	11.29	11.75	11.52
FeO:	0.74	0.86	0.83	0.84	0.86	0.68	0.87	0.82
MnO:	0.06	0.01	0.00	0.00	0.03	0.00	0.05	0.01
MgO:	0.05	0.07	0.07	0.08	0.06	0.08	0.07	0.07
CaO:	0.76	0.83	0.82	0.88	0.80	0.70	0.81	0.83
Na2O:	2.40	2.31	2.33	2.52	2.45	2.47	2.25	2.27
K2O:	4.85	5.28	5.35	5.25	5.28	5.25	5.57	5.41
Total:	88.44	91.83	92.70	93.08	93.12	92.67	93.91	93.59
"volatiles":	11.56	8.17	7.30	6.92	6.88	7.33	6.09	6.41

sample:	89-050	89-050	89-050	Can 13	Can 13	Can 13	Can 14	Can 14
inclusion:	G-34	A-48	A-33	#128	#129	#129	F-3	D-2
spot:		B			A	B		
beam-size: (microns)	15	10	20	15	15	20	30	20
SiO2:	72.68	72.75	73.57	74.45	71.75	72.32	72.98	70.41
TiO2:	0.10	0.07	0.08	0.31	0.22	0.13	0.13	0.06
Al2O3:	11.55	11.61	11.26	11.09	11.36	11.30	11.43	11.51
FeO:	0.82	0.83	0.77	0.98	1.10	0.70	0.76	0.17
MnO:	0.00	0.02	0.00	0.06	0.12	0.13	0.08	0.04
MgO:	0.07	0.06	0.06	0.25	0.17	0.17	0.05	0.01
CaO:	0.84	0.87	0.75	1.61	1.71	1.62	0.85	0.69
Na2O:	2.30	2.33	2.38	2.58	3.32	3.33	2.98	3.04
K2O:	5.31	5.27	5.31	2.15	1.79	1.81	4.65	4.72
Total:	93.67	93.83	94.18	93.47	91.53	91.51	93.91	90.65
"volatiles":	6.33	6.17	5.82	6.53	8.47	8.49	6.09	9.35

Appendix A continued

sample:	Can 14 (Na2O)	Can 14 (Na2O)	Can 14	Can 14	Flat 14	Flat 14	Flat 14	Flat 14	Flat 14
inclusion:	C-24	F-22	E-6	F-22	B-4	B-2	B-1	B-3	#105
spot:		B		A					
beam-size: (microns)	5	5	20	20	20	20	20	20	20
SiO2:	74.43	74.01	72.01	72.53	72.44	67.11	71.70	71.07	72.35
TiO2:	0.08	0.05	0.02	0.05	0.00	0.00	0.00	0.05	0.12
Al2O3:	11.80	11.66	11.53	11.46	11.34	10.96	11.78	11.49	11.38
FeO:	0.77	0.78	0.88	0.87	0.75	0.69	0.85	0.90	0.93
MnO:	0.09	0.08	0.00	0.10	0.09	0.07	0.05	0.06	0.05
MgO:	0.02	0.03	0.09	0.02	0.02	0.02	0.03	0.02	0.04
CaO:	0.61	0.63	1.07	0.60	0.63	0.52	0.61	0.59	0.79
Na2O:	2.80	3.09	2.53	3.29	2.93	2.98	2.93	2.75	3.27
K2O:	4.27	4.43	4.48	4.50	4.43	4.46	4.50	4.67	3.73
Total:	94.88	94.75	92.61	93.43	92.62	86.82	92.46	91.57	92.65
"volatiles":	5.12	5.25	7.39	6.57	7.38	13.18	7.55	8.43	7.35

sample:	Flat 14	Tioga-F	Tioga-F	Tioga-F	Tioga-F	Tioga-F	Tioga-F	Tioga-F	Tioga-F
inclusion:	B-5	1	2.1	2.2	2.2	3	4.1	4.2	5.1
spot:		A	A	A	A	A	A	A	A
beam-size: (microns)	20	30	30	10	15	30	30	15	20
SiO2:	67.65	73.38	71.91	72.95	71.93	71.83	72.36	72.92	72.13
TiO2:	0.10	0.10	0.14	0.06	0.11	0.19	0.10	0.04	0.09
Al2O3:	11.11	11.89	12.10	12.04	12.03	12.04	12.06	11.93	12.07
FeO:	0.70	0.79	0.80	0.73	0.77	0.86	0.82	0.74	0.84
MnO:	0.12	0.03	0.05	0.05	0.05	0.02	0.04	0.01	0.03
MgO:	0.00	0.11	0.10	0.12	0.11	0.12	0.11	0.10	0.12
CaO:	0.58	0.60	0.59	0.67	0.65	0.76	0.64	0.65	0.64
Na2O:	2.96	2.85	2.82	2.52	2.61	2.88	2.86	2.81	2.79
K2O:	4.20	4.58	4.69	4.72	4.64	4.74	4.74	4.77	4.77
Total:	87.42	94.33	93.21	93.87	92.90	93.45	93.73	93.96	93.48
"volatiles":	12.59	5.67	6.80	6.13	7.11	6.55	6.27	6.04	6.52

Appendix B

Recalculation procedure for conversion of original melt inclusion (glass) analyses into modeled altered ash compositions following these steps:

1. All analyses are recalculated to 100 weight percent, anhydrous and CaO-free.

2. Assuming loss of SiO_2, Na_2O and K_2O from the glassy material, the concentrations of these oxides are preset to the concentrations which are actually measured in the bentonite sample (preset oxides are marked by asterik).

3. Concentrations of all remaining oxides are recalculated by multiplication of the original value (glass) with a factor *c* to adjust for the overall loss of SiO_2, Na_2O and K_2O.

4. Factor *c* is calculated as difference of the sum of preset concentrations for SiO_2, Na_2O and K_2O to 100 weight percent, divided by the difference of the sum of the original concentrations for SiO_2, Na_2O and K_2O (in glass) to 100 weight percent.

$$c = (100\text{wt\%} - \text{sum}(\text{oxide}_{\text{preset}})\text{wt\%}) \,/\, (100\text{wt\%} - \text{sum}(\text{oxide}_{\text{glass}})\text{wt\%})$$

where oxides are only SiO_2, Na_2O and K_2O.

Appendix C
Relative abundances of morphology types in zircon populations from Ordovician K-bentonites; classified after the scheme of Pupin and Turco (1972b).

Morphology	Can 1	Can 2	Can 10	Can 13	Can 14	Can 27
H	-	-	-	-	-	-
L1	-	-	-	-	-	-
L2	-	-	-	-	-	-
L3	-	-	-	-	-	-
L4	-	-	-	-	-	-
L5	-	-	-	-	-	-
G1,2,3	-	-	-	-	-	-
Q1	-	-	-	-	-	-
S1	-	-	-	-	0.1	-
S2	-	-	1.0	2.1	-	-
S3	-	0.3	-	-	0.4	-
S4	-	-	-	1.1	1.0	-
S5	-	-	-	2.1	3.4	-
P1	-	-	-	-	5.1	-
Q2	-	-	-	-	-	-
S6	0.2	-	-	-	0.1	-
S7	1.9	0.5	2.7	6.4	5.1	-
S8	0.4	0.8	1.7	2.1	3.0	-
S9	0.2	0.3	-	-	5.1	1.4
S10	0.2	-	-	-	5.9	-
P2	0.2	-	-	7.4	20.4	-
Q3	-	-	-	-	-	-
S11	0.2	-	-	-	0.4	-
S12	0.9	-	6.7	-	2.3	-
S13	0.6	0.3	1.3	2.1	1.0	2.4
S14	-	-	1.3	-	1.7	3.4
S15	-	-	-	-	0.8	-
P3	-	-	-	-	2.5	-
Q4	-	-	-	-	-	-
S16	1.3	-	0.3	2.1	0.6	-
S17	15.3	8.5	13.4	8.5	14.5	6.8
S18	18.0	8.2	20.4	8.5	3.9	4.1
S19	6.4	6.4	12.0	3.2	5.5	23.9
S20	0.2	-	-	-	2.2	5.1
P4	-	-	-	2.1	4.8	0.7
Q5	-	-	-	-	-	-
S21	0.4	-	-	-	-	-
S22	6.1	7.2	11.7	4.3	4.7	2.7
S23	17.4	20.6	8.4	-	1.4	2.0
S24	17.0	21.1	11.0	2.1	3.1	37.2
S25	5.5	4.6	1.3	24.5	0.7	7.8
P5	0.2	-	-	21.3	0.4	2.4
E	-	-	-	-	-	-
J1	-	-	0.3	-	-	-
J2	1.7	3.3	3.3	-	-	-
J3	1.7	7.5	1.7	-	-	-
J4	1.7	8.2	1.3	-	-	-
J5	2.3	2.1	-	-	-	-
D	-	-	-	-	-	-

Appendix C continued

Morphology	Flat 6	Flat 13	Flat 14	Flat 26
H	-	-	-	-
L1	-	-	-	-
L2	-	-	-	-
L3	-	-	-	-
L4	-	-	-	-
L5	-	-	-	-
G1,2,3	-	-	-	-
Q1	-	-	-	-
S1	-	-	0.4	-
S2	1.2	5.7	1.3	-
S3	-	-	0.4	-
S4	-	-	1.0	-
S5	-	-	2.9	-
P1	-	2.9	4.1	-
Q2	-	-	-	-
S6	-	-	-	-
S7	20.1	-	5.6	-
S8	2.4	2.9	3.4	-
S9	1.2	-	5.6	0.9
S10	-	-	5.6	0.9
P2	-	2.9	16.8	-
Q3	-	-	-	-
S11	-	-	0.1	-
S12	11.4	1.4	1.1	1.3
S13	1.2	-	1.1	0.9
S14	1.6	1.4	1.7	4.3
S15	-	-	0.5	1.7
P3	-	-	2.1	1.7
Q4	-	-	-	-
S16	-	1.4	0.4	-
S17	39.0	14.3	13.1	1.7
S18	7.1	-	4.2	6.4
S19	7.9	4.3	8.6	16.3
S20	0.4	2.9	2.1	2.1
P4	1.2	-	5.2	2.1
Q5	-	-	-	-
S21	-	-	0.9	-
S22	2.4	11.4	3.8	2.6
S23	-	2.9	1.8	2.1
S24	2.4	24.3	5.6	42.0
S25	0.4	10.0	0.4	10.7
P5	0.4	11.4	0.2	2.1
E	-	-	-	-
J1	-	-	-	-
J2	-	-	-	-
J3	-	-	-	-
J4	-	-	-	-
J5	-	-	-	-
D	-	-	-	-

Appendix C continued

Morphology	Hounsfield	Trenton-1	89-050	Millbrig	Dickeyville	Nasset
H	-	-	-	-	-	-
L1	-	-	-	-	-	-
L2	-	-	-	-	-	-
L3	-	-	-	-	-	-
L4	-	-	-	-	-	-
L5	-	-	-	-	-	-
G1,2,3	-	-	-	-	-	-
Q1	-	-	-	-	-	-
S1	-	-	-	-	-	-
S2	-	-	-	-	-	-
S3	-	-	0.2	-	-	-
S4	-	-	-	-	-	-
S5	-	-	0.3	-	-	1.3
P1	-	-	0.2	0.5	0.2	1.0
Q2	-	-	-	-	-	-
S6	-	-	-	-	-	-
S7	0.5	-	0.2	0.6	0.5	1.7
S8	0.3	-	0.2	0.6	0.5	1.0
S9	0.3	-	0.5	0.2	0.2	3.6
S10	1.4	-	0.6	0.6	-	5.3
P2	1.6	0.4	0.2	1.2	-	1.0
Q3	-	-	-	-	-	-
S11	-	-	-	-	-	-
S12	0.5	0.9	-	0.2	0.9	1.3
S13	1.4	0.4	0.3	1.1	1.4	3.3
S14	1.1	-	2.0	0.3	0.5	1.3
S15	0.3	-	0.5	1.8	-	2.7
P3	0.8	-	-	1.7	-	1.0
Q4	-	-	-	-	-	-
S16	-	0.4	-	-	0.5	0.7
S17	6.5	3.4	2.3	5.4	2.6	2.0
S18	4.9	5.9	3.9	8.0	8.0	5.6
S19	25.5	5.9	31.8	16.4	10.8	14.6
S20	2.4	3.0	6.4	3.8	2.1	13.2
P4	9.0	-	2.5	8.1	-	2.3
Q5	-	0.4	-	-	-	-
S21	-	3.8	-	1.1	2.6	-
S22	8.7	5.1	0.9	7.2	9.6	0.3
S23	7.3	15.3	2.1	12.0	14.1	3.3
S24	17.1	23.3	38.5	20.3	21.6	16.6
S25	5.7	11.4	5.5	4.8	9.9	13.9
P5	4.6	2.1	0.8	4.4	0.5	3.0
E	-	-	-	-	0.5	-
J1	-	2.1	-	-	1.6	-
J2	-	2.1	-	-	1.9	-
J3	-	3.8	-	-	3.1	-
J4	-	5.5	0.2	-	4.5	-
J5	-	3.4	-	-	1.4	-
D	-	1.3	0.1	-	0.7	-

Appendix D

Generalized map of the upper Mohawk Valley near the town of Canajoharie in New York State, showing the sample localities for K-bentonites in Canajoharie Creek and Flat Creek (from Bock, 1990).

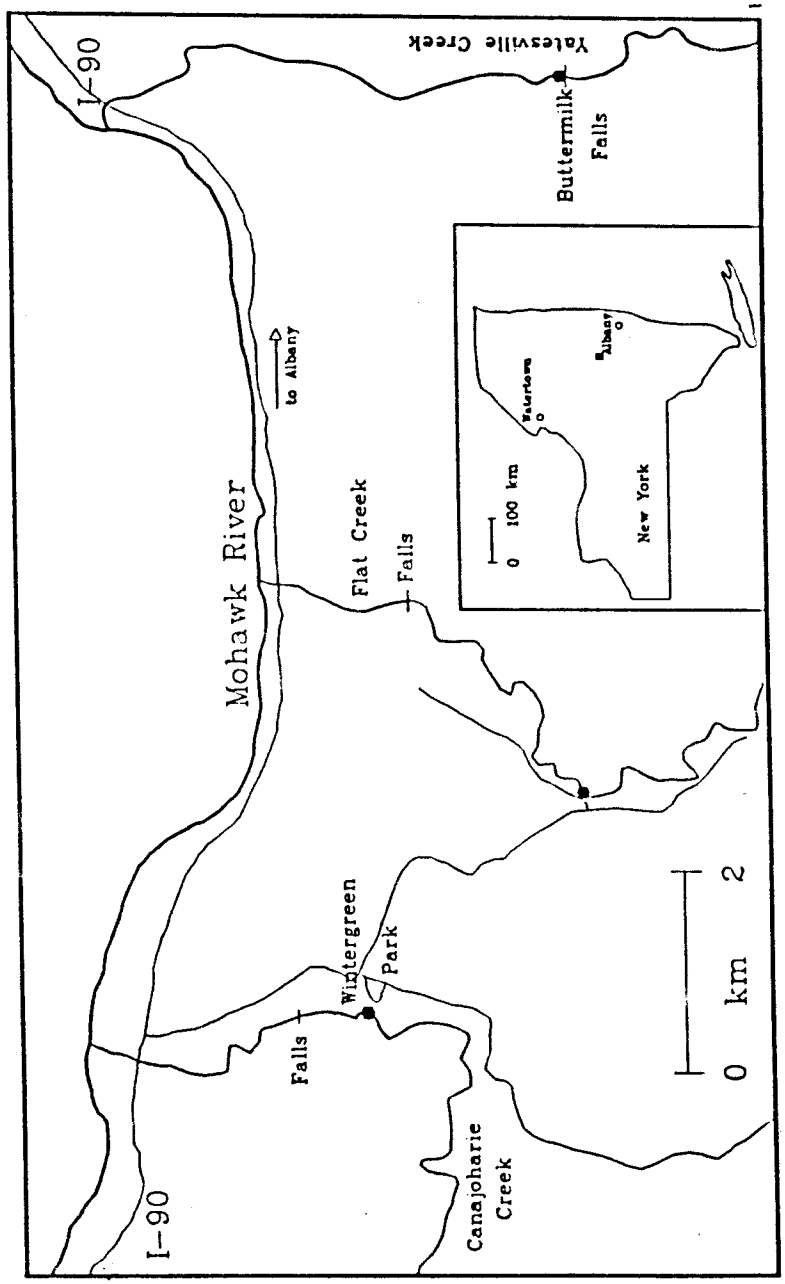

Appendix E

Closeup of Canajoharie Creek and Flat Creek, showing the sample localities for each creek (from Bock, 1990). Stratigraphy and terminology of the K-bentonites is given in Table I and Figure 3.

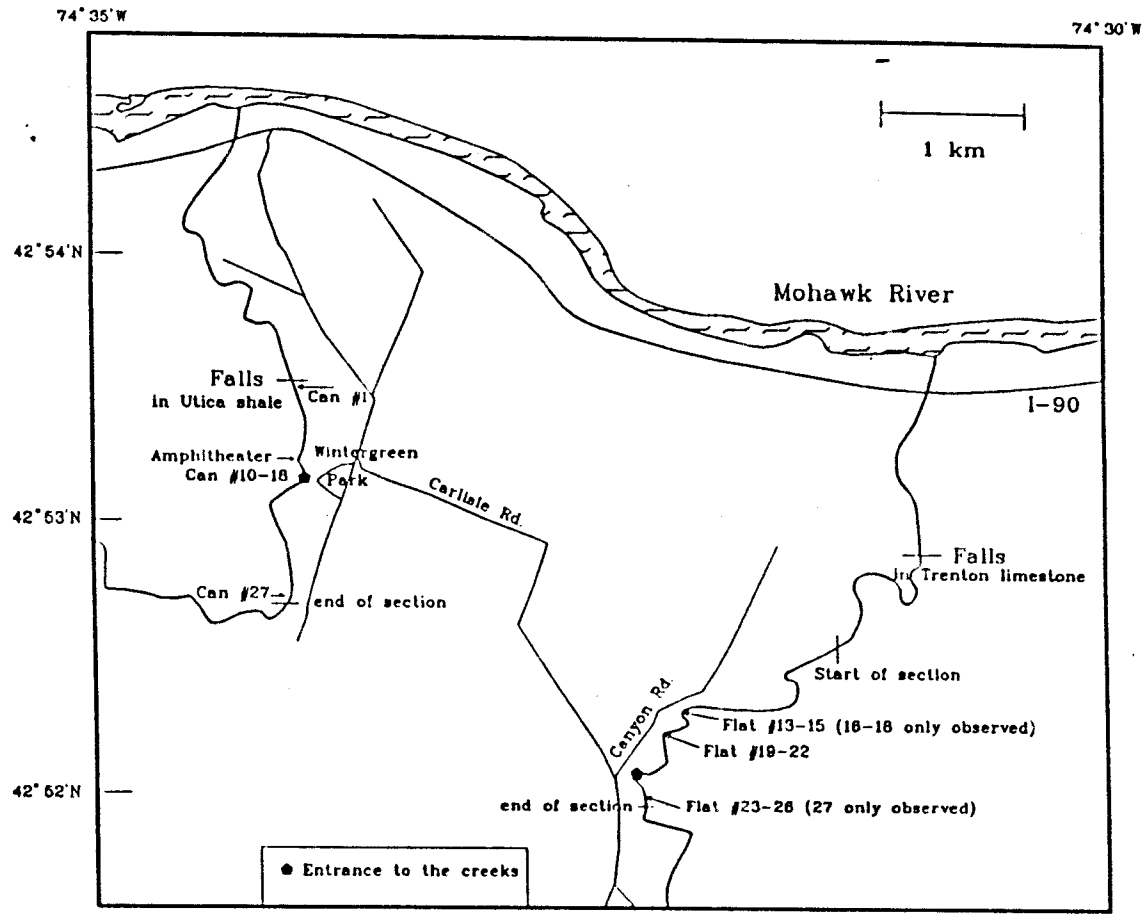

Appendix F

Sample localities:

K-bentonites Can 1 thru 27:
Canajoharie Creek, Montgomery County NY (74°33.9'W, 42°53.3'N)

K-bentonites Flat 5 thru 27:
Flat Creek, Montgomery County NY (74°31.5W, 42°52.5'N)

Trenton-1 K-bentonite: Abandoned quarry along U.S. Highway 169, east of Middleville (Cameron and Kamal, 1977) (74°57.6'W, 43°54.3'N).

89-050 K-bentonite:
In waterfall along second side stream south of County Home, about 500 meters west of U.S. Highway 28 (Kay, 1953) (74°59'W, 43°07'N).

Hounsfield K-bentonite:
About 3 kilometers east of Dexter, Jefferson County NY, in abandoned quarry (160 centimeters above quarry floor) along road Dexter-Brownville; type locality for Hounsfield K-bentonite (Kay, 1930, 1931) (76°00.1'W, 44°01.6'N).

Glacial sediment:
Small quarry west of U.S. Highway 12, about 2 kilometers north of Copenhagen, Lewis County NY (75°42.6'W, 43°54.3N).

Millbrig and Dickeyville K-bentonites:
Roadcut along U.S. Highway 61, 6.4 kilometers northwest of Dickeyville, Wisconsin; type locality for Dickeyville K-bentonite (Kolata et al., 1986) (42°37'N, 90°37'W).

Nasset K-bentonite:
Roadcut along U.S. Highway 52, north of Guttenberg, Iowa (about 1 kilometer) (Willman and Kolata, 1978) (42°48'N, 91°06'W).